Sonoma Technology, Inc.

1360 Redwood Way, Suite C
Petaluma, CA 94954-1104
707 / 665-9900
Fax 707 / 665-9800
www.sonomatech.com

ANALYSES OF THE CAUSES OF HAZE FOR THE CENTRAL STATES (PHASE II)

SUMMARY OF FINDINGS

EXECUTIVE SUMMARY
STI-904780.08-2754-ES

By:
Dana Coe Sullivan
Hilary R. Hafner
Steven G. Brown
Clinton P. MacDonald
Sean M. Raffuse
Bryan M. Penfold
Paul T. Roberts
Sonoma Technology, Inc.
1360 Redwood Way, Suite C
Petaluma, CA 94954-1169

Prepared for:
Central States Regional Air Planning Association
10005 S. Pennsylvania, Suite C
Oklahoma City, OK 73159

August 31, 2005

TABLE OF CONTENTS

LIST OF FIGURES

Figure **Page**

LIST OF FIGURES

Figure **Page**

LIST OF FIGURES

LIST OF TABLES

1. INTRODUCTION

The Central States Regional Air Planning Association (CENRAP) is researching visibility-related issues for its region, which includes the states of Texas, Oklahoma, Louisiana, Arkansas, Kansas, Missouri, Nebraska, Iowa, and Minnesota, and is developing a regional haze plan in response to the U.S. Environmental Protection Agency's (EPA) mandate to protect visibility in Class I areas. In order to develop an effective regional haze plan, the CENRAP ultimately must develop a conceptual model of the phenomena that lead to episodes of low and high visibility in the CENRAP region.

This Executive Summary describes the findings of data analyses and assessments of phenomena that govern regional haze in the CENRAP region. (Methods, information sources, and graphical and tabular illustrations of available data are documented in the appendices.) It is intended to be used for reference during preparation for photochemical modeling and during consideration of strategies to improve or protect visibility conditions in CENRAP's Class I areas. Specifically, the findings in this document should be useful for (1) selection of year-2002 episodes and geographic areas that should be treated at 12-km spatial resolution for photochemical modeling and (2) preliminary consideration of potentially effective control scenarios. In addition, CENRAP and its member states, tribes, and stakeholders will likely build on the results of this project in the future when more air quality data are available or periodically as EPA Regional Haze Rule milestones arise. Therefore, the analyses presented in this document may be used as a foundation for future analyses.

2. PURPOSE AND OBJECTIVES

Air quality regulators are faced with the challenge of (1) characterizing the causes of impairments to visibility when visibility is reduced and when visibility is at its best (when presumably impairments to visibility are minimized); and (2) identifying the most effective means to preserve the conditions when visibility is at its best and to gradually improve the visibility when it is most impaired. Thus, the objectives of the data analyses reported in this Executive Summary, "Analyses of the Causes of Haze for the Central States (Phase II)" (CENRAP Work Assignment Number 04-0628-RPO-017), were to determine the causes of hazy conditions and variations in haziness for Class I areas and other Interagency Monitoring of Protected Visual Environments (IMPROVE)-Protocol monitoring sites in the CENRAP region. Consistent with the requirements of the Regional Haze Rule, the analyses focused on the 20% of days with the worst visibility conditions and the 20% of days with the best visibility conditions at Class I sites during the period 2000-2004 ("20%-worst" and "20%-best" days, respectively). The analyses were formulated to address several key questions and issues:

1. To what extent are visibility-impairing emissions within the control of CENRAP air regulators?
   - Can specific source types, geographic locations, or temporal patterns of emissions sources impacting Class I areas during episodes of good or poor visibility be distinguished?

- What connections can be drawn between sample periods showing unusual species concentrations and sporadic emission sources (e.g., dust storms and large forest fires)? How can this information be used to estimate the impacts of sporadic emission sources?

2. What specific types of meteorological events should most concern CENRAP air regulators when considering strategies to improve or protect visibility?
   - What are the archetypal meteorological conditions associated with episodes of good visibility and poor visibility? On which dates of 2002 did such conditions occur?
   - Which days or episodes in 2002 best represent these good and poor visibility events and should be considered for modeling?
   - Was the meteorology in 2002 and 2003 normal compared to climatological averages?

3. Can trends in emissions on the time scale of years be related to trends in the causes of haze?
   - Are changes in the aerosol components responsible for changes in haze?
   - For any detectable changes in aerosol components responsible for haze, are the changes related to variations in meteorological conditions or emissions?
   - Where emissions are known to have changed substantially (based on emission inventory data), are there corresponding changes in haze levels?

The analyses reported in this document reflect a simplified approach to these questions and issues—they are not intended to substitute for rigorous assessments based on photochemical and meteorological modeling. Instead, they provide a preliminary understanding of the important phenomena governing haze in the CENRAP region and a preview of what might be expected to result from modeling assessments. The understanding gained from a simplified approach is useful in the interim period until modeling exercises are complete; can be used to help guide the specific modeling plans (e.g., selection of episode dates or modeling domains); and can simplify CENRAP's task of developing haze mitigation strategies. With the information presented in this document, CENRAP can begin considering likely haze mitigation alternatives, understand the types of meteorological and emissions events that are associated with episodes of good and poor visibility, and select the specific dates that would be good candidates for base-year episodic photochemical modeling.

Four representative subregions of CENRAP (illustrated in **Figure 2-1**) were identified in which aerosol extinctions and concentrations of $PM_{2.5}$ components significantly covary in space and time (for the 20%-best and 20%-worst days). Visibility conditions within each of these subregions are thought to be affected by common influences, such as emissions sources, clean-air corridors,[1] and prevailing meteorological conditions.[2] Therefore, analyses were oriented toward these representative subregions (rather than individual monitoring sites)—a cost-effective

[1] Clean-air corridor is defined as the transport pathway predominantly associated with 20%-best days.
[2] Supporting evidence for the definition of these subregions is summarized in Section 4 and documented in Appendix A of this Executive Summary.

approach to considering most of the geographic extent of the CENRAP region. Representative sites from each of the subregions received most of the attention: Cedar Bluff (CEBL1), Kansas, for the Western Plains; Sikes (SIKE1), Louisiana, for Southeastern Plains; Hercules-Glades (HEGL1), Missouri, for the Upper Midwest; and Voyageurs National Park (VOYA2), Minnesota, for Minnesota.

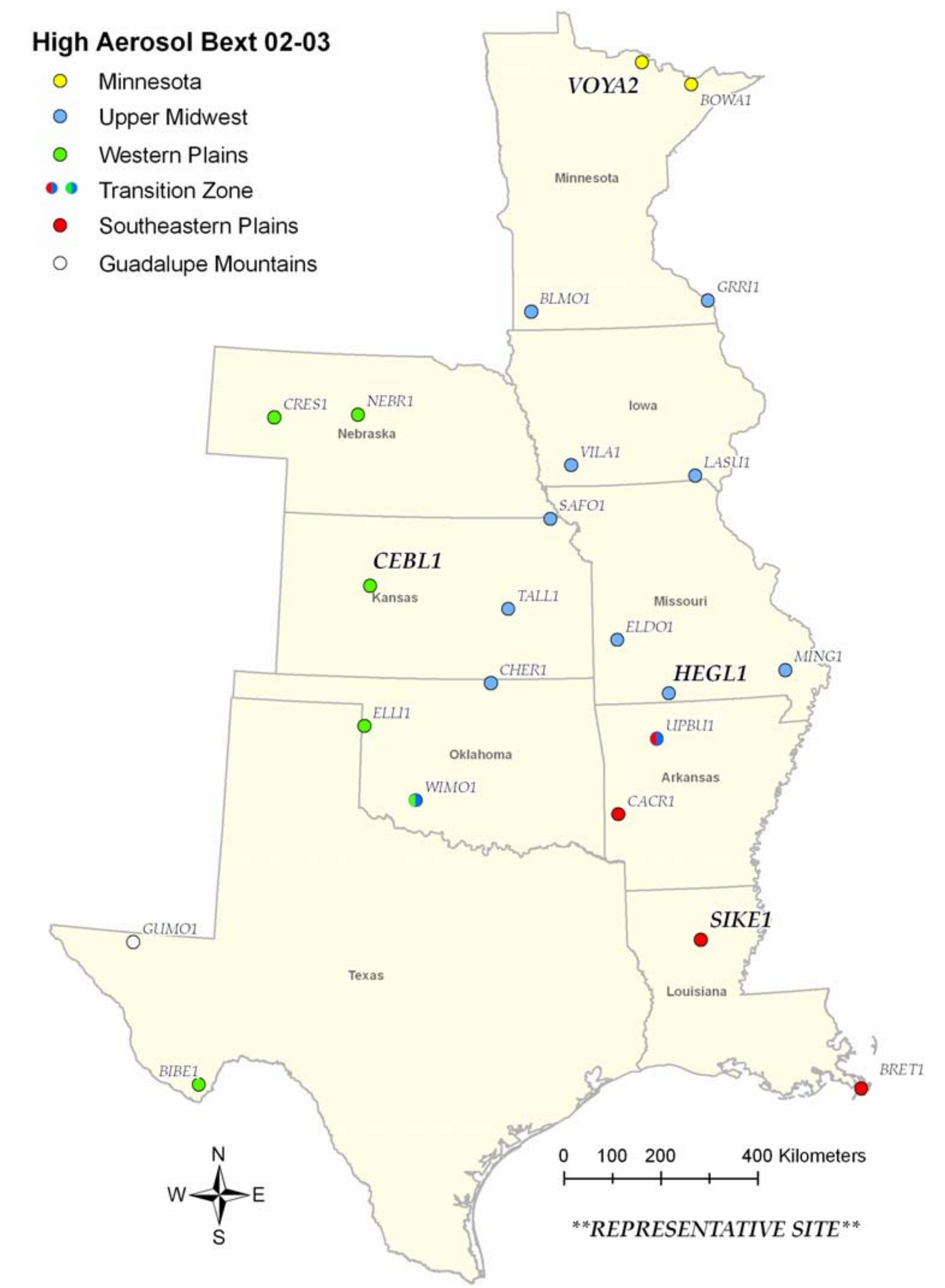

Figure 2-1. IMPROVE and IMPROVE-Protocol monitoring sites in the CENRAP domain classified by representative subregion for the 20%-worst visibility days in 2002-2003.

The following sections of this Executive Summary include a summary of primary conclusions (Section 3) followed by additional supporting evidence in Section 4. References for the Executive Summary are provided in Section 5. Several appendices follow the Executive Summary to provide additional documentation of methods, graphical and tabular summaries of data, and other pertinent information in support of the conclusions. Appendix A summarizes the Task 4 spatiotemporal analyses. Appendix B summarizes the Task 5 meteorological analyses. Appendix C summarizes the Task 6 emissions analyses. Appendix D includes two draft journal articles that summarize the source apportionment approach and results for Sikes and Hercules-Glades, respectively.

3. SUMMARY OF PRIMARY CONCLUSIONS

The primary conclusions derived from this project are provided in this section. Supporting evidence for each conclusion is discussed in Section 4.

1. To what extent are visibility-impairing emissions within the control of CENRAP air regulators?

    - Emission inventory analyses produced the following answers to the stated question. (However, an important area of weakness in the analyses was caused by substantial inconsistencies in the emission inventories of volatile organic compounds [VOCs], $PM_{2.5}$, PM_{10}, and ammonia [NH_3], both within and between various regions. Unless resolved, these problems are likely to affect photochemical modeling performance).

        – *CENRAP will need the cooperation of other Regional Planning Organizations (RPOs) or countries to protect clean-air corridors and to improve visibility conditions at some sites.* Emissions sources in the Midwest RPOs and Visibility Improvement State and Tribal Association of the Southeast (VISTAS) regions contribute significantly to visibility impairment on the 20%-worst days in the Southeastern Plains and Upper Midwest subregions of CENRAP. In addition, sources in northern Mexico and the Midwest RPO region contribute moderately to visibility impairment on the 20%-worst days in the Western Plains subregion. Areas of Canada and the Western Regional Air Partnership (WRAP) states are clean-air corridors for visibility-protected sites in the Northern Minnesota and Western Plains subregions. However, in most other respects, visibility conditions at CENRAP's protected sites are affected primarily by emissions sources or clean-air corridors located within CENRAP's boundaries.

        – *BART [3] requirements alone are unlikely to significantly alter visibility conditions of protected sites in the CENRAP.* An estimate of the impacts of emissions from potentially BART-eligible sources showed that such sources generally contribute very little to the oxides of sulfur (SO_x)- and oxides of nitrogen (NO_x)-associated visibility impairment at Class I areas in the CENRAP region. Additional emissions reductions will be needed to improve visibility conditions on the 20%-worst days.

[3] BART = Best Available Retrofit Technology

- Source apportionment analyses corroborated the results of emission inventory analyses.

  - *Aerosol components that contribute to poor visibility include sulfate, nitrate, and carbonaceous matter.* In the Upper Midwest and Southeastern Plains subregions, ammonium sulfate accounts for 70% (on average) of visibility impairment at CENRAP's protected sites on the 20%-worst days, computed using the standard IMPROVE equation (Malm et al., 1994; IMPROVE, 2004). In the Western Plains, sulfate and nitrate combined account for 40% (on average) of visibility impairment. In Northern Minnesota, sulfate, nitrate, and carbonaceous aerosol are important, accounting respectively for 40%, 25%, and 30% (on average) of visibility impairment. In all CENRAP subregions, carbonaceous matter causes 10% to 30% of the visibility impairment (on average), although this estimate is likely to be conservatively low because the IMPROVE visibility equation does not fully account for carbonaceous aerosol scattering.

  - *Source regions both outside and within CENRAP are important contributors to visibility impairment at the protected sites.* Coal combustion in the Ohio River Valley, St. Louis area, and Gulf States accounts for 40% to 50% of the aerosol mass (and an even larger proportion of light extinction) at CENRAP's protected sites on the 20%-worst days in the Upper Midwest and Southeastern Plains subregions. "Southeastern aged aerosol" (from areas outside the CENRAP region) and "urban carbonaceous aerosol" from the Mississippi River Valley (from areas generally within CENRAP) contribute roughly one-quarter to nearly half of the aerosol mass on the 20%-worst days in these areas. Wintertime nitrate episodes were important in the Upper Midwest and were associated with impacts from ammonia and NO_x emissions sources located mostly within the CENRAP region. Of source regions outside the CENRAP region, Ohio River Valley coal combustion contributed more heavily to visibility impairment in the Upper Midwest than in the Southeastern Plains, while transport of aerosols from the southeastern United States contributed more heavily at the Southeastern Plains sites.

  - *Fires infrequently contribute to visibility impairment observed on the 20%-worst days at most sites in the CENRAP region.* Organic carbon mass (OMC) contributed to light extinction infrequently on 20%-worst days, except at a few sites. The exceptions included Big Bend during the spring months, Nebraska National Forest during the summer, and the two sites located in the Minnesota region during the summer. (More investigation is needed to determine whether these elevated OMC contributions were due to fires.) In the Southeastern Plains and Upper Midwest regions, the influences of episodic local and regional burning events, usually within CENRAP, were successfully detected through corroborative analyses, though they were not important drivers of poor visibility in those areas. Fires may threaten clean-air corridors and visibility conditions on days with clear conditions and high winds from the northwestern U.S. or Canada—conditions likely to occur on the 20%-best days.

  - *Very infrequently does geologic material contribute appreciably to visibility impairment observed on the 20%-worst days at most sites in the CENRAP region.*

Soil and coarse mass contributed to light extinction infrequently on 20%-worst days, except at Guadalupe Mountains. (More investigation is needed to determine the sources of soil and coarse mass at Guadalupe Mountains.) In the Southeastern Plains and Upper Midwest regions, the influences of dust transported over long distances were successfully detected through corroborative analyses, though they were not important drivers of poor visibility in those areas. Dust storms may threaten clean-air corridors and visibility conditions on days with clear conditions and rapid transport through the Great Plains of the U.S. or across the Atlantic—conditions likely to occur on the 20%-best days.

2. What specific types of meteorological events should most concern CENRAP air regulators when considering strategies to improve or protect visibility?

   - *Many types of weather and transport conditions occurred on the 20%-best or 20%-worst days during 2002-2003.* On average there were about five different weather and transport clusters for each of the four CENRAP subregions for both the 20%-worst and 20%-best days. The meteorological and transport characteristics associated with the clusters for each subregion are presented in Section 4.3 and in Appendix B.

   - *Representative days and episodes in 2002 were identified that are suitable for modeling.* Recommended modeling days shown in **Tables 3-1 and 3-2** were determined by selecting episodes that were coincident among the four subregions and that captured most of the common meteorological and transport characteristics identified in the clusters.

Table 3-1. Recommended modeling dates that exhibited representative meteorological and transport conditions on the 20%-worst visibility days.

Modeling Periods in 2002	Cedar Bluff	Sikes	Voyageurs	Hercules-Glades
July 6-7	No data	Worst	Worst	Worst
August 2-10	No data	Worst	Worst	Worst
September 1-14	Worst	Worst	Worst	Worst
December 2-14	Worst	No data	Worst	Worst

"Worst" = 20%-worst visibility days.
"No data" indicates samples were not available on the specified dates.

Table 3-2. Recommended modeling dates that exhibited representative meteorological and transport conditions on the 20%-best visibility days.

Modeling Periods in 2002	Cedar Bluff	Sikes	Voyageurs	Hercules-Glades
April 20-26	No data	Best	Best	Best
May 17	No data	—	Best	Best
October 14-17	Best	—	Best	Best
December 19-31	Best	Best	Best	Best

"Best" = 20%-best visibility days.
"No data" indicates samples were not available on the specified dates.
— indicates data were available but the dates were not among the 20%-best visibility days at that site.

- *In general, the meteorology of 2002-2003 was near normal for the CENRAP region and can, therefore, be considered representative* <u>with two minor exceptions</u>:
  - Temperatures were slightly above normal in the northern portions of the CENRAP region in 2002 and in the western portions in 2003.
  - Precipitation was slightly above normal in Texas and slightly below normal in the western portions of the CENRAP region in 2002. Precipitation was slightly below normal in most of CENRAP in 2003.

3. Can trends in emissions on the time scale of years be related to trends in the causes of haze?

   - Sufficiently long histories of IMPROVE-protocol data are available for the Upper Buffalo Wilderness site (in Arkansas), the Big Bend National Park site (in Texas), and the sites in northern Minnesota (Voyageurs National Park Site No. 1, Voyageurs National Park Site No. 2, and Boundary Waters-Canoe Area). Analyses of the available data for these sites yielded the following conclusions.
     - *Sulfur dioxide (SO_2) emissions in the Ohio River Valley states (Ohio, West Virginia, Kentucky, Indiana, and Illinois), Tennessee, and Missouri declined substantially from 1990 to 1999.* These declines in SO_2 emissions were concurrent with a decline in observed ammonium sulfate concentrations and associated light extinction at the Upper Buffalo, Arkansas site (which lies in a transitional zone and shares characteristics with the Upper Midwest and Southeastern Plains subregions of CENRAP).
     - *SO_2 emissions in Texas, New Mexico, Arizona, Louisiana, Arkansas, and Mississippi increased somewhat from 1990 to 1999.* These increases in SO_2 emissions were concurrent with an increase in observed ammonium sulfate concentrations and associated light extinction at the Big Bend, Texas site. No information was readily available to characterize the historical trend in SO_2 emissions for northern Mexico, which is also an important upwind area for the Big Bend site on its 20%-worst days.
     - *In Minnesota and surrounding states, the trend in SO_2 emissions varied from state to state.* Emissions declined substantially from 1990 to 1999 in some states (Missouri, Illinois, and Wisconsin), increased substantially in North Dakota, and changed relatively little in other states (Minnesota, Iowa, Kansas, Nebraska, and South Dakota). From 1990 to 1999, ammonium sulfate concentrations and associated light extinction declined at the Voyageurs and Boundary Waters-Canoe sites. Therefore, it appears that declining SO_2 emissions in Missouri, Illinois, and Wisconsin may have benefited visibility conditions in the Northern Minnesota representative region.

4. SUPPORTING EVIDENCE

Each primary conclusion stated in Sections 2 and 3 is restated and supported with a summary of the evidence determined through data analyses.

4.1 EVIDENCE IN SUPPORT OF DEFINING THE REPRESENTATIVE GEOGRAPHIC SUBREGIONS OF THE CENRAP

In order to simplify subsequent analyses (described in Sections 4.2 and 4.3), sites considered to be representative of subregions of the CENRAP region were identified. Each representative site was considered to generally share emissions and meteorological influences with other sites in the same subregion. This approach minimized the number of sites requiring detailed analytical treatment. Four subregions were identified:

- An Upper Midwest subregion, consisting of sites in southern Iowa, Missouri, and eastern Kansas, represented by the Hercules-Glades (HEGL1) site.
- The Western Plains, which included Big Bend but not Guadalupe Mountains, represented by the Cedar Bluff (CEBL1) site.
- Minnesota, consisting of the border sites, Voyageurs and Boundary Waters-Canoe, represented by the Voyageurs (VOYA2) site.
- Southeastern Plains, which includes sites in Louisiana and southern Arkansas, represented by the Sikes (SIKE1) site.

In addition, the Guadalupe Mountains subregion in which the Guadalupe Mountains site is located showed only a loose relationship with Big Bend and other CENRAP sites. Two more sites—Upper Buffalo and Wichita Mountains—appeared to fall in “transition zones” between the Western Plains and upper Midwest or Southeastern Plains.

The differences between Big Bend and Guadalupe Mountains were surprising given their geographic proximity to one another. However, further investigation of the light extinction budgets and the meteorological patterns on the 20%-worst days at each site demonstrated convincingly that the two sites are often affected by different emissions sources and transport patterns. Comparison of **Figure 4-1** to **Figure 4-2** shows that coarse mass is a more important factor in light extinction at the Guadalupe Mountains site than at the Big Bend site, while ammonium sulfate is a more important factor at the Big Bend site than at the Guadalupe Mountains. **Figure 4-3** illustrates the differences, using spatial probability density (SPD) and conditional probability integrated analysis (CoPIA) (detailed in Appendix A), in the geographic areas most likely to influence these two sites on the 20%-worst days. Areas of west Texas, northern Mexico, and the Big Bend area of Texas likely to influence the Guadalupe Mountains site on its 20%-worst days are very unlikely to influence the Big Bend site on its 20%-worst days. Conversely, areas around Austin and San Antonio, Texas, and areas of Tamaulipas and Nuevo León, Mexico, are important zones of influence for the Big Bend site on its 20%-worst days, but less so for the Guadalupe Mountains site.

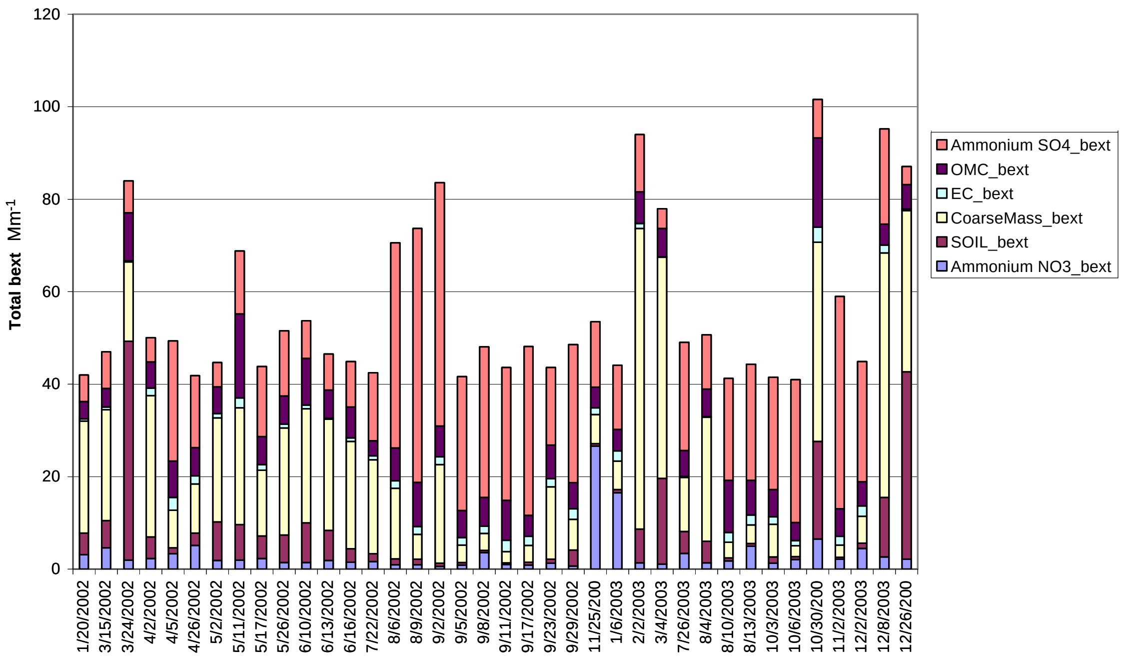

Figure 4-1. Light extinction (b_{ext}) budget by component (using standard IMPROVE calculations) for the 20%-worst visibility days at Guadalupe Mountains in 2002-2003.

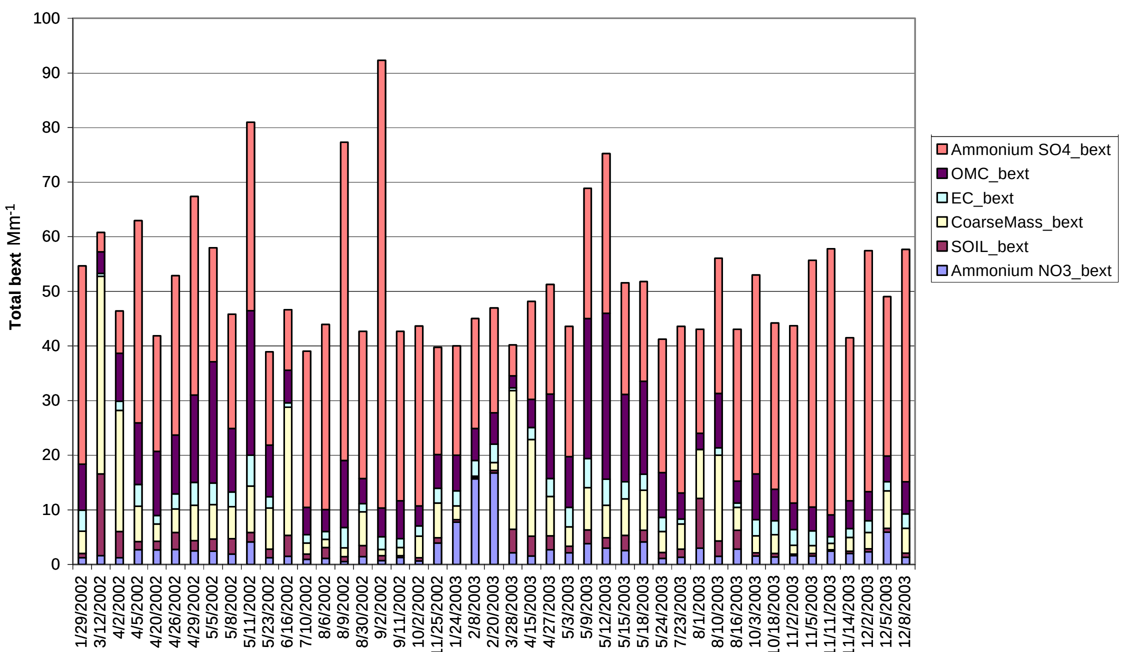

Figure 4-2. Light extinction (b_{ext}) budget by component (using standard IMPROVE calculations) for the 20%-worst visibility days at Big Bend in 2002-2003.

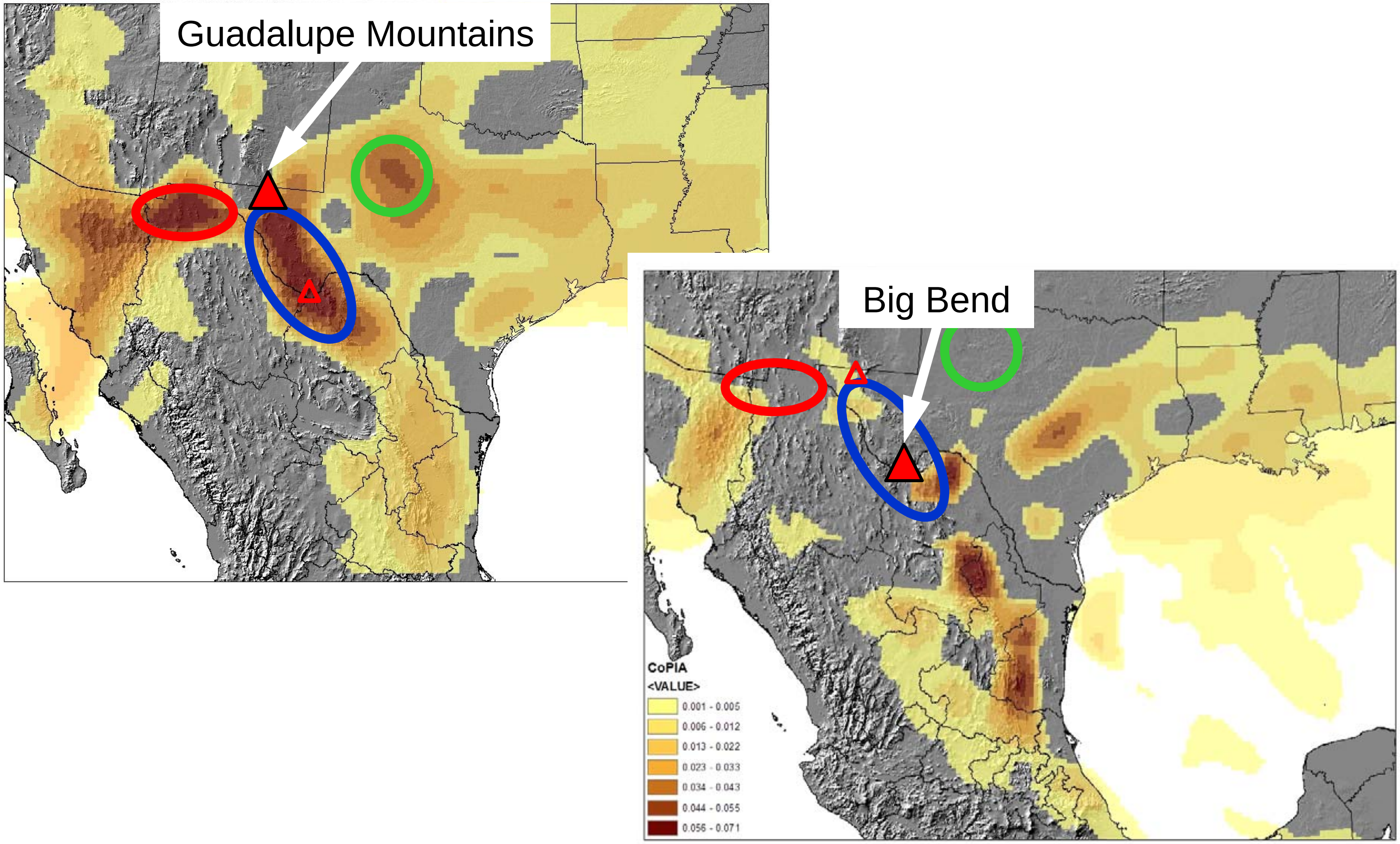

Figure 4-3. The geographic zones of influence on the Guadalupe Mountains and Big Bend sites on the 20%-worst visibility days. (Red, green, and blue ovals are placed to aid in visual comparisons of the two maps.) The resulting value for each grid cell is the conditional probability of air traveling over a grid cell on the 20%-worst visibility days relative to the probability over a grid cell for all days. Details are provided in Appendix A.

4.2 EVIDENCE FOR IDENTIFYING EMISSIONS SOURCES OR SOURCE REGIONS THAT CONTRIBUTE TO HAZE

CENRAP will need the cooperation of other RPOs or countries to protect clean-air corridors and to improve visibility conditions at some sites.

SO_2 and NO_x emission inventories and 72-hr backward wind trajectories were analyzed for four representative sites—one site from each of the four representative subregions of the CENRAP—and for the 20%-best and 20%-worst days observed at each site. The products of these analyses were maps of emissions impact potentials (EIP), where the EIP for a specific geographic area was proportional to (a) the probability of transport from that area to the receptor site and (b) the scale of emissions in the area. EIP assigns weightings to emissions according to the likelihood that the emissions will be transported to a selected receptor site. **Figure 4-4** illustrates the calculation of EIP for the Hercules-Glades site in southwestern Missouri: emissions density multiplied by the density of backward wind trajectory hourly endpoints yields EIP. More details about the methods and sources of data are provided in Appendix C.

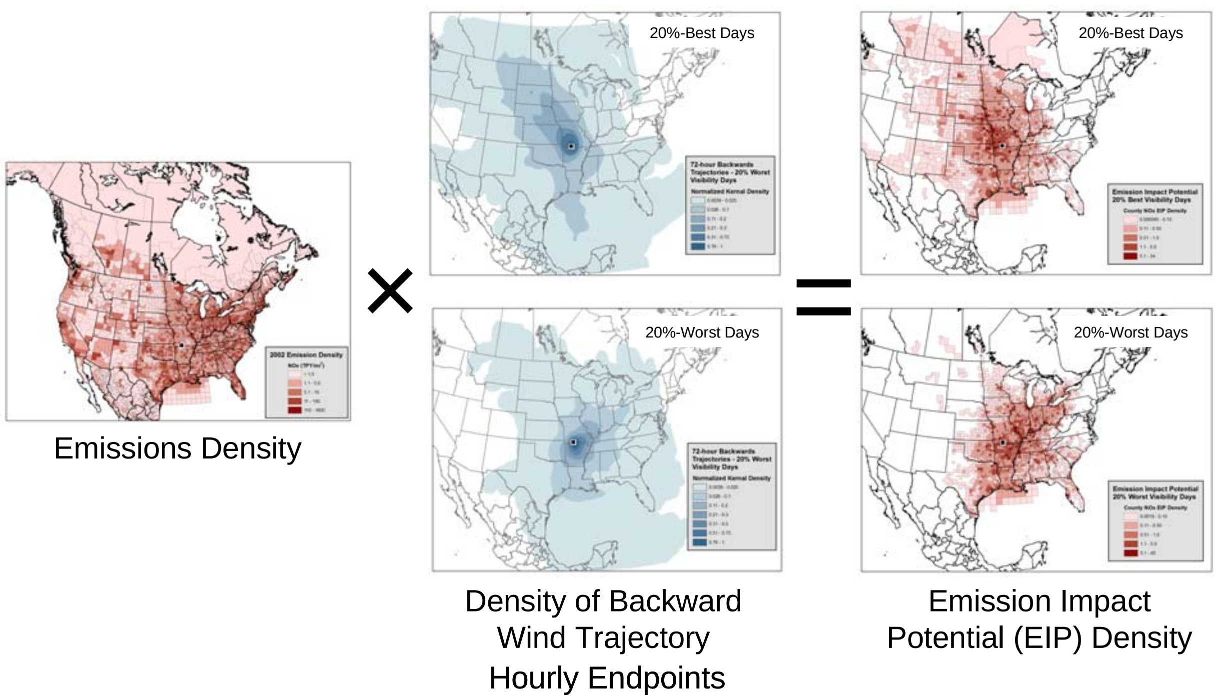

Figure 4-4. Illustration of the procedure to calculate EIP.

Illustrations of the geographic distributions of EIP (**Figures 4-5 and 4-6**) show the locations of emissions sources most likely to impact the four representative sites and subregions of the CENRAP region. **Figure 4-7** illustrates the distribution of backward wind trajectory hourly endpoints observed on the 20%-best days, which can be used to help define the clean-air corridors for a given site. (**Table 4-1** summarizes some of the conclusions that can be drawn from these figures.) In summary, CENRAP can only partly control the clean-air corridors and emissions source regions that are important to Class I areas within its borders. Areas of Canada and/or WRAP states comprise significant portions of the clean-air corridors for the Minnesota and Western Plains subregions. In addition, emissions sources in some Midwest RPO states and VISTAS states contribute significantly to impaired visibility conditions on the 20%-worst days in the Upper Midwest and Southeastern Plains subregions.

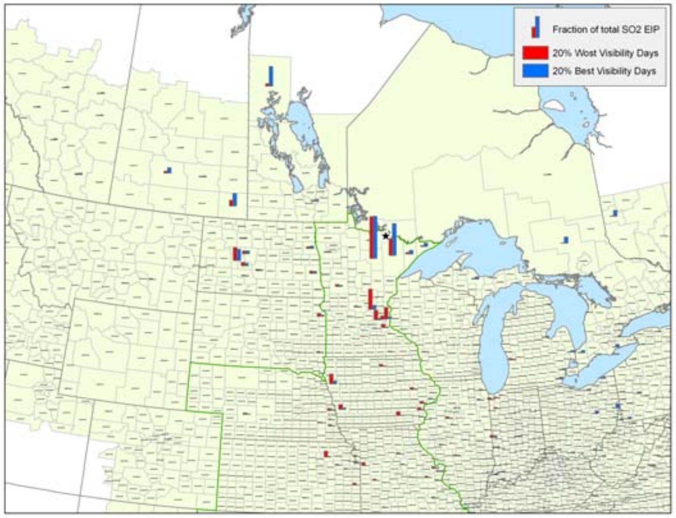

(a) Voyageurs, Minnesota (Minnesota subregion)*

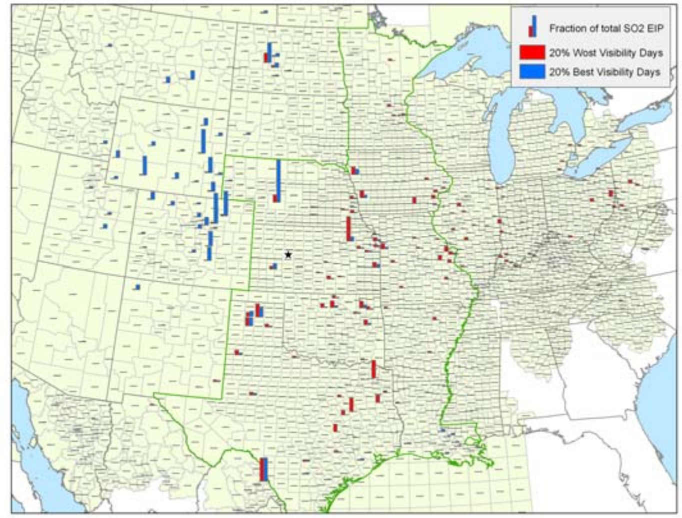

(b) Cedar Bluff, Kansas (Western Plains subregion)

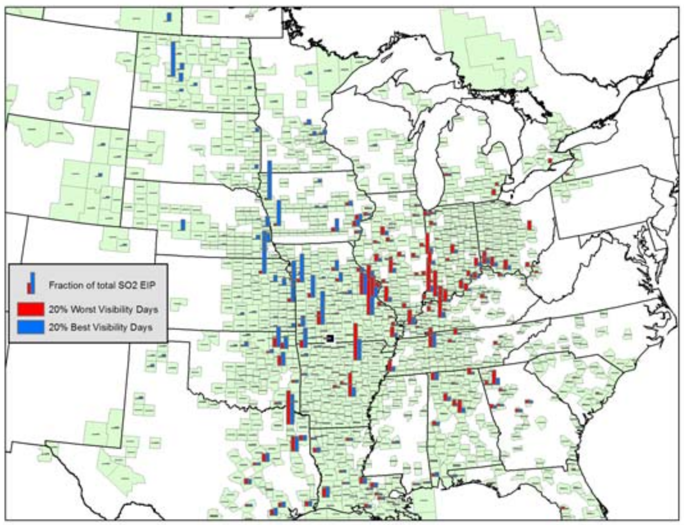

(c) Hercules-Glades, Missouri (Upper Midwest subregion)

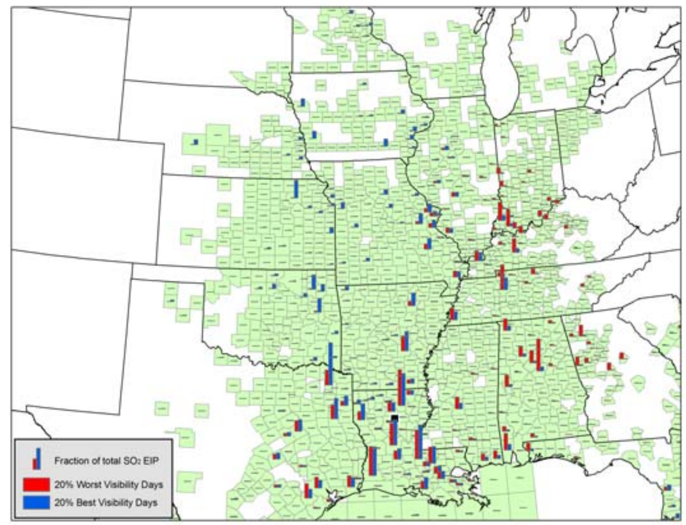

(d) Sikes, Louisiana (Southeastern Plains subregion)

* Note: Many trajectory hourly endpoints for the 20%-best days extended far northward into Canada and therefore dropped out of the analysis.

Figure 4-5. Geographic distributions of SO_2 EIP for the 20%-worst visibility days (red bars) and 20%-best visibility days (blue bars) observed at four representative sites.

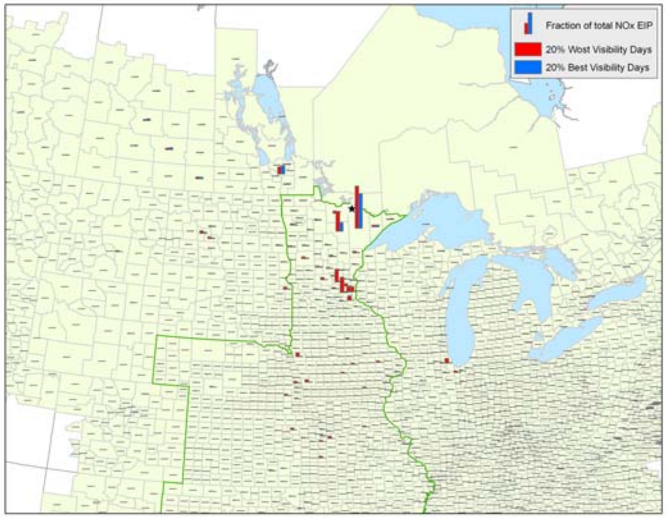

(a) Voyageurs, Minnesota (Minnesota subregion)*

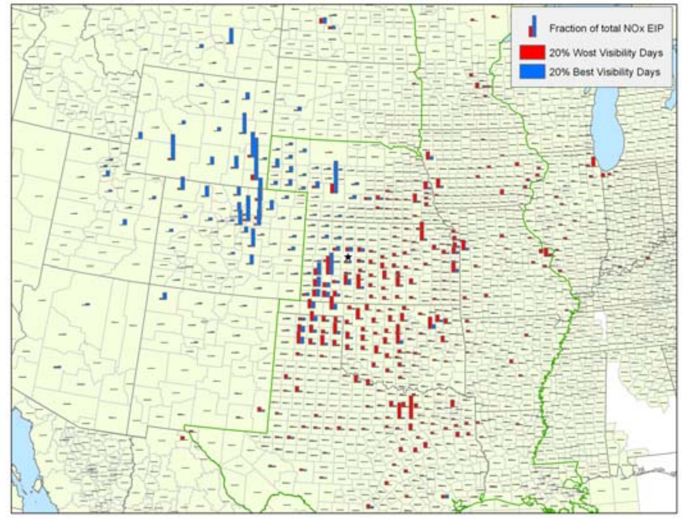

(b) Cedar Bluff, Kansas (Western Plains subregion)

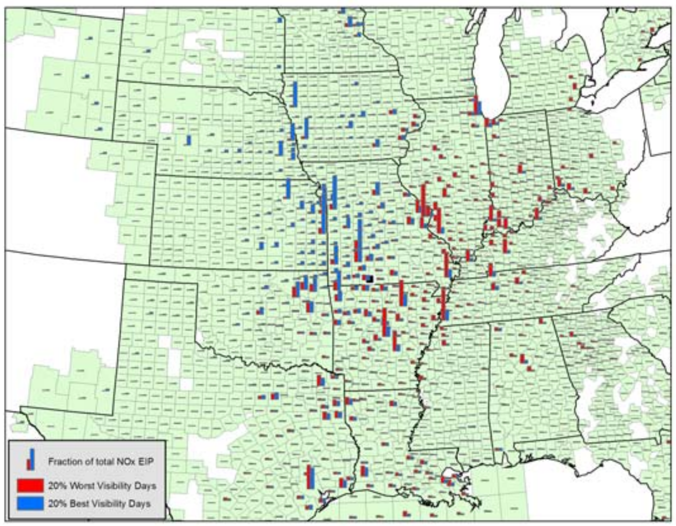

(c) Hercules-Glades, Missouri (Upper Midwest subregion)

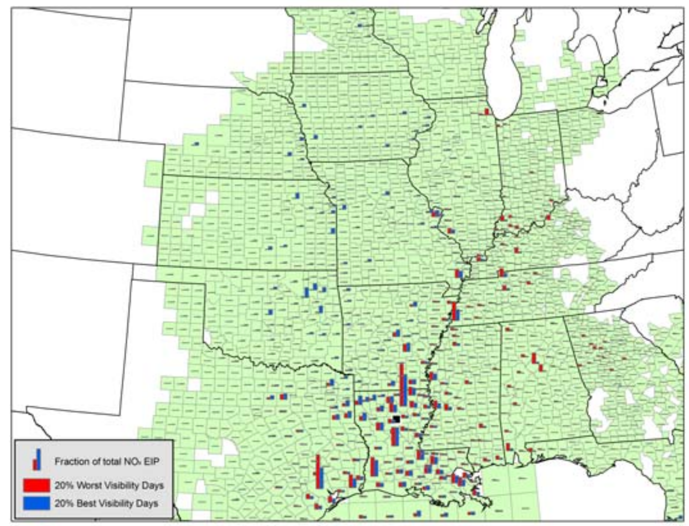

(d) Sikes, Louisiana (Southeastern Plains subregion)

* Note: Many trajectory hourly endpoints for the 20%-best days extended far northward into Canada and therefore dropped out of the analysis.

Figure 4-6. Geographic distributions of NO_x EIP for the 20%-worst visibility days (red bars) and 20%-best visibility days (blue bars) observed at four representative sites.

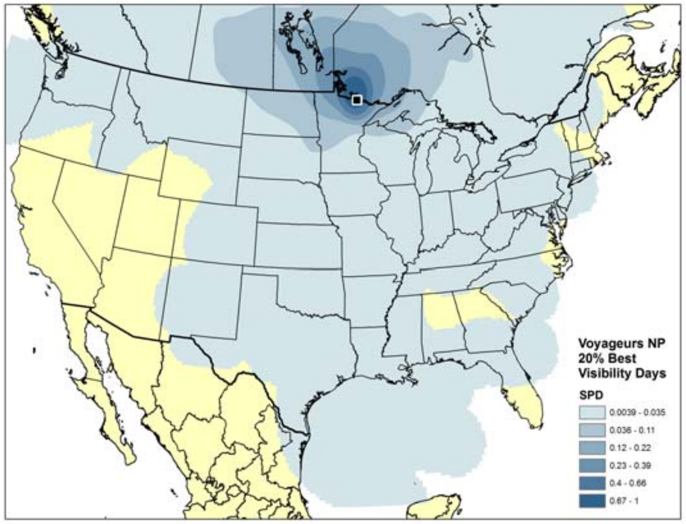

(a) Voyageurs, Minnesota (Minnesota subregion)*

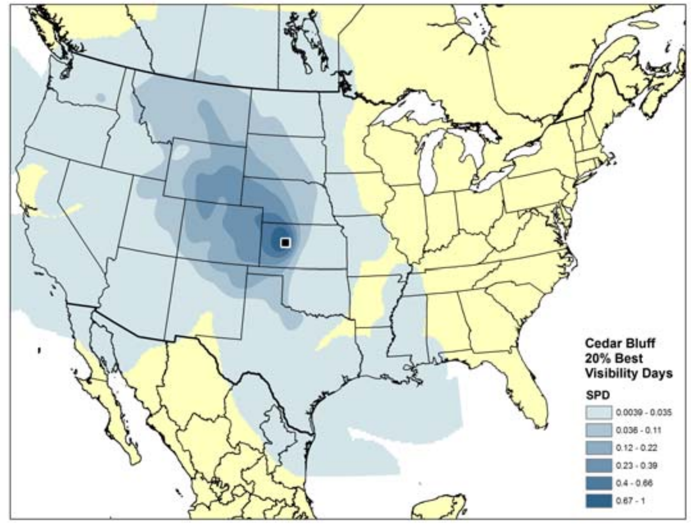

(b) Cedar Bluff, Kansas (Western Plains subregion)

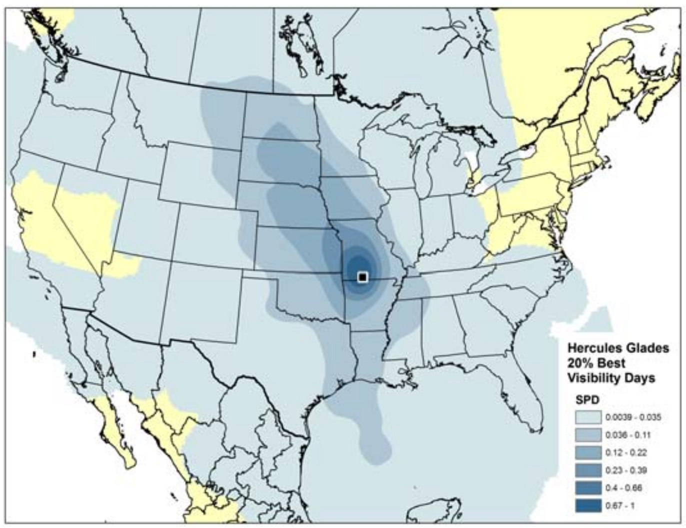

(c) Hercules-Glades, Missouri (Upper Midwest subregion)

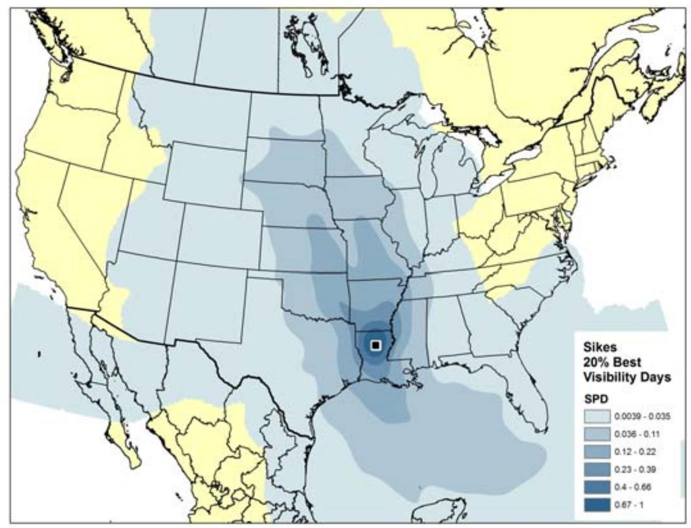

(d) Sikes, Louisiana (Southeastern Plains subregion)

* Note: Many trajectory hourly endpoints for the 20%-best days extended far northward into Canada and therefore dropped out.

Figure 4-7. Geographic distributions of 72-hr backward wind trajectories for the 20%-best visibility days observed at four representative sites. Spatial probability density (SPD) is detailed in Appendix A. A value of one indicates that all trajectories passed near the grid cell, while a value closer to zero denotes an area over which very few trajectories passed.

Table 4-1. Summary of geographic emissions source areas impacting representative sites and subregions of the CENRAP region.

Representative Site (Subregion)	20%-Best Days		20%-Worst Days	
	Important Clean-Air Corridors	Internal or External to CENRAP	Important Emissions Source Regions	Internal or External to CENRAP
Voyageurs, Minnesota (Minnesota)	Canada* Minnesota	Largely external	Minnesota, North Dakota	Largely internal
Cedar Bluff, Kansas (Western Plains)	WRAP states, Western Kansas, Western Nebraska	Largely external	Kansas, Texas, Missouri, Oklahoma, Iowa, Illinois, Northern Mexico	Largely internal
Hercules-Glades, Missouri (Upper Midwest)	Arkansas, Oklahoma, Kansas, Missouri, Nebraska, Iowa, South Dakota, North Dakota	Largely internal	Several MRPO States, Missouri, Arkansas, Texas, Oklahoma, VISTAS states	Largely external
Sikes, Louisiana (Southeastern Plains)	Louisiana, Texas, Oklahoma, Arkansas, Kansas, Missouri, Nebraska, Gulf of Mexico	Largely internal	VISTAS States, MRPO States, Louisiana, Texas, Arkansas	Largely external

*Note: Many trajectory hourly endpoints for the 20%-best days extended far northward into Canada and therefore dropped out of the GIS analysis. However, Canada contains most of the clean air corridor for Northern Minnesota.

BART requirements alone are unlikely to significantly alter visibility conditions at protected sites in the CENRAP.

EIPs were calculated using conservatively high estimates of emissions from BART-eligible sources. BART-eligible sources are defined in the Code of Federal Regulations (U.S. Environmental Protection Agency, 2004)as stationary point sources meeting the following criteria:

1. They have the potential to emit 250 tons or more of a visibility-impairing air pollutant, including SO_2, NO_x, particulate matter (PM), or VOCs.
2. They were put in place between August 7, 1962 and August 7, 1977.
3. They are located at any of 26 specific types of facilities, such as fossil-fuel fired steam electric plants of more than 250 million British thermal units (BTU) per hour heat input, coal cleaning plants, etc. (See Appendix C for the full list of facility types.)

Sources meeting the third criteria were identified as *potentially* BART-eligible; however, insufficient information was available to restrict the list of sources according to the first and second criteria. Therefore, this analysis produced a conservatively high estimate of potentially BART-eligible sources (i.e., not all the sources identified will meet all three criteria).

Figures 4-8 and 4-9 illustrate the geographic distributions of SO_x and NO_x EIPs attributable to potentially BART-eligible sources and BART-ineligible point sources on the 20% worst visibility days. From 7% to 19% of point-source SO_x EIP and from 6% to 13% of point-source NO_x EIP were attributable to potentially BART-eligible sources, based on the total SO_x and NO_x EIP at the four representative sites. Note that about 90% of total United States SO_x emissions are attributable to point sources; however, only about 40% of total United States NO_x emissions are attributable to point sources. (The balances are emitted by area and mobile sources.) Therefore, the relative importance of potentially BART-eligible sources is diluted substantially by the contributions of area and mobile sources of NO_x, but only slightly by the contributions of area and mobile sources of SO_x. In addition, the inclusion of emissions from Mexico and Canada would further dilute the importance of potentially BART-eligible sources.

Because the EIPs of potentially BART-eligible sources are relatively small, we expect that enforcement of BART requirements will produce limited improvement in the visibility conditions on the CENRAP region's 20%-worst days. Therefore, we expect that additional emissions reduction strategies will be needed to meet the goals of the Regional Haze Rule.

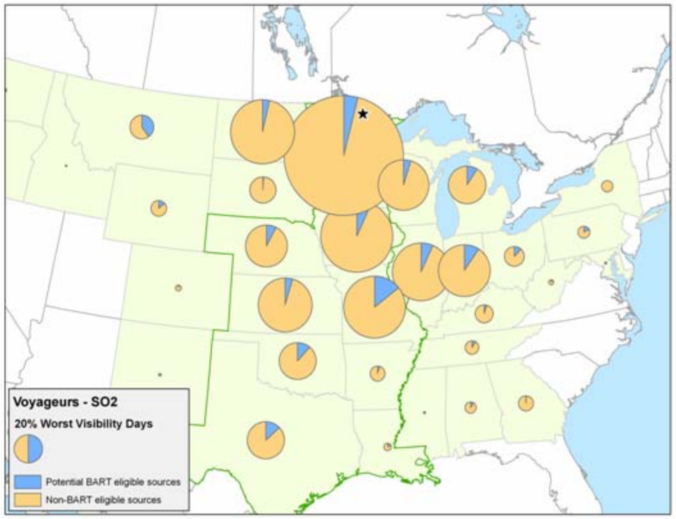

(a) Voyageurs, Minnesota (Minnesota subregion)*

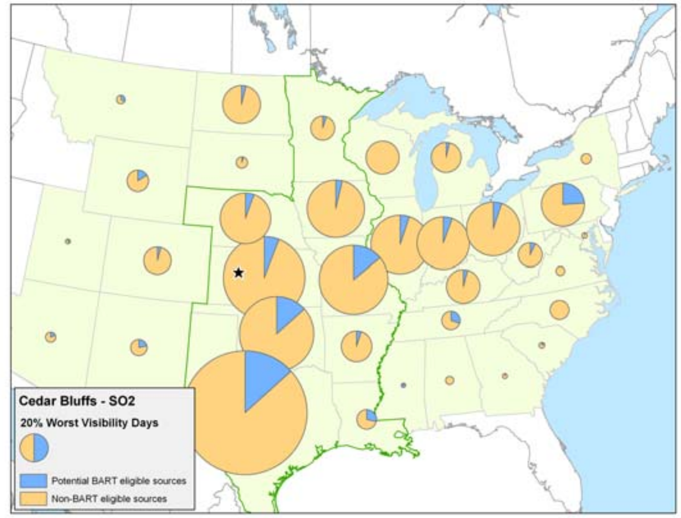

(b) Cedar Bluff, Kansas (Western Plains subregion)

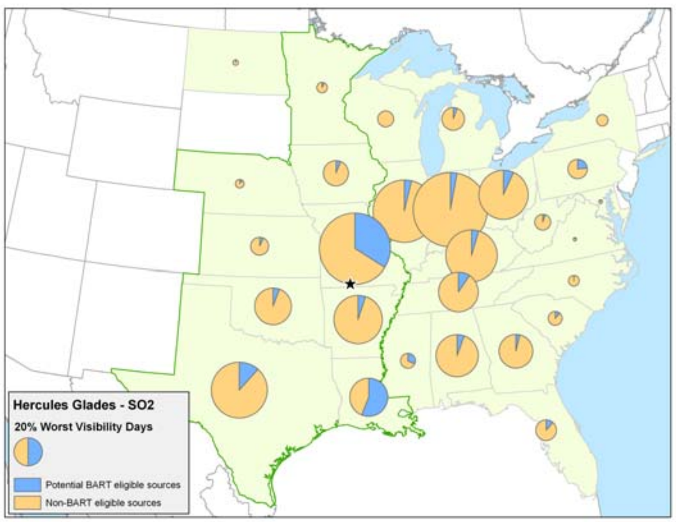

(c) Hercules-Glades, Missouri (Upper Midwest subregion)

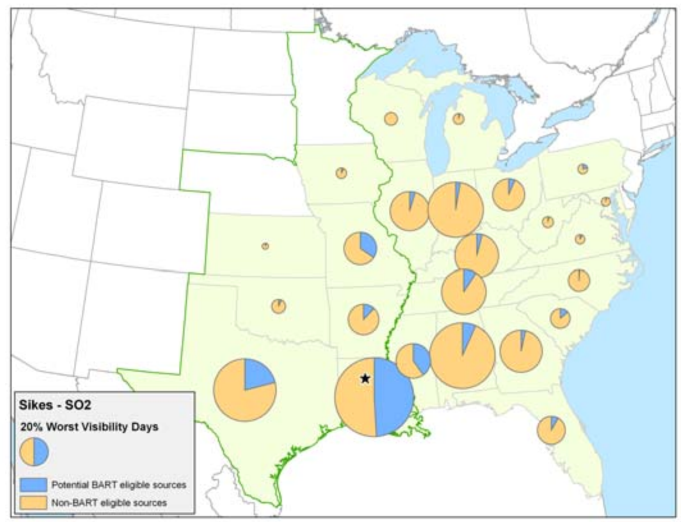

(d) Sikes, Louisiana (Southeastern Plains subregion)

*Note: Many trajectory hourly endpoints for the 20%-best days extended far northward into Canada and therefore dropped out of the analysis.

Figure 4-8. Geographic distributions of SO_2 EIP from point sources on the 20%-worst visibility days observed at four representative sites.

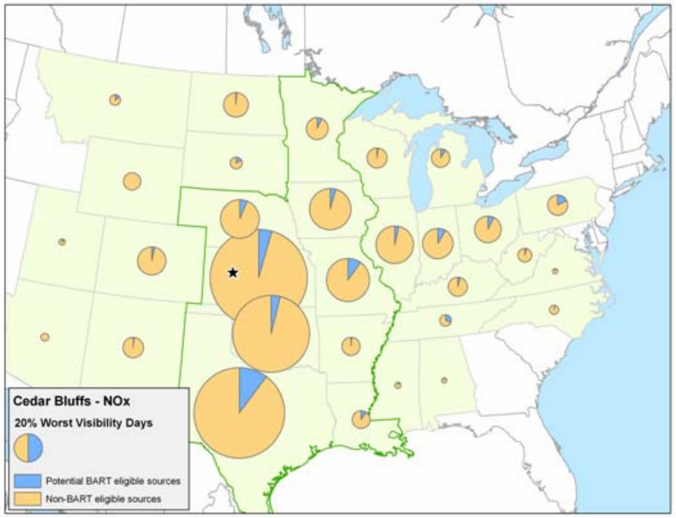

(a) Voyageurs, Minnesota (Minnesota subregion)*

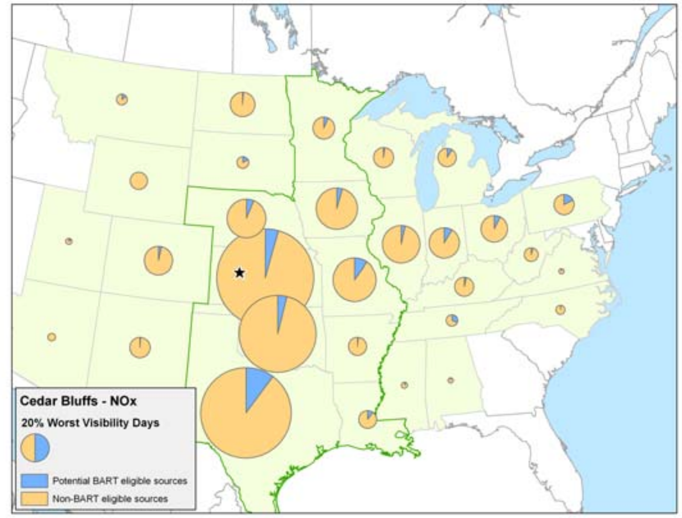

(b) Cedar Bluff, Kansas (Western Plains subregion)

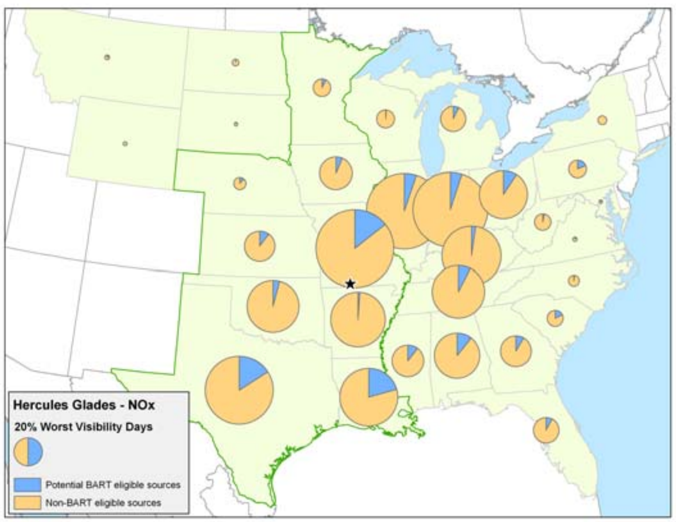

(c) Hercules-Glades, Missouri (Upper Midwest subregion)

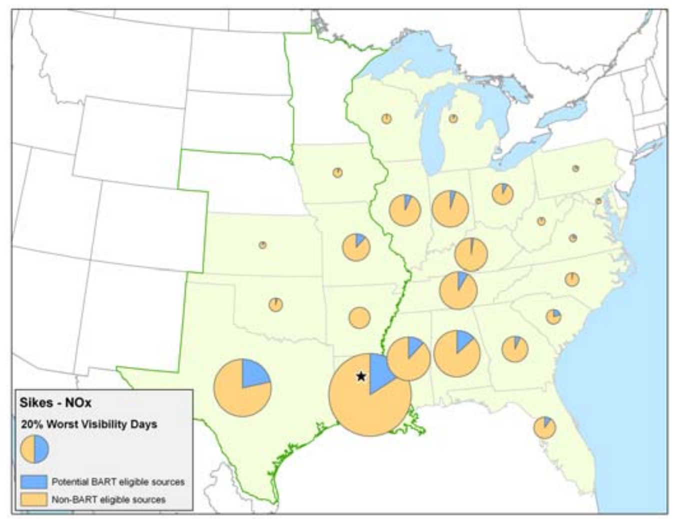

(d) Sikes, Louisiana (Southeastern Plains subregion)

*Note: Many trajectory hourly endpoints for the 20%-best days extended far northward into Canada and therefore dropped out of the analysis.

Figure 4-9. Geographic distributions of NO_x EIP from point sources on the 20%-worst visibility days observed at four representative sites.

Aerosol components that contribute to poor visibility include sulfate, nitrate, and carbonaceous matter.

Average $PM_{2.5}$ compositions for the 20%-worst days observed at each representative site are illustrated in **Figures 4-10 through 4-13**. The IMPROVE equation (Malm et al., 1994; IMPROVE, 2004) was used to calculate the total light extinction (b_{ext}) contribution of each chemical component. However, we note the likelihood that the IMPROVE equation does not fully account for extinction by OC (Lowenthal and Kumar, 2003); therefore, OC may be somewhat more important than the figures indicate.

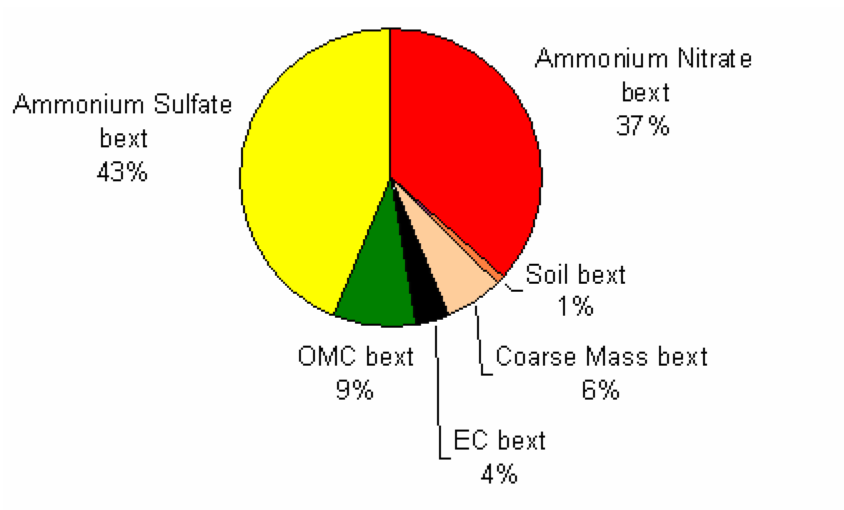

Figure 4-10. Average light extinction budget (b_{ext}, based on the IMPROVE visibility equation) on the 20%-worst visibility days at Cedar Bluff during 2002-2003.

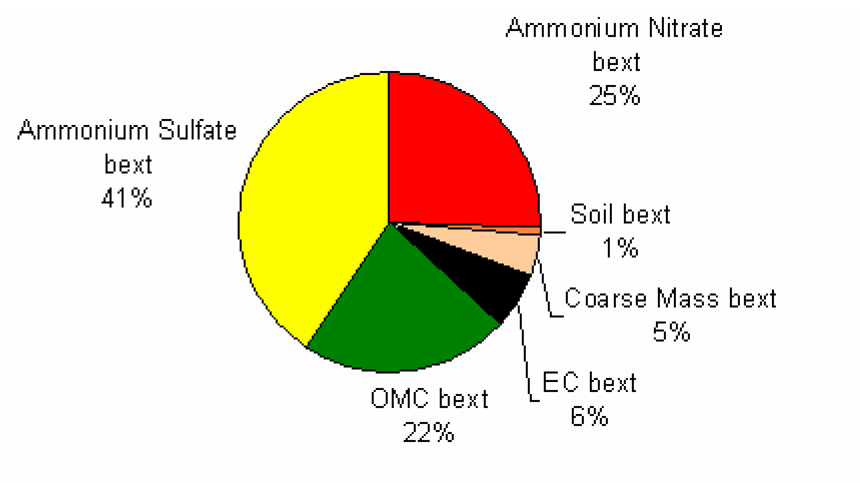

Figure 4-11. Average light extinction budget (b_{ext}, based on the IMPROVE visibility equation) on the 20%-worst visibility days at Voyageurs during 2002-2003.

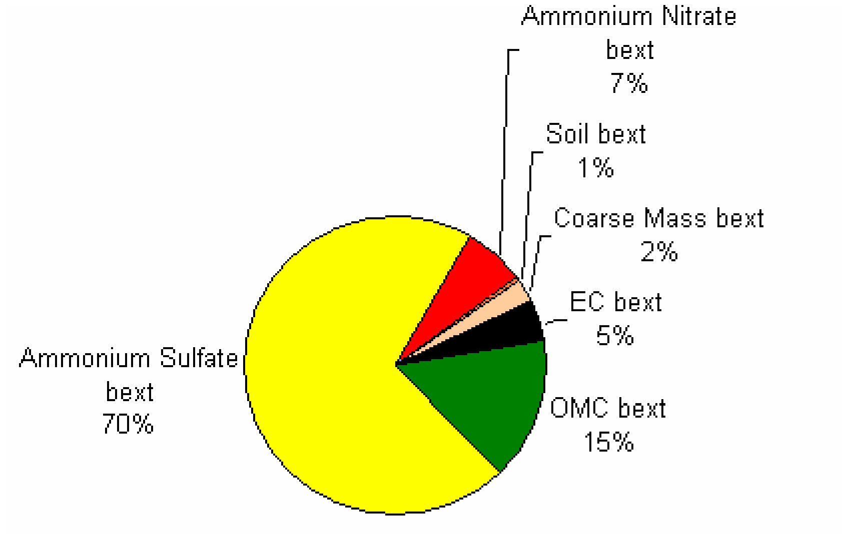

Figure 4-12. Average light extinction budget (b_{ext}, based on the IMPROVE visibility equation) on the 20%-worst visibility days at Sikes during 2002-2003.

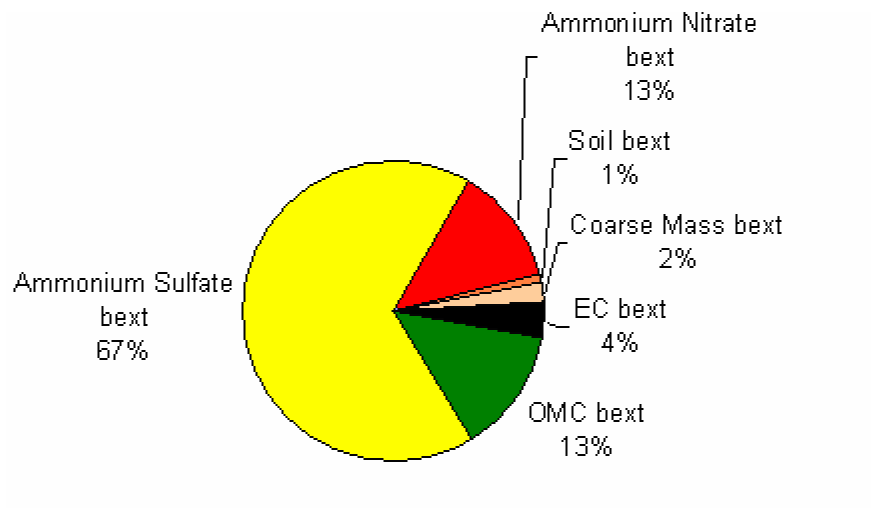

Figure 4-13. Average light extinction budget (b_{ext}, based on the IMPROVE visibility equation) on the 20%-worst visibility days at Hercules-Glades during 2002-2003.

Source regions both outside of and within CENRAP are important contributors to visibility impairment at the protected sites.

"Factors" (i.e., statistical results from which we infer types of emissions sources) contributing to $PM_{2.5}$ mass were identified at Sikes and Hercules-Glades using the receptor modeling tool Positive Matrix Factorization (PMF). At both sites, eight factors best characterized the ambient data, with predicted mass comparing well to measured mass (i.e., $r^2 > 0.97$ and slope between 0.98 and 0.99). These factors were inferred to represent specific source types. The average mass composition overall, and on the 20%-worst days observed at Sikes and Hercules-Glades, are shown in **Figures 4-14 and 4-15**.

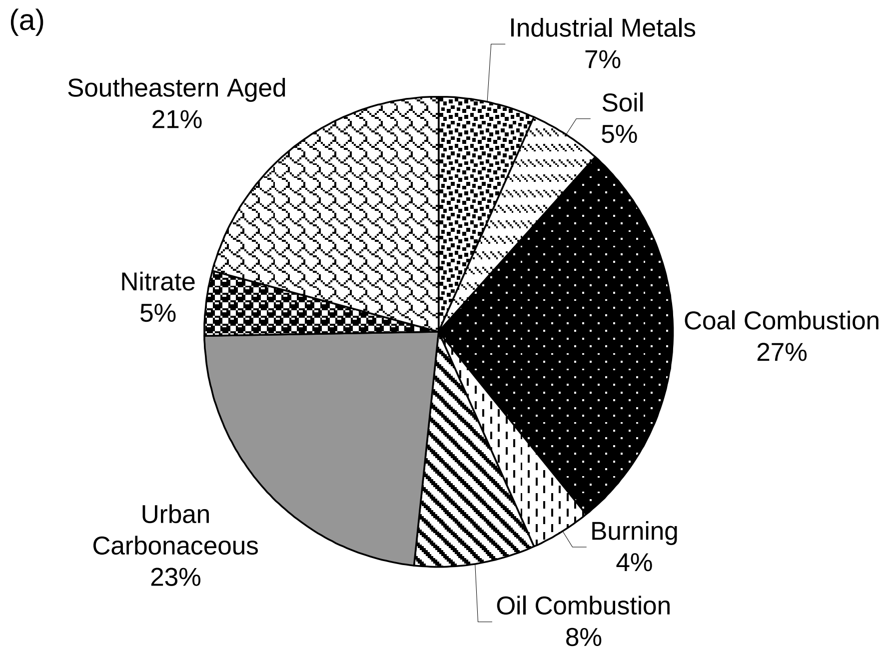

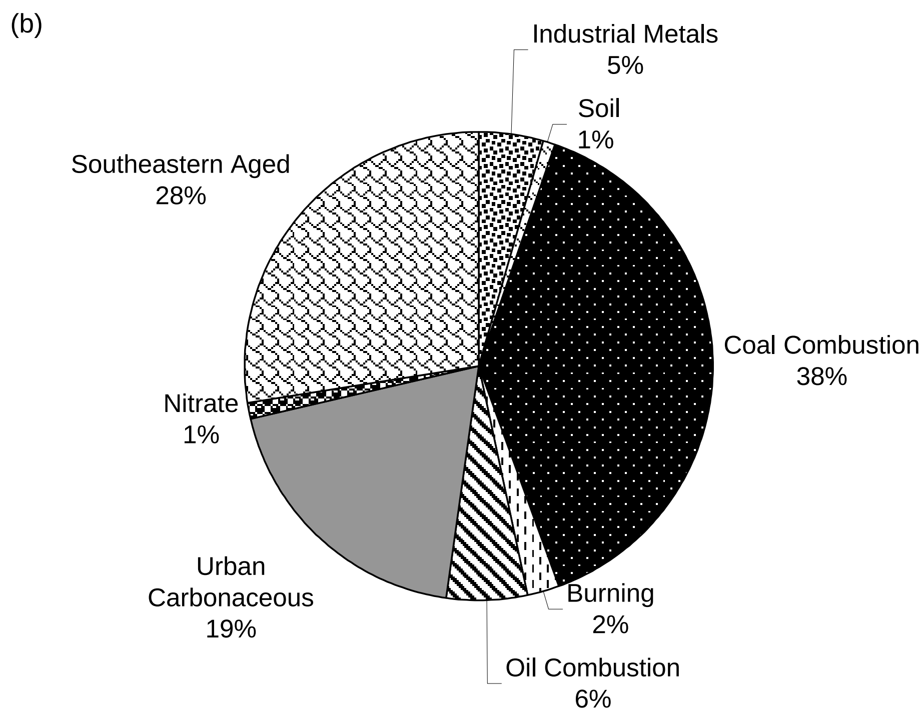

Figure 4-14. Average factor contributions to mass at Sikes for (a) all samples and (b) the 20%-worst visibility days.

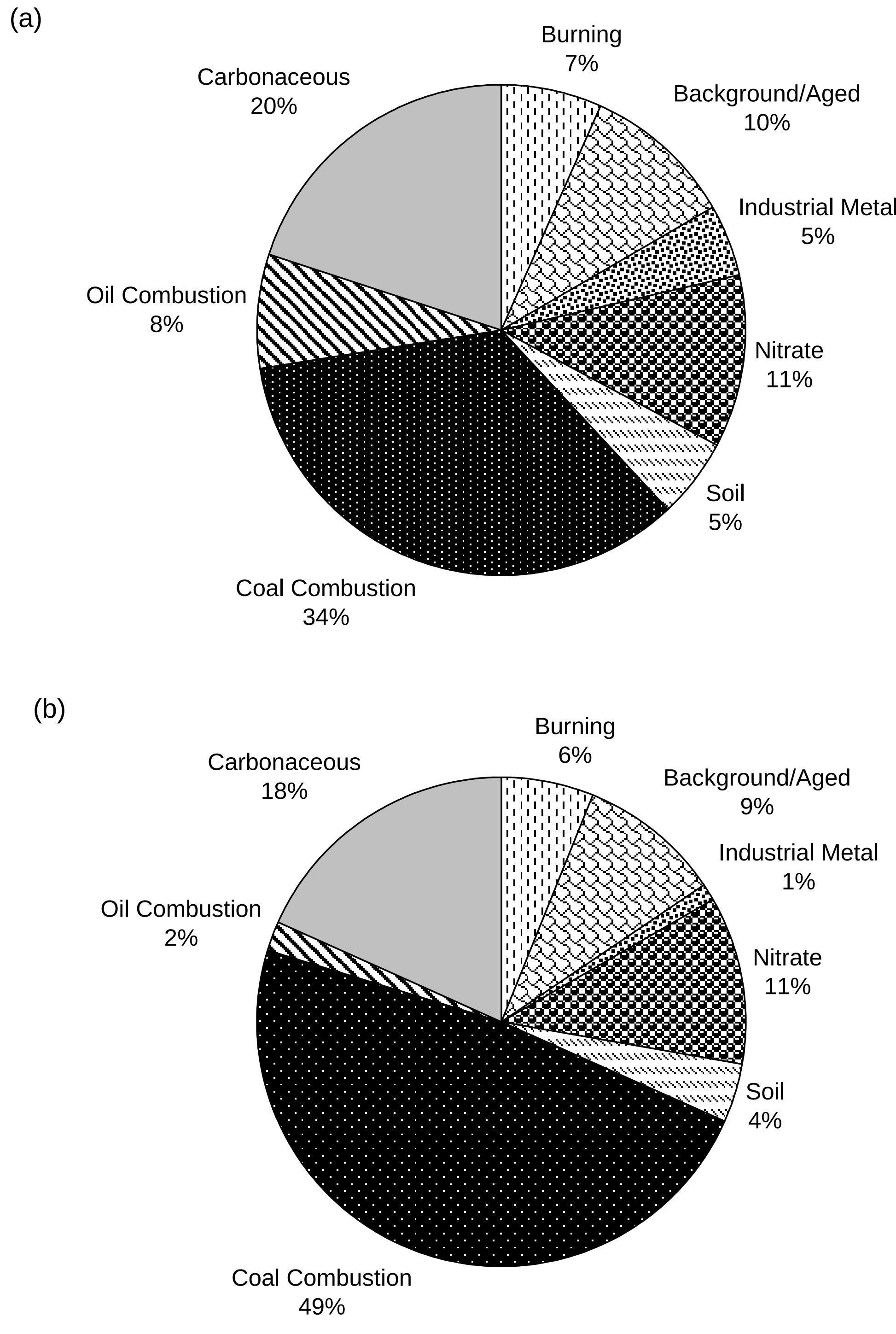

Figure 4-15. Average factor contributions to mass at Hercules-Glades for (a) all samples and (b) the 20%-worst visibility days.

Fires infrequently contribute to visibility impairment observed on the 20%-worst days at most sites in the CENRAP region.

Contributions of OMC to light extinction were evaluated for the 20%-worst days. At all but four sites, OMC contributions infrequently exceeded 20% of total light extinction on poor-visibility days.[4] The exceptions included Big Bend during the spring months, Nebraska National Forest during the summer, and the two sites located in the Minnesota region during the summer. In other areas—the Southeastern Plains and Upper Midwest regions—the results of PMF analyses were available to combine with backward wind trajectories and satellite-detected fire data (as discussed below). These types of analyses would be useful to help determine if fires are the sources of elevated OMC at the Big Bend, Nebraska National Forest, and Minnesota region sites.

A biomass burning factor inferred at the Hercules-Glades and Sikes sites did not have a clear temporal trend, but appeared to be episodic. Air mass trajectories were combined with satellite-detected fire locations and geographic extents in an attempt to better characterize the sources associated with the biomass burning factor. The analyses suggest that the biomass burning factor is significant only when local burning and conducive meteorology occur.

At Sikes, on two days when the highest levels of the biomass burning factor were present (August 4, 2003, and April 19, 2001), air mass trajectories showed transport from nearby fire locations (**Figure 4-16**), indicating the likelihood that the factor is correctly associated with impacts from biomass burning. However, none of the days on which the highest levels of the biomass burning factor occurred were among the 20%-worst days, indicating that while biomass burning is episodic and detectable, it does not appear to be an important contributor to poor visibility on the 20%-worst days at Sikes. Overall, the biomass factor accounted for only 4% of the median mass, and only 2% of the mass on the 20%-worst days.

Similar observations were made with the data analyzed for Hercules-Glades. On two days when the highest levels of the biomass burning factor were present (April 12, 2003, and May 9, 2003), air mass trajectories showed transport from nearby fire locations (**Figure 4-17**). Periods of time when the biomass burning factor was high were associated with nearby fires, rather than with long-range multi-day transport. Overall, the biomass burning factor accounted for 7% of the median mass, and 6% of the mass on the worst visibility days. Some of the days showing high levels of the biomass burning factor coincided with episodes of poor visibility. However, on average, the biomass burning factor was substantially less important than coal combustion and other factors.

We note that our analyses likely produced a lower limit estimate of the influence of biomass burning. PMF is unable to fully quantify a burning factor because the chemical fingerprint of the factor profile varies with distance from the source (or aging air mass), fuel type, and atmospheric chemistry during transport. If samples were collected every day during spring and summer, or if observations of organic molecular markers such as levoglucosan (Sheesley et al., 2003; Zheng et al., 2002; Schauer et al., 2001a; Fine et al., 2004; Brown et al., 2002; Fine et al., 2002; Schauer et al., 2001b; Nolte et al., 2001) were available, these analyses could be substantially improved.

[4] The contribution of OMC to total light extinction exceeded 20% on fewer than 20% of the 20%-worst days.

Very infrequently does geologic material contribute appreciably to visibility impairment observed on the 20%-worst days at most sites in the CENRAP region.

The combined contribution of soil plus course mass infrequently exceeded 20% of total light extinction on 20%-worst days.[5] The Guadalupe Mountains site was the only exception. At that site, soil plus course mass contributed from 20% to 86% of total light extinction on roughly two-thirds of the poor-visibility days. In the Southeastern Plains and Upper Midwest regions PMF results were available to combine with backward wind trajectories (as discussed below) to determine likely sources of geologic material. These types of analyses would be useful to help identify the sources of dust impacting the Guadalupe Mountains site.

An event-driven soil factor comprised of silicon, iron, and titanium was identified for the Hercules-Glade and Sikes sites. This soil factor yielded relatively high contributions to $PM_{2.5}$ mass during a few events, the two principal of which occurred on July 1 and 31, 2002. On these two dates, the soil factor approached a mass contribution of 20 $\mu g/m^3$ at Sikes and Hercules-Glades, where it more typically averaged 0.6 $\mu g/m^3$ (or 5% of the mass). Ten-day backward wind trajectories calculated for July 1 and 31, 2002, such as the example shown in **Figure 4-18**, indicate rapid transport across the Atlantic Ocean. This transport pattern suggests that Saharan dust contributed to $PM_{2.5}$ masses at Sikes and Hercules-Glades on July 1 and 31, 2002. Other days with relatively large soil factor contributions were associated with transport over the Great Plains. However, none of the days with especially large soil factor contributions occurred on the 20%-worst visibility days at Sikes or Hercules-Glades. Thus, long-range transport of dust appears to have little effect on the 20%-worst days in the Southeastern Plains and Upper Midwest regions.

---

[5] The contribution of soil plus course mass to toal light extinction exceeded 20% on fewer than 20% of the 20%-worst days.

(a)

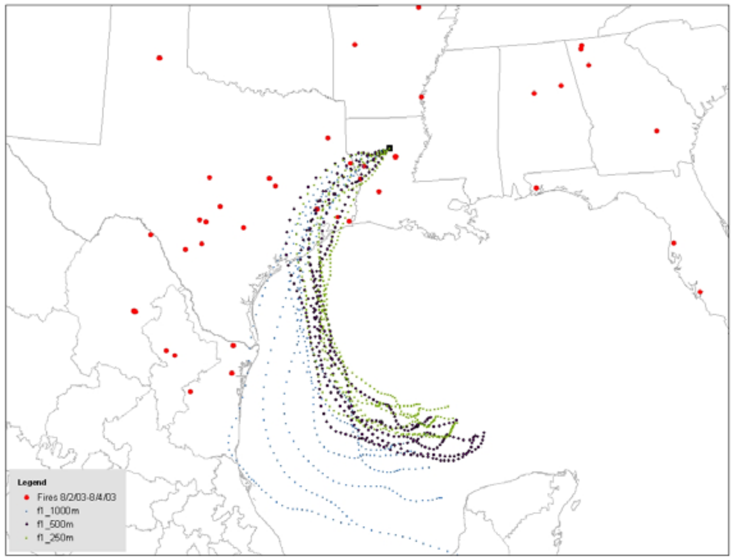

(b)

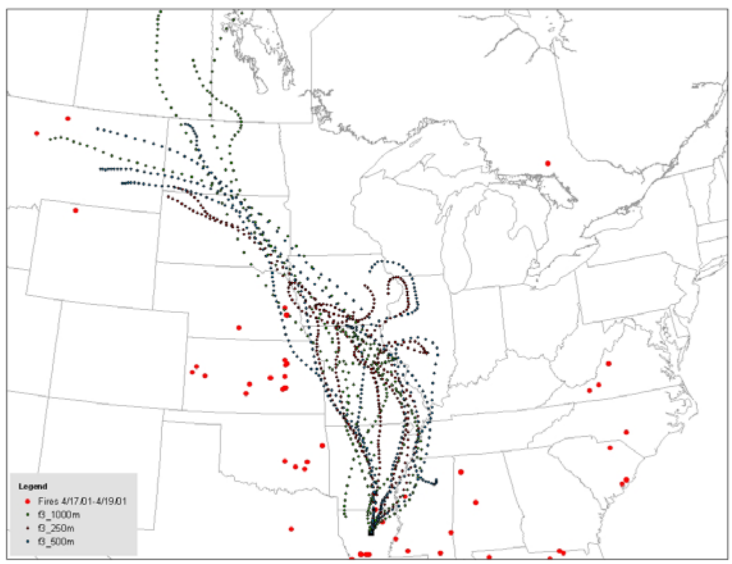

Figure 4-16. Three-day air mass backward trajectories using the NOAA HYSPLIT model with 250-m, 500-m, and 1000-m ending heights at Sikes and fire locations on (a) August 4, 2003, and (b) April 19, 2001.

(a)

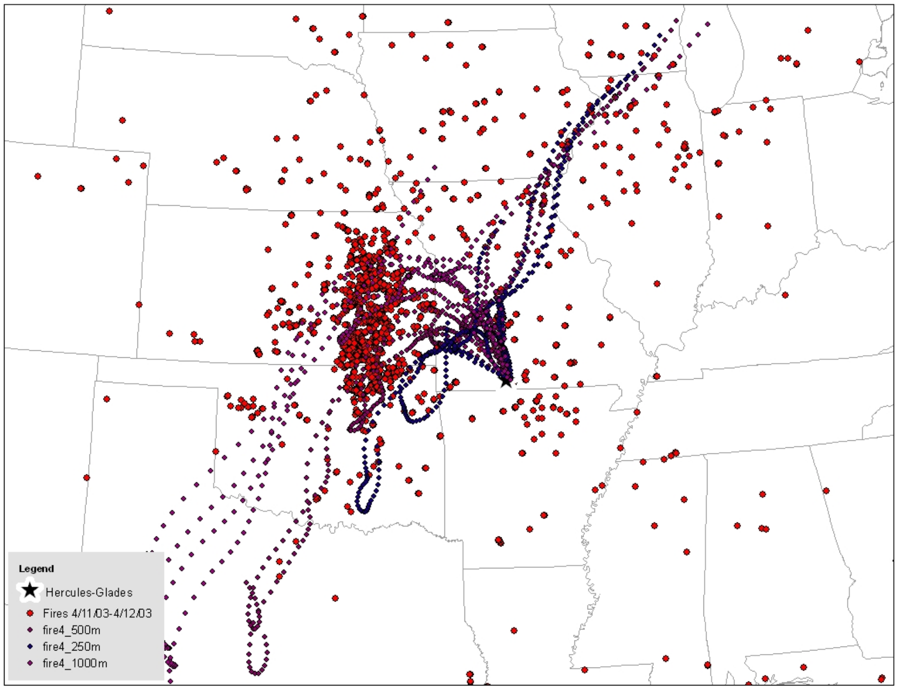

(b)

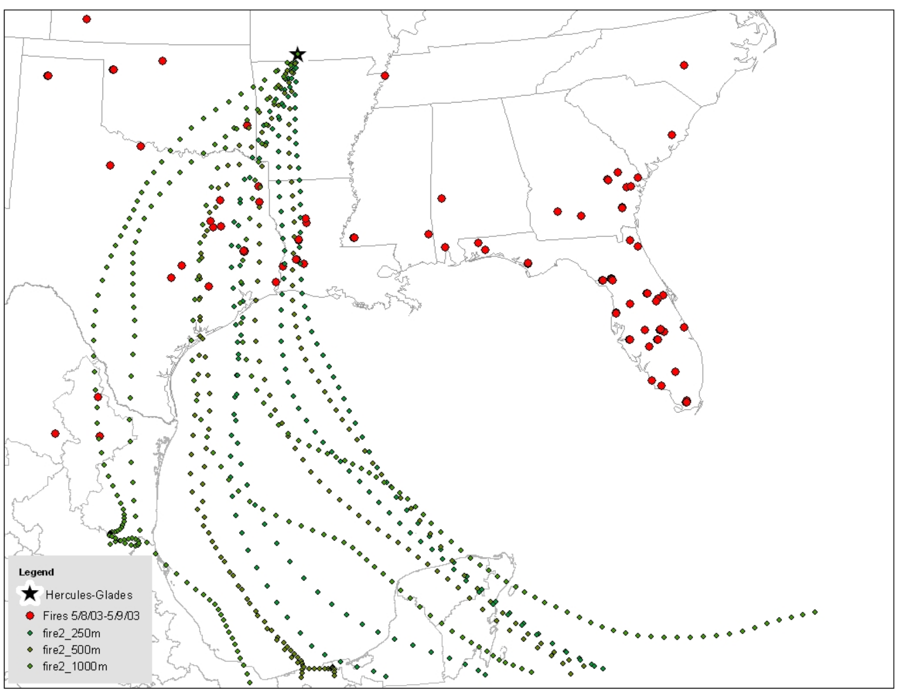

Figure 4-17. Three-day air mass backward trajectories using the NOAA HYSPLIT model with 250-m, 500-m, and 1000-m ending heights at Hercules-Glades and fire locations on the burning event day of (a) April 12, 2003, and (b) May 9, 2003.

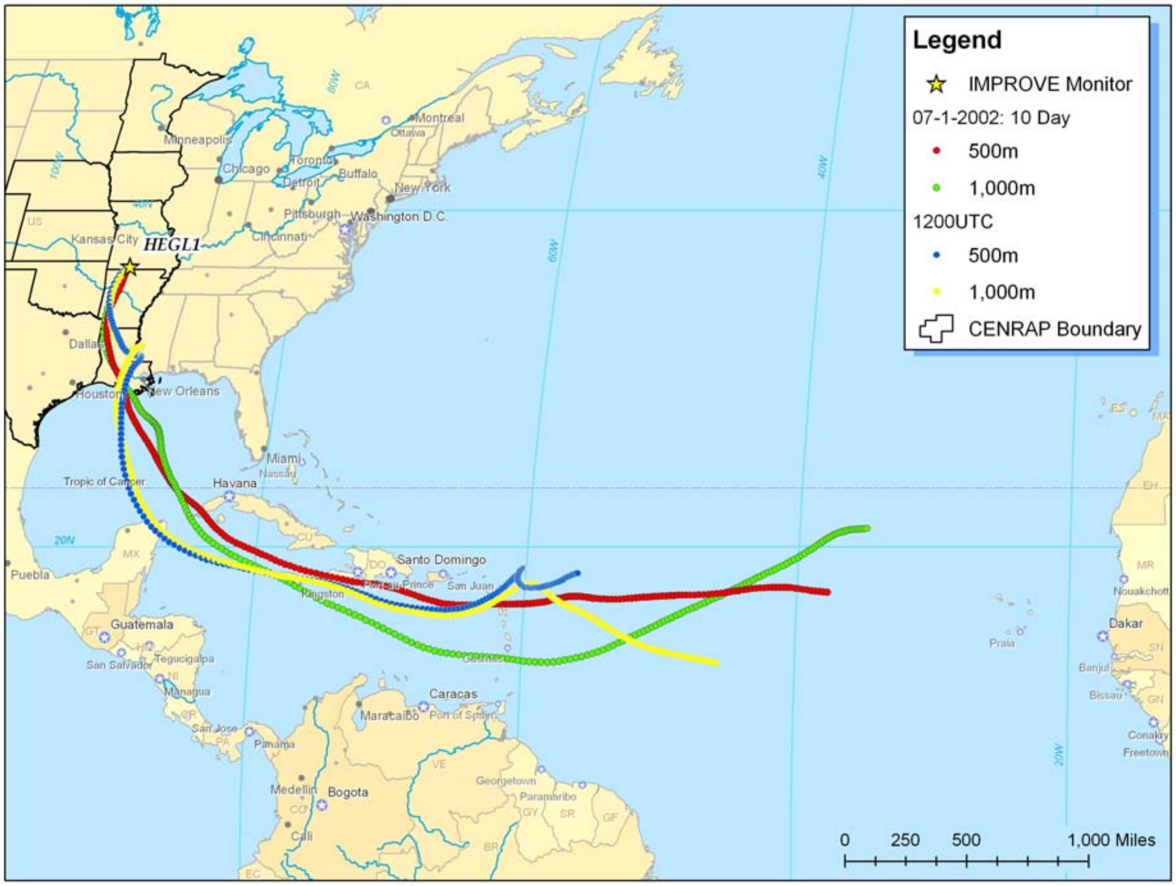

Figure 4-18. Air mass trajectories on the dust event of July 1, 2002.

4.3 EVIDENCE FOR IDENTIFYING THE PREDOMINANT METEOROLOGICAL CONDITIONS DURING PERIODS OF GOOD OR POOR VISIBILITY

In general, the meteorology of 2002-2003 was near normal for the CENRAP region and can, therefore, be considered "representative".

Figures 4-19 and 4-20 show National Climatic Data Center 2002 and 2003 state precipitation and temperature rankings in the context of the past 108 years. For example, in 2002, Texas' temperature rank was 61; over 108 years, about one-half of Texas' average temperatures were greater than, and about one-half of the average temperatures were less than, the average temperature in 2002. Thus, 2002 is classified as normal for Texas. There are four gradations on either side of normal, ranging from a near-normal to a record year. Very few states fall outside the near-normal ranking in 2002 or 2003 for either precipitation or temperature.

(a)

(b)

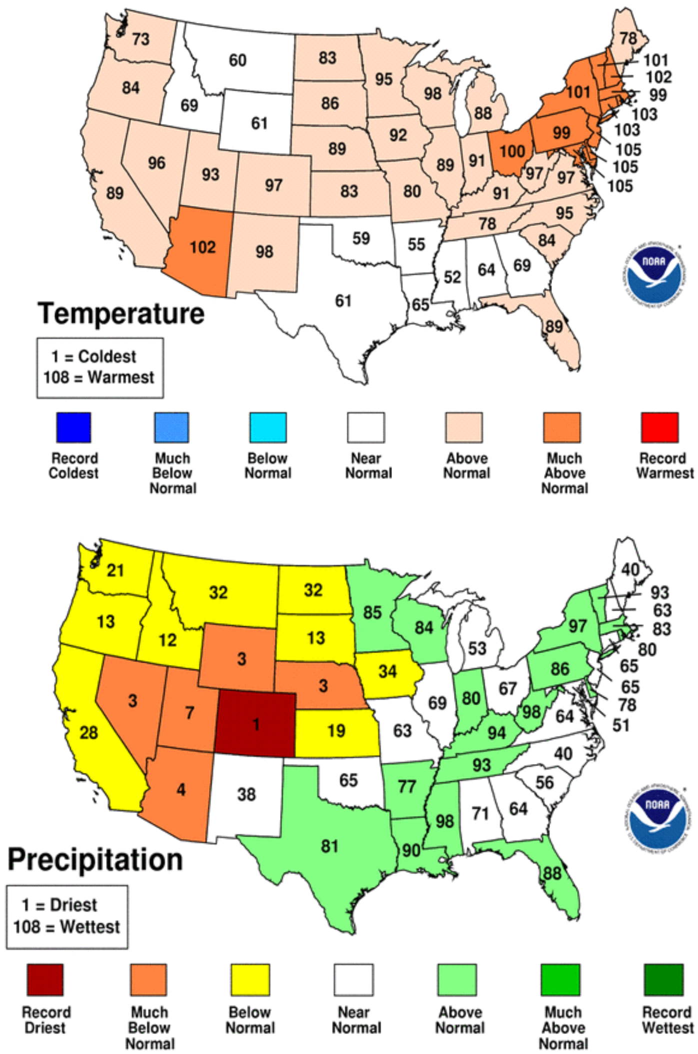

Figure 4-19. January through December 2002 statewide ranks for (a) temperature and (b) precipitation. (Figures from the National Climatic Data Center.)

(a)

(b)

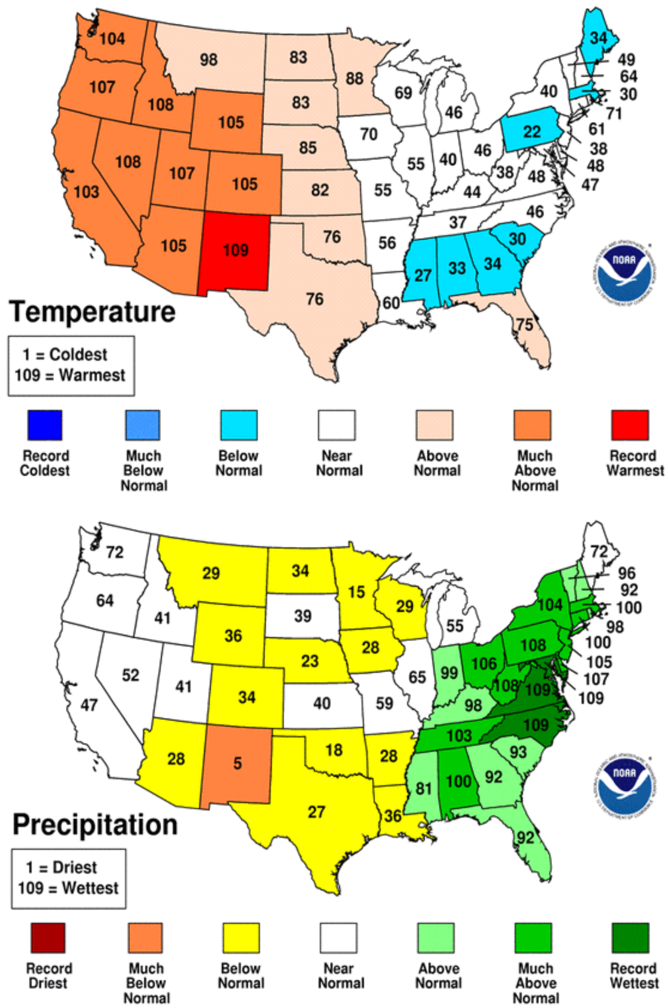

Figure 4-20. January through December 2003 statewide ranks for (a) temperature and (b) precipitation. (Figures from the National Climatic Data Center.)

There are numerous types of weather and transport conditions that occur on the 20%-best or 20%-worst days during 2002-2003, and there are representative days and episodes in 2002 that are suitable for modeling.

Cluster analysis was used to group days based on meteorological and transport characteristics for four CENRAP subregions for the 20%-best and 20%-worst days. The variables used, and the resulting clusters obtained, in the analysis are presented in the Appendix B**.** The transport and meteorological parameters that were used to define individual days are illustrated in daily schematics in Appendix B. An example of a schematic for one day is shown in **Figure 4-21**. The variables in the schematic capture large-scale weather patterns, transport, local stability, temperature, relative humidity, winds, and the predominant PM species. Based on evaluation of these schematics, days with similar transport and meteorology characteristics were grouped. On average, we identified five groups of days with the same characteristics for each subregion for both the 20%-worst and 20%-best days. The general meteorological and transport characteristics associated with the groups for each subregion are summarized below. Recommended modeling days shown in Tables 3-1 and 3-2 were determined by selecting episodes that coincided among the subregions and reflected most of the common meteorological and transport characteristics identified in the clusters.

- For the Northern Minnesota subregion (represented by Voyageurs), the 20%-worst days occurred during both winter and summer and typically coincided with high levels of relative humidity in the morning. In winter, nitrates were the predominant light-scattering species and westerly transport generally prevailed. In summer, southeasterly transport coincided with large light-scattering contributions from sulfates, while stagnant conditions were associated with relatively large contributions from OC species.
- In the Northern Minnesota subregion, the 20%-best days typically occurred during the cold season, tended to exist with weak atmospheric stabilities (compared to the 20%-worst days), and coincided with northerly transport conditions.
- For the Western Plains subregion (represented by Cedar Bluff), the 20%-worst days occurred during both cold and warm seasons and typically coincided with high morning relative humidity. In winter, nitrates were the predominant light-scattering species, and transport tended to be northerly. In summer, high light-scattering contributions from sulfates tended to correlate with southeasterly transport and quiescent upper-level meteorological patterns.
- In the Western Plains, the 20%-best days typically paired with northwesterly transport during the cold season.
- For the Upper Midwest subregion (represented by Hercules-Glades), the 20%-worst days typically occurred during the warm season when transport was easterly or southeasterly and sulfates dominated visibility impairment.
- In the Upper Midwest, the 20%-best days occurred in both cold and warm seasons when upper-level low-pressure troughs over the central or eastern United States paired with transport from the north and northwest.
- For the Southeastern Plains subregion (represented by Sikes), the 20%-worst days usually occurred during the warm season. Southeasterly or north-northeasterly transport conditions corresponded to the predominance of sulfate in visibility impairment.
- For the Southeastern Plains subregion, the 20%-best days occurred primarily in the cold season when transport patterns carried air masses from the northwest or over the Gulf of Mexico from the southeast.

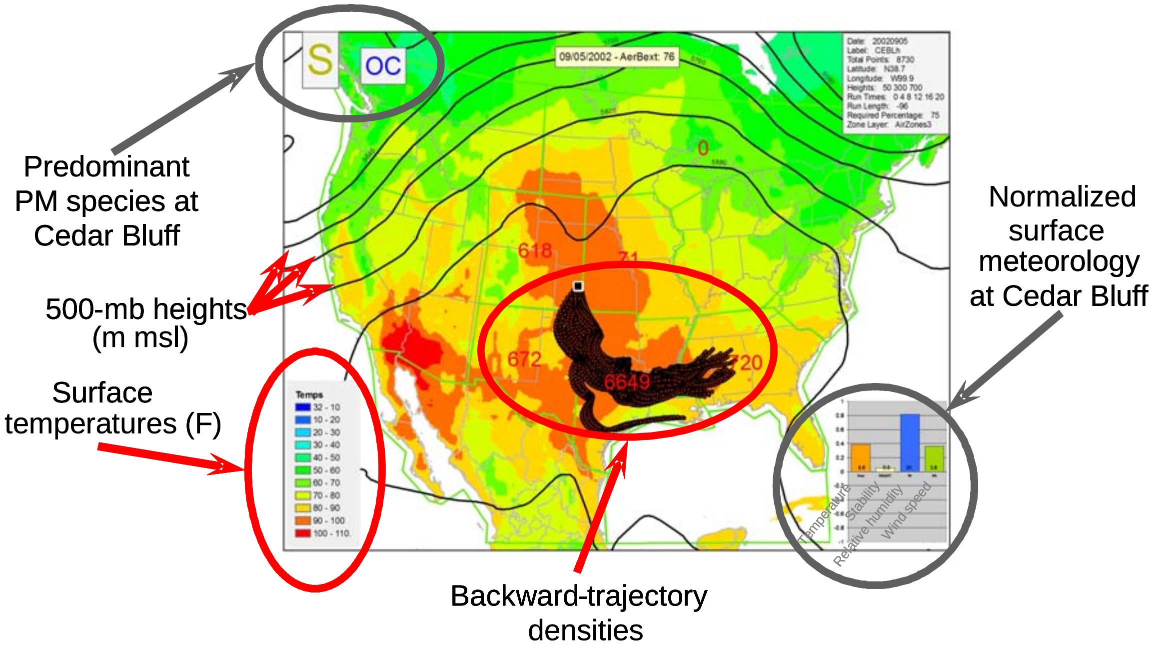

Figure 4-21. An annotated schematic depicting meteorology and transport conditions for one of the 20%-worst visibility days at the Cedar Bluff site.

4.4 EVIDENCE RELATING MULTI-YEAR EMISSIONS TRENDS TO TRENDS IN THE CAUSES OF HAZE

SO_2 emissions in the Ohio River Valley states (Ohio, West Virginia, Kentucky, Indiana, and Illinois), Tennessee, and Missouri declined substantially from 1990 to 1999.

Trends in state-level SO_2 emissions from 1990 to 1999 are illustrated in **Figure 4-22.** Five-year average ammonium sulfate concentrations observed on the 20%-worst days declined from about 11 $\mu g/m^3$ in 1993/1994 to 9 $\mu g/m^3$ in 1999/2000 (**Figure 4-23**) at the Upper Buffalo site. (Details about how five-year averages were computed and plotted are available on the VIEWS web site). Light extinction due to ammonium sulfate on the 20%-worst days declined during the same period from about 100 Mm^{-1} to 80 Mm^{-1} (**Figure 4-24**), while total light extinction declined from about 140 Mm^{-1} to 120 Mm^{-1} (**Figure 4-25**). Visibility conditions on the 20%-best days also benefited slightly from declining ammonium sulfate concentrations (**Figure 4-26**).

Figure 4-22. State-level trends in SO_2 emissions for the period 1990-1999. (Source: Schichtel et al., 2004)

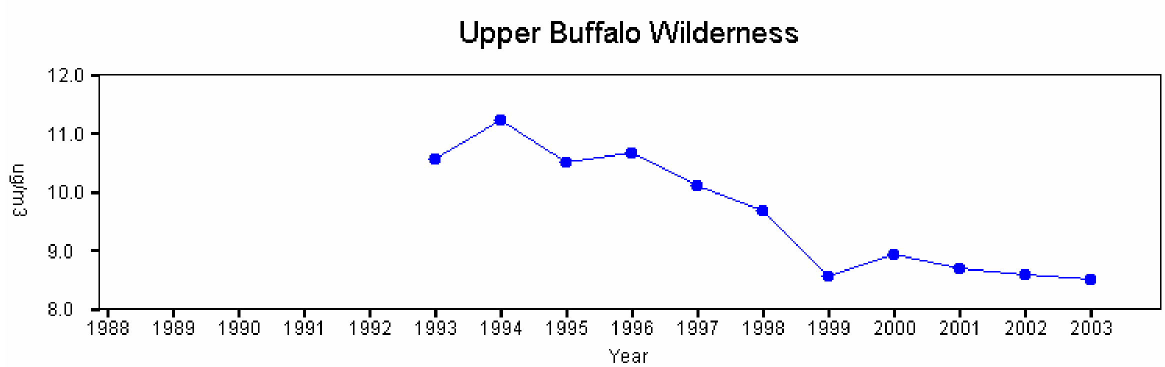

Figure 4-23. Five-year average ammonium sulfate concentrations observed on the 20%-worst visibility days at the Upper Buffalo site from 1993-2003. (Source: Visibility Information Exchange Web System)

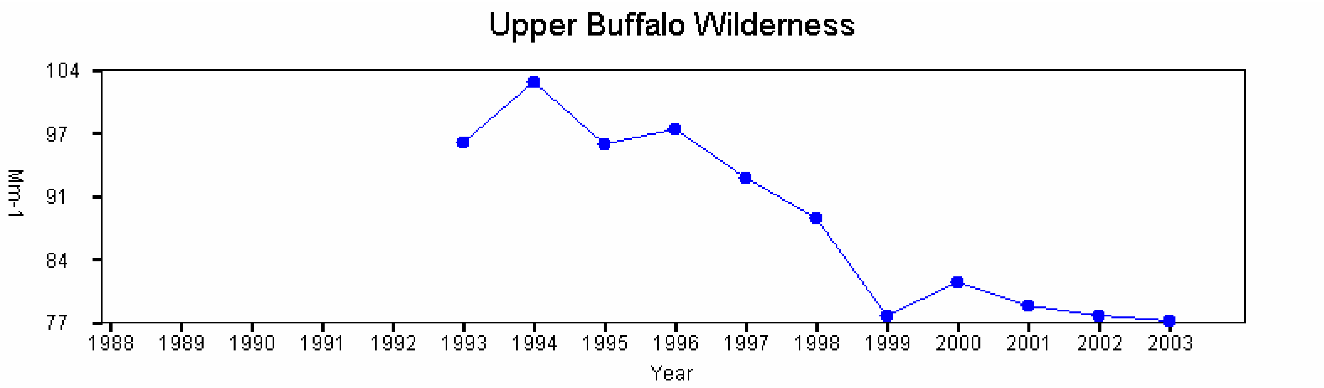

Figure 4-24. Five-year average light extinction due to ammonium sulfate observed on the 20%-worst visibility days at the Upper Buffalo site from 1993-2003. (Source: Visibility Information Exchange Web System)

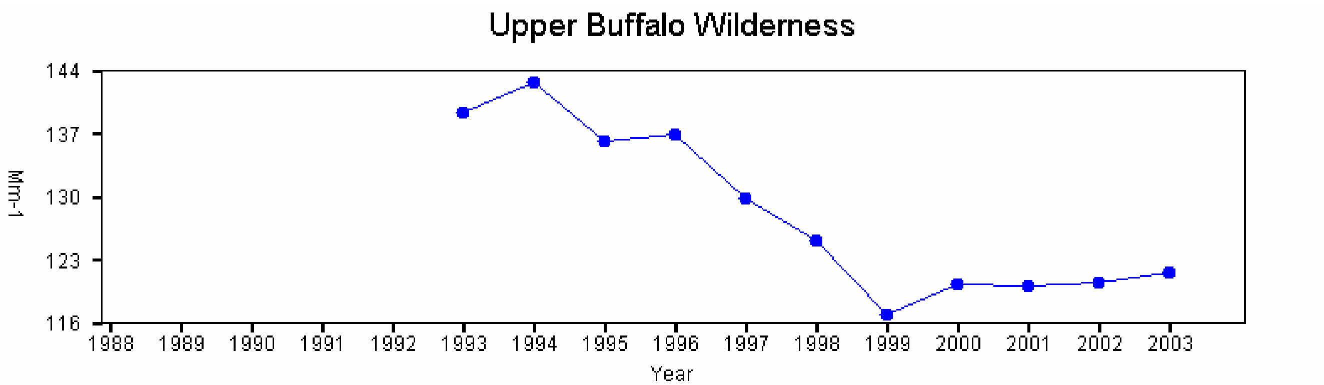

Figure 4-25. Five-year average total light extinction observed on the 20%-worst visibility days at the Upper Buffalo site from 1993-2003. (Source: Visibility Information Exchange Web System)

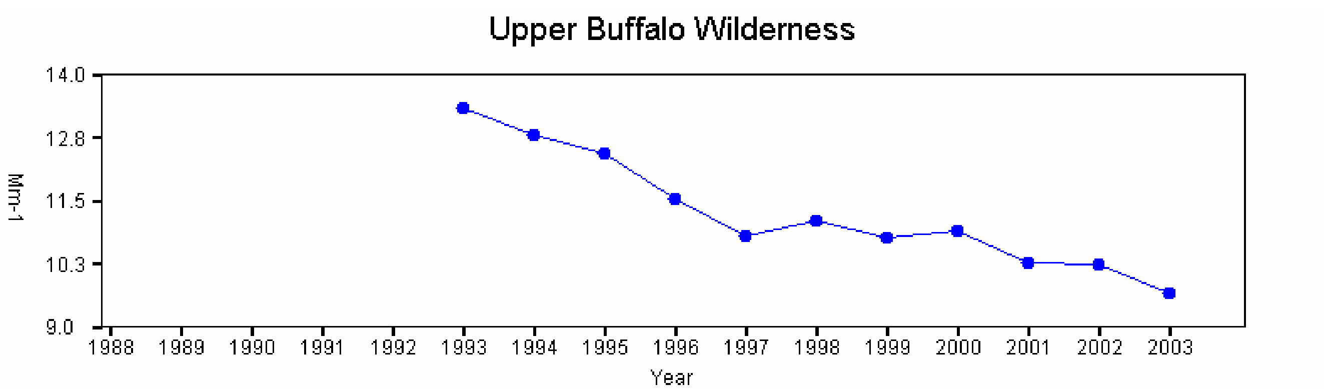

Figure 4-26. Five-year average light extinction due to ammonium sulfate observed on the 20%-best visibility days at the Upper Buffalo site from 1993-2003. (Source: Visibility Information Exchange Web System)

SO_2 emissions in Texas, New Mexico, Arizona, Louisiana, Arkansas, and Mississippi increased somewhat from 1990 to 1999.

Trends in state-level SO_2 emissions from 1990 to 1999 are illustrated in Figure 4-22. Five-year average ammonium sulfate concentrations observed on the 20%-worst days increased from about 4 $\mu g/m^3$ in 1990/1991 to 5-6 $\mu g/m^3$ in 1999/2000 (**Figure 4-27**) at the Big Bend site. Light extinction due to ammonium sulfate on the 20%-worst days increased during the same period from about 20 Mm^{-1} to 28 Mm^{-1} (**Figure 4-28**), while total light extinction increased from about 41 Mm^{-1} to 54 Mm^{-1} (**Figure 4-29**). Visibility conditions on the 20%-best visibility days did not change noticeably (**Figure 4-30**).

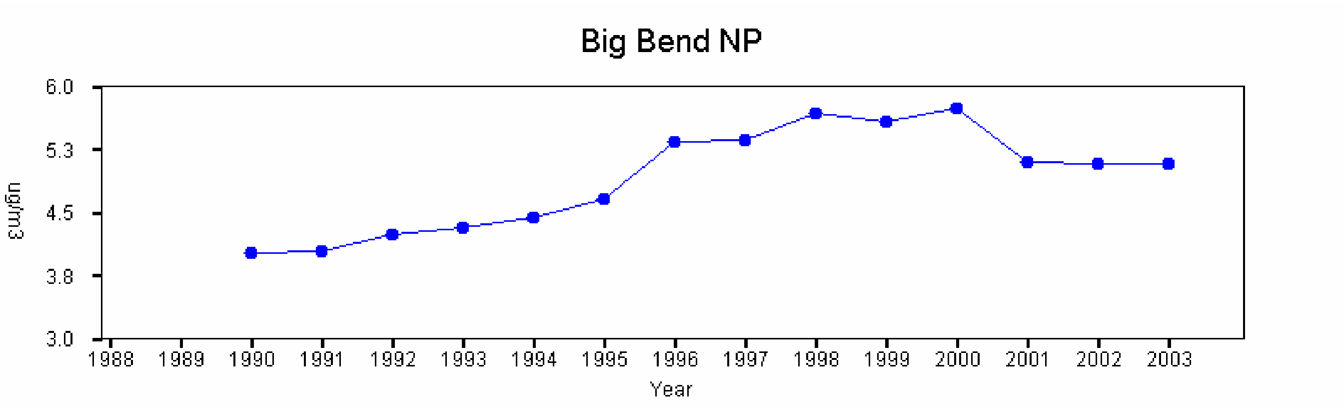

Figure 4-27. Five-year average ammonium sulfate concentrations observed on the 20%-worst visibility days at the Big Bend site from 1990-2003. (Source: Visibility Information Exchange Web System)

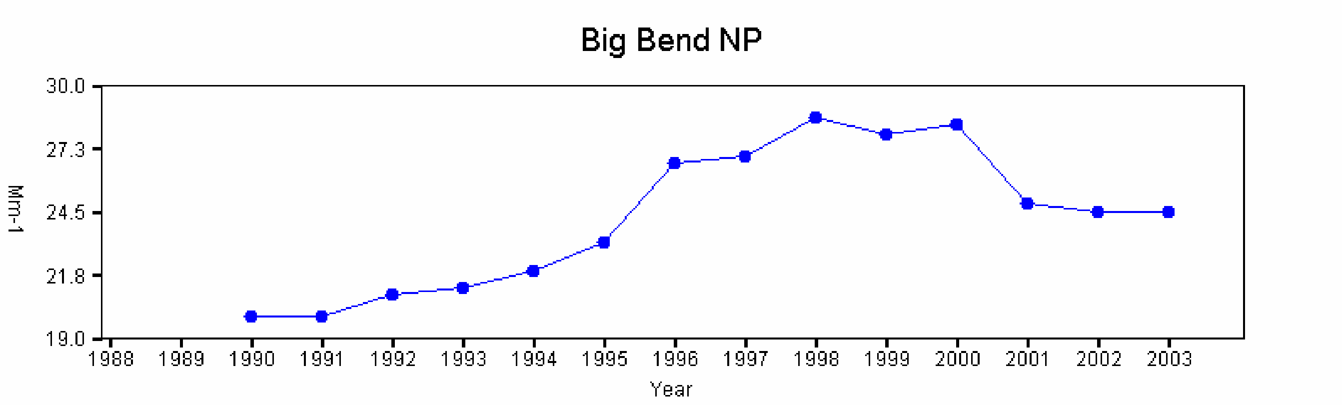

Figure 4-28. Five-year average light extinction due to ammonium sulfate observed on the 20%-worst visibility days at the Big Bend site from 1990-2003. (Source: Visibility Information Exchange Web System)

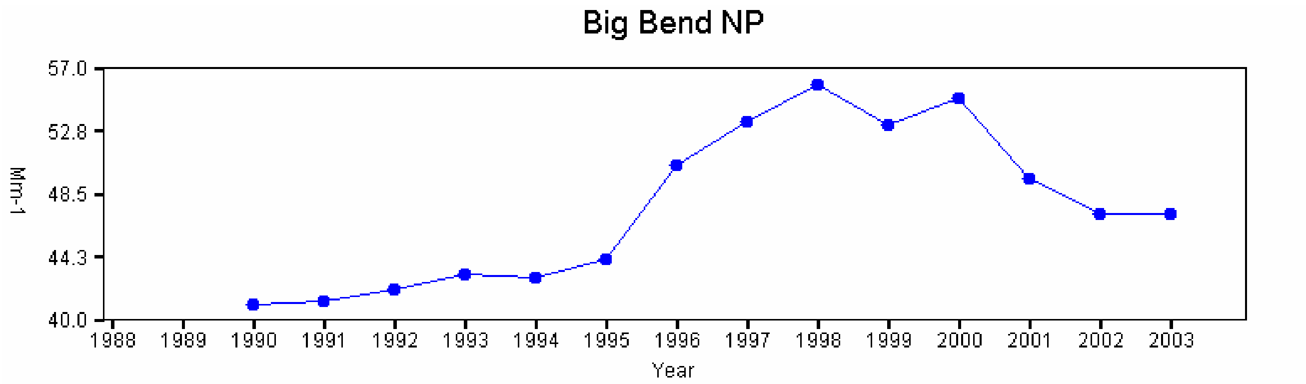

Figure 4-29. Five-year average total light extinction observed on the 20%-worst visibility days at the Big Bend site from 1990-2003. (Source: Visibility Information Exchange Web System)

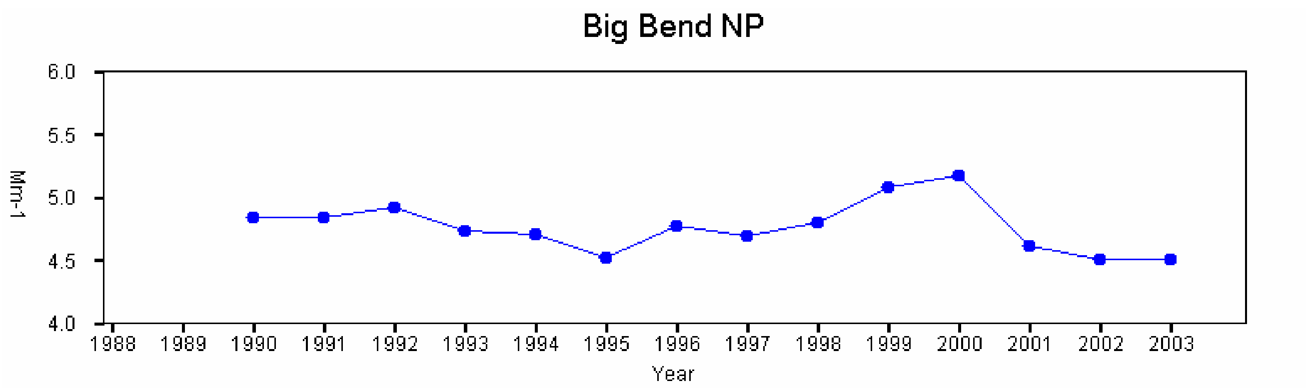

Figure 4-30. Five-year average light extinction due to ammonium sulfate observed on the 20%-best visibility days at the Big Bend site from 1990-2003. (Source: Visibility Information Exchange Web System)

In Minnesota and surrounding states, the trend in SO_2 emissions varied from state to state.

Trends in state-level SO_2 emissions from 1990 to 1999 are illustrated in Figure 4-22. . Five-year average ammonium sulfate concentrations observed on the 20%-worst days declined from about 4.5 µg/m^3 in the early 1990s to 2.8-3.8 µg/m^3 in 1999/2000 (**Figure 4-31**) at the Boundary Waters-Canoe and Voyageurs sites. Light extinction due to ammonium sulfate on the 20%-worst days declined during the same period from 35-40 Mm^{-1} to 20-30 Mm^{-1} (**Figure 4-32**), while total light extinction increased from 70-75 Mm^{-1} to 55-67 Mm^{-1} (**Figure 4-33**). Visibility conditions on the 20%-best days did not change noticeably at the Boundary Waters-Canoe site, but may have improved slightly at Voyageurs (**Figure 4-34**).

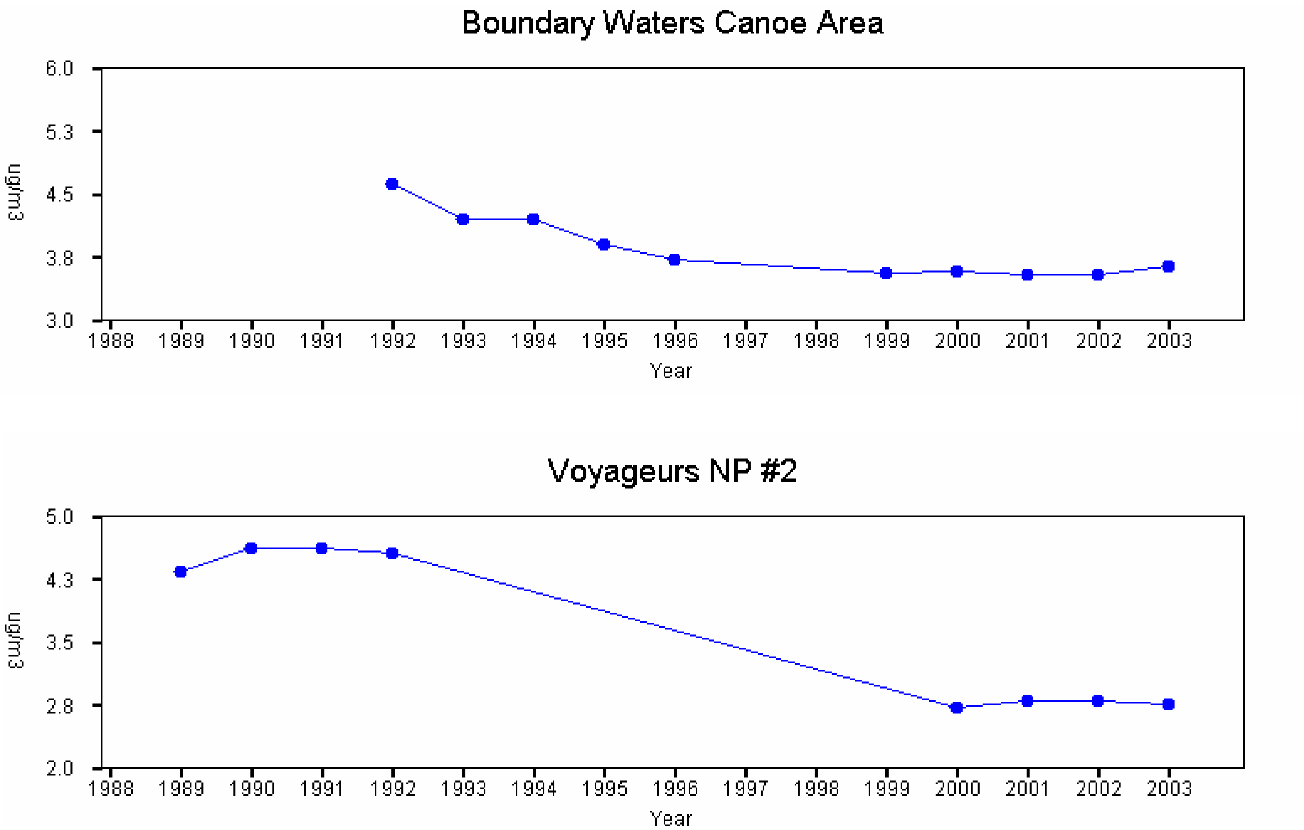

Figure 4-31. Five-year average ammonium sulfate concentrations observed on the 20%-worst visibility days at the Northern Minnesota sites, Boundary Waters-Canoe and Voyageurs (VOYA2), from 1989-2003. (Source: Visibility Information Exchange Web System)

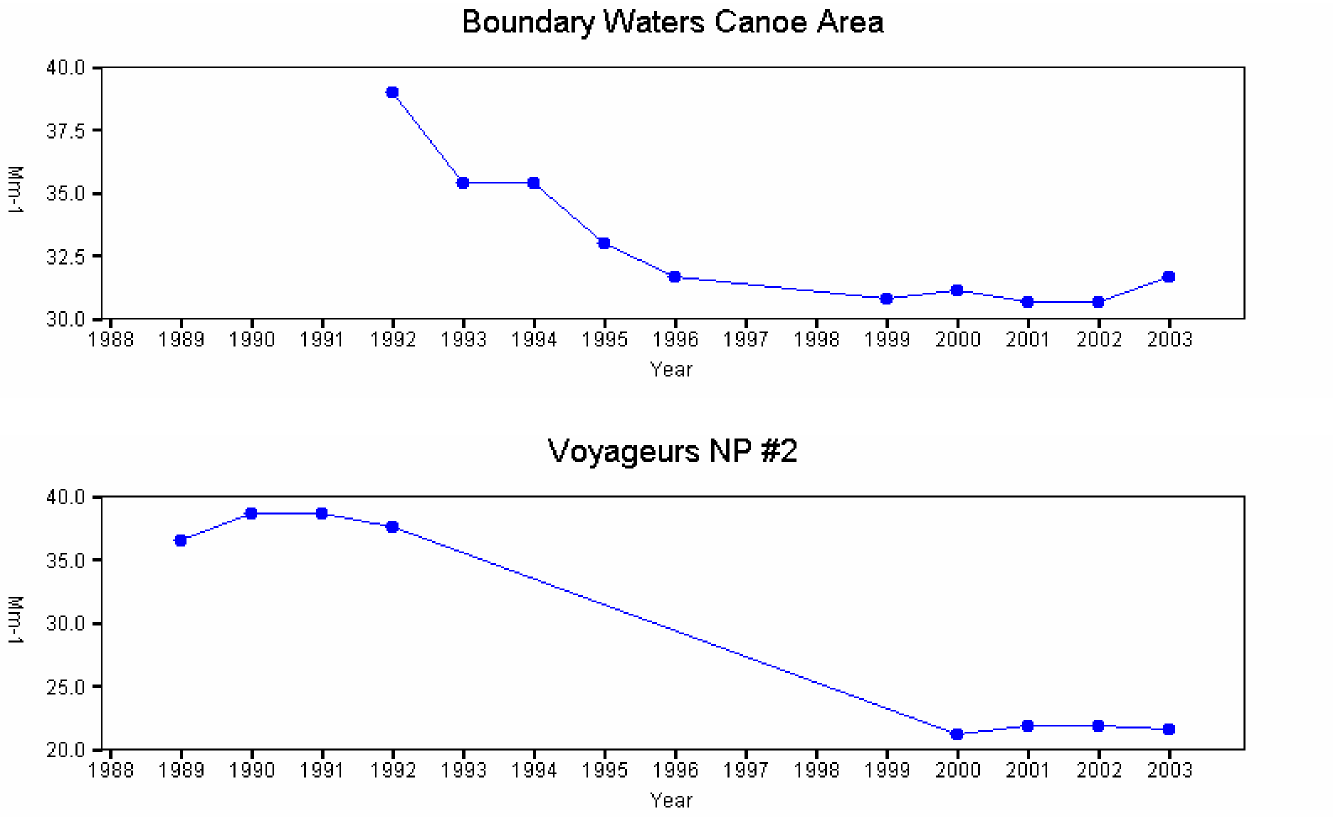

Figure 4-32. Five-year average light extinction due to ammonium sulfate observed on the 20%-worst visibility days at the Northern Minnesota sites, Boundary Waters-Canoe and Voyageurs (VOYA2), from 1989-2003. (Source: Visibility Information Exchange Web System)

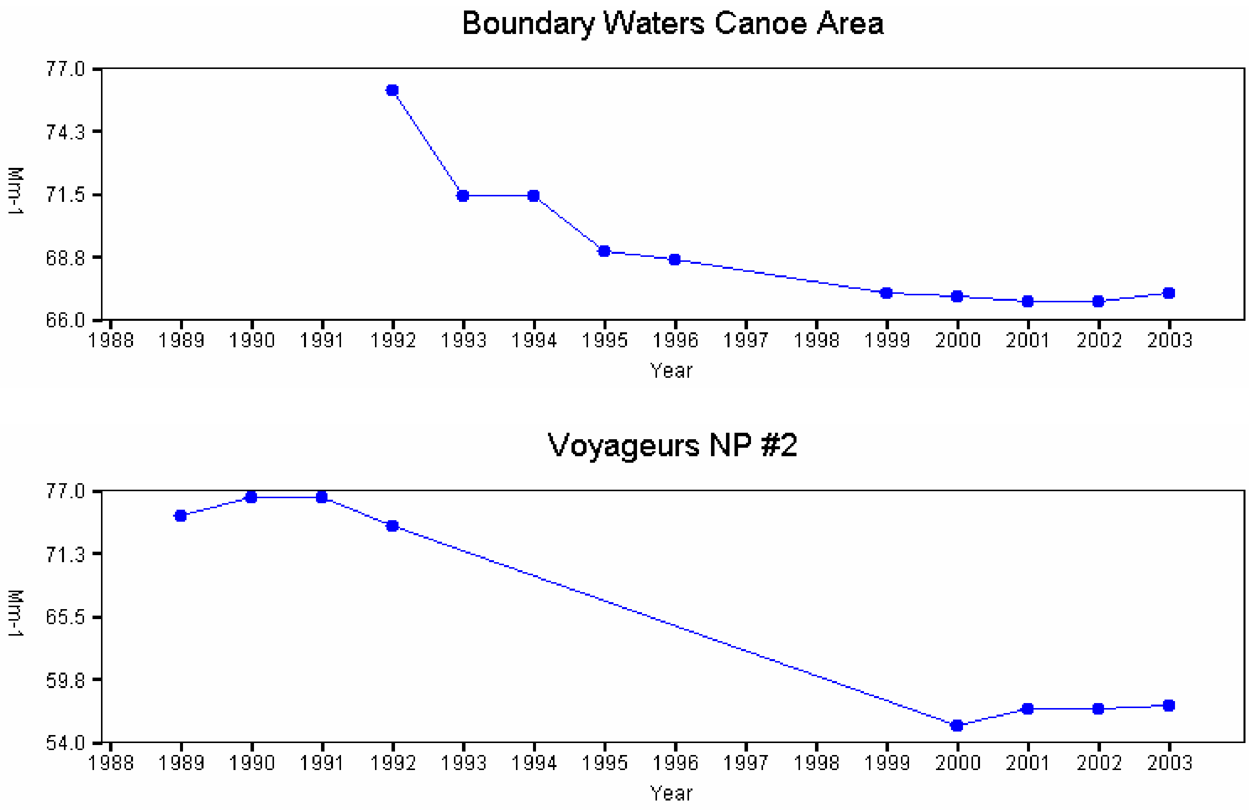

Figure 4-33. Five-year average total light extinction observed on the 20%-worst visibility days at the Northern Minnesota sites, Boundary Waters-Canoe and Voyageurs (VOYA2), from 1989-2003. (Source: Visibility Information Exchange Web System)

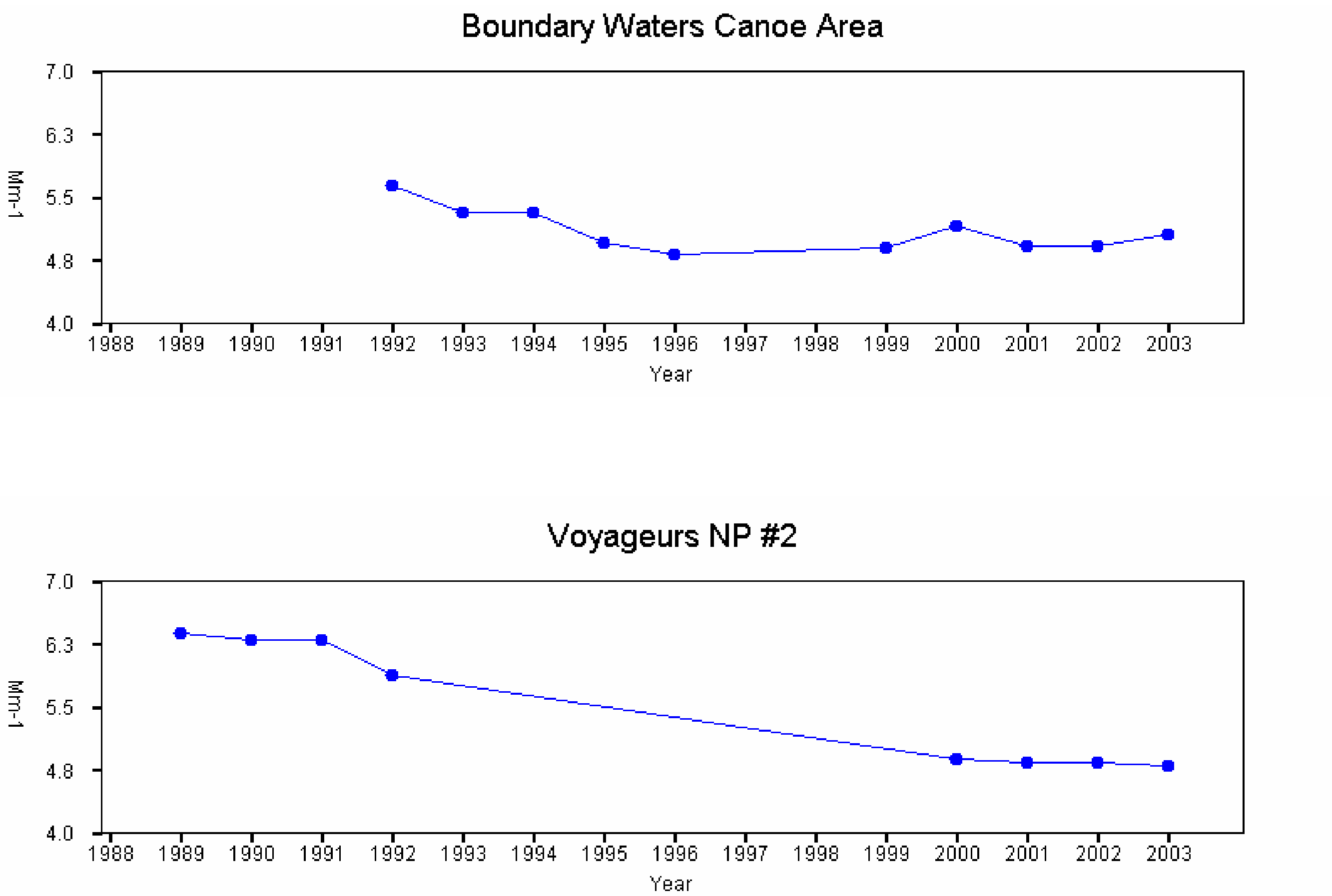

Figure 4-34. Five-year average light extinction due to ammonium sulfate observed on the 20%-best visibility days at the Northern Minnesota sites, Boundary Waters-Canoe and Voyageurs (VOYA2), from 1989-2003. (Source: Visibility Information Exchange Web System)

5. REFERENCES

Brown S.G., Herckes P., Ashbaugh L., Hannigan M.P., Kreidenweis S.M., and Collett J.L., Jr. (2002) Characterization of organic aerosol in Big Bend National Park, Texas. *Atmospheric Environment* **36** (38), 5807-5818.

Fine P.M., Cass G.R., and Simoneit B.R.T. (2002) Organic compounds in biomass smoke from residential wood combustion: emissions characterization at a continental scale. *Journal of Geophysical Research-Atmospheres* **107** (D21).

Fine P.M., Cass G.R., and Simoneit B.R.T. (2004) Chemical characterization of fine particle emissions from the fireplace combustion of wood types grown in the Midwestern and Western United States. *Environmental Engineering Science* **21** (3), 387-409.

IMPROVE (2004) Overview of IMPROVE and visibility. Available on the Internet at <http://vista.cira.colostate.edu/improve/Overview/Overview.htm> last accessed June 15, 2005.

Lowenthal D. and Kumar N. (2003) $PM_{2.5}$ mass and light extinction reconstruction in IMPROVE. *Journal of Air and Waste Management Association* **53** (9), 1109-1120.

Malm W.C., Sisler J.F., Huffman D., Eldred R.A., and Cahill T.A. (1994) Spatial and seasonal trends in particulate concentration and optical extinction in the United States. *Journal of Geophysical Research* **99** (D1), 1347-1370.

Nolte C.G., Schauer J.J., Cass G.R., and Simoneit B.R.T. (2001) Highly polar organic compounds present in wood smoke and in the ambient atmosphere. *Environmental Science & Technology* **35** (10), 1912-1919.

Schauer J.J., Fraser M.P., Cass G.R., and Simoneit B.R.T. (2001a) Source reconciliation of atmospheric gas-phase and particle-phase pollutants using organic compounds as tracers. (submitted for publication).

Schauer J.J., Kleeman M.J., Cass G.R., and Simoneit B.R.T. (2001b) Measurement of emissions from air pollution sources. 3. C_1 through C_{29} organic compounds from fireplace combustion of wood. *Environmental Science & Technology* **35** (9), 1716-1728.

Schichtel B., Malm W., Pitchford M., Ashbaugh L., Eldred R., and Ames R. (2004) Spatial and seasonal patterns in speciated fine particle concentration in the rural United States. Presentation at *A Science Colloquium on Modeling and Measuring Aerosols, University of Maryland, Baltimore, MD, June14-16*.

Sheesley R.J., Schauer J.J., Chowdhury Z., Cass G.R., and Simoneit B.R.T. (2003) Characterization of organic aerosols emitted from the combustion of biomass indigenous to South Asia. *Journal of Geophysical Research-Atmospheres* **108** (D9).

U.S. Environmental Protection Agency (2004) Regional haze regulations and guidelines for Best Available Retrofit Technology (BART) determinations; proposed rule. 40 CFR Part 51. *Federal Register*, Vol. 69, No. 87, pp. 25184-25232. May 5.

Visibility Information Exchange Web System (2004) Trends. Available on the Internet at <http://vista.cira.colostate.edu/views/Web/AnnualSummary/Trends.aspx >, last accessed June 8, 2005.

Zheng M., Cass G.R., Schauer J.J., and Edgerton E.S. (2002) Source apportionment of $PM_{2.5}$ in the southeastern United States using solvent-extractable organic compounds as tracers. *Environmental Science & Technology* **36**, 2361-2371.

APPENDIX A

DOCUMENTATION OF METHODS AND GRAPHICAL SUMMARY OF DATA FOR TASK 4

SPATIOTEMPORAL ANALYSIS

A.1 INTRODUCTION

The objective of this task is to identify subregions within CENRAP where aerosol extinction and concentrations of $PM_{2.5}$ components significantly covary in space and time. This analysis will help in selecting representative sites for further analysis which will eliminate the need to model and characterize every site. This task uses recent speciated $PM_{2.5}$ data for 2002-2003 collected as part of the IMPROVE program. The primary tool used in this task is principal component analysis (PCA) with Varimax rotation. PCA was applied to identify groups of sites that have similar variance of aerosol extinction (by b_{ext}) or a given species concentration (e.g., organic carbon [OC], nitrate, sulfate, etc.) using data from all sites (Lehman et al., 2004; Eder et al., 1993). The analyses performed in this task built on previous work conducted in Phase I by Desert Research Institute (DRI), in which areas of covariance of $PM_{2.5}$ concentrations in the CENRAP and WRAP regions were identified. The results of this task are sets of sites (i.e., subregions of CENRAP) that share characteristically varying air quality on the 20%-worst and 20%-best visibility days. Representative sites for each subregion are also selected for detailed analyses in later tasks.

A.2 METHOD

IMPROVE data collected on a 1-in-3 day schedule for 2002-2003 at 23 sites in the CENRAP region were obtained from the IMPROVE web site. Basic quality control (QC) was conducted by comparing the measured $PM_{2.5}$ mass to the reconstructed fine mass (RCFM) for every sample at every site (Hafner, 2003). If the comparison showed the measured mass and RCFM were not within 50%-150%, that sample was labeled as suspect and not used in subsequent data analyses. From this check, 44 samples were labeled as suspect. Next, the 20%-worst and 20%-best visibility days at each site for 2002-2003 were determined from visibility extinction (b_{ext}). All days on which at least one site had a 20%-worst day were combined in one subset, and all days on which at least one site had a 20%-best day were combined in another subset. PCA analyses were then conducted for the 20%-worst and 20%-best days using the aerosol extinction, sulfate, OC, and nitrate concentrations. Varimax rotation was used to achieve a simple structure among factor loadings (e.g., limit components with non-zero loadings on the same variable). Data at Mingo were used, though it was recently discovered (in late summer 2005) that these data may be invalid, so results from this site should be ignored until the status of the data is confirmed.

A.3 PCA RESULTS FOR AEROSOL EXTINCTION

Results are given in **Table A-1 and Figures A-1 and A-2**. Six and five subregions were identified from the aerosol extinction on the 20%-worst and 20%-best days, respectively. These were:

- An Upper Midwest subregion, consisting of sites in southern Iowa, Missouri, and eastern Kansas.
- The Western Plains, which included Big Bend National Park (Big Bend) but not Guadalupe Mountains National Park (Guadalupe Mountains).
- The Guadalupe Mountains, which consistently showed a poor relationship with Big Bend and other CENRAP sites.
- Minnesota, consisting of the border sites Voyageurs National Park Site 2 (Voyageurs) and Boundary Waters/Canoe Area (Boundary Waters).
- Southeastern Plains, which includes sites in Louisiana and southern Arkansas.
- A "transition zone" between the western plains and the upper Midwest and Southeastern Plains, consisting of Upper Buffalo Wilderness (Upper Buffalo) and Wichita Mountains.

Table A-1. PCA results (variance explained by the factor) on the 20%-worst and 20%-best visibility days for aerosol extinction.

Subregion	% Variance on the 20%-Worst Days	% Variance on the 20%-Best Days	Representative Site
Minnesota	12	8	Voyageurs
Upper Midwest	36	42	Hercules-Glades
Western Plains	16	23	Cedar Bluff
Transition Zone	11	–	–
Southeastern Plains	10	12	Sikes
Guadalupe Mountains	7	9	–

From these results, four representative sites were selected: Cedar Bluff (CEBL1), Kansas, for the Western Plains; Sikes Aerosol (Sikes, SIKE1), Louisiana, for Southeastern Plains; Hercules-Glades (HEGL1), Missouri, for the Upper Midwest; and Voyageurs (VOYA2), Minnesota, for Minnesota. The influences on the transition zone sites are approximated by the selected sites, so neither transition zone site was selected for additional work.

The selection of the representative sites was confirmed by comparing the number of 20%-worst and 20%-best visibility days each site had in common with the other sites in its subregion. Minnesota only had two sites, so Voyageurs was selected since it had more data than Boundary Waters. In the Upper Midwest, El Dorado Springs was the most representative site, followed by Tallgrass and Hercules-Glades. However, Hercules-Glades was selected since it has twice as much data as El Dorado Springs, and is still very representative for the region. This site's representativeness was confirmed by trajectory analysis in the meteorology characterization task (Appendix B). In the Western Plains, all sites but Big Bend shared nearly all the same days, with Cedar Bluff being the most representative. The connection between Big Bend and the other Western Plains sites exists because these sites shared many of the same high-extinction days when sulfate or coarse mass were large contributors to light extinction. (A different conclusion might have been drawn if particulate mass and/or average visibility days had been of interest for these analyses.) In the Southeastern Plains, Sikes was the most representative site in its subregion.

A.4 PCA RESULTS FOR $PM_{2.5}$ COMPONENTS

In addition to aerosol extinction, groupings among sites for dominant aerosol components were explored with PCA. This analysis helped us understand the underlying variability of the PCA analysis on aerosol extinction, the representativeness of the selected sites, and the extent of regional versus local effects.

PCA results using OC, nitrate (NO_3), and sulfate (SO_4) on the 20%-worst and 20%-best visibility days are shown in **Figures A-3 through A-8**. Results were consistent with the aerosol extinction analysis, but showed some underlying trends that will be useful in later analyses:

- Nitrate concentrations varied more on a local level than on a regional level; five to seven factors were found for nitrate. The Upper Midwest factor identified by b_{ext} was split into two, which may be due to the greater availability of ammonia for ammonium nitrate formation in Iowa compared to Missouri.
- Sulfate showed a distinctive regional character, with the Minnesota, Upper Midwest, Transition Zone, and Southeastern Plains being grouped together. The Western Plains, Big Bend, and Guadalupe visibility trends are likely distinguished from the other sites by the sulfate differences.
- PCA results for OC were similar to aerosol extinction results, except that the Western Plains and Minnesota were grouped together. This may be indicative of a "western" OC influence in these subregions versus a more localized OC influence in the eastern subregions.

A.5 CASE STUDY: GUADALUPE MOUNTAINS

The Guadalupe Mountains site consistently showed different results than other sites in CENRAP, even Big Bend, which is also in western Texas. Extensive work has been conducted on Big Bend aerosol as part of the Big Bend Regional Aerosol and Visibility Observational (BRAVO) study (Pitchford et al., 2004). Sulfate is the main chemical component of poor visibility, and transport from Mexico, Texas, and the Southeast affect the worst visibility days. To investigate the differences between Guadalupe Mountains and Big Bend, we examined the extinction composition on the 20%-worst days at these two sites for 2002-2003, shown in **Figures A-9 and A-10**. Of the 38 worst days, the two sites only have 11 of the days in common. While the 20%-worst days at Big Bend are dominated mostly by sulfate and to a lesser extent OC, at Guadalupe, sulfate, OC, and coarse mass are all important.

The differences in poor visibility days and the composition on these days are likely due to different meteorological transport regimes affecting the two sites. To further investigate this, 72-hr back trajectories were run for all sample dates at each site using the NOAA HYSPLIT model (Draxler and Hess, 1997), which were then mapped as a spatial probability density (SPD^0):

$$SPD = \frac{\text{Count of hourly trajectory endpoints within search radius}}{\text{Count of trajectories run}}$$

The largest SPD values are in areas where the backward trajectories have spent the most time. Then, a conditional probability function (CPF) was applied to help interpret the results (Kim and Hopke, 2004; Kim et al., 2003, 2004; Ashbaugh et al., 1985). In CPF, the transport patterns of the 20%-highest concentration days of a given factor are compared to the climatological transport patterns. After finding SPD^0, back trajectories for the 20%-worst visibility days were run and mapped (SPD'). This density is then compared to the SPD for all days (i.e., the climatology), so that the differences in transport and source areas on high concentration days of a given factor are highlighted:

$$CoPIA' = SPD' - SPD^0 \qquad (1)$$

This Conditional Probability Integrative Analysis (CoPIA) is very similar to the CPF analyses employed in other studies (Kim and Hopke, 2004; Kim et al., 2003, 2004; Ashbaugh et al., 1985); however, CoPIA is adapted to take advantage of tools available in a Geographic Information System (GIS) framework. Ensemble backward trajectories were run every 4 hours to account for wind variability over a 24-hr sampling period.

CoPIA results for the 20%-worst visibility days at Big Bend and Guadalupe for 2002-2003 are shown in **Figures A-11 and A-12**; the higher values are in areas where the backward trajectories spent the most time. The results show that different transport regimes affect these two sites, confirming what was observed in the compositional analysis. Transport from Mexico, Texas, and the Southeast affect Big Bend. While, in addition to Texas, transport (likely soil and coarse mass) from western Mexico, New Mexico, and Arizona affect Guadalupe. While Guadalupe is not a representative site for CENRAP, it would be interesting to analyze this site in the future to determine west versus east trends and the importance of transport into the CENRAP region.

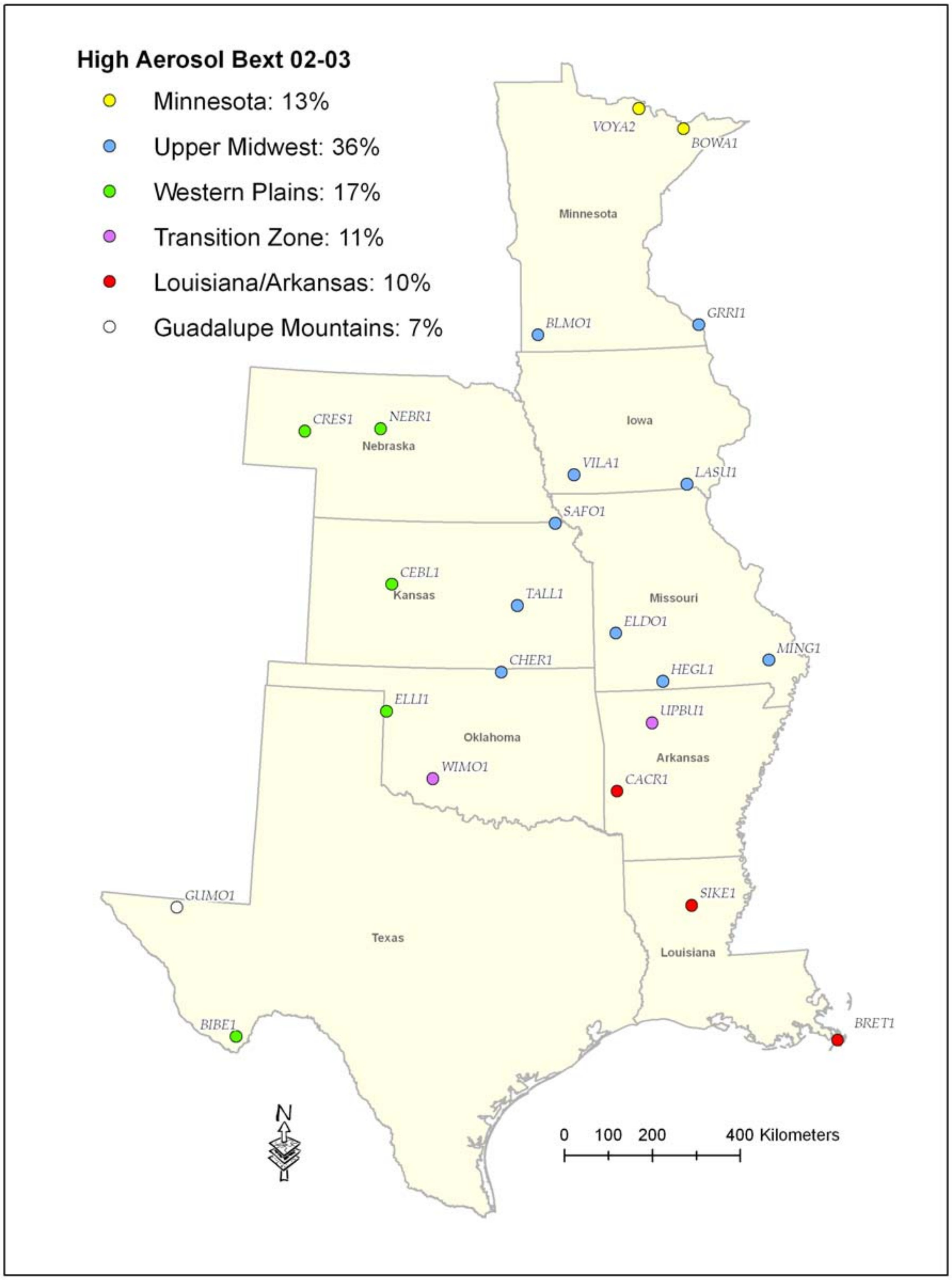

Figure A-1. PCA results (grouping and % of data variability explained) for aerosol extinction on the 20%-worst visibility days in 2002-2003.

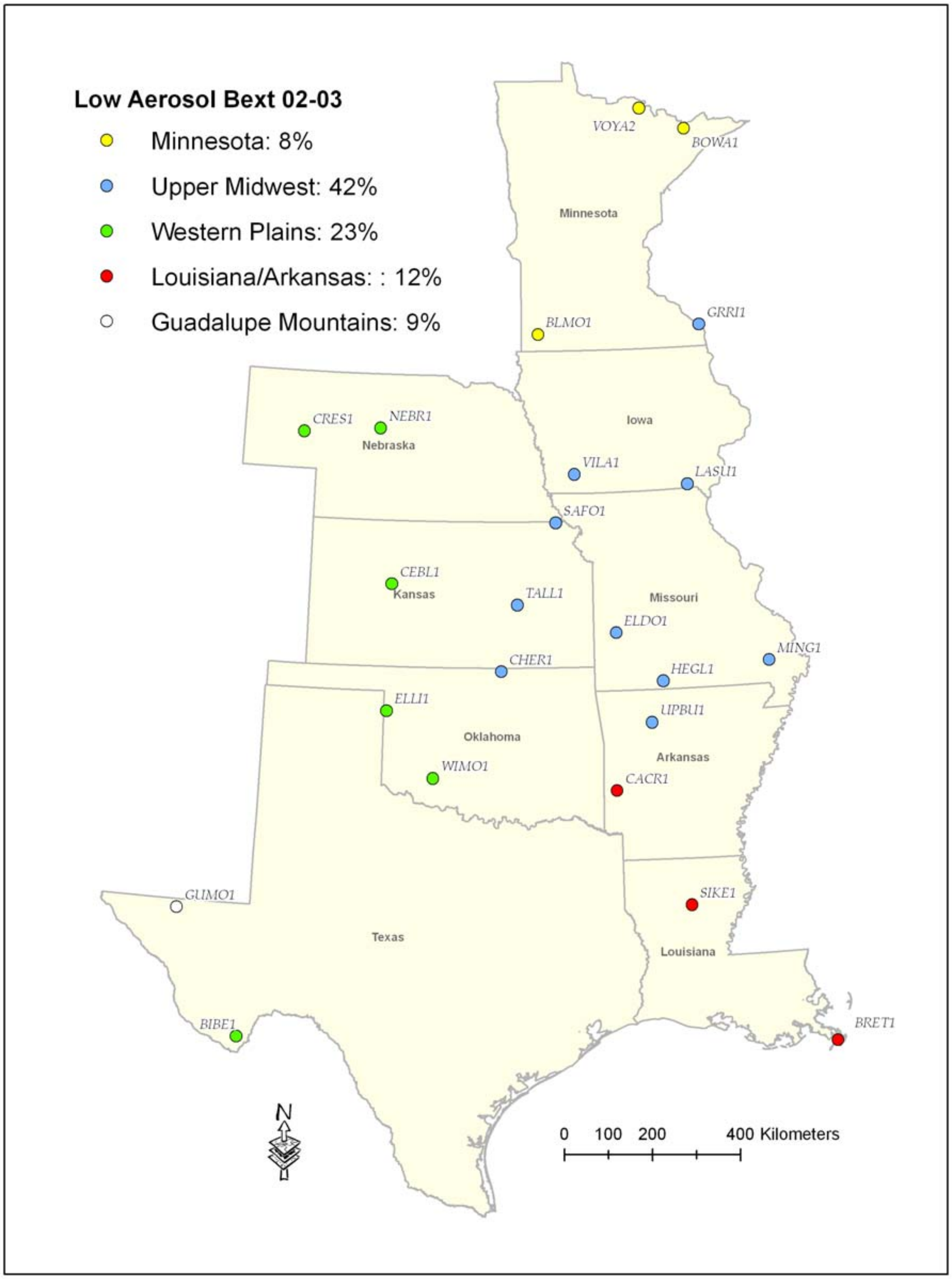

Figure A-2. PCA results (grouping and % of data variability explained) for aerosol extinction on 20%-best visibility days in 2002-2003.

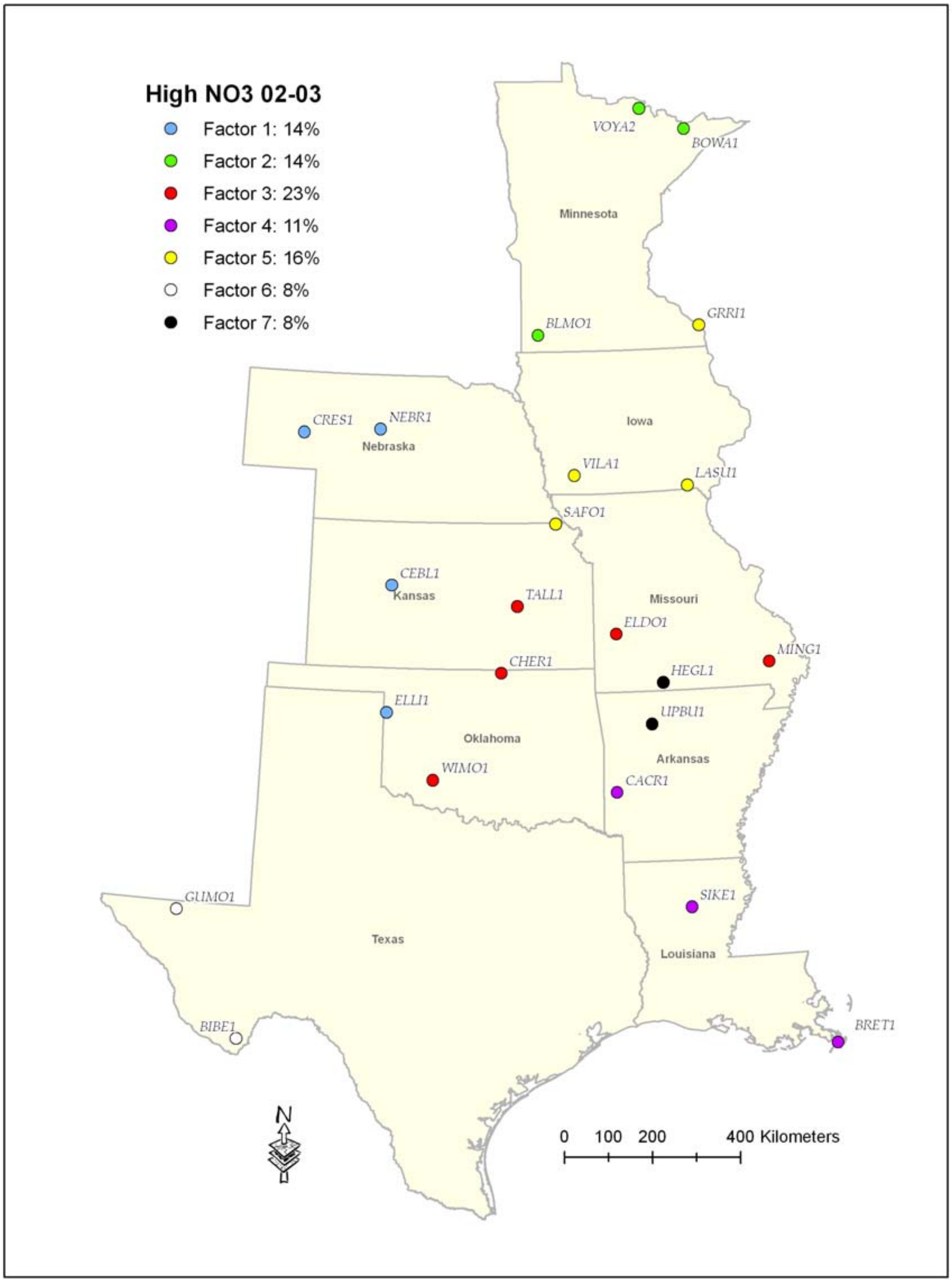

Figure A-3. PCA results (grouping and % of data variability explained) for nitrate on the 20%-worst visibility days in 2002-2003.

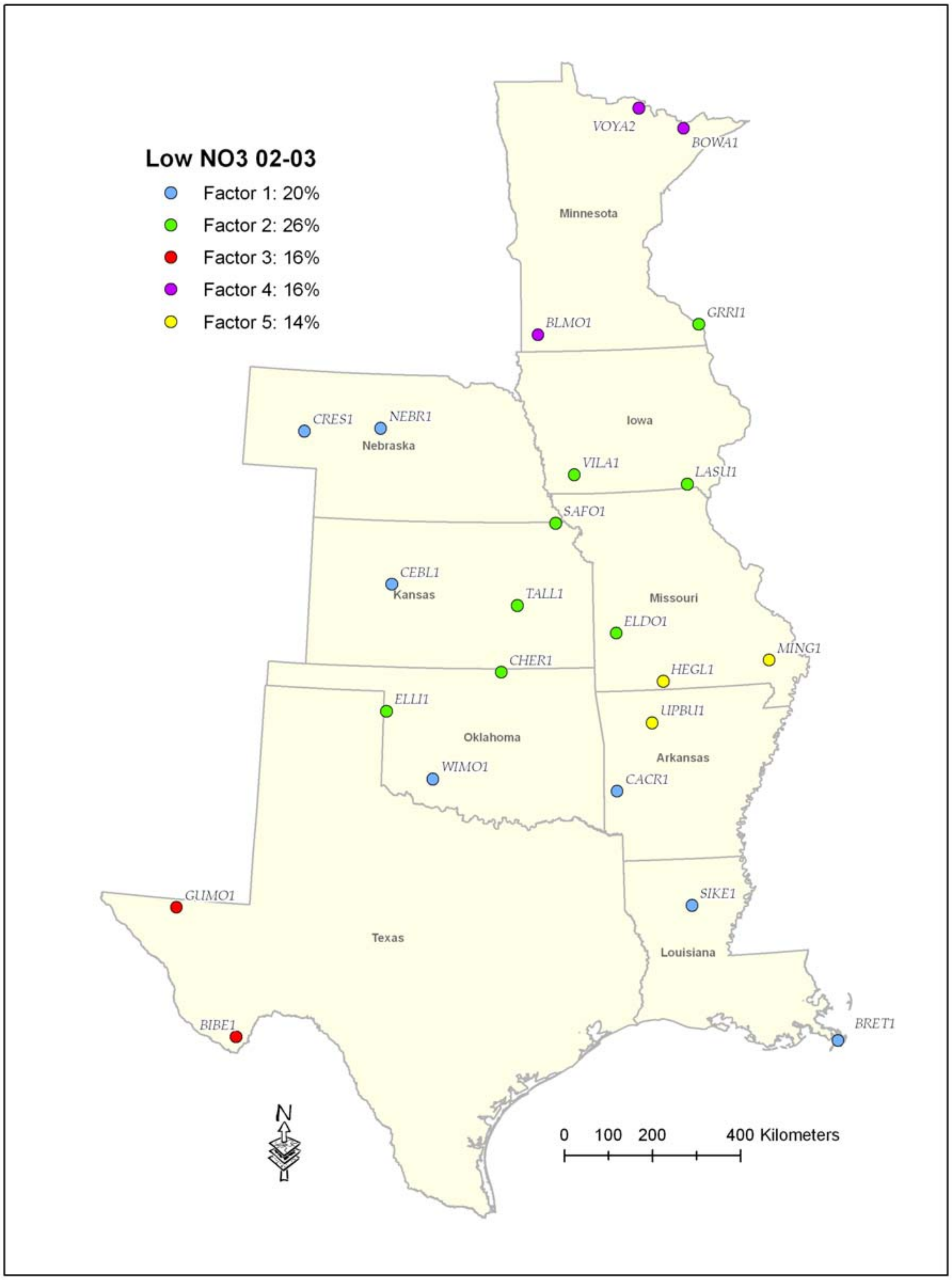

Figure A-4. PCA results (grouping and % of data variability explained) for nitrate on the 20%-best visibility days in 2002-2003.

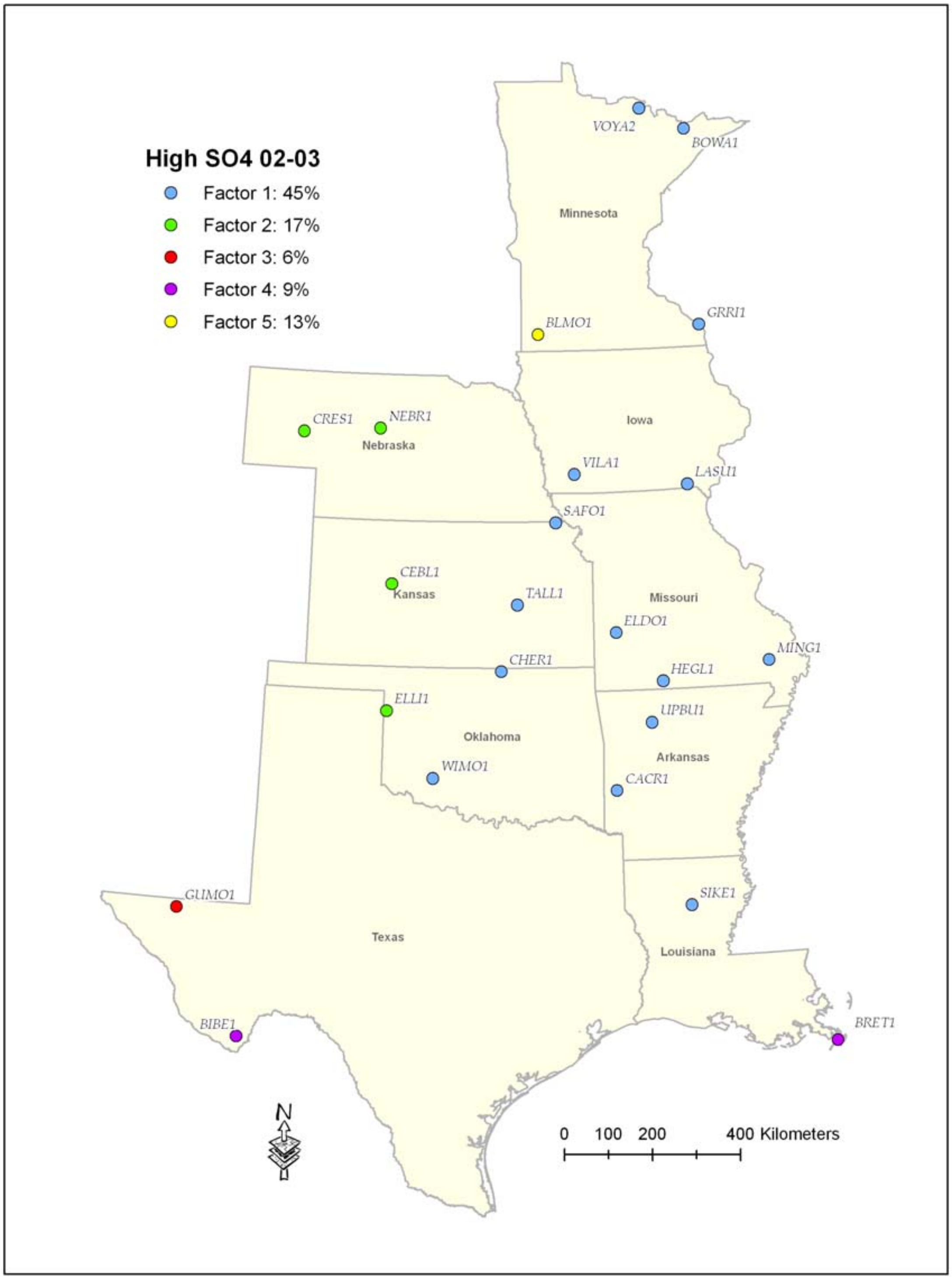

Figure A-5. PCA results (grouping and % of data variability explained) for sulfate on the 20%-worst visibility days in 2002-2003.

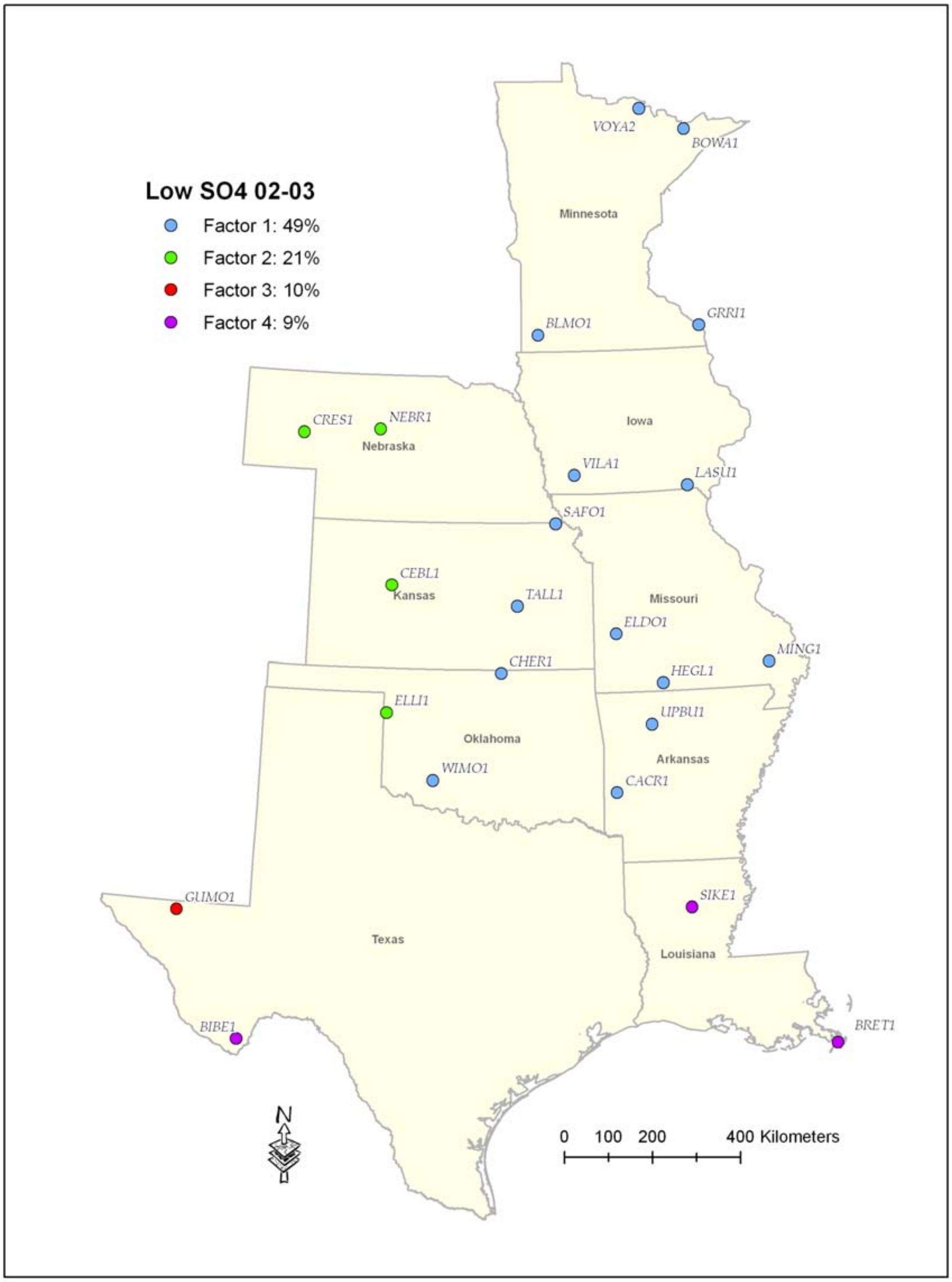

Figure A-6. PCA results (grouping and % of data variability explained) for sulfate on the 20%-best visibility days in 2002-2003.

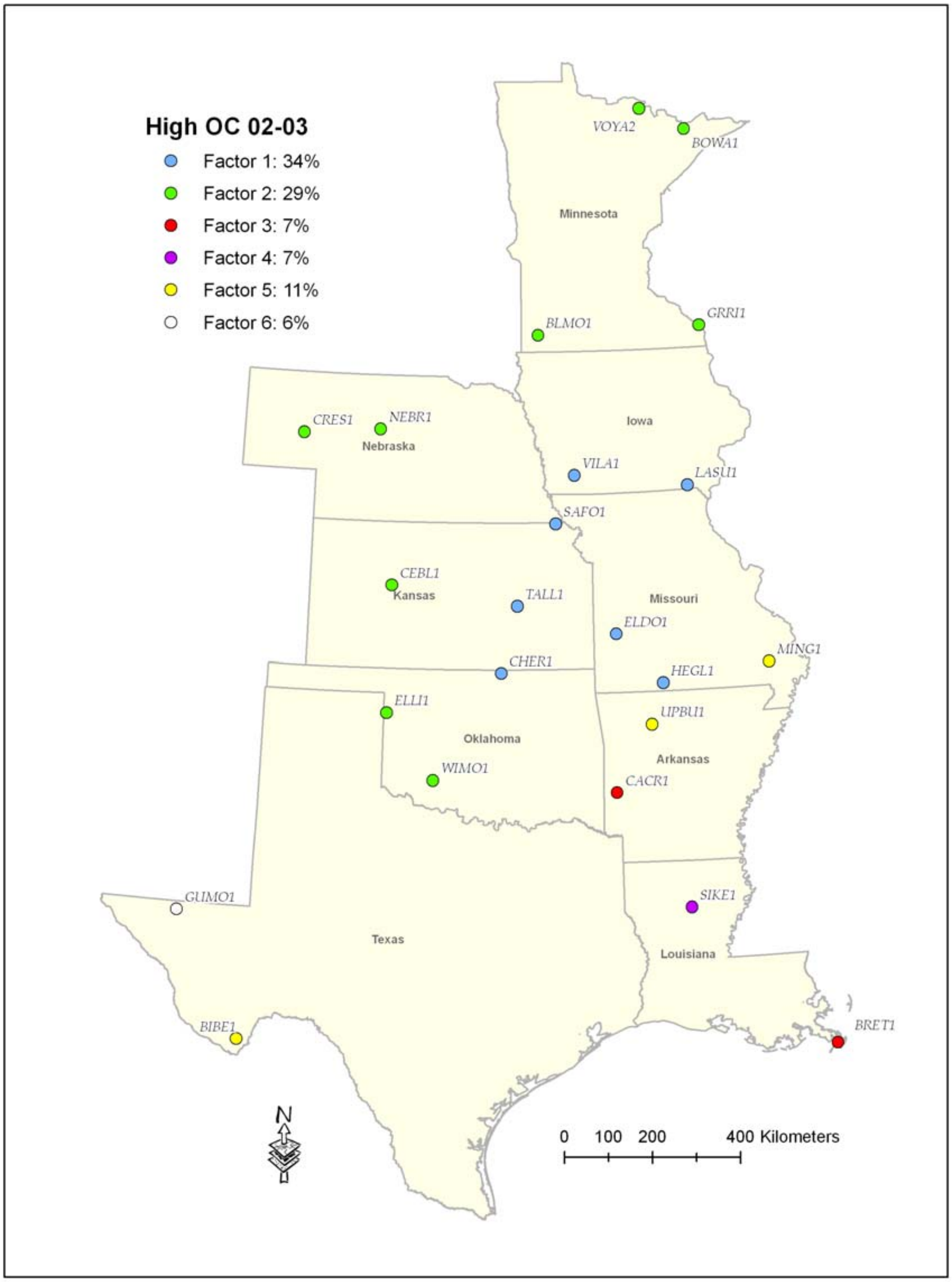

Figure A-7. PCA results (grouping and % of data variability explained) for OC on the 20%-worst visibility days in 2002-2003.

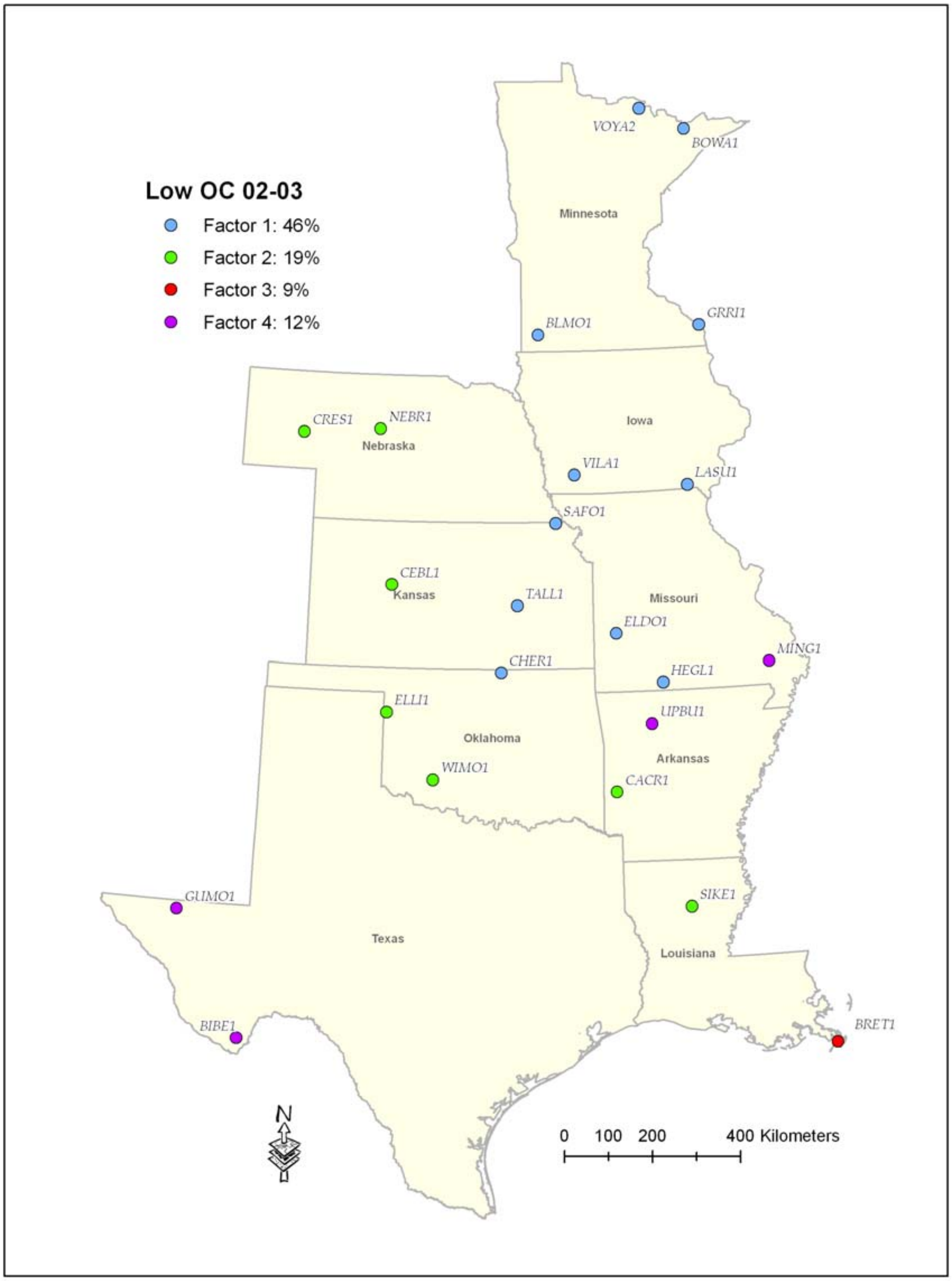

Figure A-8. PCA results (grouping and % of data variability explained) for OC on the 20%-best visibility days in 2002-2003.

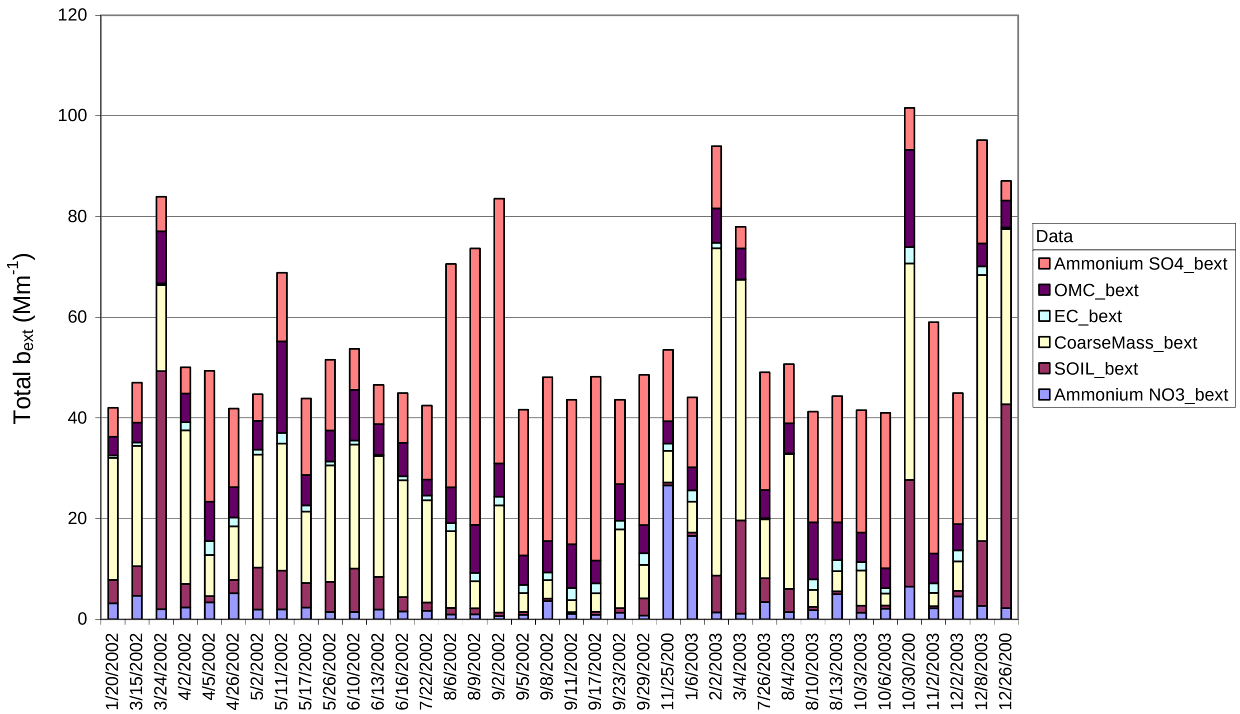

Figure A-9. Extinction (b_{ext}) composition by component (using standard IMPROVE calculations) for the 20%-worst visibility days at Guadalupe Mountains in 2002-2003.

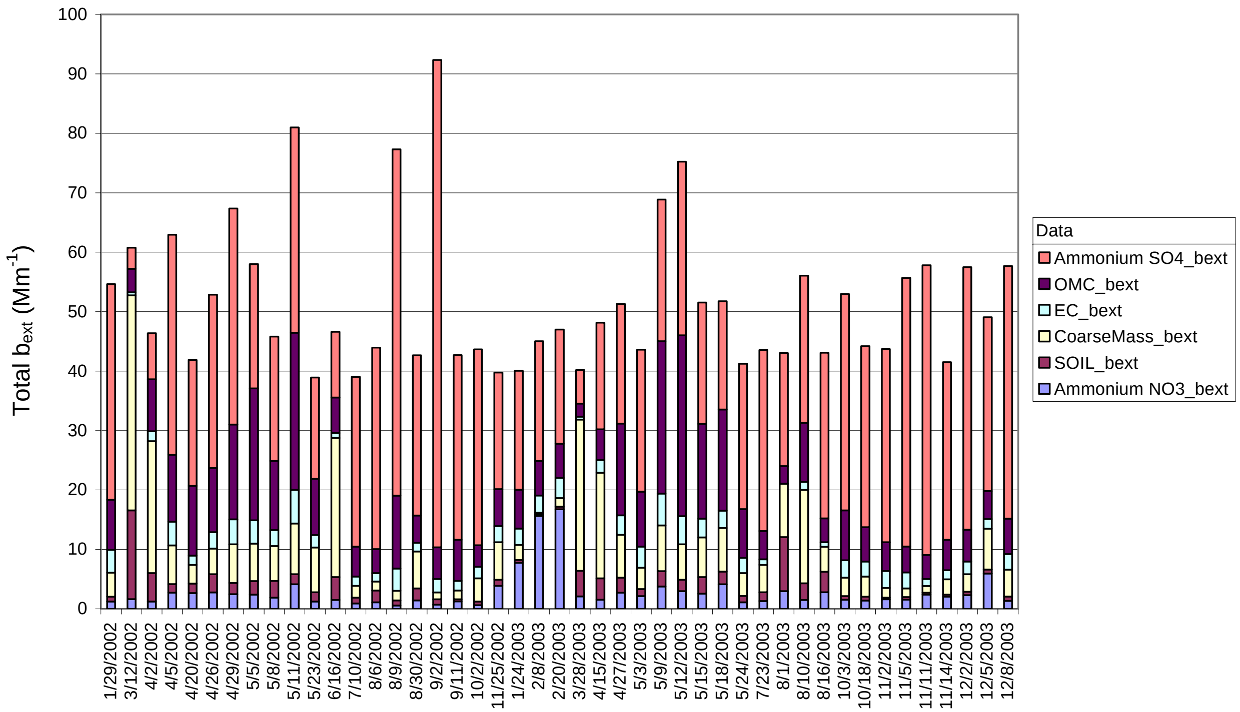

Figure A-10. Extinction (b_{ext}) composition by component (using standard IMPROVE calculations) for the 20%-worst visibility days at Big Bend in 2002-2003.

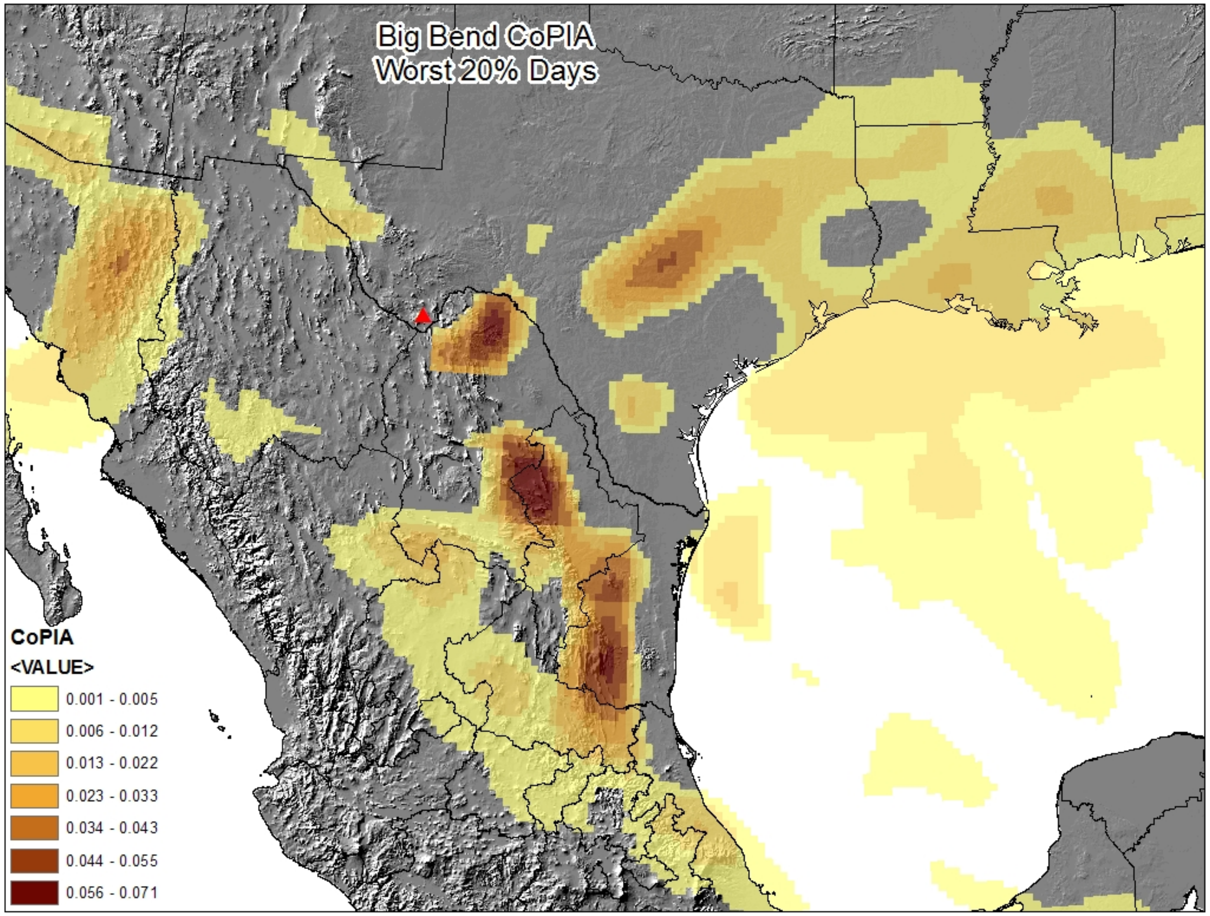

Figure A-11. CoPIA results for the 20%-worst visibility days at Big Bend for 2002-2003.

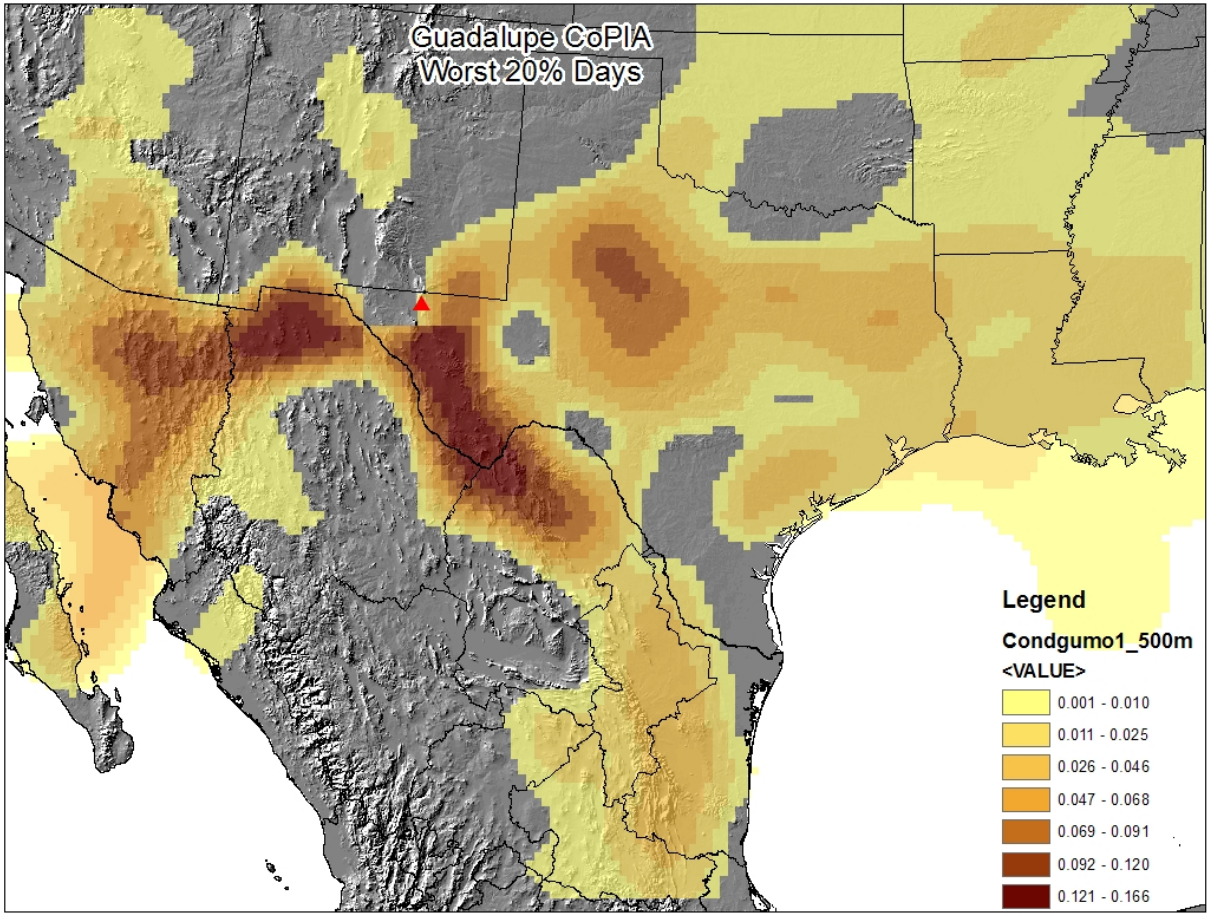

Figure A-12. CoPIA results for the 20%-worst visibility days at Guadalupe for 2002-2003.

A.6 REFERENCES

Ashbaugh L.L., Malm W.C., and Sader W.Z. (1985) A residence time probability analysis of sulfur concentrations at Grand Canyon National Park. *Atmos. Environ.* **19** (8), 1263-1270.

Draxler R.R. and Hess G.D. (1997) Description of the HYSPLIT 4 modeling system. Technical memorandum by NOAA, ERL ARL-224, December 24.

Eder B.K., Davis J.M., and Bloomfield P. (1993) A characterization of the spatiotemporal variability of non-urban ozone concentrations over the eastern United States. *Atmos. Environ.* **27A**, 2645-2668.

Hafner H.R. (2003) Data validation workshop. Prepared for the Lake Michigan Air Directors Consortium and U.S. Environmental Protection Agency, Region V, Chicago, IL, by Sonoma Technology, Inc., Petaluma, CA, STI-903510-2424, October.

Kim E., Hopke P.K., and Edgerton E.S. (2003) Source identification of Atlanta aerosol by positive matrix factorization. *J. Air & Waste Manage. Assoc.* **53**, 731-739.

Kim E. and Hopke P.K. (2004) Improving source identification of fine particles in a rural northeastern U.S. area utilizing temperature-resolved carbon fractions. *J. Geophys. Res.* **109** (D9).

Kim E., Hopke P.K., and Edgerton E.S. (2004) Improving source identification of Atlanta aerosol using temperature resolved carbon fractions in positive matrix factorization. *Atmos. Environ.* **38**, 3349-3362.

Lehman J., Swinton K., Bortnick S., Hamilton C., Baldridge E., Eder B., and Cox B. (2004) Spatio-temporal characterization of tropospheric ozone across the eastern United States. *Atmos. Environ.* **38**, 4357-4369.

Pitchford M.L., Tombach I., Barna M., Gebhart K.A., Green M.C., Knipping E., Kumar N., Malm W.C., Pun B., Schichtel B.A., and Seigneur C. (2004) Big Bend Regional Aerosol and Visibility Observational Study. Final report prepared for the U.S. Environmental Protection Agency, National Park Service and governmental agencies from Mexico, by the National Oceanic and Atmospheric Administration, Las Vegas, NV; Colorado State University, Ft. Collins, CO; National Park Service, Air Resources Division, Ft. Collins, CO; Desert Research Institute, Las Vegas, NV; EPRI, Palo Alto, CA; and Atmospheric and Environmental Research, Inc., San Ramon, CA, September.

APPENDIX B

DOCUMENTATION OF METHODS AND GRAPHICAL AND TABULAR SUMMARIES OF DATA FOR TASK 5

METEOROLOGICAL ANALYSES

B.1 OVERVIEW

The objective of this task was to determine the types of meteorological events that should most concern CENRAP air regulators when considering strategies to improve or protect visibility. To meet this objective, days were clustered based on meteorology and transport characteristics for the four subregions defined in Task 4 for the 20%-best and 20%-worst days. The subregions include Northern Minnesota (represented by Voyageurs), Western Plains (represented by Cedar Bluff), Upper Midwest (represented by Hercules-Glades), and Southeastern Plains (represented by Sikes). The transport and meteorological parameters that were used to define each day were captured in daily schematics. An example of a schematic for one day is shown in **Figure B-1**. The variables shown on the schematic are described below.

- Ensemble backward trajectories. Locations of the backward trajectories for each hour are shown as dots. For each day, the trajectories were run back for 96 hours from each representative site starting at 0000, 0004, 0008, 1200, 1600, and 2000 CST at three levels: 50 m, 300 m, and 700 m above ground level (agl). The hours when trajectories were located in predefined subregions, for all heights and start times, were totaled and are also shown on the plots. The predefined regions are shown in **Figure B-2**. The trajectories indicate the source areas of material that arrived at the site in each subregion.
- 500-mb heights. The height contours of the 500-mb pressure surface are shown as bold lines. The 500-mb height pattern has a strong influence on local and regional meteorology and air quality. In general, a ridge in the 500-mb height pattern is associated with stable boundary conditions and poor air quality, whereas a trough in the 500-mb height pattern is associated with an unstable boundary condition and good air quality.
- Surface temperature. The spatial distribution of surface temperature is shown with colored contours. Surface temperature can influence particle formation. For example, under warm conditions, nitrate will tend to favor the gas phase (i.e., nitric acid); and under cool conditions, particle nitrate formation will be enhanced.

- Morning surface relative humidity, surface wind speed, 700-mb temperature, and the 850-mb temperature and surface temperature difference. These variables are depicted as normalized fingerprint plots in the lower right corner of the schematics. The fingerprints were used to aid in the subjective clustering of days. Relative humidity is important to particle formation. Local winds can affect dispersion of local emissions and strong winds can increase crustal material. The 700-mb temperature and the 850-mb temperature and surface temperature difference are good indicators of atmospheric stability. In general, the larger the value of the 850-mb temperature minus surface temperature difference, the more stable the atmosphere; similarly, the warmer the 700-mb temperature, the more stable the atmosphere. All variables were normalized linearly as presented below. The values used for the normalizations are typical minimum and maximum values that are observed throughout a year, ignoring extreme events. However, in the case of relative humidity, 0% was used as the lower range, even though 0% relative humidity is never observed near the ground. This minimum value was chosen so that the normalized relative humidity values could easily be translated to percentages.
  - Relative humidity is normalized 0 to 1 where 0 is 0% and 1 is 100%.
  - The 700-mb temperature is normalized –1 to 1, where –1 is –25°C and 1 is 25°C.
  - The 850-mb to surface temperature difference is normalized from –1 to 1 where –1 is –15°C and 1 is 15°C.
  - Wind speed is normalized from 0 to 1 where 0 is 0 m/s and 1 is 10 m/s.
- Predominant PM species. The two dominant species that make up $PM_{2.5}$ on each day are shown in the upper left corner of the plot. On the individual plots, nitrate is depicted as N, sulfate as S, organic carbon as OC, elemental carbon as EC, and crustal material as CM. The relative amount of each species is shown by the size of the square.

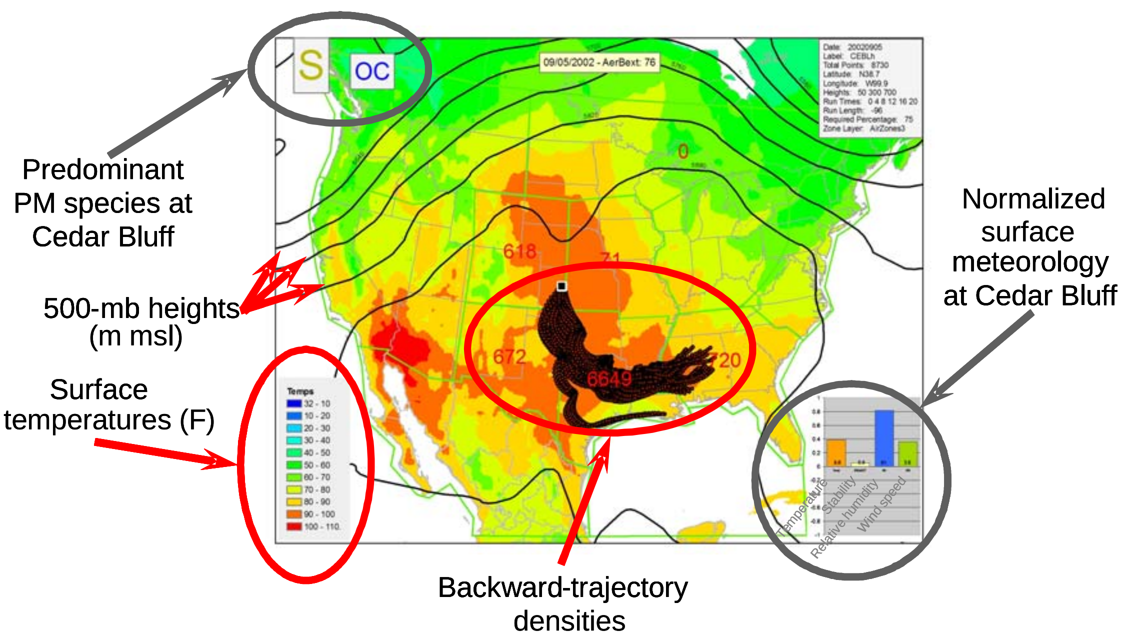

Figure B-1. Example conditions for a 20%-worst visibility day at the Cedar Bluff site.

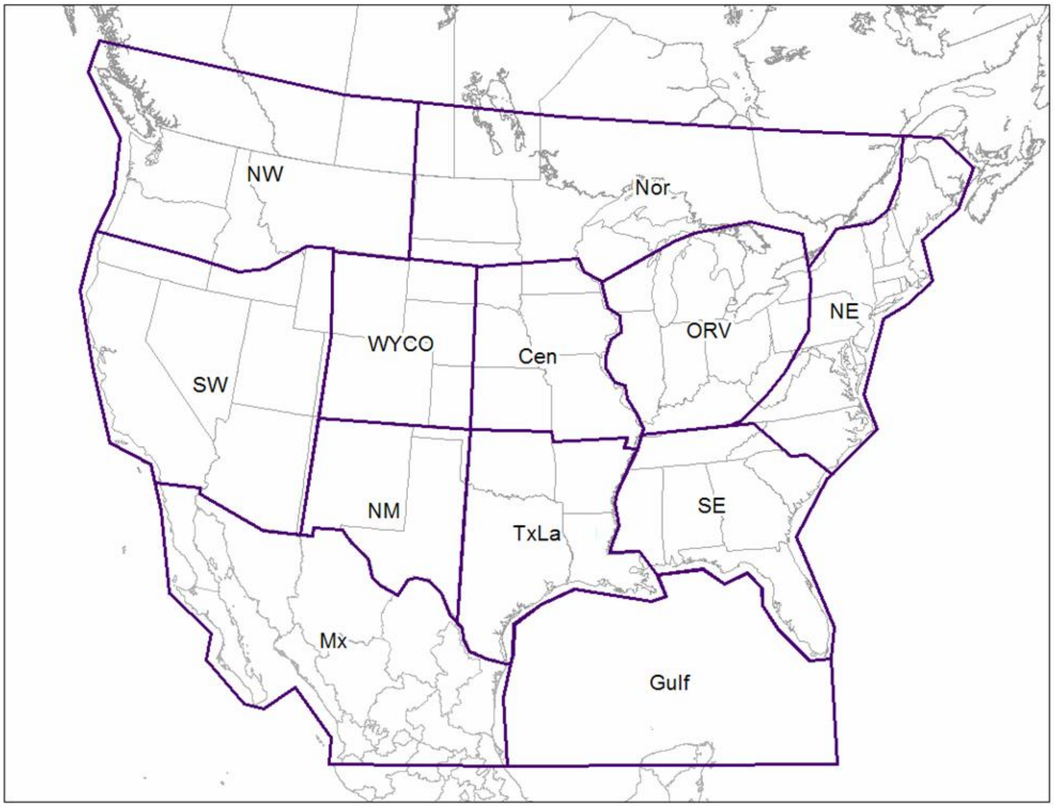

Figure B-2. Source areas defined for parcel residence time counts.

B.2 NORTHERN MINNESOTA SUBREGION

For the Northern Minnesota subregion (represented by the Voyageurs site [VOYA2]), there were five weather/transport day types for the 20%-worst days and three for the 20%-best days. The meteorological and transport characteristics associated with the 20%-worst days are summarized in **Table B-1**; in general, these days were

- characterized by high morning relative humidity (>85%) and
- as likely to occur in the winter as in the summer.

The meteorological and transport characteristics associated with the 20%-best days are summarized in **Table B-2**; in general, these days

- occurred in the cool season,
- were less stable than the 20%-worst days, and
- had a transport direction from the north.

The five weather/transport groups associated with the 20%-worst days at Voyageurs are described below and summarized in Table B-1:

1. <u>Wintertime Westerly Transport</u>. This worst visibility group is the most common, and its conditions occurred on 21 of the 65 days analyzed. $PM_{2.5}$ on the majority of these days was composed mainly of nitrate with some sulfate. This group is characterized by long-range transport from the west-northwest; the Nor source area (see Figure B-2) experienced the most parcel residence time. The meteorological pattern is characterized by an upper-level trough over the east-central or eastern United States, with northwesterly flow aloft over VOYA2. Morning inversions are strong for this group, with the 850-mb to surface-temperature difference at an average of +7.2°C. A good example day for this group is February 18, 2001 (see **Figure B-3**).

2. <u>Warm Season Southeasterly Transport</u>. This group of conditions is the second most common, occurring on 20 of the 65 days studied. $PM_{2.5}$ on the majority of these days was composed mainly of sulfate with some organic carbon. This group is characterized by transport from the south-southeast; two source areas, Cen and Nor (Figure B-2), experienced the most parcel residence time. The meteorological pattern is characterized by an upper-level ridge over the east central United States and a trough in the western United States. A few cases showed very little upper-level dynamics with weak flow aloft. The morning relative humidity was high (~92%). A good example day for this group is September 9, 2003 (see **Figure B-4**).

3. <u>Warm Season Stagnant</u>. These worst visibility group conditions occurred on 10 of the 65 days studied. $PM_{2.5}$ on the majority of these days was composed mainly of organic carbon with some sulfate. Within this group are two subgroups:

   Subgroup A conditions occurred on 7 of the 65 days and are characterized by transport from the west-northwest; the Nor source area (Figure B-2) experienced the most parcel residence time. The meteorological pattern is characterized by a weak upper-level ridge or zonal flow over the central United States and light morning surface winds. A good example day of this group is June 28, 2002 (see **Figure B-5**).

   Subgroup B conditions occurred on 3 of the 65 days and are characterized by medium-range transport from the east-northeast; the Nor and ORV source areas (Figure B-2) experienced the most parcel residence time. The meteorological pattern is characterized by a weak ridge over the central United States, and light morning surface winds. A good example day of this group is May 18, 2003 (see **Figure B-6**).

4. <u>Cool Season Pre-frontal</u>. This group of conditions is one of the least common worst visibility groups, occurring on 7 of the 65 days. $PM_{2.5}$ on the majority of these days was composed mainly of nitrate with some sulfate. This group is characterized by medium-range transport from the south-southwest; the Nor and Cen source areas (Figure B-2) experienced the most parcel residence time. The meteorological pattern is characterized as pre-cold front with an upper-level trough over the Rocky Mountains or west-central United States. This group has the least stability of all the worst visibility groups, and the average morning 700-mb temperature is -11°C. A good example day of this group is December 12, 2001 (see **Figure B-7**).

5. <u>Fall Southwesterly Transport</u>. This group of conditions is another of the least common, occurring on 7 of the 65 days studied. $PM_{2.5}$ on the majority of these days was composed

mainly of sulfate with some organic carbon. This group is characterized by medium-range transport from the southwest; the Nor and WYCO source areas (Figure B-2) experienced the most parcel residence time. The meteorological pattern is characterized by an upper-level ridge over the central U.S. A good example of this group is September 17, 2002 (see **Figure B-8**).

The three weather/transport groups associated with the 20%-best days at Voyageurs are described below and summarized in Table B-2:

1. Wintertime Northwesterly Transport. This best visibility group was the most common, and its conditions occurred on 46 of the 65 days studied. $PM_{2.5}$ on the majority of these days was composed of mainly sulfate with some organic carbon. Within this group are two subgroups. Both subgroups are characterized by medium-range transport from the north-northwest; the Nor source area (Figure B-2) experienced the most parcel residence time.

   Subgroup A conditions occurred on 30 of the 65 days, and the meteorological pattern is characterized by zonal flow aloft or an upper-level trough over the central United States. The average morning 700-mb temperature is -15°C. A good example day of this group is February 8, 2003 (see **Figure B-9**).

   Subgroup B conditions occurred on 16 of the 65 days, and the meteorological pattern is characterized by an upper-level trough over the central United States. Morning surface temperatures are similar to those of Subgroup A. However, morning wind speeds are half as large as those in Subgroup A, and the morning temperature profile is considerably more stable than that of Subgroup A. A good example day of this group is January 19, 2001 (see **Figure B-10**).

2. Spring and Summer Northeasterly Transport. This group of conditions occurred on 10 of the 65 days analyzed. $PM_{2.5}$ on the majority of these days was composed mainly of sulfate and organic carbon. This group is characterized by medium-range transport from the east-northeast; the Nor source area (Figure B-2) experienced the most parcel residence time. It is similar to the Warm Season Stagnant worst visibility group, with the exceptions of lower average wind speeds and lower average relative humidities. Within this group there are two subgroups.

   Subgroup A conditions occurred on 6 of the 65 days, and the meteorological pattern is characterized by an upper-level cutoff low-pressure system over the Plains or Midwest. This group has the lowest average morning relative humidity (78%), and the strongest morning wind speed (4 m/s). A good example day of this group is May 9, 2003 (see **Figure B-11**).

   Subgroup B conditions occurred on 4 of the 65 days. The meteorological pattern is characterized by an upper-level ridge over the west-central United States and lighter morning surface winds than those in Subgroup A (2.6 m/s). A good example day of this group is July 17, 2003 (see **Figure B-12**).

3. Spring Season Split Flow. This group of conditions is the least common of the best visibility groups, occurring on 9 of the 65 days studied. $PM_{2.5}$ on the majority of these days was composed mainly of sulfate with some organic carbon. This group is characterized by long-range transport from split directions, mainly the northwest and

south; the Nor source area (Figure B-2) experienced the most parcel residence time for this group. The meteorological pattern is characterized by both an upper-level trough in the western United States and an upper-level ridge in the eastern United States, or an upper-level ridge in the western United States and an upper-level trough in the eastern United States. The Voyageurs site is located between these upper-level features. A good example day of this group is May 8, 2002 (see **Figure B-13**).

Table B-1. The five weather/transport day types for the 20%-worst visibility days for the Northern Minnesota subregion (represented by Voyageurs [VOYA2]).

		VOYA Worst	Transport						Avg. Calcuations (12Z)			
Group	Dates	Chemistry	Distance	Directiron	Main Source Region	Secondary Source Region	Upper-Air Pattern	Max Temperature	Relative Humidity (%)	850mb Temp - Surface Temp (deg. C)	Wind Speed (m/s)	700mb Temperature (deg. C)
1	12/26/2003 01/04/2001 01/10/2001 01/13/2001 01/22/2001 02/03/2001 02/18/2001 12/09/2001 12/18/2001 01/11/2002 03/12/2002 11/28/2002 12/10/2002 12/13/2002 01/27/2003 01/30/2003 02/26/2003 11/20/2003 12/20/2003 01/26/2002 02/01/2002	N,S	long	W,NW	Nor		trough over the eastern or east-central US. NW flow aloft over YOYA.	Cold season, temperatures near freezing.	86.8	7.2	3	-9
2	06/01/2002 6/28/2002 09/11/2002 06/02/2003 05/26/2002 09/29/2002 07/29/2003	OC,S	medium - long	W,NW	Nor		Zonal flow or weak ridge over central US	Warm season	90.3	0.8	2.3	-4
3a	09/07/2001 07/16/2002 09/02/2002 10/11/2002 06/23/2003 07/02/2003 07/26/2003 08/19/2003 09/09/2003 10/09/2003 10/31/2001 03/16/2003 11/11/2003 08/16/2003 08/25/2003 09/06/2003 07/15/2001 07/18/2001 07/07/2002 08/09/2002	S,OC	long	S,SE	Cen	Nor	Ridge over east central US and a trough in the western US or very weak flow aloft (little dynamics)	Warm season	91.6	1.4	3.8	6.1
3b	05/27/2003 08/07/2003 05/18/2003	OC,S	medium - long	E,NE	Nor	ORV	Weak ridge over central US	Warm season	91.7	1	1.9	2.8
4	03/20/2001 12/12/2001 01/31/2001 03/27/2002 10/26/2002 12/05/2003 03/29/2001	N,S	medium - long	S,SW,W	Nor	Cen	Trough over the rockies or west-central US	Cool season	87.8	-4.9	3.2	-10.7
5	04/19/2001 05/16/2001 11/12/2001 11/15/2001 09/17/2002 10/18/2003 11/06/2001	S,OC	long	S,SW,W	Nor	WYCO	Ridge over the west-central or central US.	Warm season. All events were fall events.	89.4	4.6	2.7	0.7

Table B-2. The three weather/transport day types for the 20%-best visibility days for the Northern Minnesota subregion (represented by Voyageurs [VOYA2]).

		VOYA Best	Transport						Avg. Calcuations (12Z)			
Group	Dates	Chemistry	Distance	Directiron	Main Source Region	Secondary Source Region	Upper-Air Pattern	Max Temperature	Relative Humidity (%)	850mb Temp - Surface Temp (deg. C)	Wind Speed (m/s)	700mb Temperature (deg. C)
1a	03/24/2002 04/20/2002 04/26/2002 05/02/2002 05/17/2002 05/20/2002 09/23/2002 11/25/2002 12/01/2002 01/09/2003 02/08/2003 03/28/2003 04/03/2003 09/24/2003 09/30/2003 10/03/2003 10/15/2003 11/23/2003 10/17/2002 09/15/2003 02/09/2001 03/05/2001 03/08/2001 05/04/2001 10/04/2001 11/27/2001 12/24/2001 12/27/2001 02/16/2002 02/28/2002	S,OC	short-medium	N,NW	Nor		Zonal flow OR trough over the west central US	Primarily cool-cold season events	85.7	-3.4	4.2	-15.2
1b	05/05/2002 12/16/2002 12/31/2002 02/05/2003 02/14/2003 07/23/2003 01/07/2001 01/19/2001 03/11/2001 03/26/2001 06/03/2001 09/22/2001 09/25/2001 12/21/2001 01/29/2002 02/13/2002	S,OC	short-medium	N,NW	Nor		Trough over the central US	Both cool season and warm season events	82.7	4.8	2	-12.5
2a	04/07/2001 12/19/2002 04/15/2003 04/21/2003 05/09/2003 10/30/2003	S,OC	medium-long	E,NE	Nor		Cutoff low over the Plains OR Midwest	Cool season - spring events	77.5	-1.5	4.1	-5.8
2b	08/27/2002 07/17/2003 06/30/2001 08/06/2002	OC,S	short-medium	N,NE	Nor		Ridge over west central US	Warm season (60's 70's)	82.6	-2.2	2.6	3.4
3	05/08/2002 05/14/2002 09/14/2002 10/02/2002 09/03/2003 04/22/2001 05/07/2001 02/19/2002 02/25/2002	S,OC	medium-long	Split: NW and S	Nor		VOYA region is in between a ridge and a trough	Primarily cool-cold season events	83.5	-2	4.1	-4.8

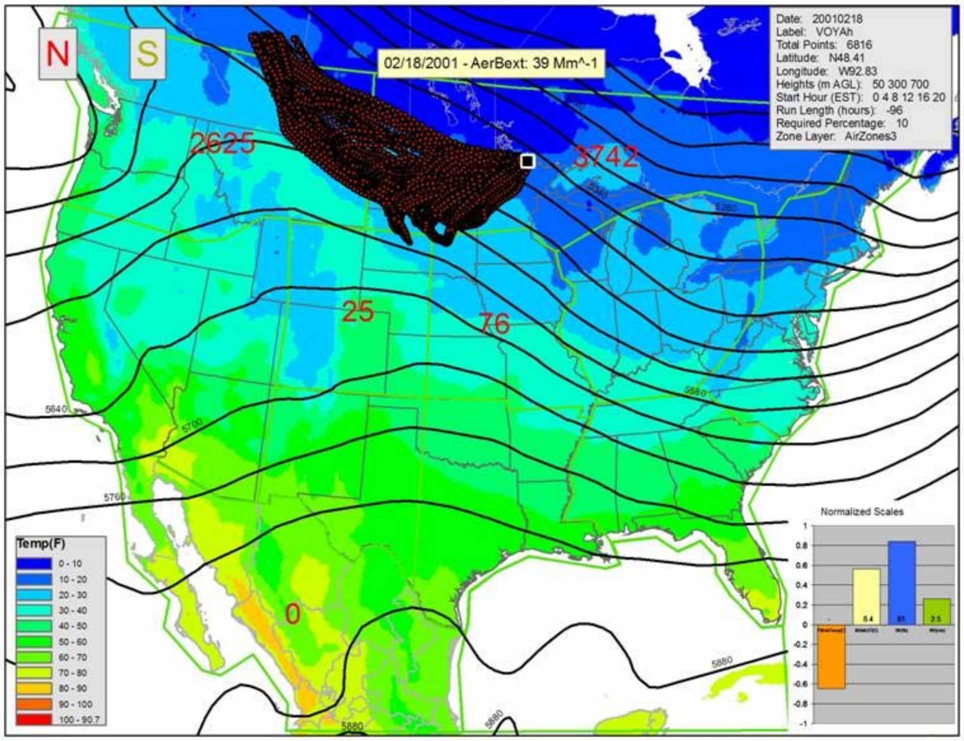

Figure B-3. Wintertime Westerly Transport example.

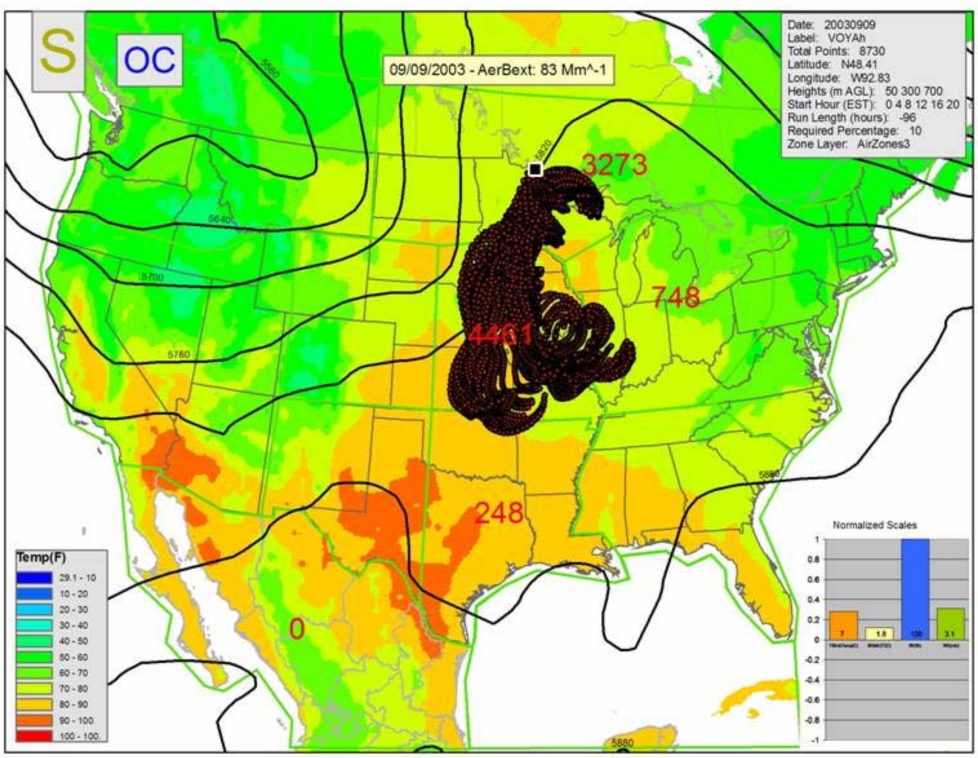

Figure B-4. Warm Season Southeasterly Transport example.

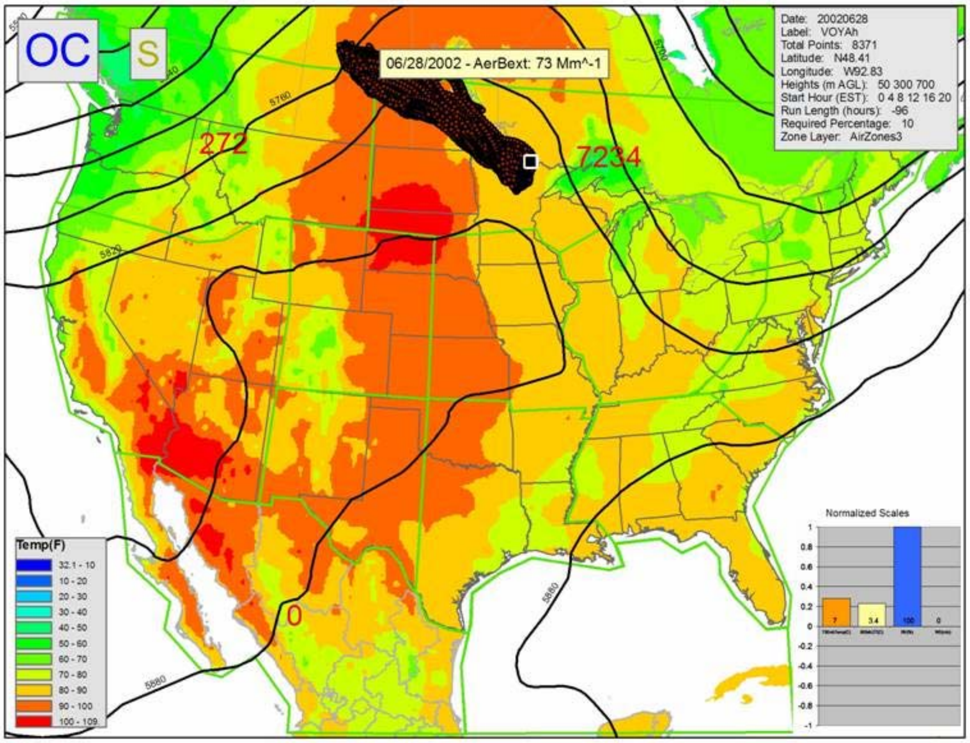

Figure B-5. Warm Season Stagnant – Subgroup A example.

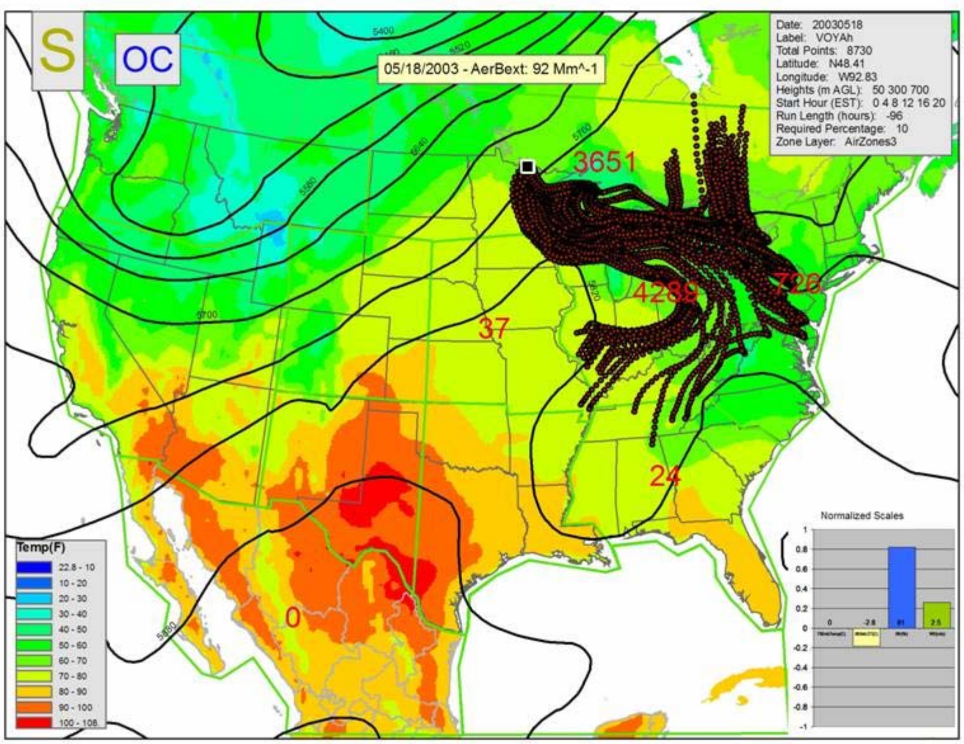

Figure B-6. Warm Season Stagnant – Subgroup B example.

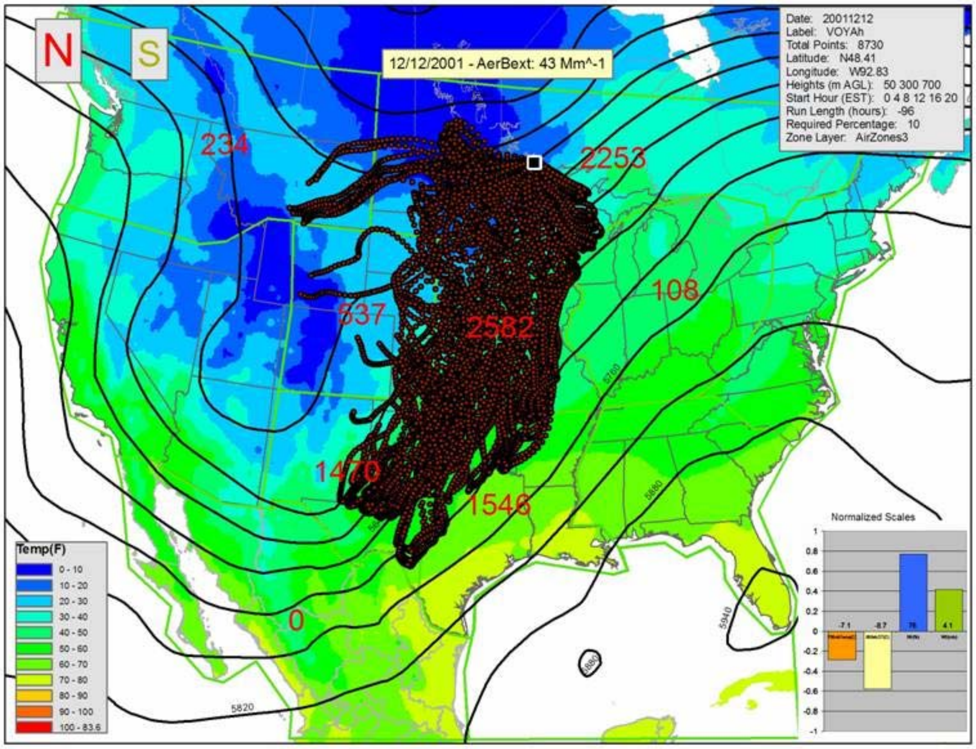

Figure B-7. Cool Season Pre-frontal example.

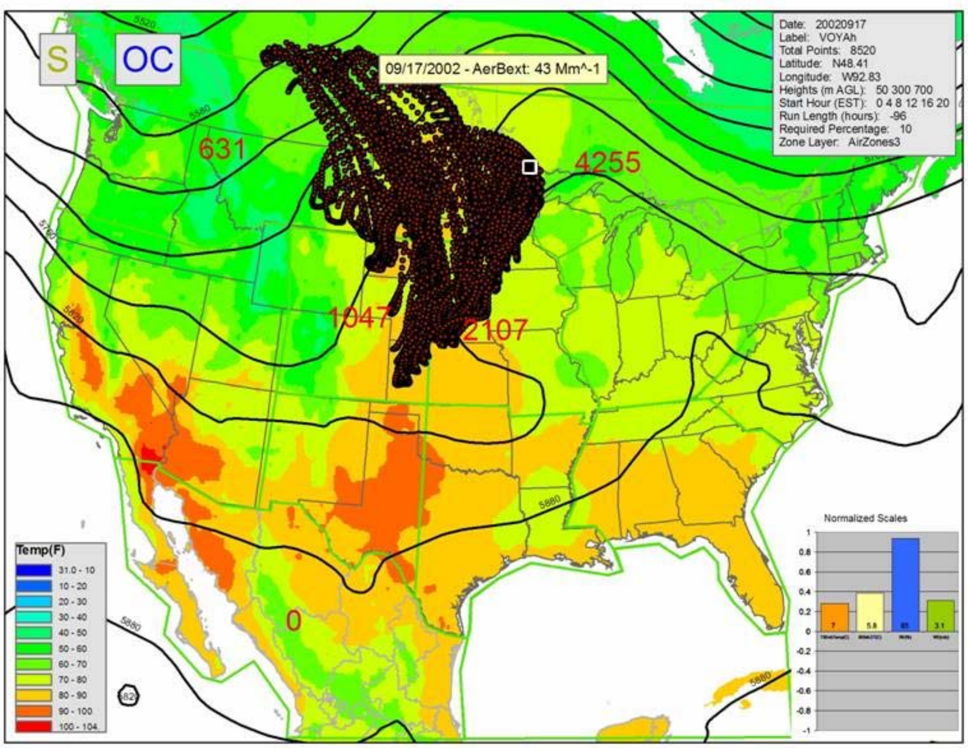

Figure B-8. Fall Southwesterly Transport example.

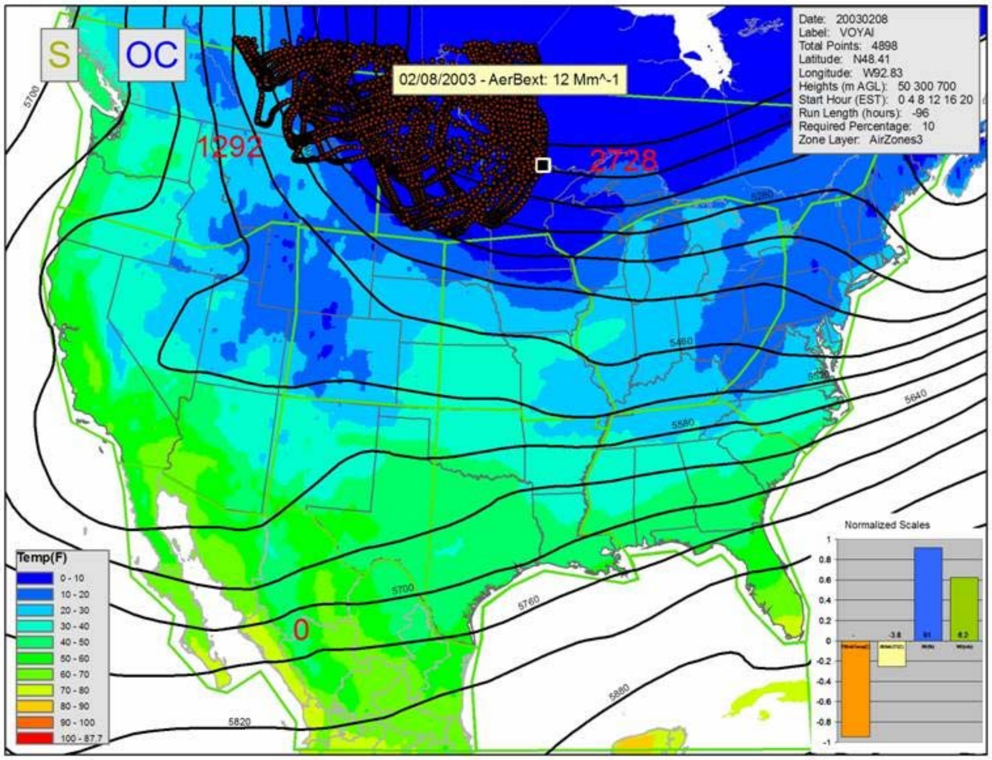

Figure B-9. Wintertime Northwesterly Transport – Subgroup A example.

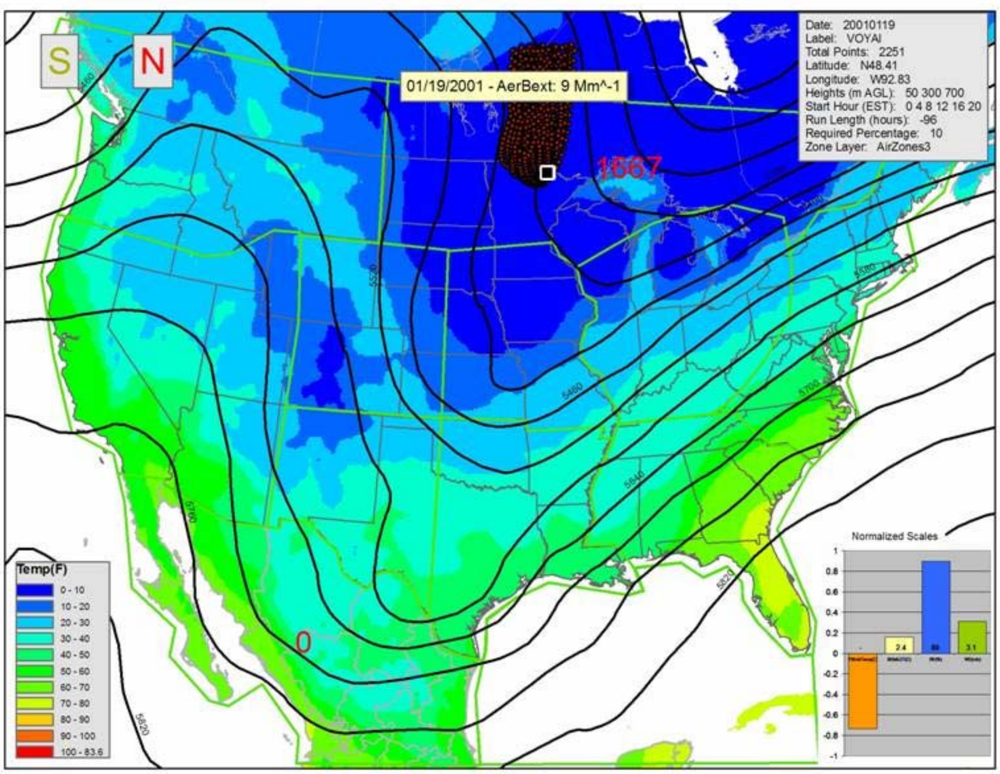

Figure B-10. Wintertime Northwesterly Transport – Subgroup B example.

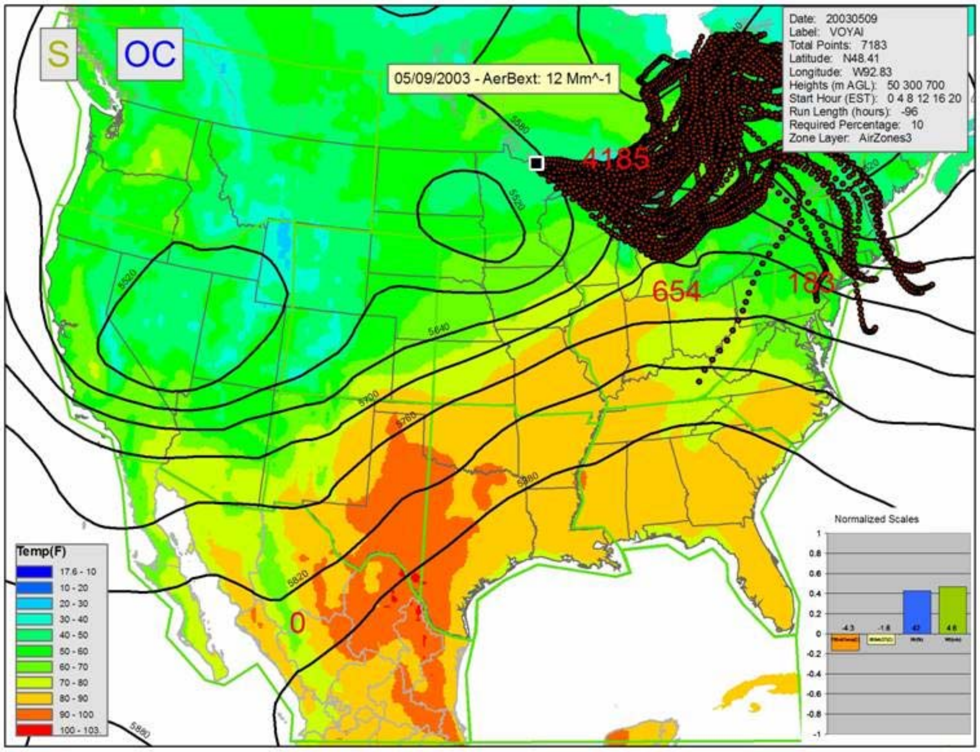

Figure B-11. Spring and Summer Northeasterly Transport – Subgroup A example.

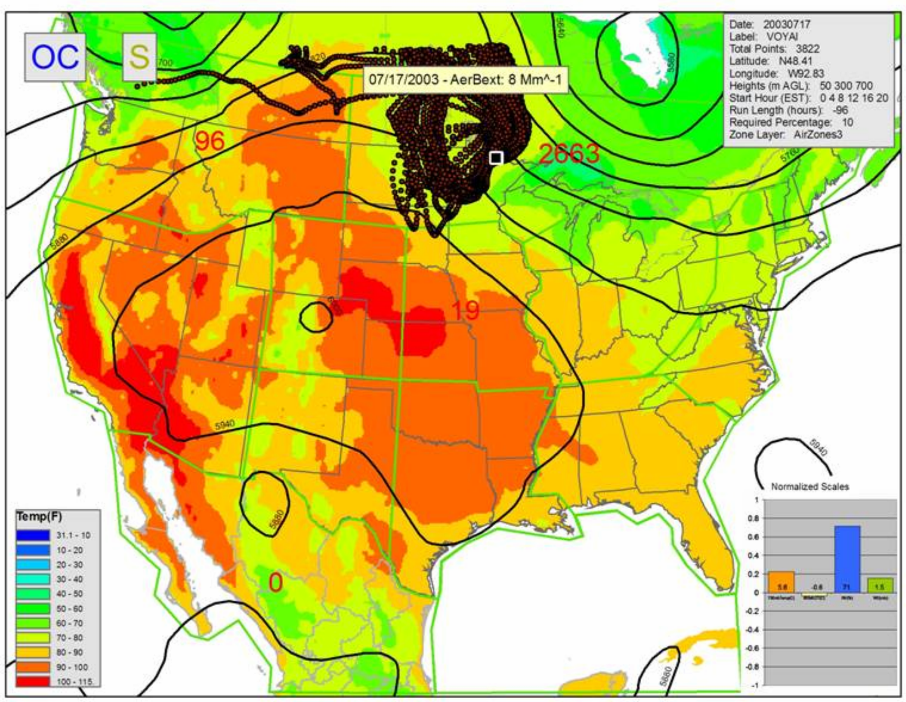

Figure B-12. Spring and Summer Northeasterly Transport – Subgroup B example.

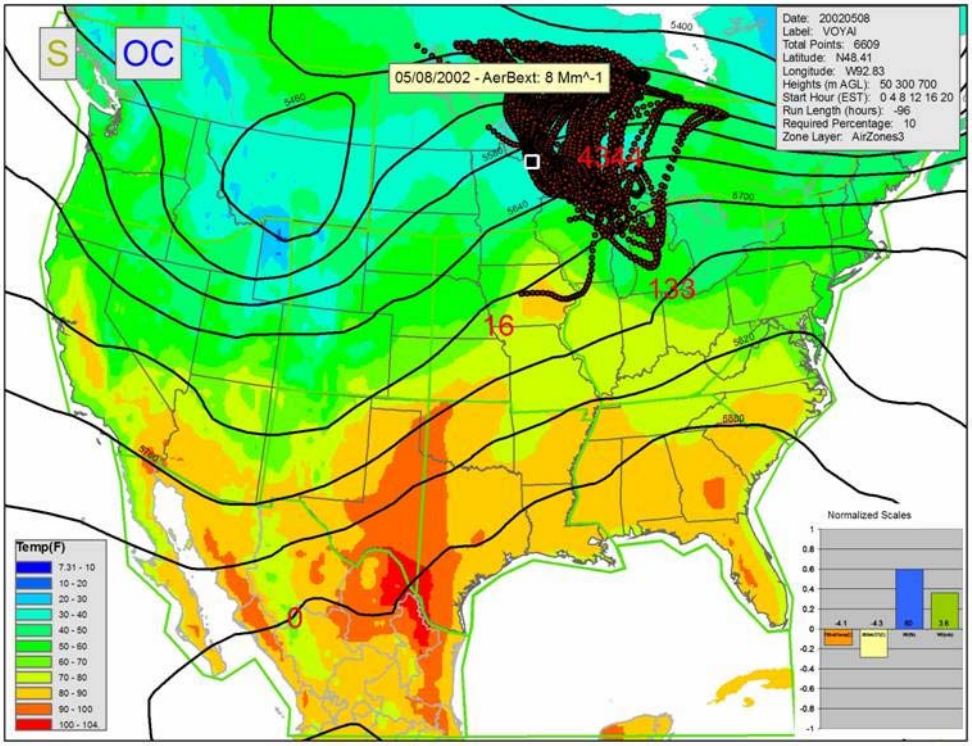

Figure B-13. Spring Season Split Flow example.

B.3 WESTERN PLAINS SUBREGION

For the Western Plains subregion (represented by the Cedar Bluff site [CEBL1], there were four weather/transport day types for the 20%-worst days, and five for the 20%-best days. The meteorological and transport characteristics associated with the 20%-worst days are summarized in **Table B-3**; in general, these days

- occurred equally as often in the wintertime as in the summertime,
- were generally more humid than the days with the best visibility, and
- were characterized by weaker upper-level dynamics than the days with the best visibility.

The meteorological and transport characteristics associated with the 20%-best days are summarized in **Table B-4**; in general, these days

- occurred most often during the cool season (late fall, winter, early spring) and
- were characterized by transport from the west.

The four weather/transport groups associated with the 20%-worst days at Cedar Bluff are described below and summarized Table B-3:

1. Wintertime Regional Re-Circulation. This worst visibility group is the most common and its conditions occurred on 15 of the 33 days analyzed. $PM_{2.5}$ on the majority of these days was composed mainly of nitrate with some sulfate. Within this group are two subgroups:

   Subgroup A conditions occurred on 10 of the 33 days and are characterized by transport from the north-northwest and local recirculation; the Cen and WYCO source areas (Figure B-2) experienced the most parcel residence time. The meteorological pattern is characterized by northwest flow aloft with a trough of low pressure over the eastern United States. A good example day of this group is January 24, 2003 (see **Figure B-14**).

   Subgroup B conditions occurred on 5 of the 33 days and are characterized by transport from split directions (mostly south-southwest and some north-northwest). The meteorological conditions are similar to those in Subgroup A, except for higher relative humidity and warmer 700-mb temperatures. A good example day of this group is March 4, 2003 (see **Figure B-15**).

2. Summertime Southeasterly Transport. This worst visibility group is the second most common and its conditions occurred on 13 of the 33 days studied. $PM_{2.5}$ on the majority of these days was composed mainly of sulfate. Within this group are two subgroups:

   Subgroup A conditions occurred on 7 of the 33 days and are characterized by medium-range transport from the southeast, with additional transport from the Ohio River Valley. The Cen source area (Figure B-2) experienced the most parcel residence time for this group. The meteorological pattern is characterized by very weak flow aloft; the Cedar Bluff site is situated under zonal flow or an upper-level ridge of high pressure. A good example day of this group is June 20, 2003 (see **Figure B-16**).

Subgroup B conditions occurred on 6 of the 33 days and are characterized by transport from the southeastern United States or Gulf of Mexico; the TxLa source area (Figure B-2) experienced the most parcel residence time. The meteorological pattern is characterized by very weak flow aloft; the Cedar Bluff site is situated under zonal flow or an upper-level ridge of high pressure. This group differs from Subgroup A because the transport is longer-range, and there is more morning stability. A good example day of this group is September 5, 2002 (see **Figure B-17**).

3. Wintertime Stagnant. This group of conditions occurred on only 3 of the 33 days. $PM_{2.5}$ on the majority of these days was composed mainly of nitrate with some sulfate. This group is characterized by short-range transport; the WYCO source area (Figure B-2) experienced the most parcel residence time. The meteorological pattern on these days shows very weak flow aloft. A good example day of this group is December 10, 2002 (see **Figure B-18**).

4. Summertime Northeasterly Transport. This group of conditions was the least common, occurring on only 2 of the 33 days analyzed. $PM_{2.5}$ on the majority of these days was composed mainly of sulfate with some organic carbon. This group is characterized by long-range transport from the east-northeast through Illinois, Missouri, and the Great Lakes area; the Cen source areas(Figure B-2) experienced the most parcel residence time. The meteorological pattern is characterized by an upper-level ridge over the central United States, with high relative humidity at the surface. A good example day of this group is August 13, 2003 (see **Figure B-19**).

The five weather/transport groups associated with the 20%-best days at Cedar Bluff are described below and summarized in Table B-4:

1. Late Fall – Winter Northwesterly Flow. This best-visibility group of conditions was the most common and occurred on 12 of the 34 days analyzed. $PM_{2.5}$ on the majority of these days was composed mainly of crustal material and nitrate. This group is characterized by transport from the west-northwest; the WYCO source area (Figure B-2) experienced the most parcel residence time. The meteorological pattern is characterized by an upper-level ridge over the western United States and an upper-level trough over the eastern United States. Despite the crustal material in the $PM_{2.5}$ composition, morning surface winds were no stronger than those in other groups. A good example day is November 22, 2002 (see **Figure B-20**).

2. Fall – Spring Post-Cold Front. This group of conditions was the second most common and occurred on 10 of the 34 days studied. $PM_{2.5}$ on the majority of these days was composed mainly of sulfate with some crustal material. This group is characterized by long-range transport from the northwest; the NW and WYCO source areas (Figure B-2) experienced the most parcel residence time. The meteorological pattern is characterized by a post-cold frontal pattern, a weak to moderately strong upper-level trough over the Cedar Bluff site, or zonal flow aloft. A good example day of this group is September 27, 2003 (see **Figure B-21**).

3. Spring – Summer Pre-Trough. This group of conditions occurred on 5 of the 34 days studied. $PM_{2.5}$ on the majority of these days was composed mainly of sulfate with some

crustal material. This group is characterized by long-range transport from multiple directions, including the south, southwest, and northwest; the TxLa and WYCO source areas (Figure B-2) experienced the most parcel residence time. The meteorological pattern is characterized by an upper-level trough over the western United States, weak upper-level dynamics over the Cedar Bluff site, high relative humidity, and strong winds at the surface. A good example day of this group is May 9, 2003 (see **Figure B-22**).

4. Wintertime Stagnant. This group of conditions occurred on 4 of the 34 days analyzed, and its pattern is similar to that of Summertime Southeasterly Transport for the 20%-worst days. $PM_{2.5}$ on the majority of these days was composed mainly of nitrate with some sulfate. This group is characterized by short-range transport; the WYCO source area (Figure B-2) experienced the most parcel residence time. The meteorological pattern is characterized by an upper-level ridge over the western United States and a trough over the eastern United States. This pattern differs from Group 2 in the 20%-worst days because it shows (1) longer transport and (2) stronger upper-level dynamics. A good example day of this group is November 28, 2002 (see **Figure B-23**).

5. Late Fall Westerly Flow. This group of conditions is the least common and occurred on 3 of the 34 days analyzed. $PM_{2.5}$ on the majority of these days was composed mainly of crustal material with some nitrate. This group is characterized by long transport from the west; the WYCO and NM source areas (Figure B-2) experienced the most parcel residence time. The meteorological pattern is characterized by zonal flow aloft and a low relative humidity at the surface (~60%). The surface winds were relatively strong. A good example day of this group is November 13, 2002 (see **Figure B-24**).

Table B-3. The four weather/transport day types for the 20%-worst visibility days for the Western Plains subregion (represented by Cedar Bluff [CEBL1]).

		CEB Worst	Transport						Avg. Calcuations (12Z)			
Group	Dates	Chemisty	Distance	Directiron	Main Source Region	Secondary Source Region	Upper-Air Pattern	Max Temperature	Relative Humidity (%)	850mb Temp - Surface Temp (deg. C)	Wind Speed (m/s)	700mb Temperature (deg. C)
1a	12/04/2002 12/25/2002 01/21/2003 01/24/2003 02/05/2003 02/26/2003 03/10/2003 10/06/2003 11/08/2003 12/02/2003	N, S	Long	Local Re-circulation	Nor	WYCO	Upper-level trough over the eastern U.S. NW flow over CEB	Cool to cold season. Temperatures mainly below freezing.	79.4	5.7	5	-2.4
1b	03/04/2003 03/07/2003 03/13/2003 04/18/2003 10/03/2003	N, S	Long	Mainly SW with some NW	mixed: NM, WYCO, TxLa		Upper-level trough over the eastern U.S. Zonal flow OR	Cool season. Fall, early spring. Temps near or just above	93.9	6.9	5.2	2.3
2a	08/30/2002 03/19/2003 04/30/2003 05/03/2003 05/18/2003 06/20/2003 08/07/2003	S	Mixed. Some long, some short.	S-SE but with components from the Ohio River Valley	Cen		Weak flow aloft. Zonal flow or under a ridge.	Warm season. Temps in the 80's or above.	88.3	-1.6	5.7	7.4
2b	09/02/2002 09/05/2002 04/27/2003 08/22/2003 08/25/2003 09/09/2003	S, OC	Long	S-SE or from the Gulf of Mexico	TxLa	NM	Weak flow aloft. Zonal or under a ridge.	Warm season. Temps in the 80's or above.	77.5	3.5	4.4	10.7
3	12/10/2002 03/01/2003 12/08/2003	N, S	Short, recirculatio n through	Local. Some north, some south.	WYCO		Weak flow aloft. No deep	Cool season. Temps near or just above	85.9	6.8	3.6	-2.6
4	06/17/2003 08/13/2003	S, OC	Long	E-NE through	Cen		Upper level ridge	Warm season. Temps in the	84.9	1.7	3.4	4.3

Table B-4. The five weather/transport day types for the 20%-best visibility days for the Western Plains subregion (represented by Cedar Bluff [CEBL1]).

		CEB Best	Transport						Avg. Calcuations (12Z)			
Group	Dates	Chemistry	Distance	Directiron	Main Source Region	Secondary Source Region	Upper-Air Pattern	Max Temperature	Relative Humidity (%)	850mb Temp - Surface Temp (deg. C)	Wind Speed (m/s)	700mb Temperature (deg. C)
1	11/22/2002 01/09/2003 01/18/2003 10/15/2003 10/27/2003 11/29/2003 12/13/2002 12/28/2002 01/03/2003 02/11/2003 12/31/2002 03/31/2003	CM,N	Medium	W-NW	WYCO		Ride over the western US and a trough over the east (or a cutoff low just east of the region)	Cool to cold season. Temps near freezing.	68.1	6.4	4.8	-0.3
2	10/20/2002 09/27/2003 10/12/2003 03/25/2003 09/12/2003 12/29/2003 03/28/2003 12/19/2002 10/05/2002 06/08/2003	S,CM	Long	NW	NW	WYCO	Weak to Moderate trough over the region or zonal flow aloft.	Mostly cool season. Late fall, early spring.	76.6	2	4.7	-2.4
3	10/02/2002 09/18/2003 06/29/2003 05/06/2003 05/09/2003	S,CM	Long	Multipe Directions	TxLa	WYCO	Weak trough over the CEB region or very little	Warm season. Temps 60's+	87.5	1.7	5.8	6.4
4	11/07/2002 11/28/2002 11/19/2002 12/05/2003	N,S	Short	W-NW - Slight recirculation from the N.	WYCO		Ride over the western US and a trough over	Cool to cold season. Temps near freezing.	69.5	5.8	5.2	-3.1
5	11/20/2003 11/13/2002 11/10/2002	CM,N	Long	W-SW	WYCO	NM	Zonal flow aloft	Cool season. Late fall events.	59.5	7.1	7.4	2.6

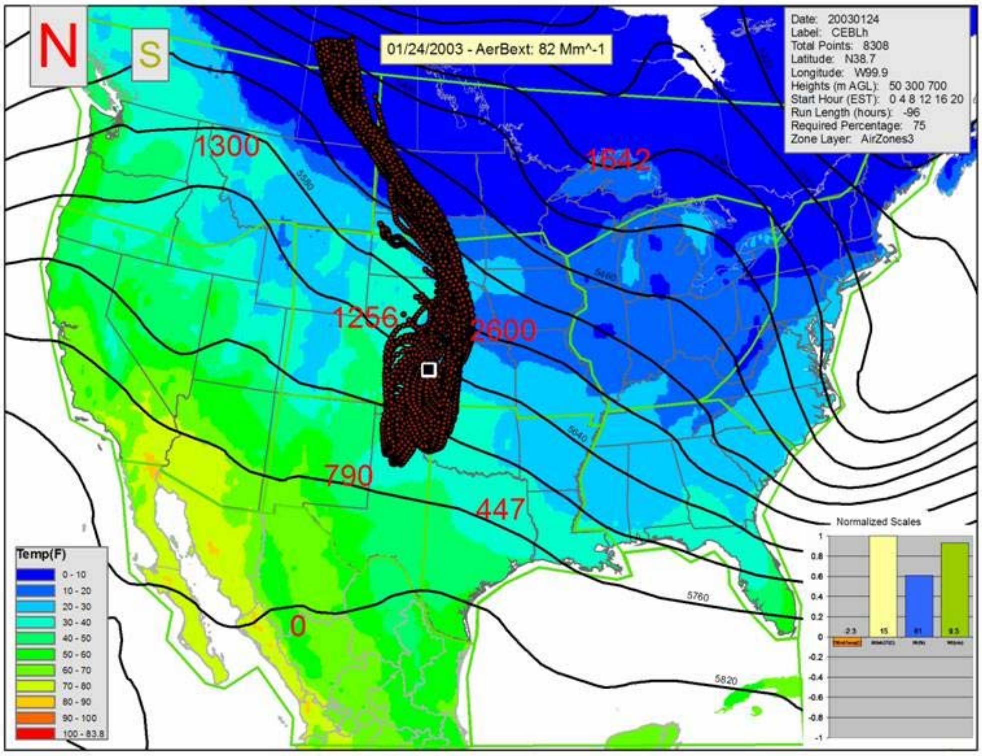

Figure B-14. Wintertime Regional Recirculation – Group A example.

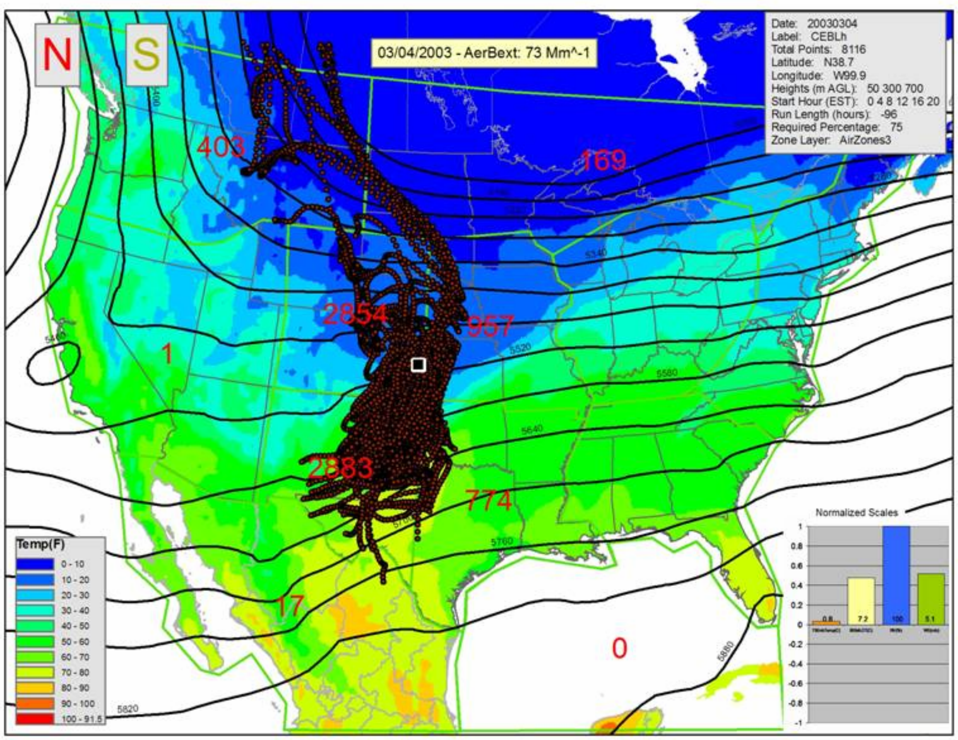

Figure B-15. Wintertime Regional Recirculation – Group B example.

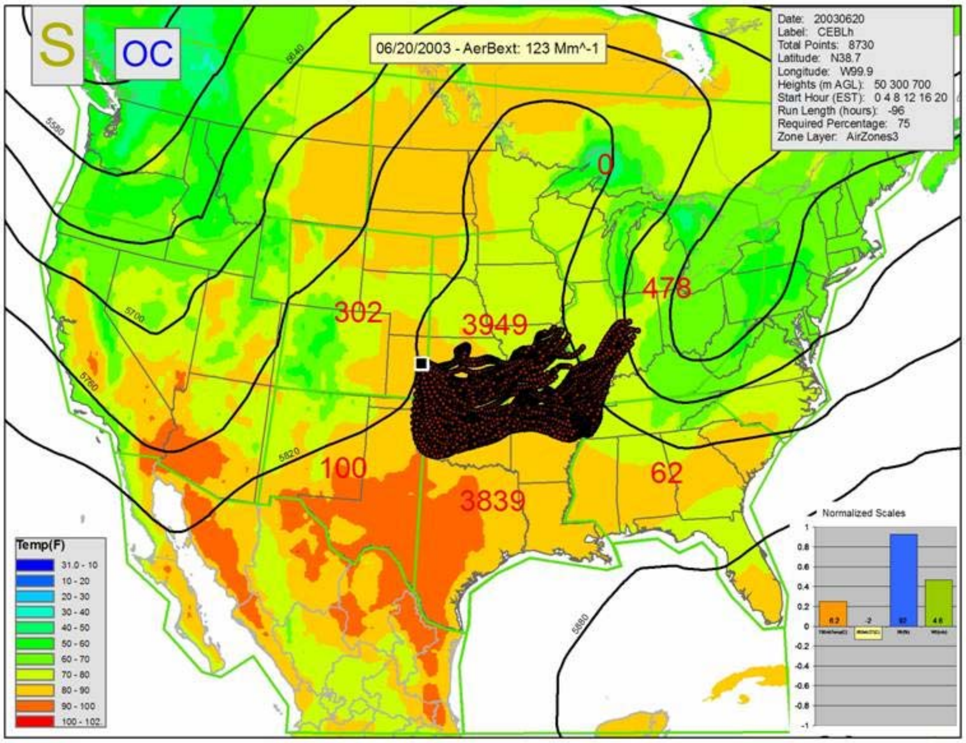

Figure B-16. Summertime Southeasterly Transport – Group A example.

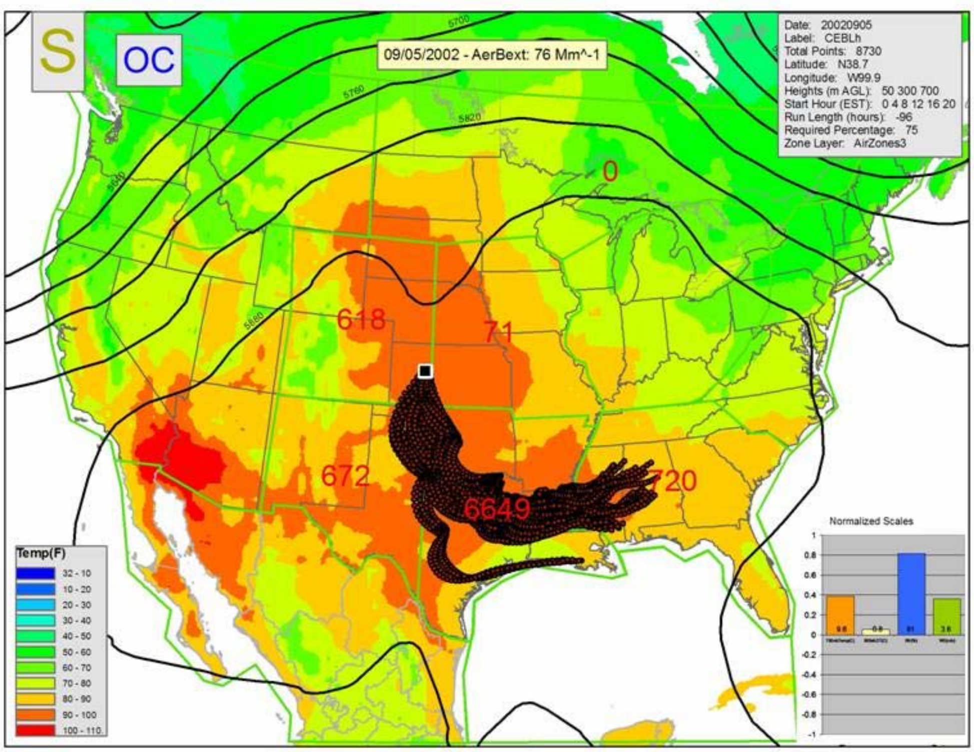

Figure B-17. Summertime Southeasterly Transport – Group B example.

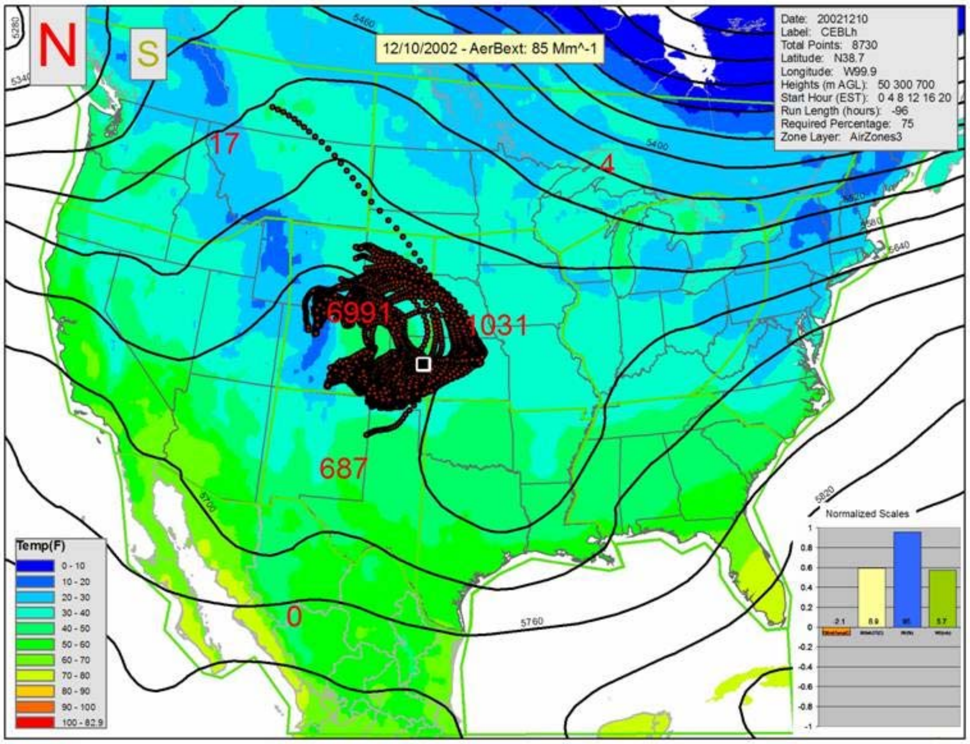

Figure B-18. Wintertime Stagnant example.

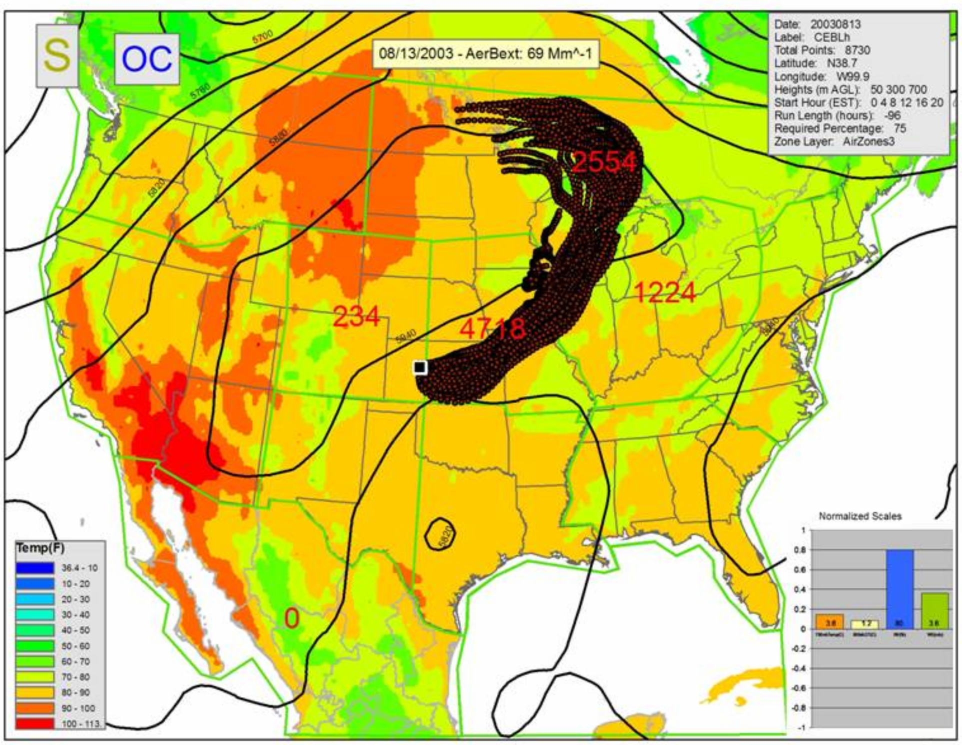

Figure B-19. Summertime Northeasterly Transport example.

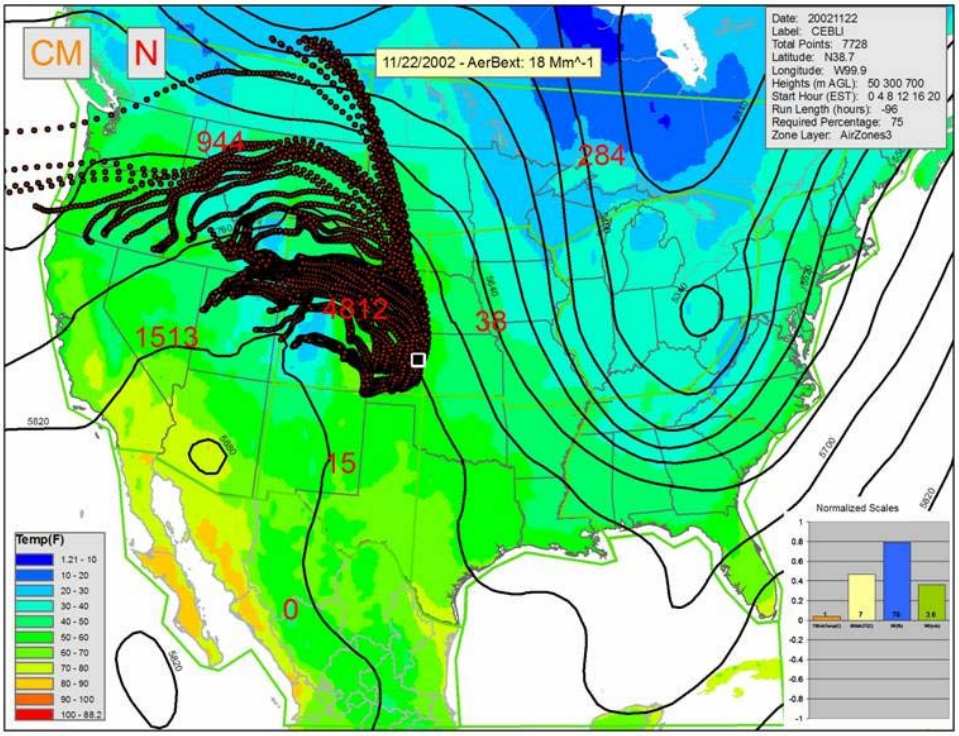

Figure B-20. Late Fall – Winter Northwesterly Flow example.

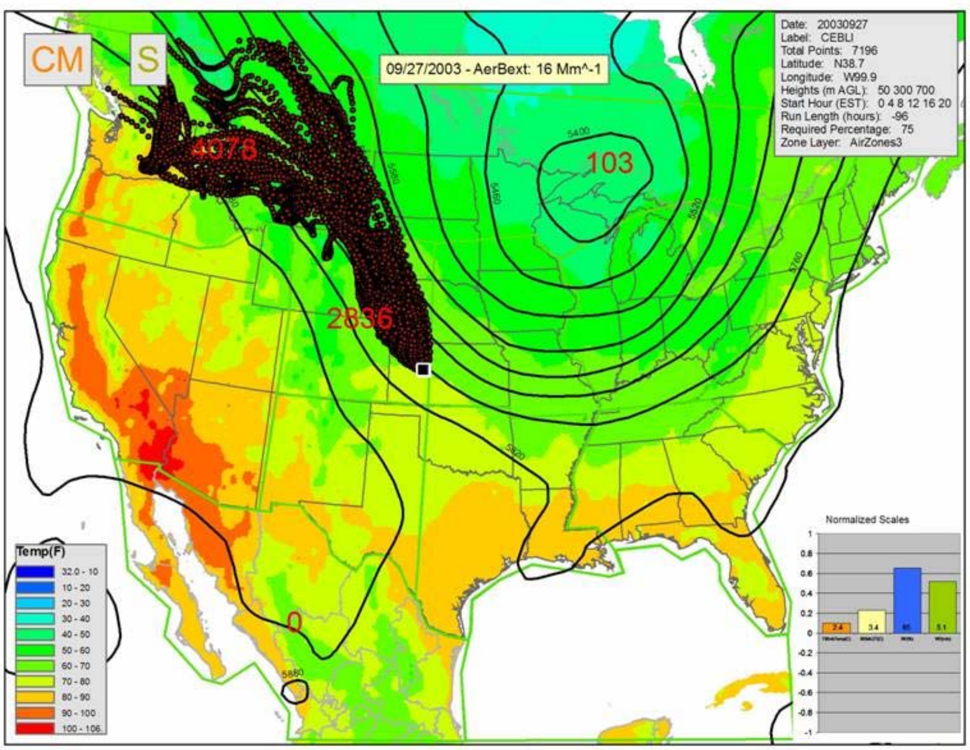

Figure B-21. Fall – Spring Post-Cold Front example.

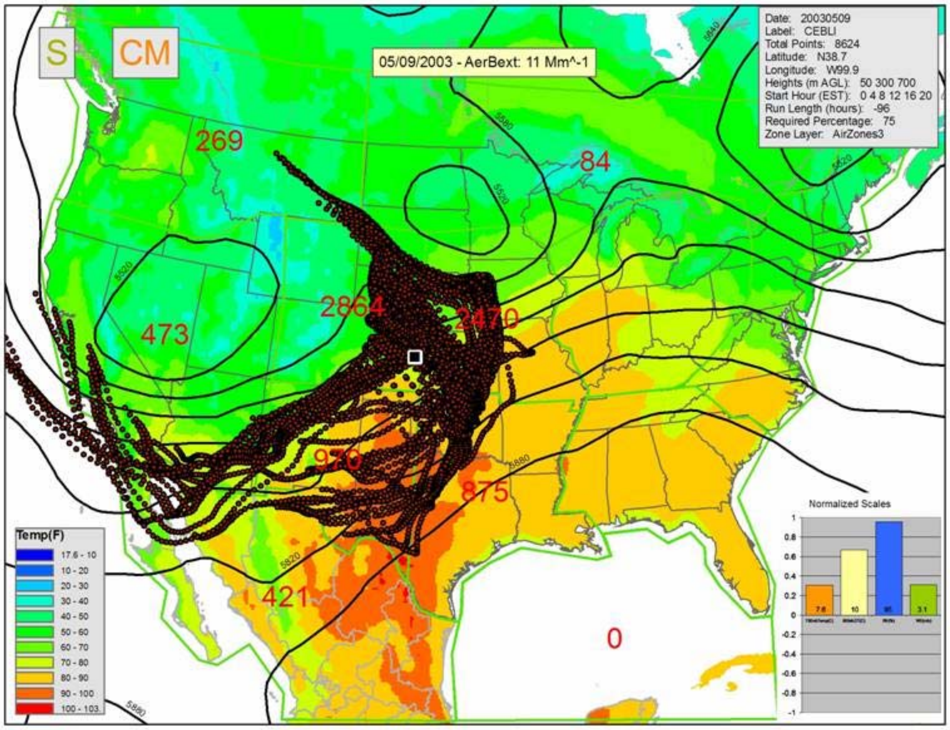

Figure B-22. Spring – Summer Pre-Trough example.

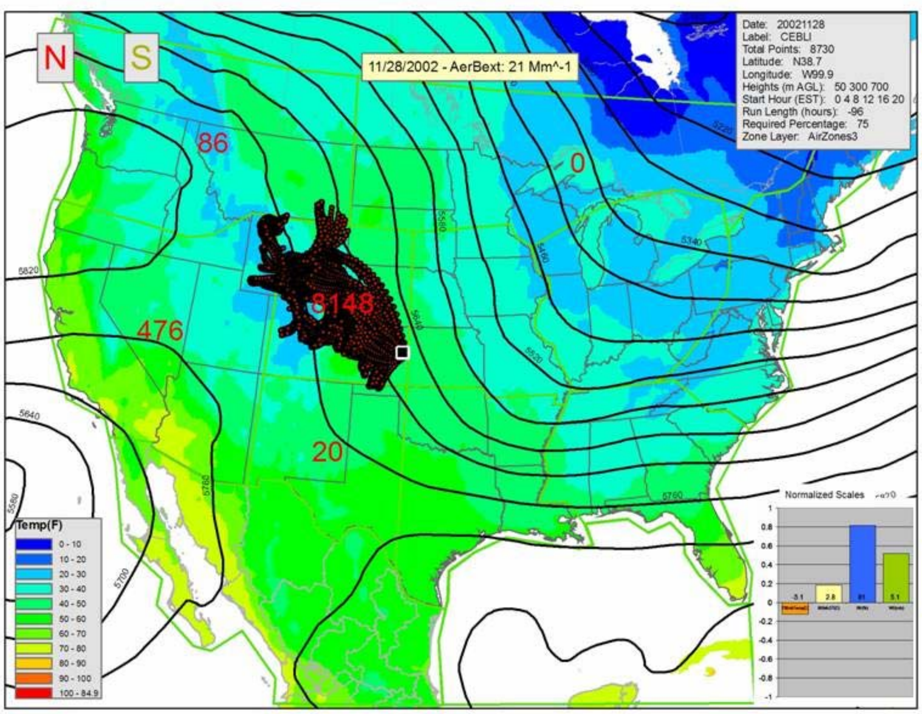

Figure B-23. Wintertime Stagnant example.

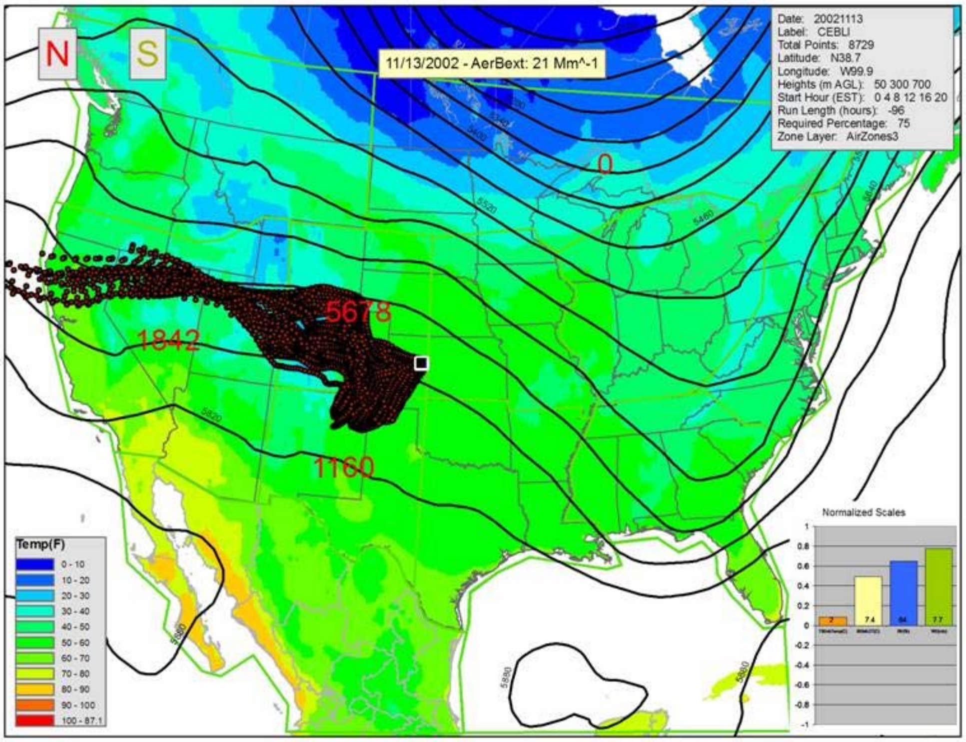

Figure B-24. Late Fall Westerly Flow example.

B.4 UPPER MIDWEST SUBREGION

For the Upper Midwest subregion (represented by the Hercules-Glades site [HEGL1]), there were five weather/transport day types for the 20%-worst days and three for the 20%-best days. The meteorological and transport characteristics associated with the 20%-worst days are summarized in **Table B-5**; in general, these days

- occurred more often in the warm season (late spring, summer, early fall),
- were characterized by sulfate-dominated $PM_{2.5}$ concentrations, and
- frequently showed transport from an easterly or southerly direction

The meteorological and transport characteristics associated with the 20%-best days are summarized in **Table B-6**; in general, these days

- occurred equally as often in the cool season as in the warm season,
- were usually associated with a weather pattern that featured an upper-level trough of low pressure over the central or eastern United States, and
- were characterized by transport from the north-northwest.

The five weather/transport groups associated with the 20%-worst days at Hercules-Glades are described below and summarized in Table B-5:

1. <u>Warm Season Northeasterly Transport</u>. These worst visibility group conditions are the most common and occurred on 26 of the 66 days analyzed. $PM_{2.5}$ on the majority of these days was composed mainly of sulfate with some organic carbon. Within this group are two subgroups:

   Subgroup A conditions occurred on 17 of the 66 days and are characterized by relatively short-range transport from the northeast; the Cen and ORV source areas (Figure B-2) experienced the most parcel residence time. The meteorological conditions are characterized by a weak upper-level ridge over the central United States. A good example day of this group is August 8, 2001 (see **Figure B-25**).

   Subgroup B conditions occurred on 9 of the 66 days and are characterized by long-range northeasterly transport; the ORV source area (Figure B-2) experienced the most parcel residence time. The meteorology is characterized by a weak upper-level pattern, often with zonal winds over the central United States. The relative humidity was generally lower for Subgroup B than for that for Subgroup A. A good example day of this group is August 30, 2002 (see **Figure B-26**).

2. <u>Summertime Southeasterly Transport</u>. These worst visibility group conditions are the second most common and occurred on 21 of the 66 days analyzed. $PM_{2.5}$ on the majority of these days was composed mainly of sulfate with some organic carbon. Within this group are two subgroups:

   Subgroup A conditions occurred on 12 of the 66 days and are characterized by transport from the east-southeast; the SE and TxLa source areas (Figure B-2) experienced the most parcel residence time. The meteorological pattern on these days is characterized by a moderately strong ridge over the eastern United States. A good example day of this group is September 8, 2002 (see **Figure B-27**).

Subgroup B conditions occurred on 9 of the 66 days and are characterized by relatively short-range transport from the southeast; the TxLa and SE source areas (Figure B-2) experienced the most parcel residence time. The meteorological pattern on these days is characterized by a strong ridge over the eastern United States and very warm temperatures. The morning winds for Subgroup B were half the speed of the morning winds for Subgroup A. A good example day of this group is July 21, 2001 (see **Figure B-28**).

3. Warm Season Southerly Transport. This group of conditions occurred most often in the spring on 8 of the 66 days analyzed. $PM_{2.5}$ on the majority of these days was composed mainly of sulfate with some organic carbon. This group is characterized by long-range transport from the south-southeast; the TxLa and Gulf source areas (Figure B-2) experienced the most parcel residence time. The meteorological pattern on these days is characterized by a weak upper-level ridge over the southeastern United States. A good example day of this group is April 30, 2003 (see **Figure B-29**).

4. Cool Season Split Flow. This group of conditions occurred on 6 of the 66 days studied. $PM_{2.5}$ on the majority of these days was composed mainly of nitrate with some sulfate. This group is characterized by long-range transport from several directions, mostly from the north and from recirculation over the Gulf of Mexico; the TxLa source area (Figure B-2) experienced the most parcel residence time. The meteorological pattern on these days is characterized by an upper-level trough over the west-central United States and a relatively strong morning temperature inversion. A good example day of this group is February 25, 2002 (see **Figure B-30**).

5. Cool Season Northwesterly Transport. This group of conditions is the least common of the worst visibility groups and occurred on only 5 of the 66 days analyzed. $PM_{2.5}$ on the majority of these days was composed mainly of nitrate with some sulfate. This group is characterized by transport from the north-northwest; the Cen and Nor source areas (Figure B-2) experienced the most parcel residence time. The meteorological pattern on these days is characterized by a strong upper-level trough over the Great Lakes region and cold, morning 700-mb temperatures. A good example day of this group is January 6, 2003 (see **Figure B-31**).

The three weather/transport groups associated with the 20%-best days at Hercules-Glades are described below and summarized in Table B-6:

1. Northwesterly Transport. These best visibility group conditions are the most common and occurred on 38 of the 67 days analyzed. $PM_{2.5}$ on the majority of these days was composed mainly of sulfate with some nitrate. Within this group are two subgroups:

Subgroup A conditions occurred on 21 of the 67 days and are characterized by long-range transport from the north-northwest; the Cen and Nor source areas (Figure B-2) experienced the most parcel residence time. This subgroup contains an equal number of warm-season and cool-season days. The meteorological pattern is characterized by an upper-level trough over the eastern United States. A good example day of this group is December 1, 2002 (see **Figure B-32**).

Subgroup B conditions occurred on 17 of the 67 days and are characterized by long-range transport from the north-northwest; the Cen and Nor source areas (Figure B-2) experienced the most parcel residence time. This subgroup contains both warm-season and cool-season days; the majority were warm season days. The meteorological pattern is characterized by an upper-level trough or cutoff low pressure system over the central United States and less morning stability than that in Subgroup A. A good example day of this group is June 8, 2003 (see **Figure B-33**).

2. Cool Season Split Flow. These best visibility group conditions are the second most common and occurred on 23 of the 67 days analyzed. $PM_{2.5}$ on the majority of these days was composed mainly of sulfate with some nitrate and organic carbon. Within this group are two subgroups:

   Subgroup A conditions occurred on 17 of the 67 days and are characterized by medium-range transport from several directions; Gulf and TxLa source areas (Figure B-2) experienced the most parcel residence time. The meteorological pattern is characterized by an upper-level trough over the west central United States and many days saw an upper-level cutoff low pressure system over the north central United States. The average morning surface wind speed for this group is also the strongest of all the best visibility groups. A good example day of this group is December 31, 2002 (see **Figure B-34**).

   Subgroup B conditions occurred on 6 of the 67 days and are characterized by medium- and long-range transport from several directions: west, northwest, south, and southeast. No source areas stood out with the most parcel residence time for this group. The meteorological pattern is characterized by a weak upper-level trough over the eastern United States or zonal flow aloft. The morning stability for this group is the highest of all the best visibility groups. A good example day of this group is January 9, 2003 (see **Figure B-35**).

3. Spring Season Recirculating Transport. This group of conditions is the least common and occurred on only 6 of the 67 days analyzed. $PM_{2.5}$ on the majority of these days was composed mainly of sulfate, with some nitrate and organic carbon. This group is characterized by short- to medium-range transport from numerous directions; the Cen source area (Figure B-2) experienced the most parcel residence time. The meteorological pattern is characterized by an upper-level trough over the central or eastern United States. A good example day of this group is March 12, 2002 (see **Figure B-36**).

Table B-5. The five weather/transport day types for the 20%-worst visibility days for the Upper Midwest subregion (represented by Hercules-Glades [HEGL1]).

		HEGL Worst	Transport						Avg. Calcuations (12Z)			
Group	Dates	Chemistry	Distance	Directiron	Main Source Region	Secondary Source Region	Upper-Air Pattern	Max Temperature	Relative Humidity (%)	850mb Temp - Surface Temp (deg. C)	Wind Speed (m/s)	700mb Temperature (deg. C)
1a	06/09/2001 08/05/2001 08/08/2001 09/13/2001 07/25/2002 08/27/2002 09/17/2002 10/23/2002 09/26/2002 06/17/2003 08/07/2003 09/09/2003 06/12/2001 06/27/2001 09/05/2002 12/13/2002 03/16/2003	S,OC	short-medium	N,NE with recirculation over HEGL	Cen	ORV	weak ridge over the central US	Mostly warm season, 70's - 80's. A few cool season cases.	90.6	-1.9	2.7	5.8
1b	04/12/2003 07/15/2001 09/16/2001 07/07/2002 08/09/2002 08/30/2002 09/14/2002 08/13/2003 08/25/2003	S,OC	long	NE	ORV		weak ridge or zonal flow over the central US	Warm season, 70's - 80's	85.1	-1.6	2.5	6.6
2a	11/15/2001 06/22/2002 08/12/2002 09/02/2002 09/08/2002 10/09/2003 05/01/2001 05/04/2001 07/18/2001 05/29/2002 09/29/2002 11/11/2003	S,OC	long	E,SE	SE	TxLa	Ridge over the Eastern US	Warm season, 70's - 80's	89.4	-2.4	5.1	5.2
2b	06/19/2002 07/21/2001 07/24/2001 11/18/2001 06/28/2002 07/10/2002 08/03/2002 08/06/2002 08/19/2003	S,OC	short-medium	SE,S	TxLa	SE	Ridge over the central US	Hot. Summertime pattern. Temps 80's - 90's	88.6	-1.9	2.5	8.4
3	04/18/2003 04/07/2001 05/09/2003 05/18/2003 03/13/2003 04/04/2001 10/04/2001 01/29/2002	S,OC,N	long	SE,S	TxLa	Gulf	Weak upper level ridge over the Southern US	Mild - Warm season temps (50's - 60's)	88.3	-0.8	5.2	6
4	12/14/2003 03/29/2001 01/05/2002 02/25/2002 12/07/2002 12/08/2003	N,S	long	Split directions. Some Northerly, some recirculation	TxLa		Trough over the west-central US	Cool season, 30's - 50's	84.2	2.7	4.1	-2.7
5	03/08/2001 11/16/2002 11/28/2002 10/06/2003 01/06/2003	N,S	long	N,NW	Cen	Nor	trough over the great lakes region	Cool season 40's - 50's	90.9	1.7	3.3	-6.4

Table B-6. The three weather/transport day types for the 20%-best visibility days for the Upper Midwest subregion (represented by Hercules-Glades [HEGL1]).

		HEGL Best	Transport						Avg. Calcuations			
Group	Dates	Chemistry	Distance	Directiron	Main Source Region	Secondary Source Region	Upper-Air Pattern	Surface Temperature	Relative Humidity (%)	850mb Temp - Surface Temp (deg. C)	Wind Speed (m/s)	700mb Temperature (deg. C)
1a	20031015 20010317 20011121 20031220 20031114 20031202 20010820 20010922 20011007 20020923 20021005 20021008 20021014 20021201 20031027 20010413 20010925 20030322 20031018 20021107 20031129	Variable - All types	long	N,NW	Cen	Nor	Trough over the eastern US	Both warm season and cool season cases.	83.7	3.7	2.8	3.7
1b	20020213 20010416 20010910 20011016 20020426 20021017 20030608 20030915 20030927 20030930 20031217 20010522 20011224 20030512 20030723 20011025 20020114	S,N	long	N,NW	Cen	Nor	Trough over central US. A few cases have cutoff lows over the central US.	Both warm season and cool season cases. Primarily more warm season than cool season.	80.1	-3.7	2.6	-3.7
2a	20021219 20021231 20010507 20011124 20020309 20020517 20020815 20030626 20011127 20031229 20021029 20030319 20030702 20031105 20011212 20030214 20031117	S,N	medium	Split directions. Recirculatio n near HEGL from S.	Gulf	TxLa	Trough over west central US. Many cases have a cutoff low over north central US.	Primarily cool season cases.	87.7	-0.5	4.8	-0.5
2b	20020429 20031012 20020126 20030109 20010314 20031120	S,OC	split - half long, half short	Multiple directions	none		Zonal flow or a weak trough over the eastern US.	Primarily cool season cases.	80.8	5.8	3.4	5.8
3	20010615 20020312 20020330 20020423 20020514 20030421	S,N.OC	short to medium	Multiple directions - Local sources	Cen		Trough over central or eastern US.	Cool to mild season (Spring) cases.	83.8	-1.6	3.5	-1.6

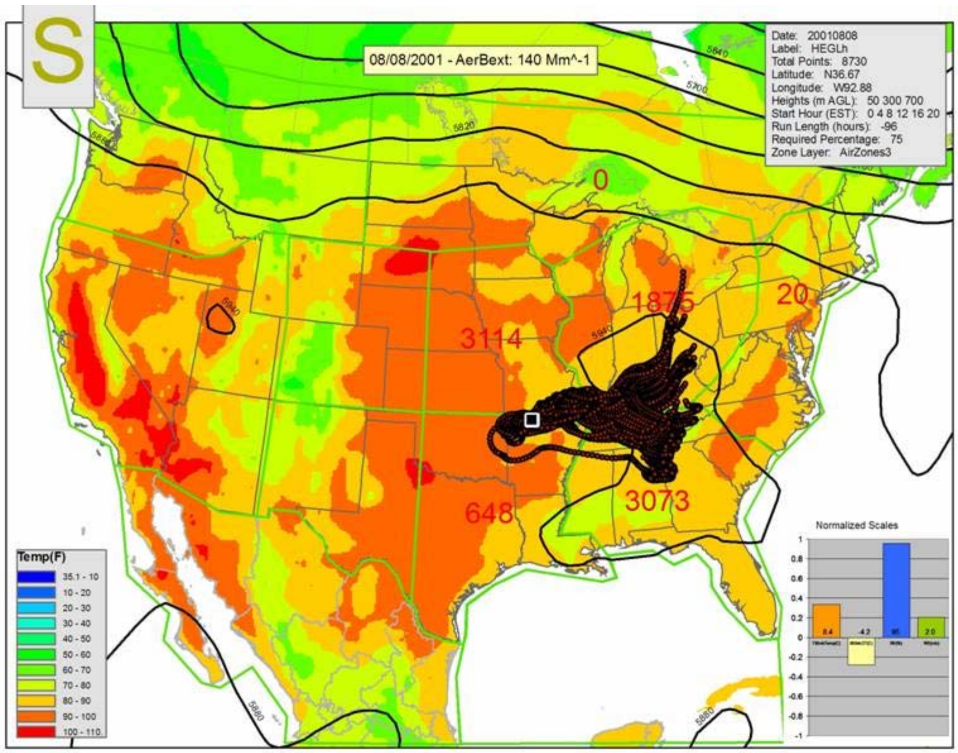

Figure B-25. Warm Season Northeasterly Transport – Subgroup A example.

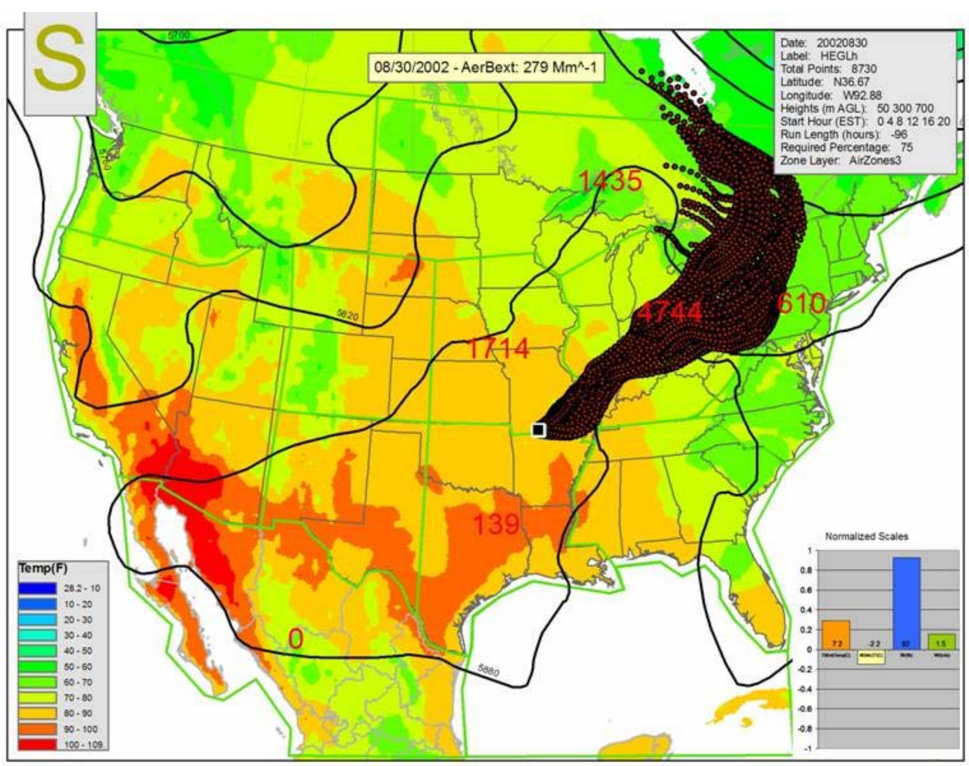

Figure B-26. Warm Season Northeasterly Transport – Subgroup B example.

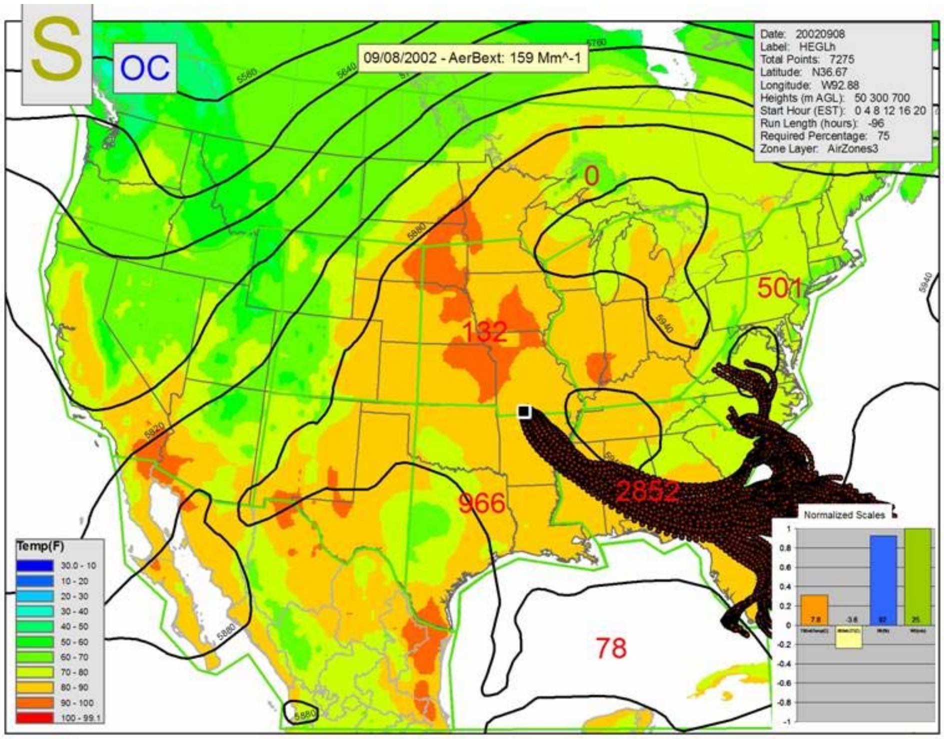

Figure B-27. Summertime Southeasterly Transport – Subgroup A example.

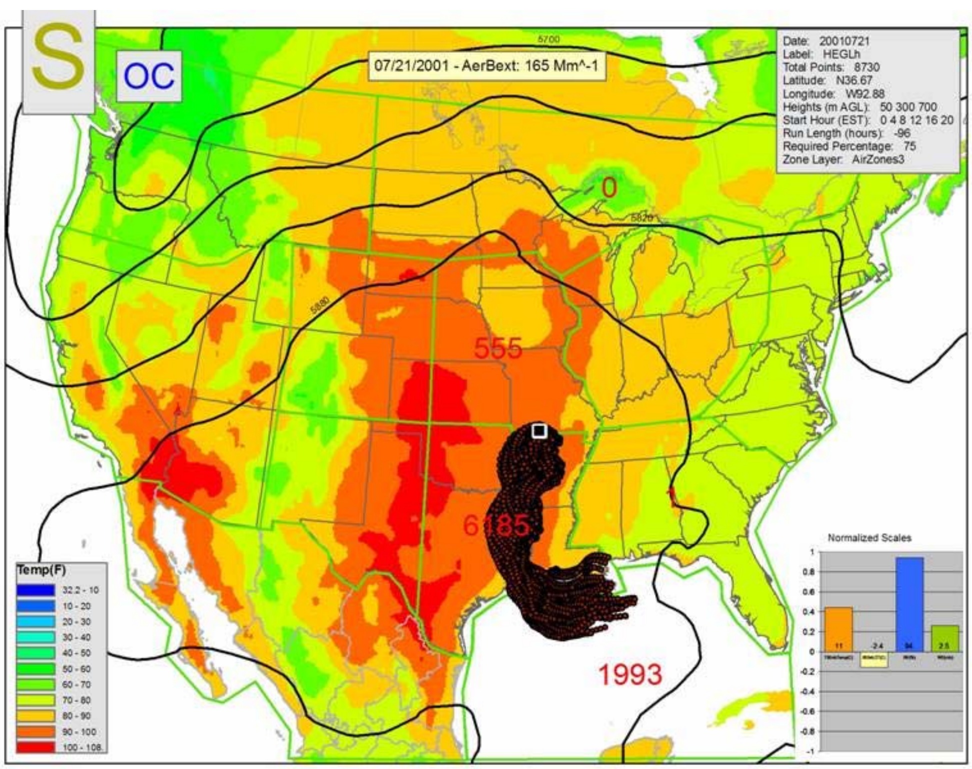

Figure B-28. Summertime Southeasterly Transport – Subgroup B example.

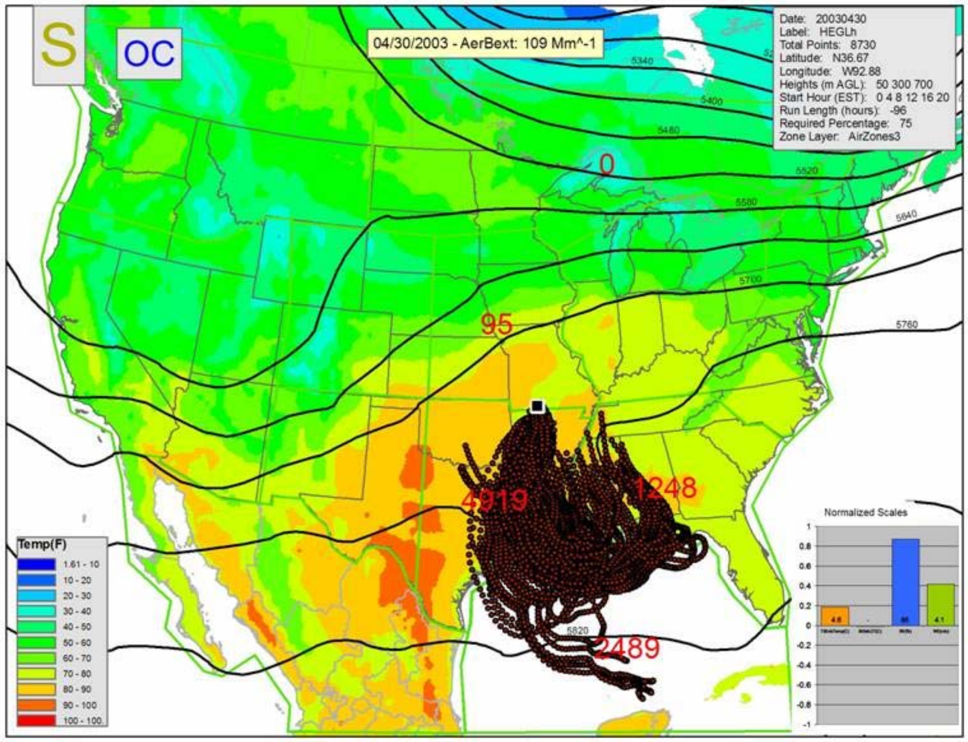

Figure B-29. Warm Season Southerly Transport example.

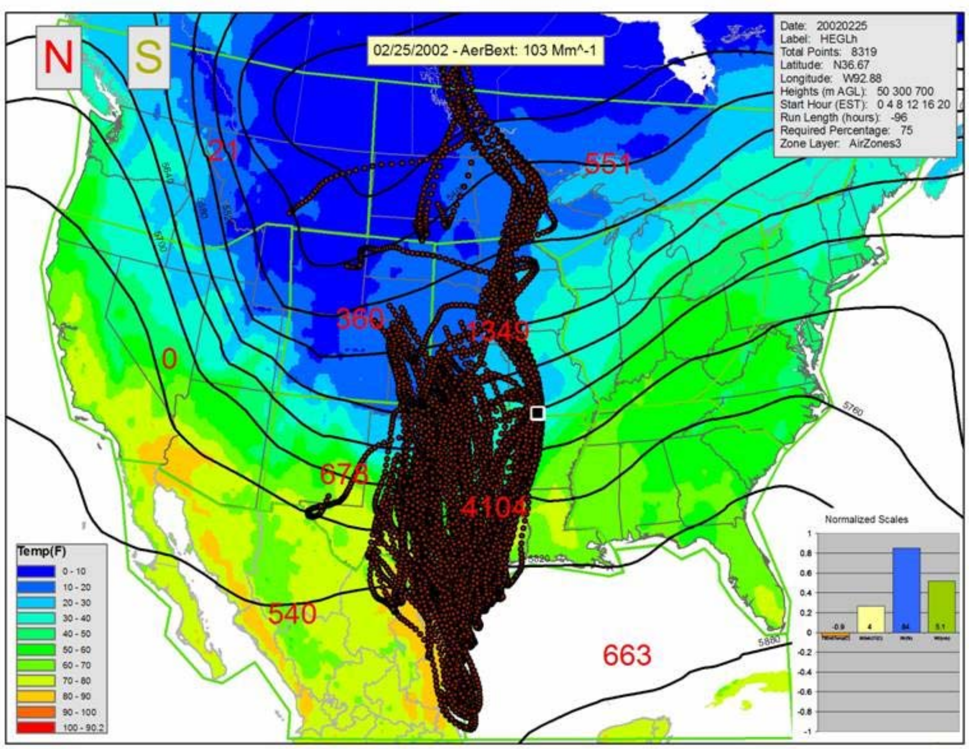

Figure B-30. Cool Season Split Flow example.

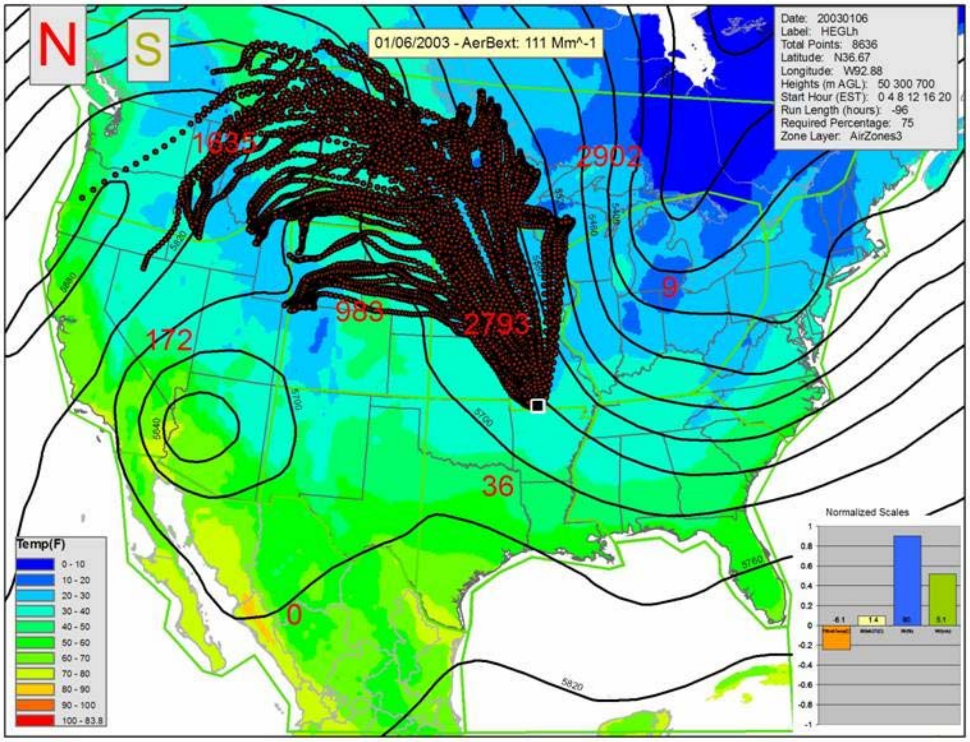

Figure B-31. Cool Season Northwesterly Transport example.

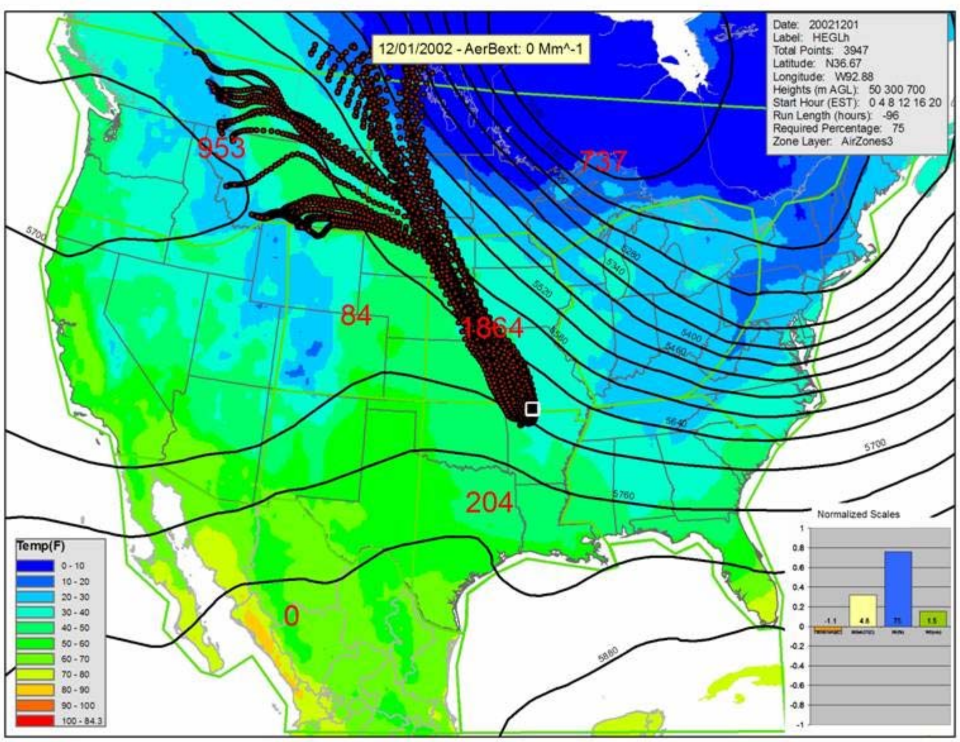

Figure B-32. Northwesterly Transport – Subgroup A example.

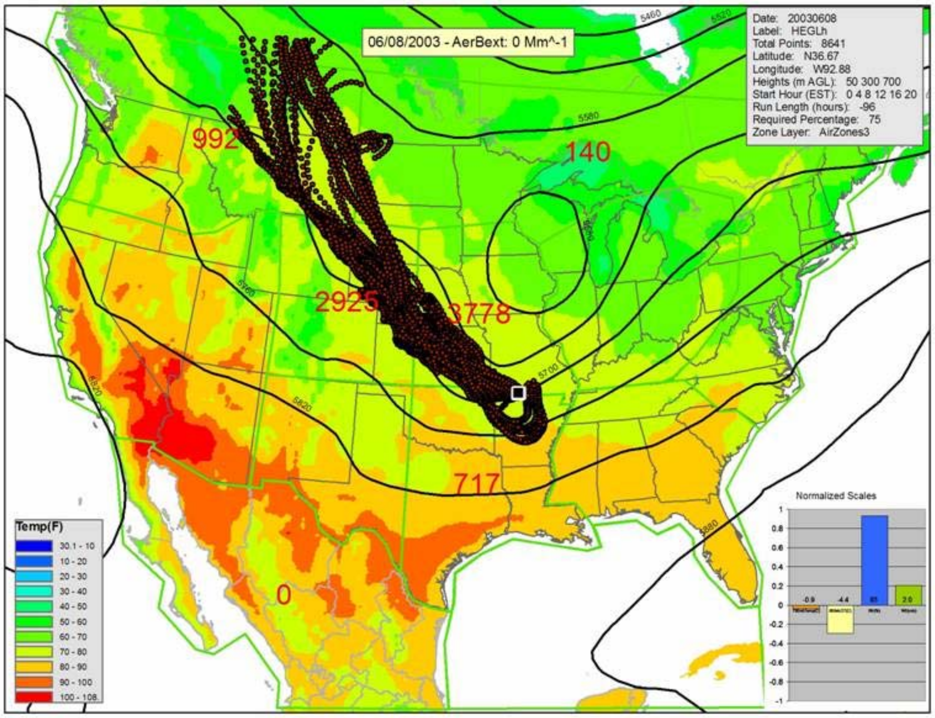

Figure B-33. Northwesterly Transport – Subgroup B example.

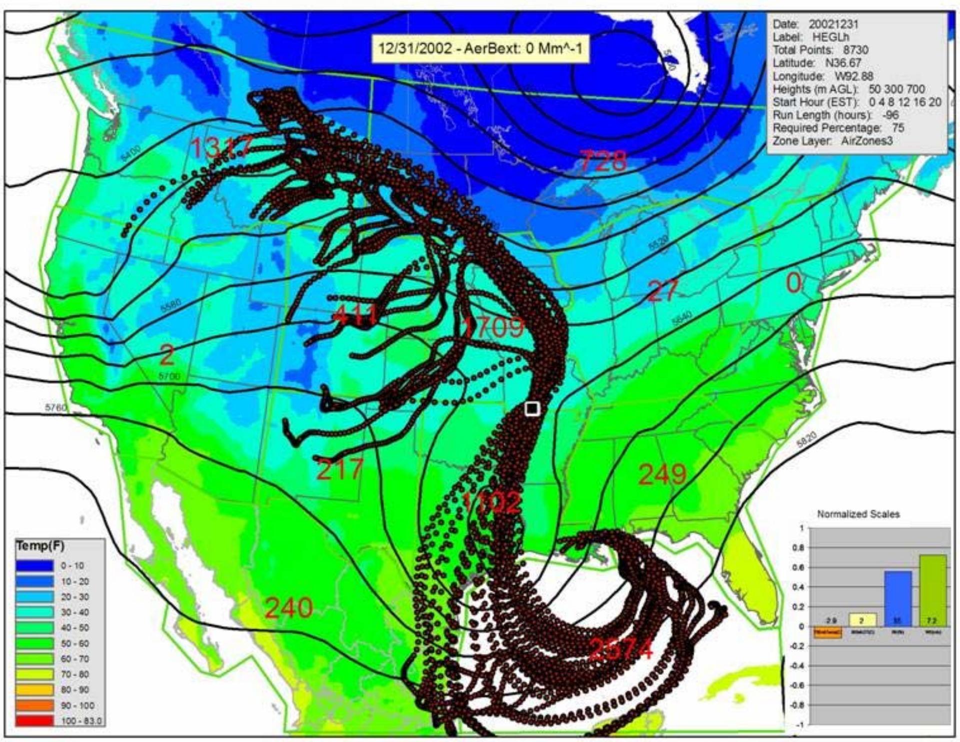

Figure B-34. Cool Season Split Flow – Subgroup A example.

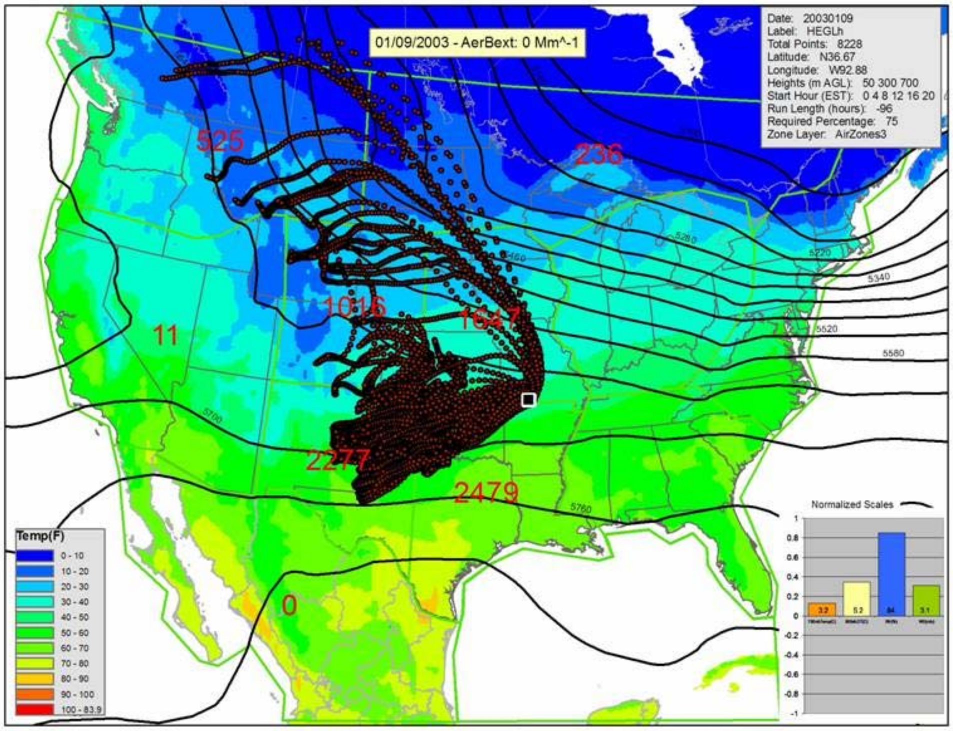

Figure B-35. Cool Season Split Flow – Subgroup B example.

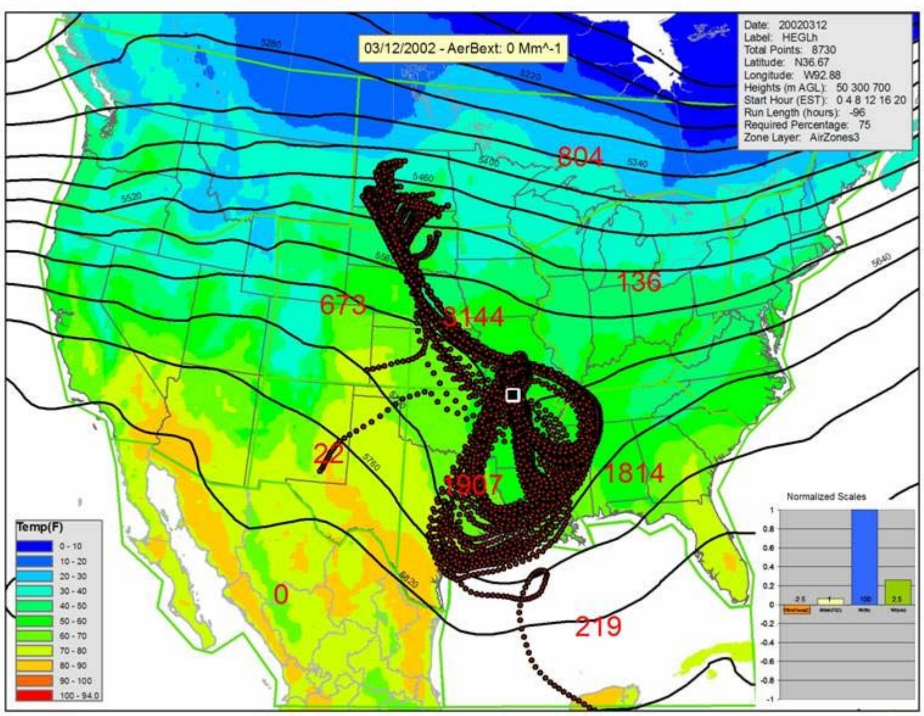

Figure B-36. Spring Season Recirculating Transport example.

B.5 SOUTHEASTERN PLAINS SUBREGION

For the Southeastern Plains subregion (represented by Sikes [SIKE1]), there were four weather/transport day types for the 20%-worst days and four for the 20%-best days. The meteorological and transport characteristics associated with the 20%-worst days are summarized in **Table B-7**; in general, these days were characterized by

- transport from the SE or NE,
- high humidity and light winds, and
- $PM_{2.5}$ consisting primarily of sulfate.

The meteorological and transport characteristics associated with the 20%-best days are summarized in **Table B-8**; in general, these days were characterized by

- transport from the NW and
- cool season temperatures.

The four weather/transport groups associated with the 20%-worst days at Sikes are described below and summarized in Table B-7:

1. Summertime Ridge. This worst visibility group of conditions is the most common and occurred on 29 of 57 days analyzed. $PM_{2.5}$ on the majority of these days was composed mainly of sulfate with some organic carbon. Within this group are two subgroups. The meteorological pattern for both subgroups is characterized by an upper-level ridge over the central or eastern United States, very warm surface temperatures, light morning winds, and high relative humidity.

   Subgroup A conditions occurred on 16 of the 57 days and are characterized by long-range transport from the east-southeast; the SE and Gulf source areas (Figure B-2) experienced the most parcel residence time. A good example day of this group is August 16, 2003 (see **Figure B-37**).

   Subgroup B conditions occurred on 13 of the 57 days and are characterized by short- to medium-range transport circulating clockwise through the Gulf of Mexico and up to Sikes from the south. The Gulf and TxLa source areas (Figure B-2) experienced the most parcel residence time. A good example day of this group is July 21, 2001 (see **Figure B-38**).

2. Warm Season Northeasterly Transport. This group of conditions is the second most common and occurred on 13 of the 57 days studied. $PM_{2.5}$ on the majority of these days was composed mainly of sulfate with some organic carbon. This group is characterized by long-range transport from the northeast; the ORV and SE source areas (Figure B-2) experienced the most parcel residence time. The meteorological pattern is characterized by an upper-level trough or cutoff low over the eastern United States. A good example day of this group is August 10, 2003 (see **Figure B-39**).

3. Warm Season Stagnant. This group of conditions occurred on 9 of the 57 days analyzed. $PM_{2.5}$ on the majority of these days was composed mainly of sulfate with some organic carbon. This group is characterized by short-range transport from numerous directions;

the TxLa and SE source areas (Figure B-2) experienced the most parcel residence time. The meteorological pattern is characterized by an upper-level ridge over the west-central United States and/or an upper-level trough over the northeastern United States. This group has the highest average morning relative humidity (93%) and the lowest average morning wind speed (1.4 m/s) of all the worst visibility groups. A good example of this group day is June 20, 2003 (see **Figure B-40**).

4. Cool Season Split Flow. This group of conditions is the least common of the worst visibility groups, occurring on only 6 of the 57 days. $PM_{2.5}$ on the majority of these days was composed mainly of sulfate and nitrate with some organic carbon. This group is characterized by transport from split directions, mainly the north-northwest and south; the TxLa source areas (Figure B-2) experienced the most parcel residence time. The meteorological pattern is characterized by an upper-level trough over the Northeast with northwest flow over the Sikes site. This group has the lowest average morning humidity (85%) and highest average morning wind speed (3.5 m/s) of all the worst visibility groups. A good example day of this group is January 9, 2003 (see **Figure B-41**).

The four weather/transport groups associated with the 20%-best days at Sikes are described below and summarized in Table B-8:

1. Wintertime Northwesterly Transport. This best visibility group of conditions is the most common and occurred on 26 of the 57 days studied. $PM_{2.5}$ on the majority of these days was composed of sulfate, organic carbon, and nitrate. This group is characterized by long-range transport from the north-northwest; the Cen and Nor source areas (Figure B-2) experienced the most parcel residence time. The meteorological pattern is characterized by an upper-level trough over the Northeast and strong northwesterly flow over the Sikes site. This group has the lowest morning humidity of all the best visibility groups (74%). A good example day of this group is January 12, 2003 (see **Figure B-42**).

2. Gulf of Mexico Transport. This group of conditions occurred on 17 of the 57 days analyzed. $PM_{2.5}$ on the majority of these days was composed mainly of sulfate with some organic carbon. Within this group are two subgroups. Both subgroups are characterized by transport circulating clockwise through the Gulf of Mexico and up to Sikes from the southeast direction. The Gulf and TxLa source areas (Figure B-2) experienced the most parcel residence time.

   Subgroup A conditions occurred on 9 of the 57 days during the late fall and early spring. The meteorological pattern is characterized by a strong upper-level trough over the central United States. A good example day of this group is December 19, 2002 (see **Figure B-43**).

   Subgroup B conditions occurred on 8 of the 57 days during the summer months. The meteorological pattern is characterized by a weak upper-level pattern. The morning average humidity is high (~96%). A good example day of this group is May 31, 2001 (see **Figure B-44**).

3. Wintertime Pre-Trough. This group of conditions occurred on 8 of the 57 days. $PM_{2.5}$ on the majority of these days was composed mainly of sulfate with some organic carbon. This group is characterized by transport from several directions, with recirculation over the Sikes site. The TxLa source area (Figure B-2) experienced the most parcel residence

time for this group. The meteorological pattern is characterized by southwesterly flow aloft over Sikes, with an approaching upper-level trough. A good example day of this group is January 14, 2002 (see **Figure B-45**).

4. Cool Season Cutoff Low. This group of conditions is the least common of the best visibility groups, occurring on only 6 of the 57 days analyzed. $PM_{2.5}$ on the majority of these days was composed mainly of sulfate with some organic carbon. This group is characterized by split long-range transport, from both the north-northwest and south; the TxLa source area (Figure B-2) experienced the most parcel residence time. The meteorological pattern is characterized by an upper-level cutoff low or strong trough over the Midwest. A good example day of this group is May 22, 2001 (see **Figure B-46**).

Table B-7. The four weather/transport day types for the 20%-worst visibility days for the Southern Plains subregion (represented by Sikes [SIKE1]).

		SIKE1 Worst	Transport						Avg. Calcuations (12Z)			
Group	Dates	Chemistry	Distance	Directiron	Main Source Region	Secondary Source Region	Upper-Air Pattern	Max Temperature	Relative Humidity (%)	850mb Temp - Surface Temp (deg. C)	Wind Speed (m/s)	700mb Temperature (deg. C)
1a	12/06/2001 05/01/2001 08/02/2001 10/31/2001 06/22/2002 07/07/2002 08/09/2002 08/30/2002 09/05/2002 09/08/2002 08/16/2003 09/09/2003 09/21/2003 10/09/2003 11/11/2003 04/30/2003	S	long	E,SE	SE	Gulf	ridge over eastern US	Hot summer pattern. 80's - 90's	88.8	-5.8	1.9	7.1
1b	05/16/2001 05/19/2001 07/12/2001 07/21/2001 04/29/2002 05/02/2002 07/22/2002 01/21/2003 05/03/2003 05/15/2003 08/14/2001 08/03/2002 08/07/2003	S,OC	short-medium	S. Trajectories curve clockwise through the Gulf of Mexico, then up from the South.	Gulf	TxLa	ridge over central US	Hot summer pattern. 80's - 90's	89.9	-4.7	2.5	8.6
2	07/15/2001 10/01/2001 05/24/2003 05/27/2003 11/08/2003 09/18/2003 11/18/2001 09/14/2002 03/10/2003 06/24/2001 11/12/2001 08/27/2002 08/10/2003	S,OC	long	N,NE	ORV	SE	trough or cutoff low over the eastern US	mild - cool season. Spring and fall pattern.	86.3	-1.4	1.5	5.7
3	08/13/2003 08/25/2003 03/23/2001 10/04/2001 02/02/2003 05/30/2003 06/20/2003 08/19/2003 10/06/2003	S,OC	short. local transport	muliple directions	TxLa	SE	ridge over west central US or trough over the Northeast	Warm season (70's)	93.4	-4.3	1.4	6.3
4	11/09/2001 01/09/2003 01/15/2003 01/27/2003 01/30/2003 12/08/2003	S,N,OC	short-medium	Split N-NW and S	TxLa		NW flow alfot - trough over the Northeast	Cool season (40's-50's)	85.1	1.7	3.5	0.8

Table B-8. The four weather/transport day types for the 20%-best visibility days for the Southern Plains subregion (represented by Sikes [SIKE1]).

		SIKE1 Best	Transport						Avg. Calcuations (12Z)			
Group	Dates	Chemistry	Distance	Directiron	Main Source Region	Secondary Source Region	Upper-Air Pattern	Max Temperature	Relative Humidity (%)	850mb Temp - Surface Temp (deg. C)	Wind Speed (m/s)	700mb Temperature (deg. C)
1	01/12/2003 01/24/2003 02/08/2003 11/21/2001 01/18/2003 11/14/2003 11/29/2003 10/07/2001 12/30/2001 01/26/2002 12/25/2002 01/03/2003 09/30/2003 10/15/2003 10/27/2003 12/26/2003 12/11/2003 02/05/2003 04/26/2002 11/20/2003 12/20/2003 10/16/2001 11/30/2001 12/21/2001 12/27/2001 12/17/2003	mixed: S,OC,N	long	N,NW	Cen	Nor	NW flow aloft and/or trough in the eastern US	Cool season, temps in the 50's	74.4	3	2.1	-0.3
2a	10/13/2001 11/27/2001 03/09/2002 03/12/2002 04/08/2002 12/19/2002 12/31/2002 11/23/2003 12/29/2003	S,OC	long	clockwise circulation from the SE through the Gulf of Mexico	Gulf		strong trough inf the central US	Cool season, temps in the 50's	89.7	-4.1	4.7	2
2b	05/31/2001 06/06/2001 08/15/2002 06/14/2003 07/11/2003 06/09/2001 06/30/2001 09/03/2003	S,OC	long	clockwise circulation from the SE through the Gulf of Mexico	Gulf	TxLa	weak upper-level dynamics. Zonal flow or stagnant aloft.	Warm season (70's)	95.9	-5.6	3	7
3	03/19/2003 01/14/2002 12/24/2001 02/10/2002 12/22/2002 02/11/2003 02/20/2003 12/02/2003	S,OC	long	multiple directions. Recirculatio n over SIKE	TxLa		Zonal flow OR trough over the east-central US	Cool season, temps in the 50's	79.2	1.1	3.2	-1.7
4	04/25/2001 05/22/2001 05/25/2001 10/25/2001 04/21/2003 05/12/2003	S,OC	long	Split: N,NW and S	TxLa		Cufoff low OR trough over the Upper-Midwest.	Mild, Spring/Fall pattern	88.4	-1.6	0.9	3.6

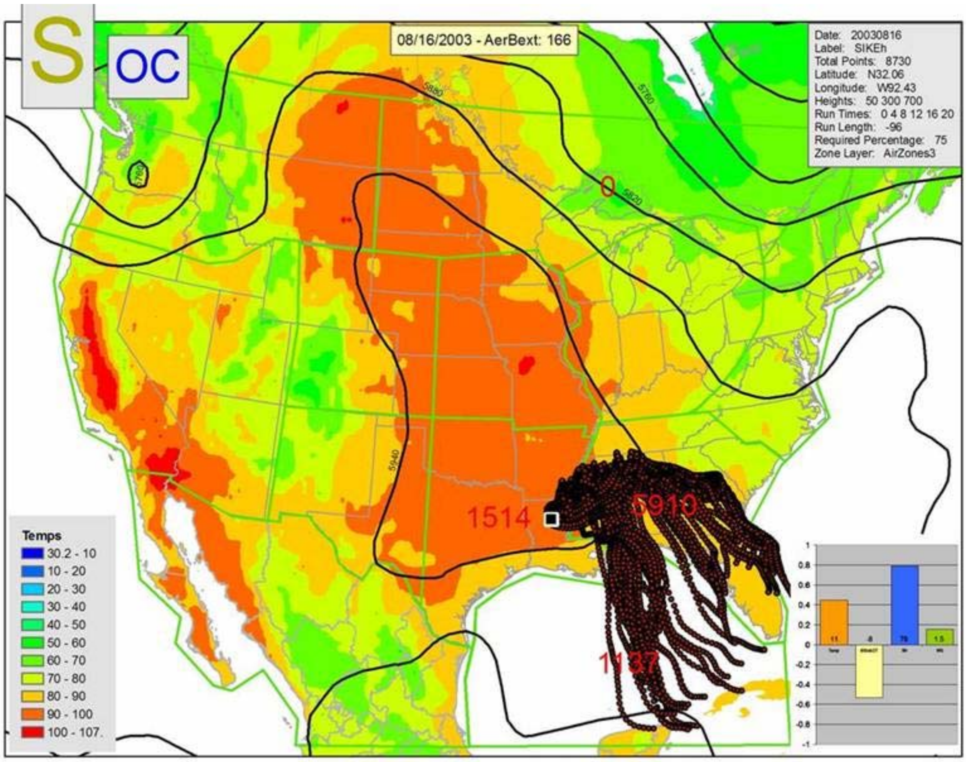

Figure B-37. Summertime Ridge – Subgroup A example.

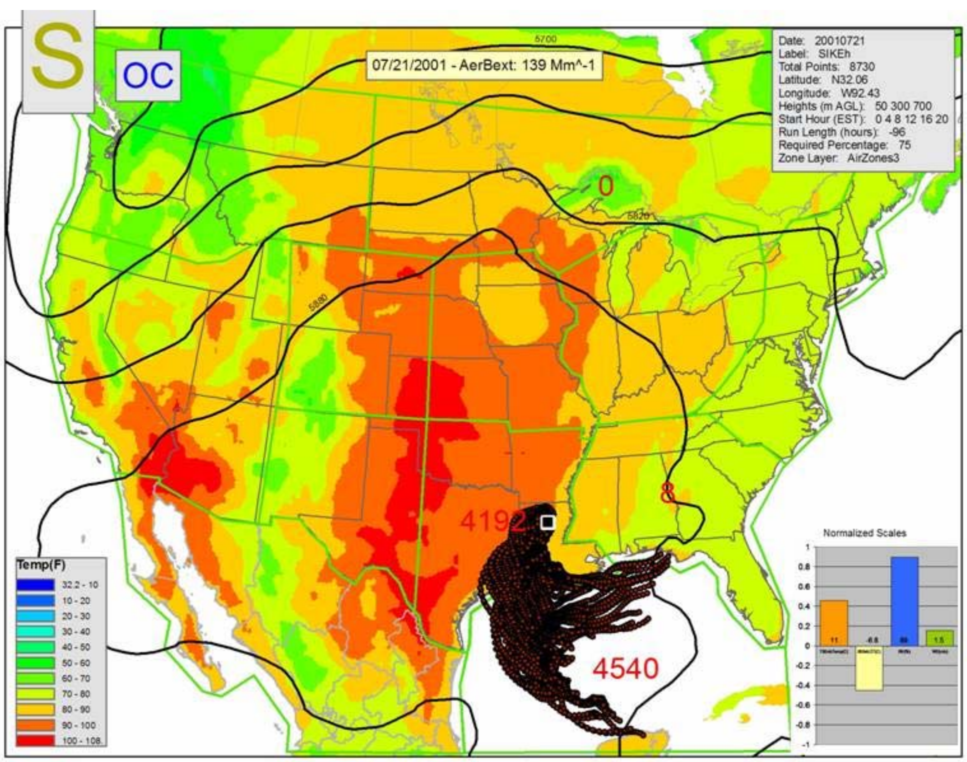

Figure B-38. Summertime Ridge – Subgroup B example.

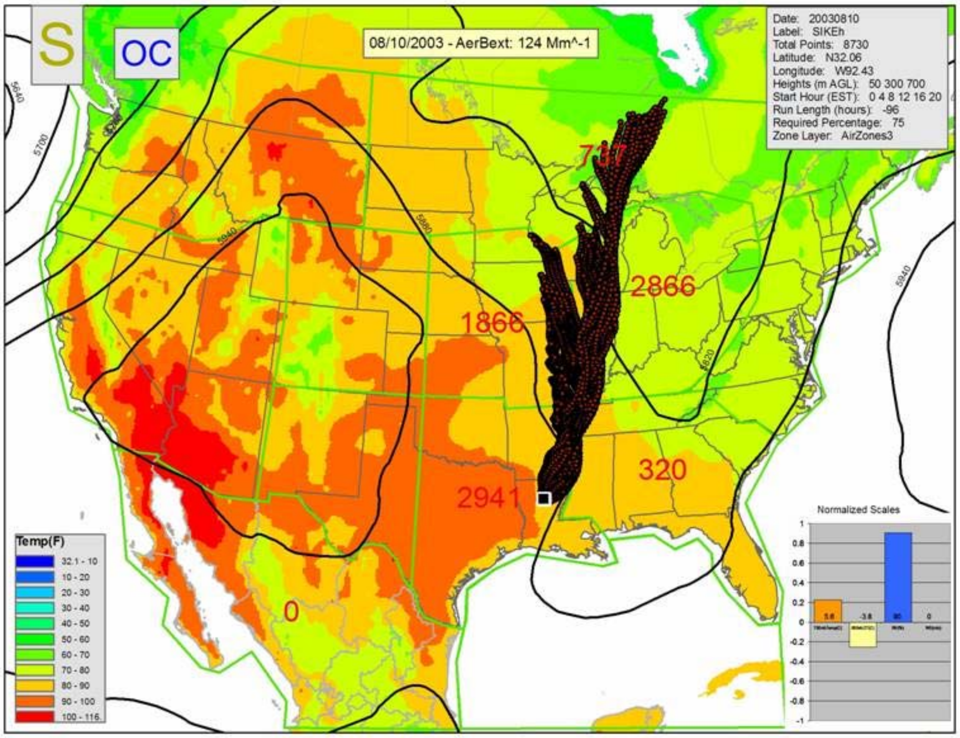

Figure B-39. Warm Season Northeasterly Transport example.

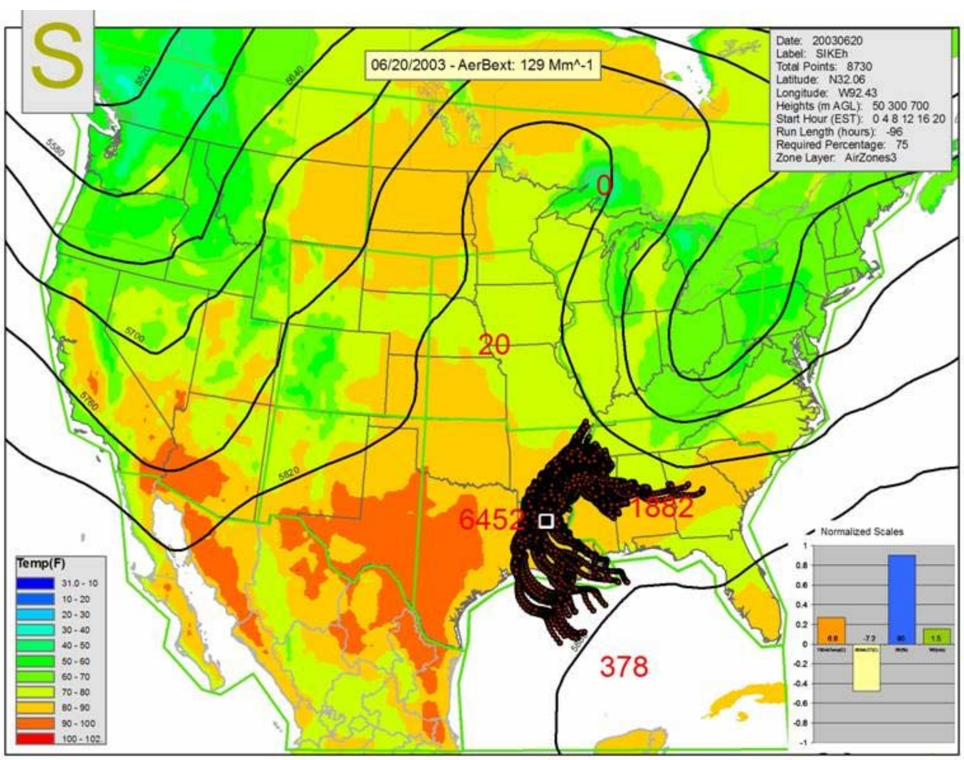

Figure B-40. Warm Season Stagnant example.

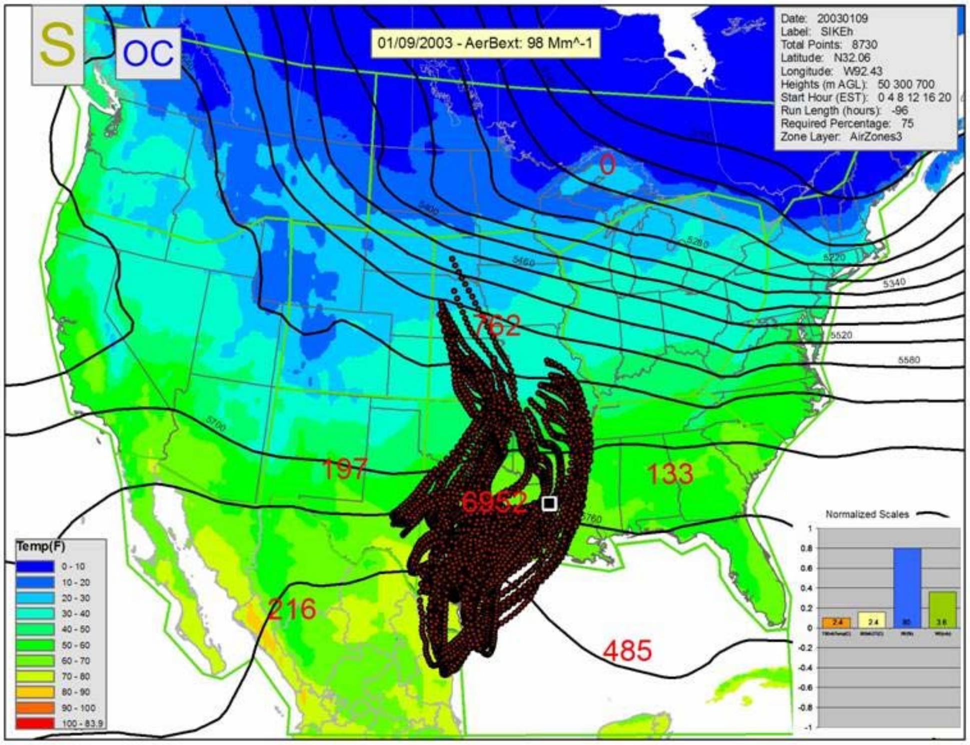

Figure B-41. Cool Season Split Flow example.

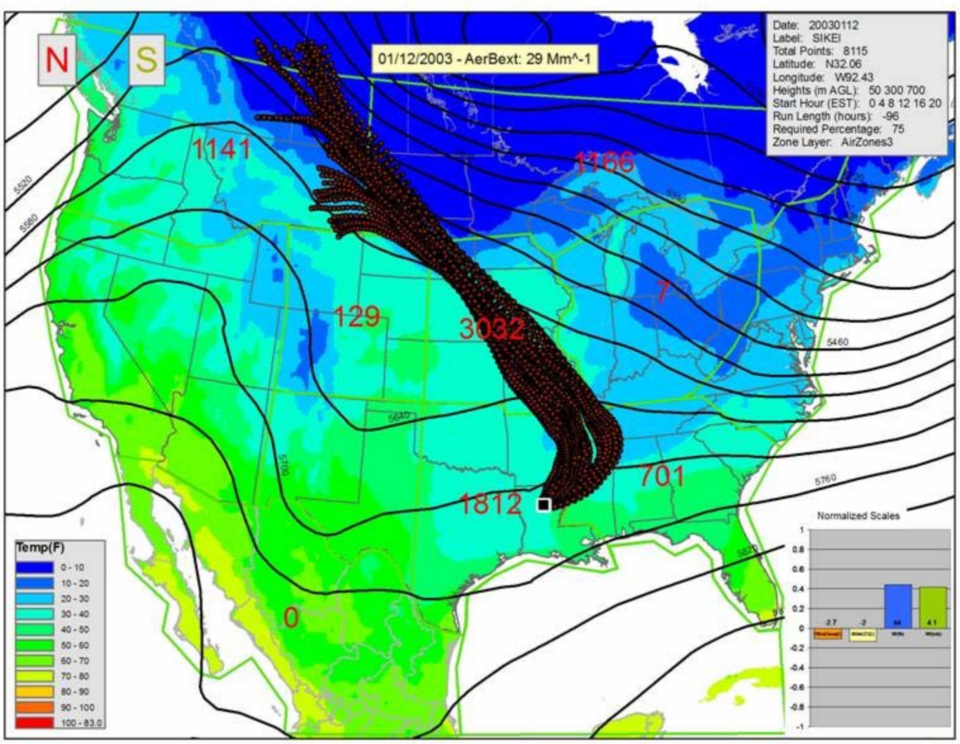

Figure B-42. Wintertime Northwesterly Transport example.

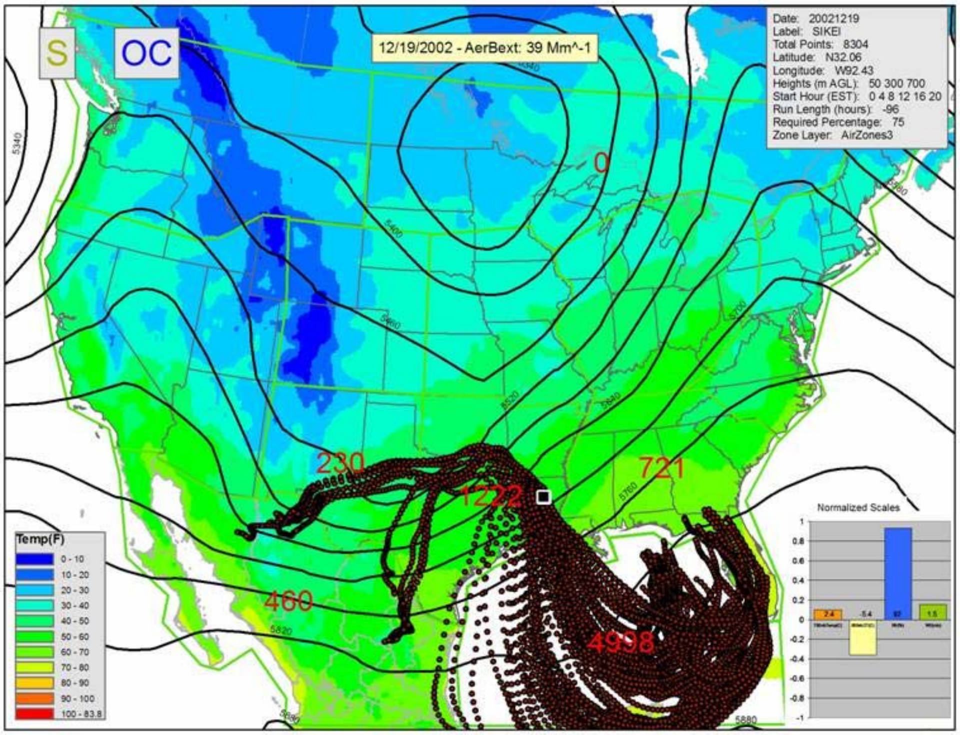

Figure B-43. Gulf of Mexico Transport – Subgroup A example.

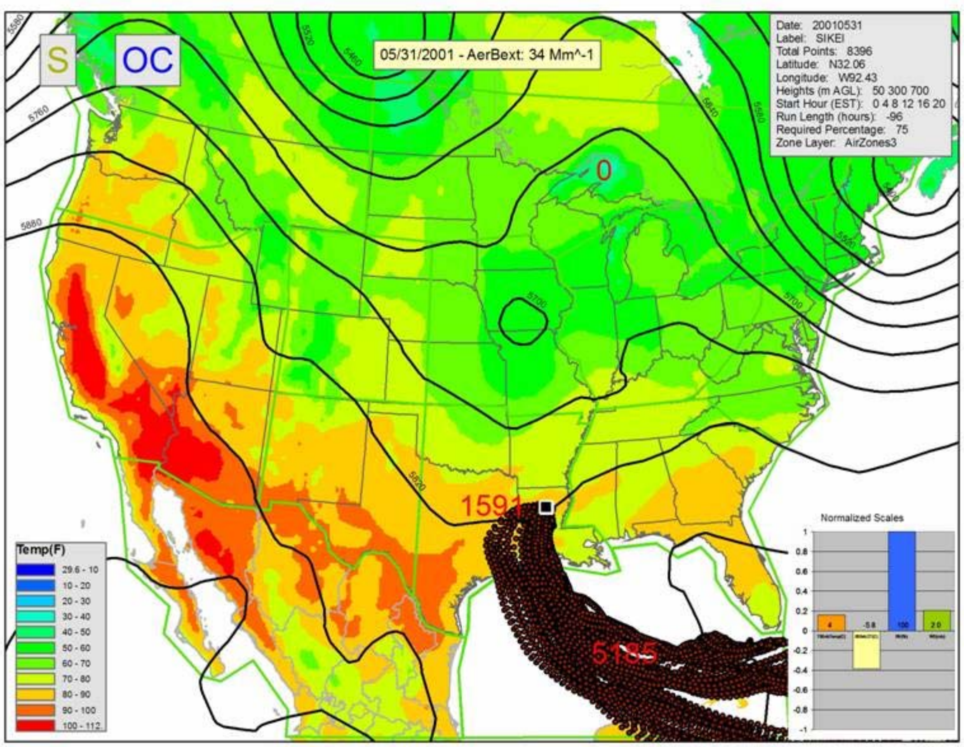

Figure B-44. Gulf of Mexico Transport – Subgroup B example.

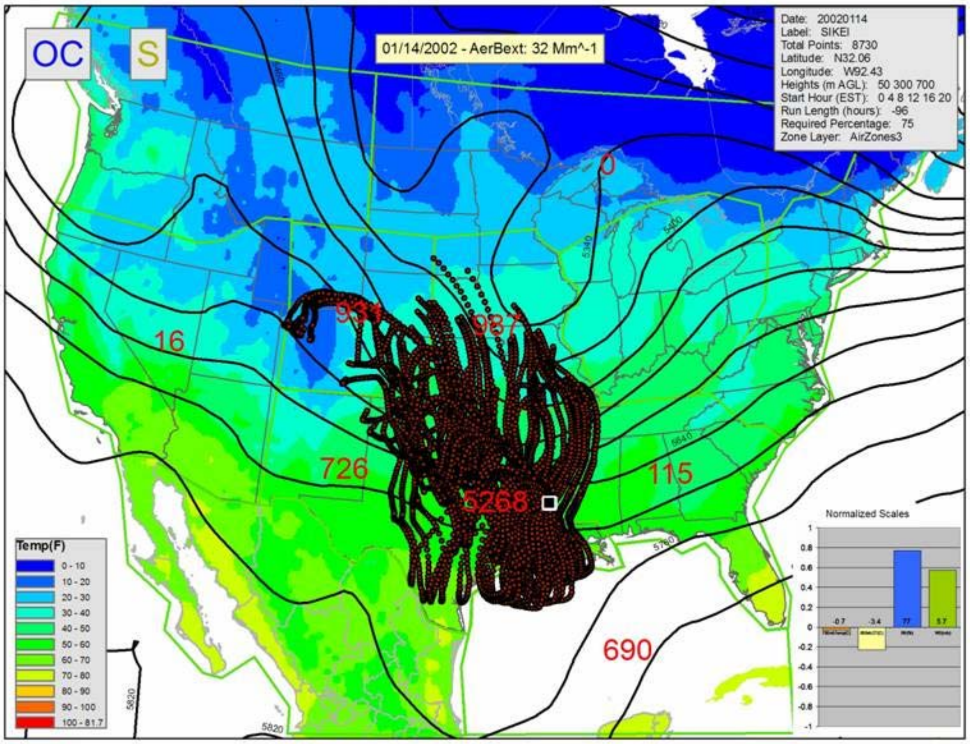

Figure B-45. Wintertime Pre-Trough example.

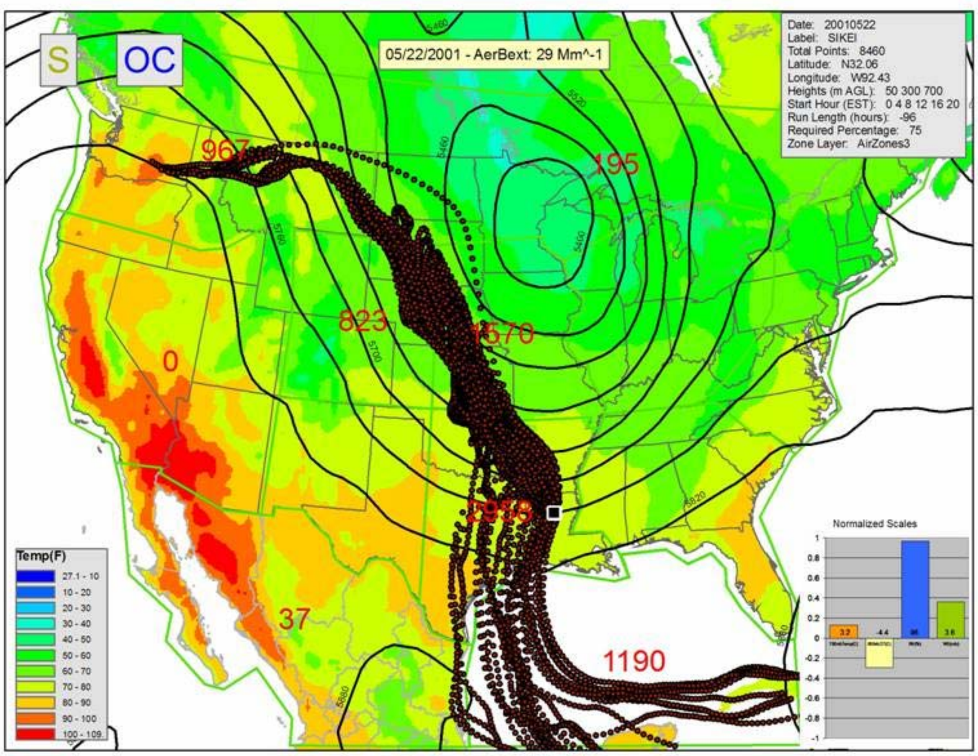

Figure B-46. Cool Season Cutoff Low example.

APPENDIX C

DOCUMENTATION OF METHODS, INFORMATION, RESOURCES, AND GRAPHICAL AND TABULAR SUMMARIES OF DATA FOR (TASK 6)

EMISSIONS ANALYSES

C.1 COMPILATION AND ASSESSMENT OF EMISSION INVENTORIES

The best available emission inventories were compiled from the following sources:

- 2002 inventories prepared by each of the five Regional Planning Organizations (RPOs) were obtained (Central Regional Air Planning Association, 2005; Mid-Atlantic/Northeast Visibility Union, 2002; The Visibility Improvement State and Tribal Association of the Southeast, 2004a, b, c; Western Regional Air Partnership, 2003a, b, c, d, e, f, g).
- The draft 2002 National Emission Inventory (NEI) was consulted for unavailable components of the RPO inventories, including inventories for on-road mobile sources in the WRAP, VISTAS, and MRPO states; and inventories of fugitive dust emissions for the WRAP states (U.S. Environmental Protection Agency, 2005b).
- The preliminary 2002 NEI was consulted for biogenic emissions in the United States (U.S. Environmental Protection Agency, 2005a).
- Environment Canada's 2002 NPRI database was accessed for emissions from Canadian point sources. Emissions were spatially allocated according to facility postal codes (Environment Canada, 2002).
- Environment Canada provided 2002 emission inventories of area, non-road mobile, and on-road mobile sources to EPA. These inventories were acquired from EPA. Province-level data were allocated to postal codes according to population density (Environment Canada, 1995).
- The 2002 Gulfwide emission inventory was consulted for emissions in the Gulf of Mexico (Wilson et al., 2004).
- The emission inventory prepared by (Kuhns et al., 1999) was acquired for emissions in Mexico (Kuhns et al., 2005).

The following information gaps and potential flaws were noted on review of the compiled emission inventories. Because of these potential problems and because the results of other tasks showed that sulfate and nitrate are the primary contributors to visibility impairment in the CENRAP region, Task 6 analyses focused exclusively on SO_2 and NO_x emissions.

- Biogenic emissions contribute substantially to VOC emissions, and we anticipate that the biogenic emissions densities in Mexico and Canada are comparable to those in the United States. However, biogenic emission inventories were unavailable for Canada and Mexico; therefore, assessments of the emission impact potentials of VOC emissions on receptors were seriously limited.
- PM_{10}, $PM_{2.5}$, and NH_3 emissions are inconsistent at state lines and/or RPO boundaries. The differences appear to be partly due to differences in emission estimation methodologies. In addition, the proportion of $PM_{2.5}$ attributed to on-road mobile sources seems too low in many areas. Rural sources of NH_3—which are likely the predominant sources of NH_3—have been omitted from the emission inventories of the WRAP states. These issues greatly limited assessments of the emission impact potentials of PM_{10}, $PM_{2.5}$, and NH_3.

  The emission inventories are illustrated in **Figures C-1 through C-7**.

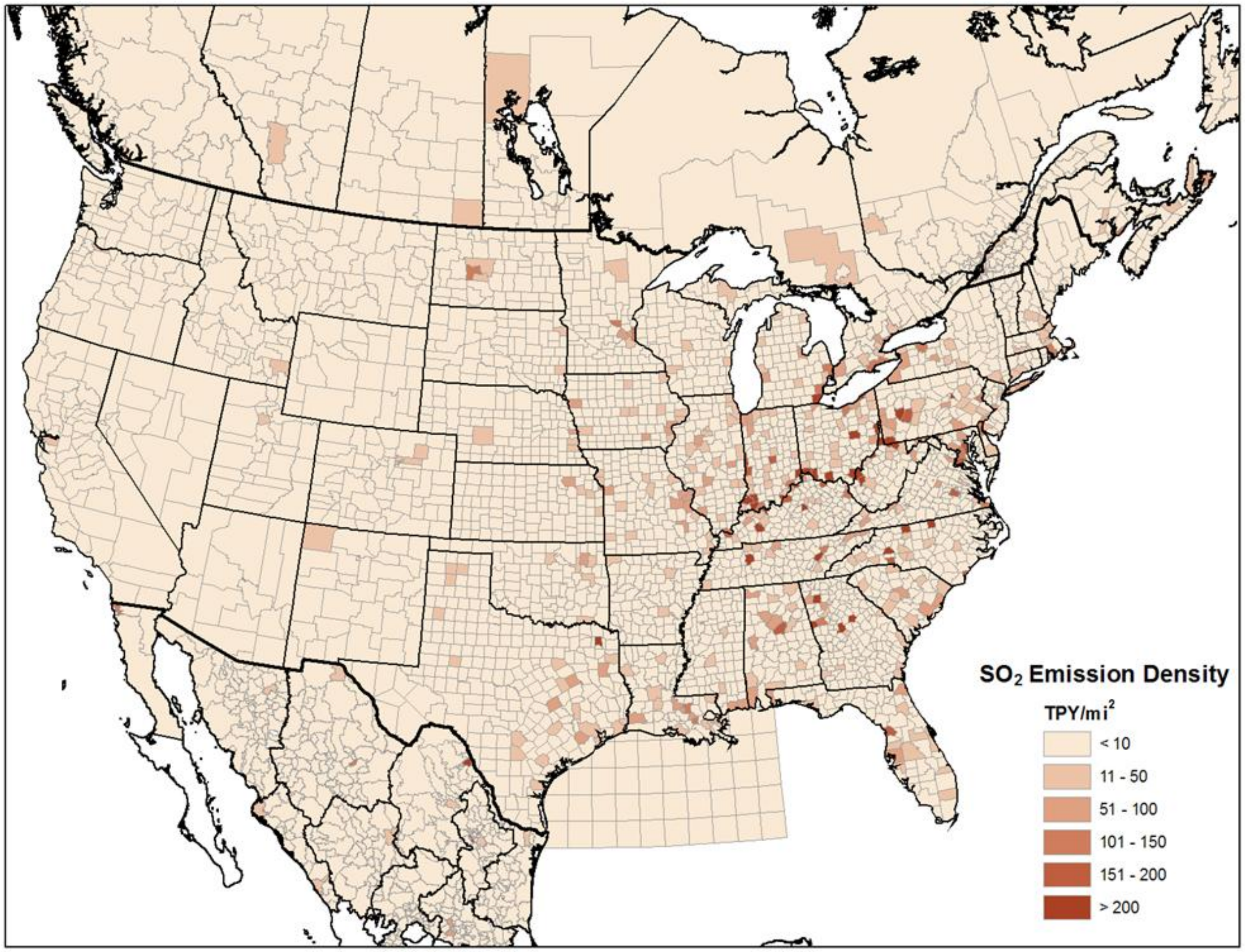

Figure C-1. SO_2 emissions density map for the United States, Canada, and Mexico.

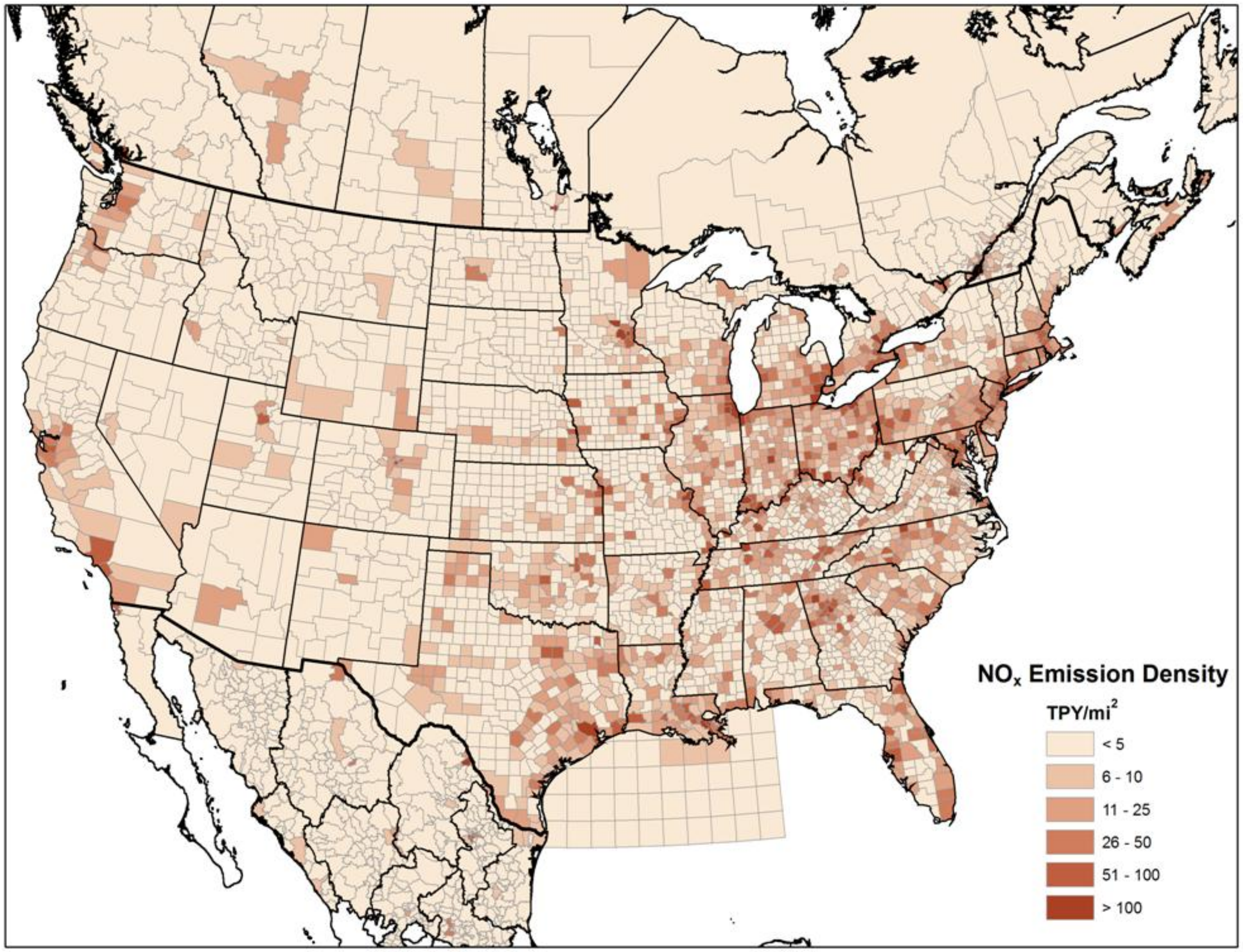

Figure C-2. NO_x emissions density map for the United States, Canada, and Mexico.

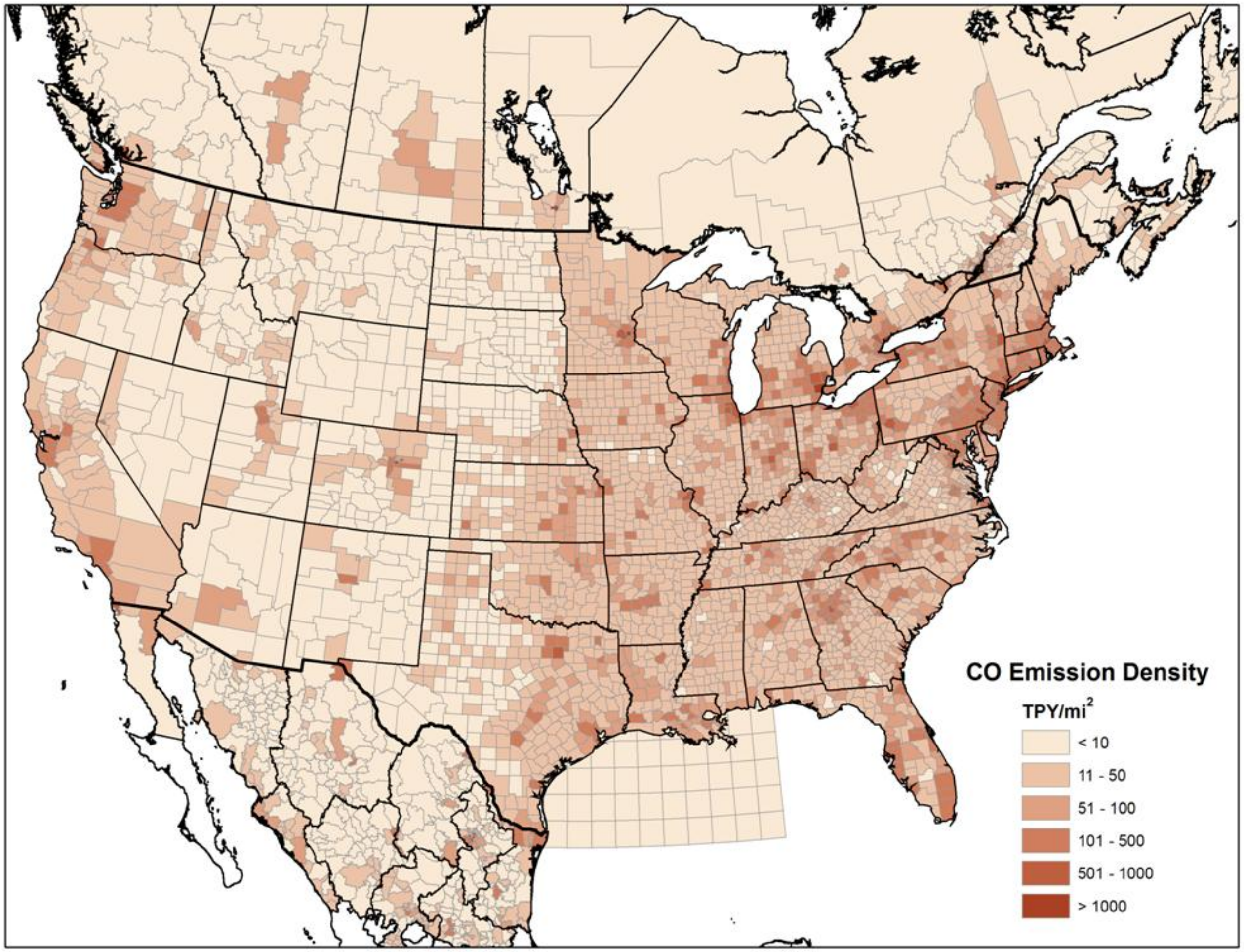

Figure C-3. Carbon monoxide (CO) emissions density map for the United States, Canada, and Mexico.

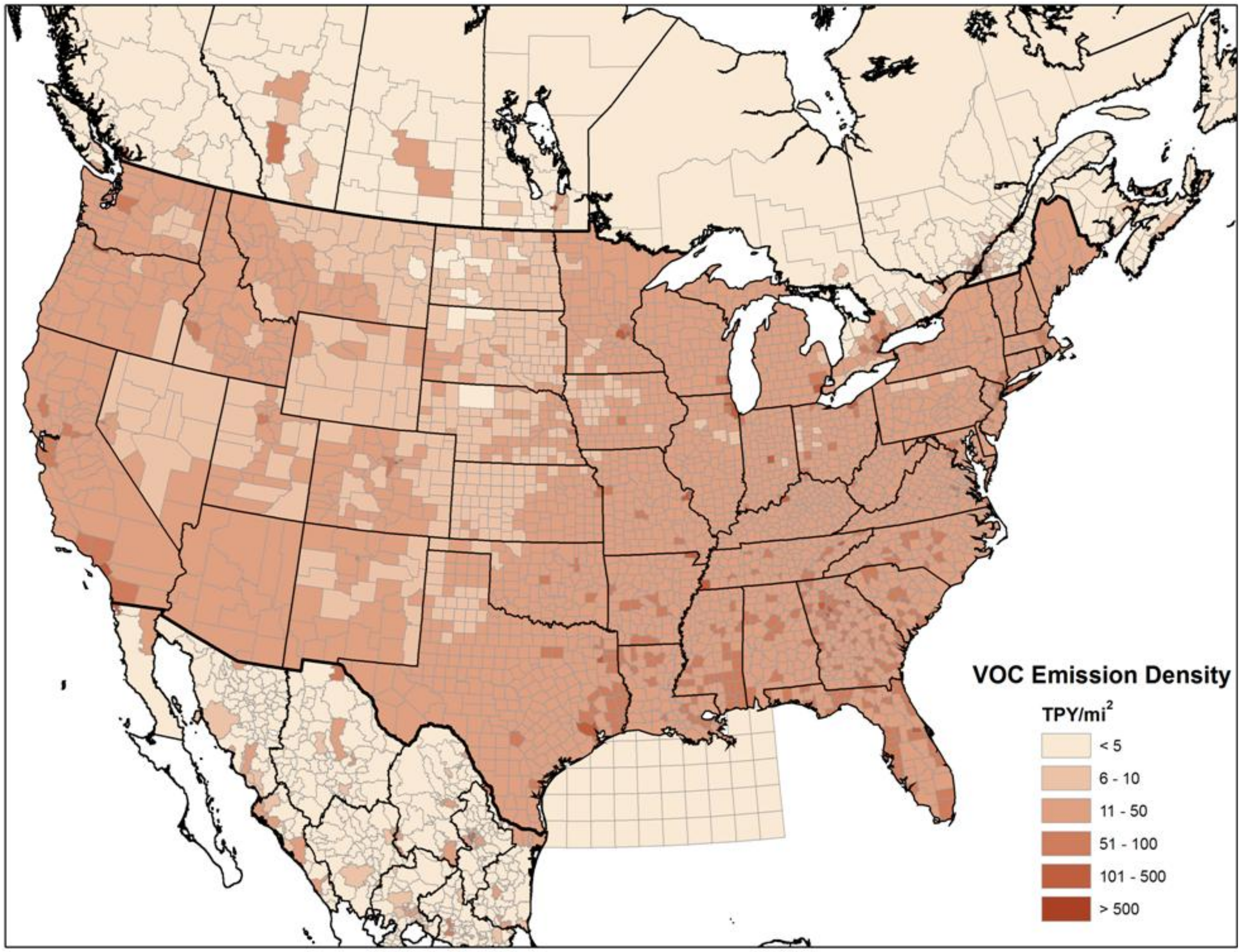

Biogenic emissions are missing for Canada and Mexico, which accounts for large discontinuities across international borders.

Figure C-4. Volatile organic compound (VOC) emissions density map for the United States, Canada, and Mexico.

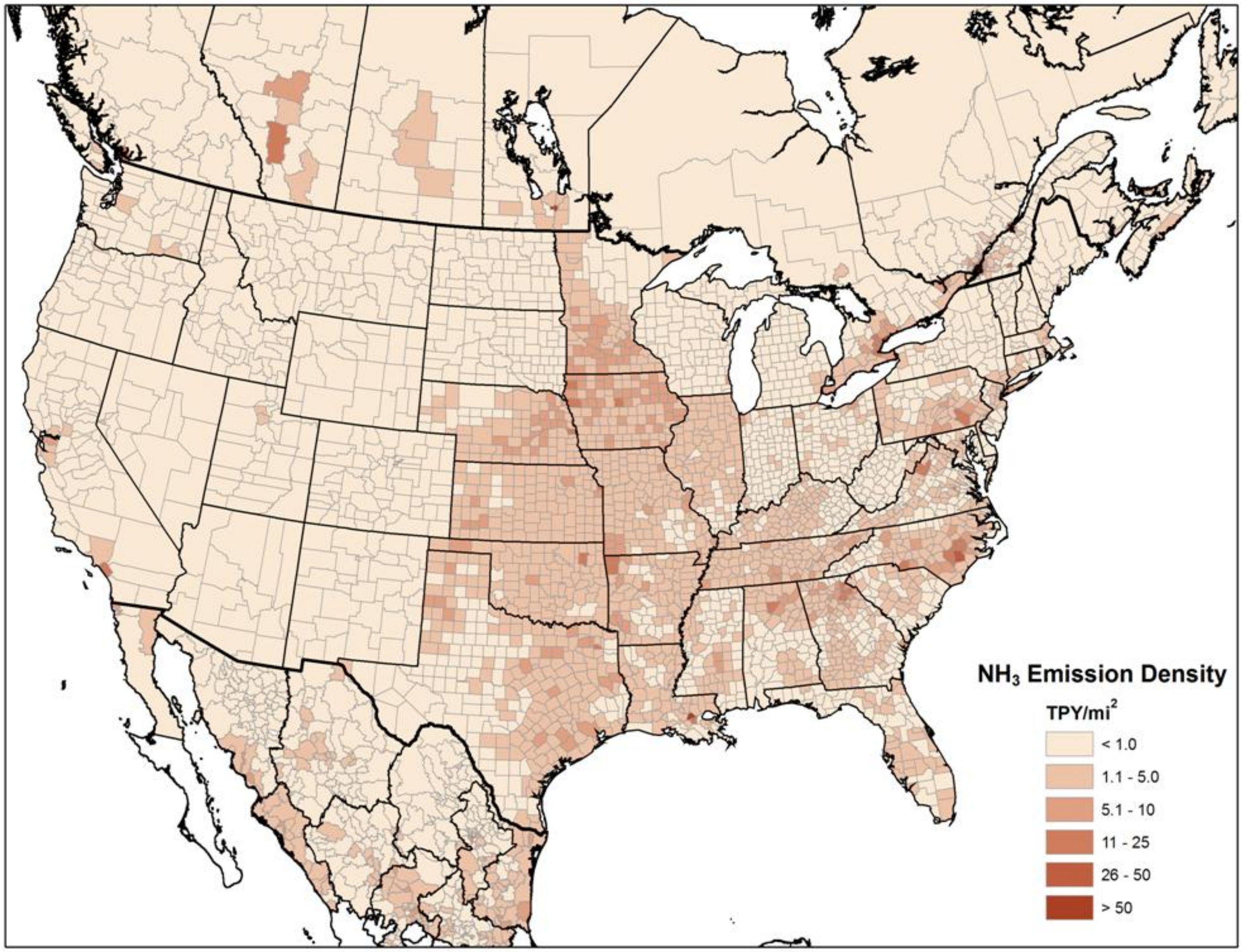

Discontinuities at state boundaries are likely due to differences in emissions estimation methodologies. Rural sources of ammonia are missing from WRAP states.

Figure C-5. Ammonia (NH_3) emissions density map for the United States, Canada, and Mexico.

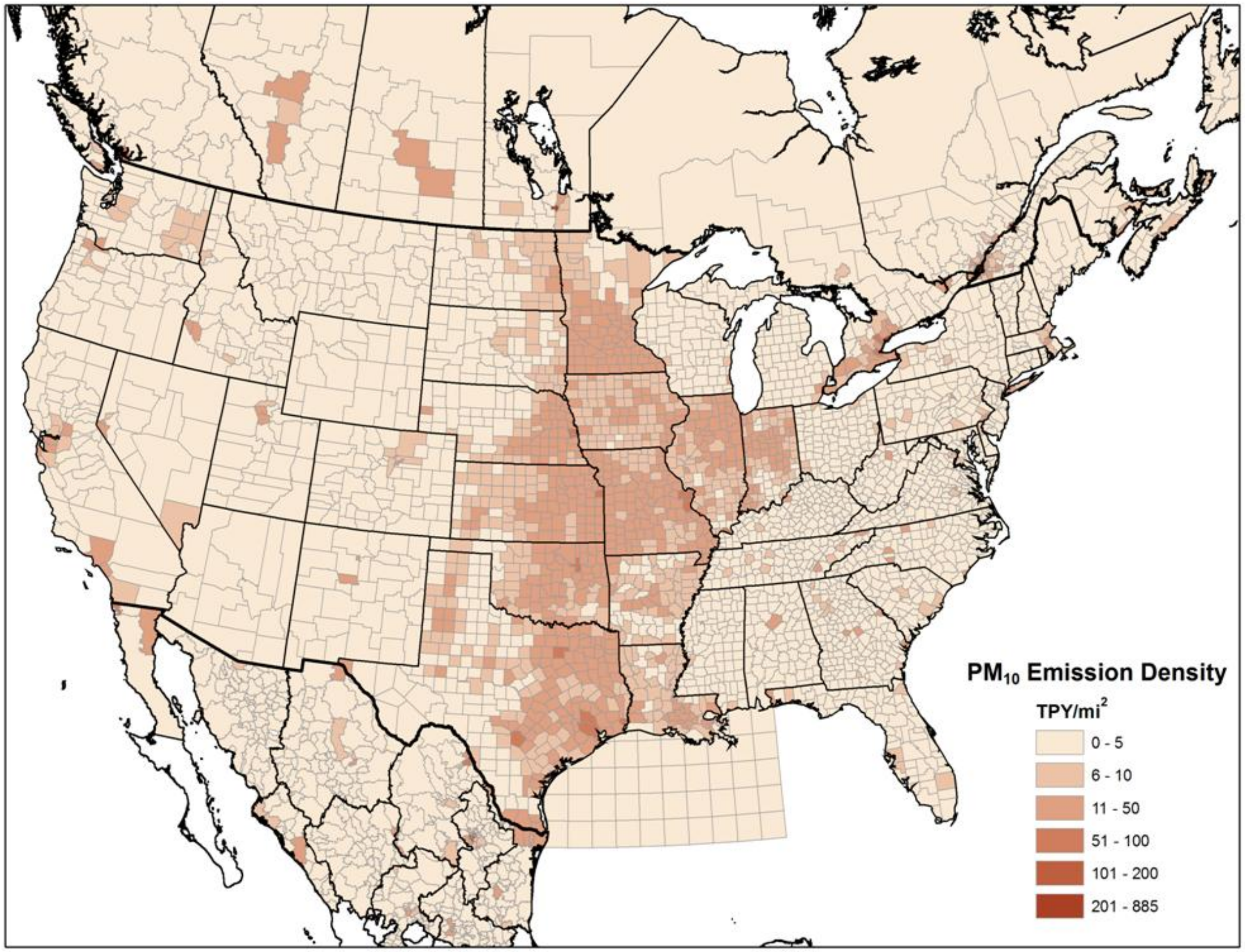

Discontinuities at state boundaries are likely due to differences in emissions estimation methodologies.

Figure C-6. Coarse particulate matter (PM_{10}) emissions density map for the United States, Canada, and Mexico.

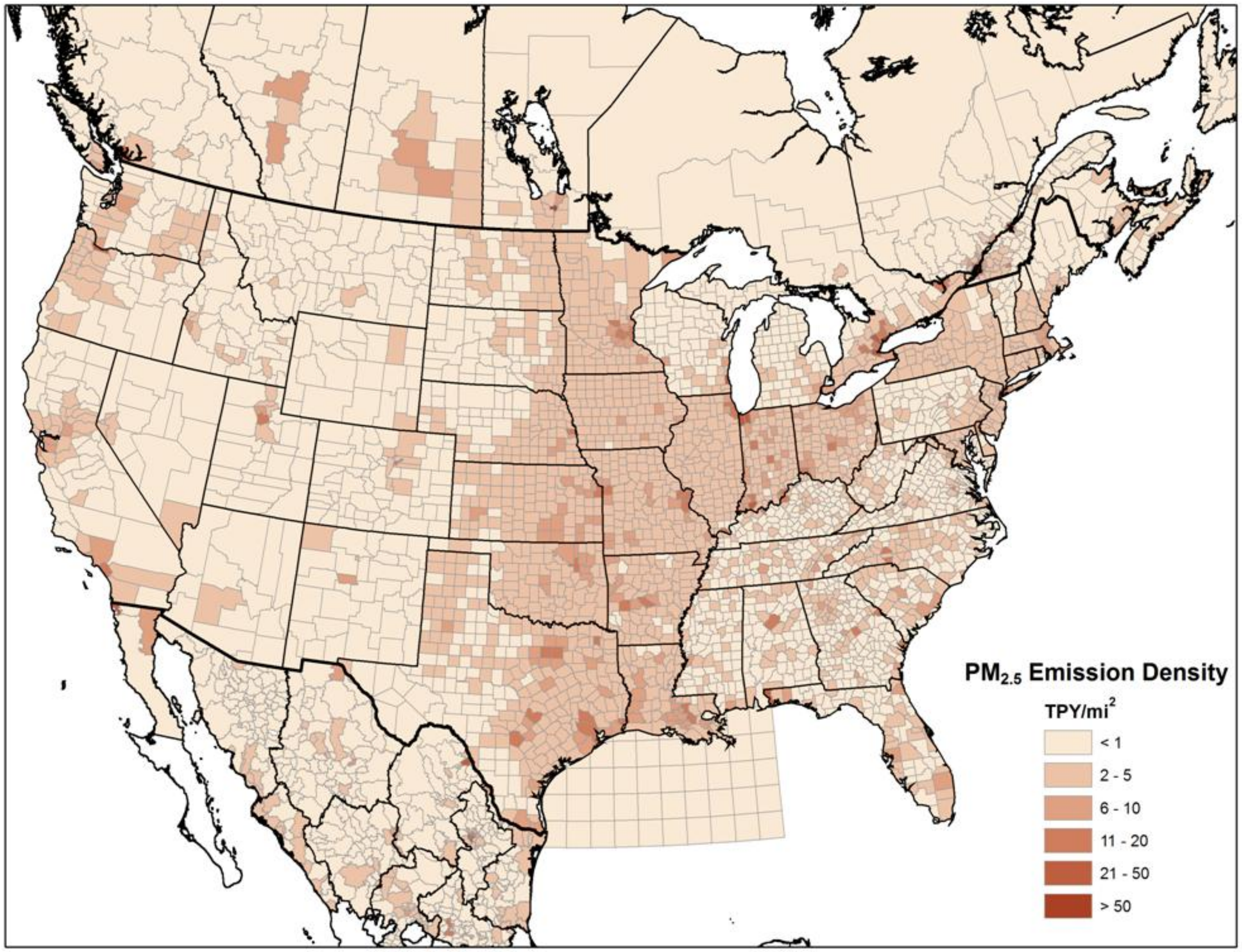

Discontinuities at state boundaries are likely due to differences in emissions estimation methodologies.

Figure C-7. Fine particulate matter (PM$_{2.5}$) emissions density map for the United States, Canada, and Mexico.

C.2 PREPARATION OF BACKWARD WIND TRAJECTORIES

The National Oceanic and Atmospheric Administration (NOAA) HYbrid Single-Particle Lagrangian Integrated Trajectory (HYSPLIT) model (Draxler and Hess, 1997) was used to determine transport patterns to the receptor site. An ensemble of backward trajectory model runs was performed to represent the various possible wind patterns on each day of interest. Days with the 20%-worst and the 20%-best visibility are of most interest. Data from the Interagency Monitoring of Protected Visual Environments (IMPROVE) network for every third day from March 2001 through 2003 were used to determine the dates of best and worst visibility. The parameters used to run the trajectories are shown in **Table C-1**. The trajectories were limited to 72 hours. Six start times were used to cover variations in meteorology during the 24-hr sampling period. Trajectories were initiated at three heights; results for all three heights were combined.

Table C-1. Parameters used to run the NOAA HYSPLIT model.

Parameter	Value
Starting heights	50, 300, 700 m
Run time	72 hours
Minimum valid data points	75%
Starting hours	0, 4, 8, 12, 16, 20
Top of model	10,000 m
Model data	EDAS
Vertical motion	Isobaric (follows height of constant pressure)

The hourly points from all trajectories over all days of interest are combined using the Spatial Probability Density (D0), which is a kernel density of all hourly trajectory points, normalized to a maximum value of one:

$$D_0 = \frac{D_c}{\hat{D}} \qquad \textbf{(C-1)}$$

where

D_c = Density at grid cell c

$\hat{D}$ = Maximum density over all grid cells (density at receptor site)

$$D_c = \sum_{i=1}^{n} \kappa_R(r_n) \qquad \textbf{(C-2)}$$

where:

r_n = distance between grid cell center and hourly trajectory point *n*

$$K_R(r) = \text{kernel density function} = \begin{cases} \dfrac{3}{\pi R^2}\left[1-\left(\dfrac{r}{R}\right)^2\right]^2 & for\ r < R \\ 0 & for\ r \geq R \end{cases}$$

R = search radius

The search radius, *R*, was determined dynamically by dividing the geographic extent of all hourly trajectory points by 30 (McCoy and Johnston, 2001; Cressie, 1993).

Figure C-8 shows the spatial probability density map for the 20%-best days at the four representative CENRAP sites. **Figure C-9** shows analogous information for the 20%-worst days. A value of one indicates that all trajectories passed near the grid cell, while a value closer to zero denotes an area over which very few trajectories passed.

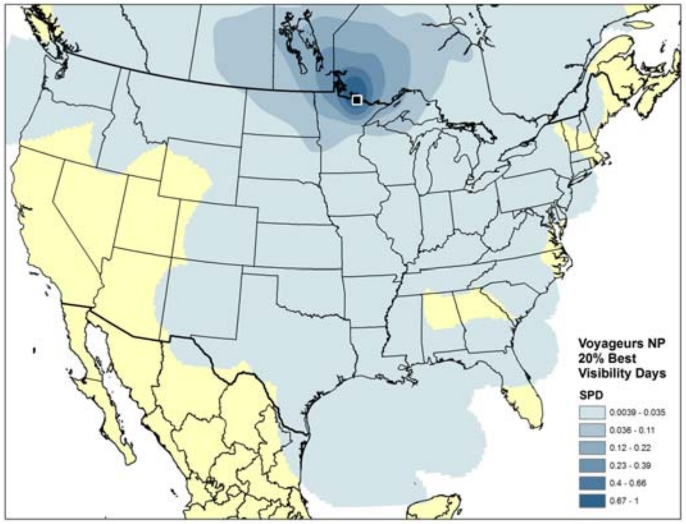

(a) Voyageurs, Minnesota (Minnesota subregion)*

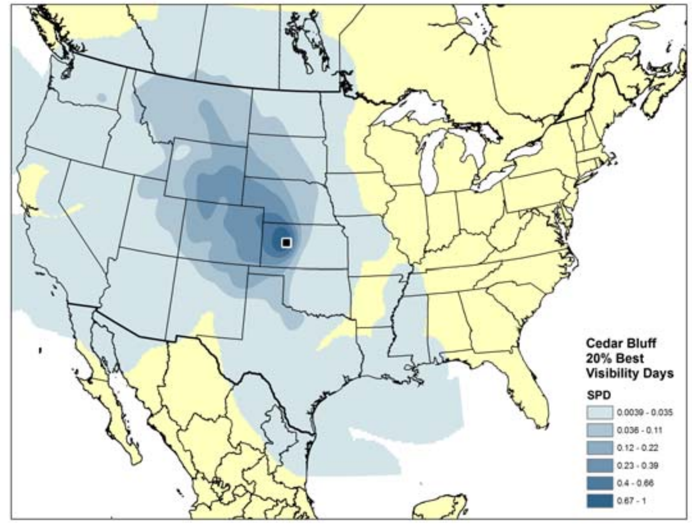

(b) Cedar Bluff, Kansas (Western Plains subregion)

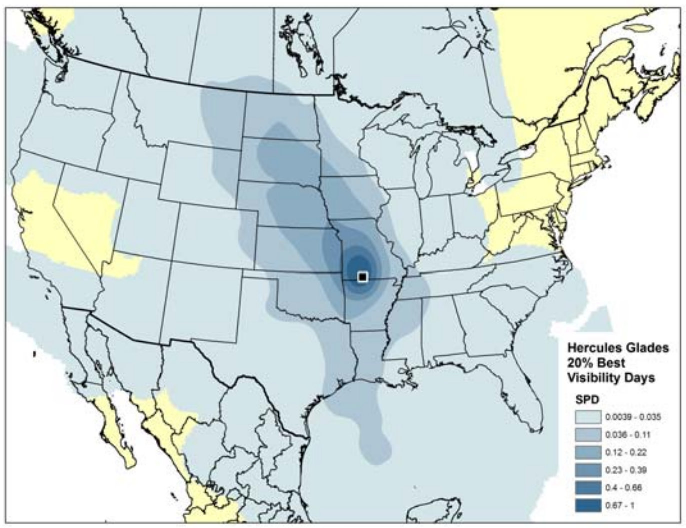

Hercules-Glades, Missouri (Upper Midwest subregion)

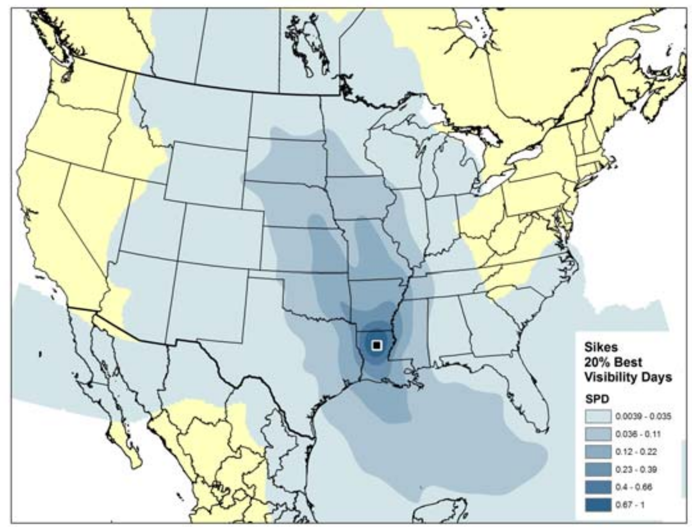

(d) Sikes, Louisiana (Southeastern Plains subregion)

* Note: Many trajectory hourly endpoints for the 20%-best days extended far northward into Canada and therefore dropped out.

Figure C-8. Geographic distributions of 72-hour backward wind trajectories for the 20%-best visibility days observed at four representative sites.

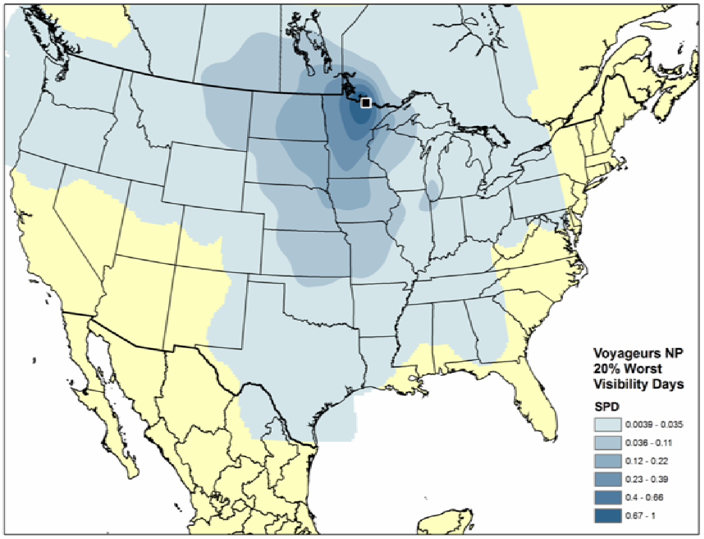

(a) Voyageurs Minnesota (Minnesota subregion)*

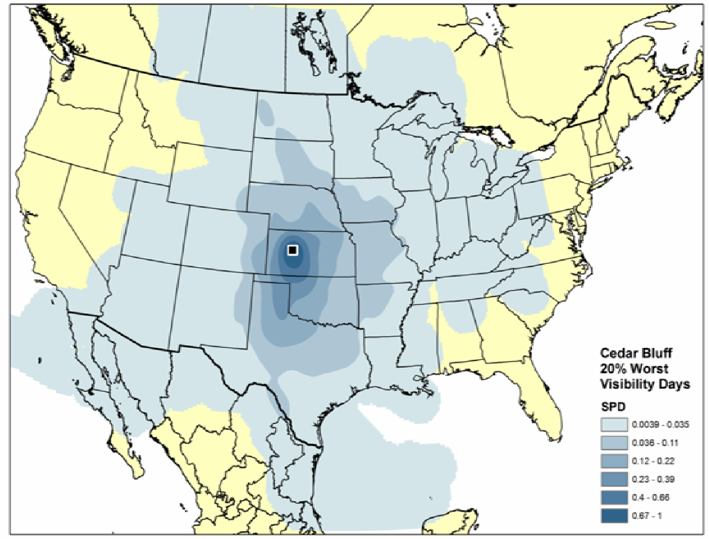

(b) Cedar Bluff, Kansas (Western Plains subregion)

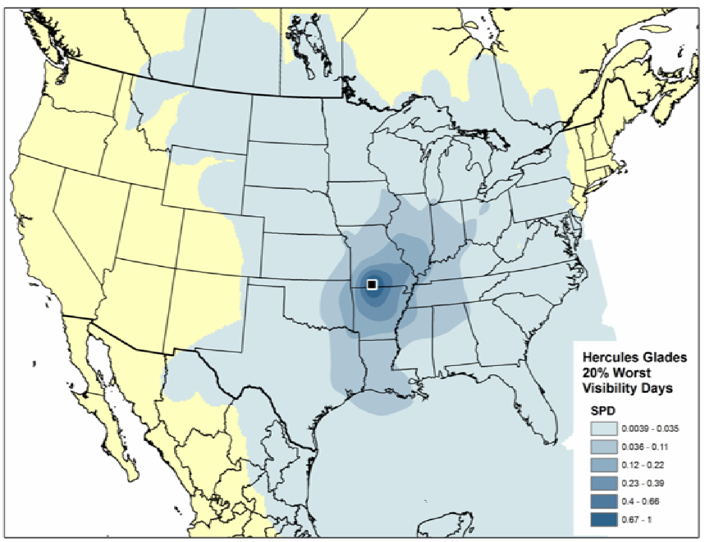

(c) Hercules-Glades, Missouri (Upper Midwest subregion)

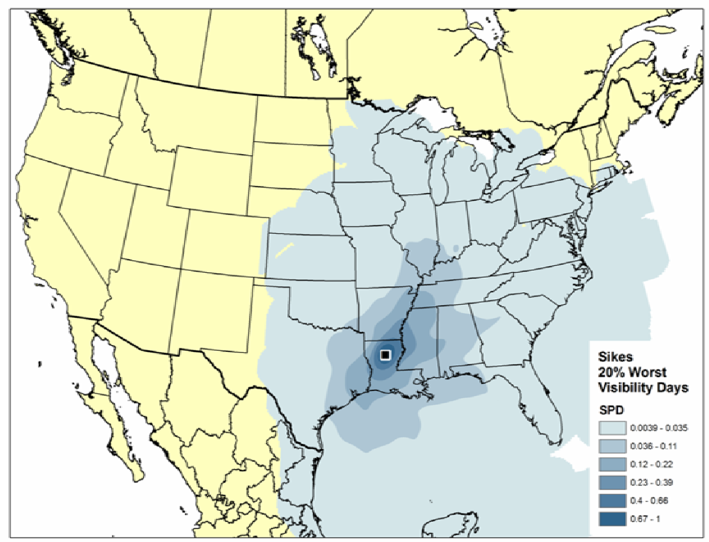

(d) Sikes, Louisiana (Southeastern Plains subregion)

Figure C-9. Geographic distributions of 72-hour backward wind trajectories for the 20%-worst visibility days observed at four representative sites.

C.3 CALCULATION OF EMISSION IMPACT POTENTIAL (EIP)

The Spatial Probability Density is used to weight the emissions from individual counties and estimate the potential for specific upwind areas to impact the receptor. The EIP of any county is calculated as:

$$EIP = \frac{E_p * D_0}{f\,(\text{distance})} \qquad \textbf{(C-3)}$$

where

E_p = county total emissions of pollutant p

D_0 = spatial probability density at the county centroid

f = function of distance between county and receptor

The EIP may be divided by a distance function to roughly account for dilution and increased uncertainty in model outputs far from the receptor site. However, for this study, f = 1. A geographic information system (GIS) tool was developed to calculate EIP values.

Figures C-10 and C-11 show the SO_x and NO_x EIP values by county for the 20%-worst and 20%-best visibility days.

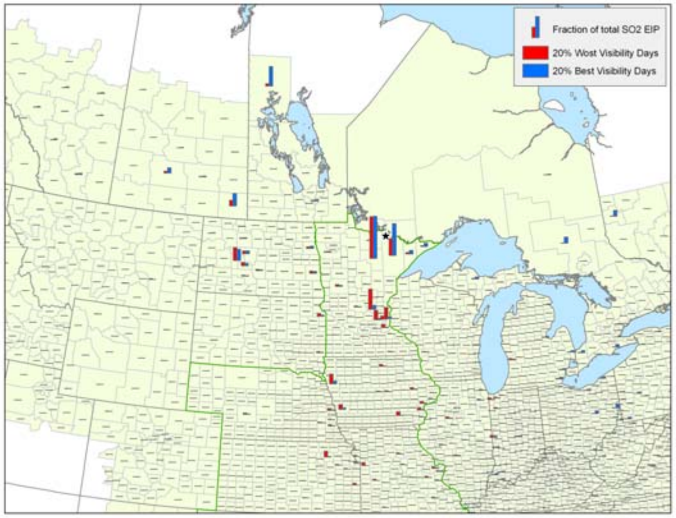

(a) Voyageurs, Minnesota (Minnesota subregion)*

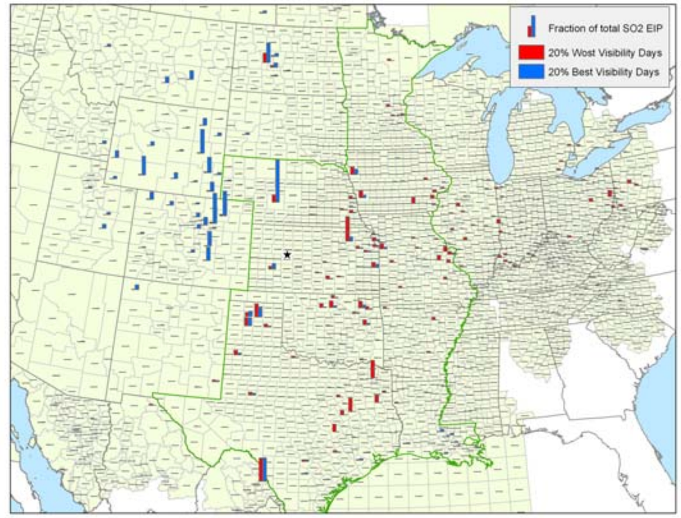

(b) Cedar Bluff, Kansas (Western Plains subregion)

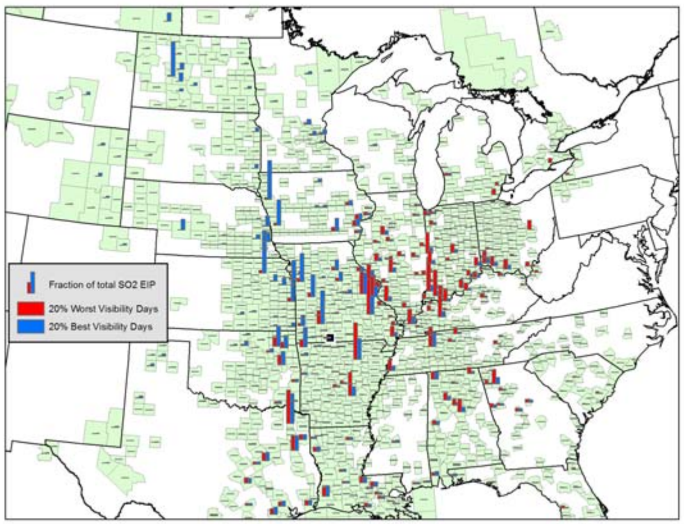

(c) Hercules-Glades, Missouri (Upper Midwest subregion)

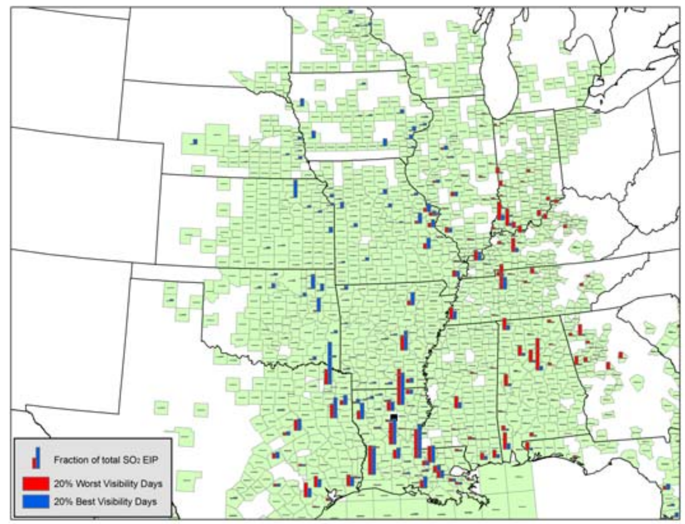

(d) Sikes, Louisiana (Southeastern Plains subregion)

* Note: Many trajectory hourly endpoints for the 20%-best days extended far northward into Canada and therefore dropped out of the analysis.

Figure C-10. Geographic distributions of SO_2 EIP for the 20%-worst visibility days (red bars) and 20%-best visibility

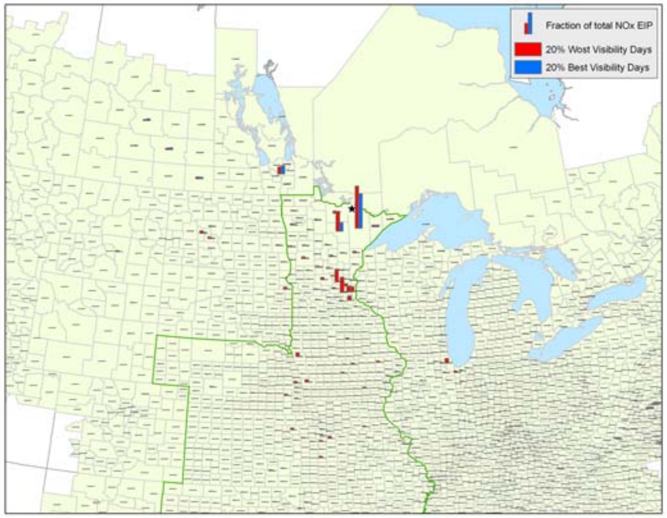

(a) Voyageurs, Minnesota (Minnesota subregion)*

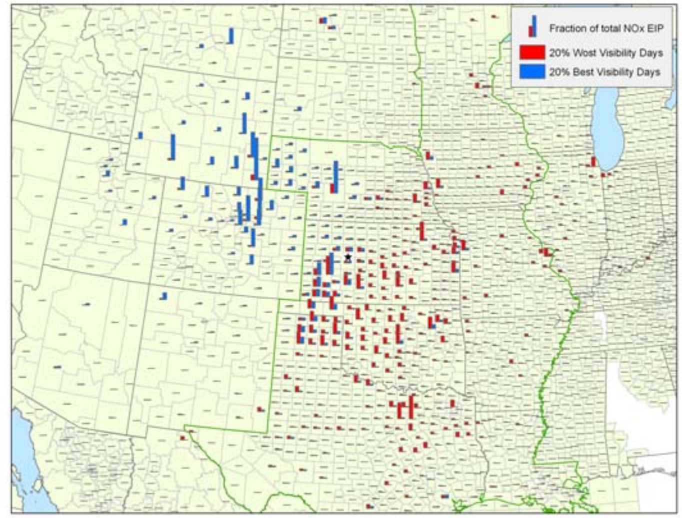

(b) Cedar Bluff, Kansas (Western Plains subregion)

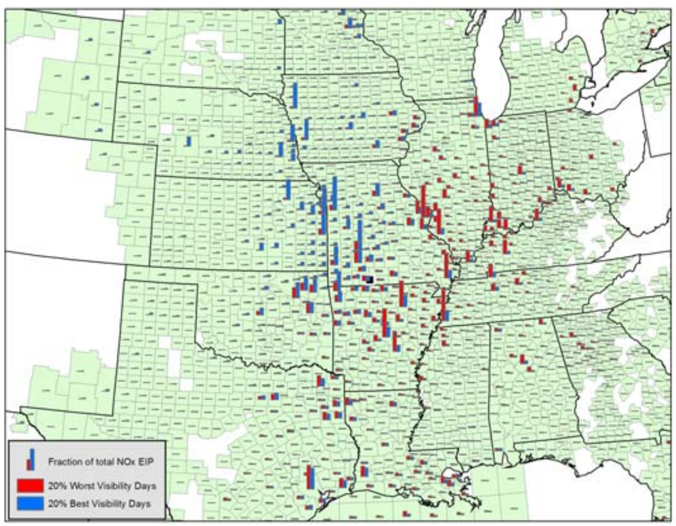

(c) Hercules-Glades, Missouri (Upper Midwest subregion)

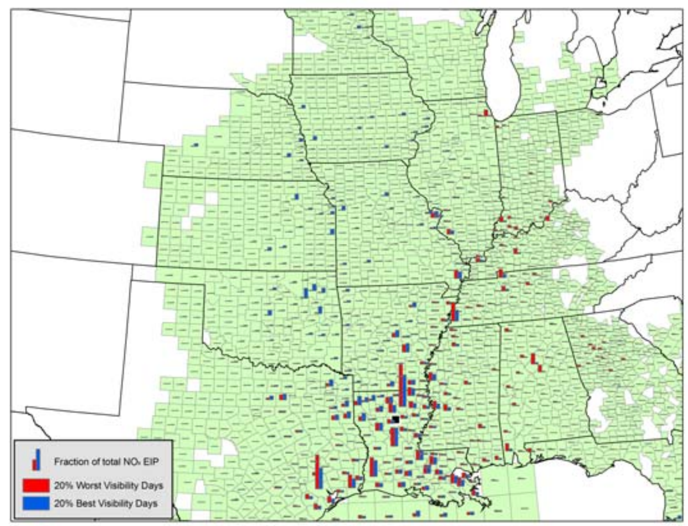

(d) Sikes, Louisiana (Southeastern Plains subregion)

* Note: Many trajectory houly endpoints for the 20%-best days extended far northward into Canada and therefore dropped out of the analysis.

Figure C-11. Geographic distributions of NO_x EIP for the 20%-worst visibility days (red bars) and 20%-best visibility days (blue bars) observed at four representative sites.

C.4 IDENTIFICATION OF POTENTIALLY BART-ELIGIBLE SOURCES

EPA's National Emissions Inventories (NEI) Draft 2002 point source inventories were compiled including all 50 states plus Washington, D.C. for use in BART Analyses. (U.S. Environmental Protection Agency, 2005b) Stationary point sources located at any of the following 26 types of facilities were identified as *potentially* BART eligible:

1. Fossil fuel-fired steam electric plants of more than 250 million British thermal units (BTU) per hour heat input
2. Coal cleaning plants (thermal dryers)
3. Kraft pulp mills
4. Portland cement plants
5. Primary zinc smelters
6. Iron and steel mill plants
7. Primary aluminum ore reduction plants
8. Primary copper smelters
9. Municipal incinerators capable of charging more than 250 tons of refuse per day
10. Hydrofluoric, sulfuric, and nitric acid plants
11. Petroleum refineries
12. Lime plants
13. Phosphate rock processing plants
14. Coke oven batteries
15. Sulfur recovery plants
16. Carbon black plants (furnace process)
17. Primary lead smelters
18. Fuel conversion plants
19. Sintering plants
20. Secondary metal production facilities
21. Chemical process plants
22. Fossil-fuel boilers of more than 250 million BTUs per hour heat input
23. Petroleum storage and transfer facilities with a capacity exceeding 300,000 barrels
24. Taconite ore processing facilities
25. Glass fiber processing plants
26. Charcoal production facilities

C.5 REFERENCES

Central Regional Air Planning Association (2005) 2002 CENRAP emissions summaries 121404. Available on the Internet at <http://www.cenrap.org/emission_document.asp> last accessed March 30, 2005.

Cressie N.A.C. (1993) *Statistics for spatial data*, John Wiley & Sons, Inc.

Draxler R.R. and Hess G.D. (1997) Description of the Hysplit 4 modeling system. Technical memorandum by NOAA, ERL ARL-224, December 24.

Environment Canada (1995) 1995 criteria emissions nonroad area source inventory. Prepared for United States Environmental Protection Agency, Research Triangle Park, NC. Available on the Internet at <ftp://ftp.cenrap.org/ei/UNC%20Task%204B/arinv.ca95_v3_nrd+stat+onrd.ida> last accessed December 6, 2004.

Environment Canada (2002) National Pollutant Release Inventory (NPRI) reporting tools and guidance. Available on the Internet at <http://www.ec.gc.ca/pdb/npri/npri_preinfo_e.cfm> last accessed June 6, 2005.

Kuhns H., Green M., Pitchford M., Vasconcelos L., White W., and Mirabella V. (1999) Attribution of particulate sulfur in the Grand Canyon to specific point sources using Tracer-Aerosol Gradient Interpretive Technique (TAGIT). *J. Air & Waste Manage. Assoc.* **49**, 906-915.

Kuhns H., Knipping E.M., and Vukovich J.M. (2005) Development of a United States - Mexico emissions inventory for the Big Bend Regional Aerosol and Visibility Observational (BRAVO) study. *J. Air & Waste Manag. Assoc.* **55** (5), 677-692.

McCoy J. and Johnston K. (2001) Using ArcGIS Spatial Analyst. ESRI.

Mid-Atlantic/Northeast Visibility Union (2002) MANE-VU final 2002 EI summaries. Database of final 2002 EI summaries. Available on the Internet at <ftp.marama.org> last accessed March 21, 2005.

The Visibility Improvement State and Tribal Association of the Southeast (2004a) 2002 VISTAS area source emission inventory. Prepared for Central Regional Air Planning Association, Oklahoma City, OK, by Alpine Geophysics, LLC, Burnsville, NC. Available on the Internet at <ftp://ftp.cenrap.org/ei/UNC%20Task%204B/ida_ar_2002_24mar04.emis.onlyVISTAS.cep.gz> last accessed December 27, 2004.

The Visibility Improvement State and Tribal Association of the Southeast (2004b) 2002 VISTAS point source emission Inventory. Prepared for Central Regional Air Planning Association, Oklahoma City, OK, by Alpine Geophysics, LLC, Burnsville, NC. Available on the Internet at <ftp://ftp.cenrap.org/ei/UNC%20Task%204B/ptinv_vistas_2002_041504.ida.onlyVISTAS.cep.gz> last accessed December 27, 2004.

The Visibility Improvement State and Tribal Association of the Southeast (2004c) 2002 VISTAS nonroad mobile source emission inventory. Prepared for Central Regional Air Planning Association, Oklahoma City, OK, by Alpine Geophysics, LLC, Burnsville, NC. Available on the Internet at <ftp://ftp.cenrap.org/ei/UNC%20Task%204B/ida_nr_2002_23mar04.emis.onlyVISTAS.cep.gz> last accessed December 27, 2004.

U.S. Environmental Protection Agency (2005a) Preliminary 2002 National Emission Inventory (NEI). Available on the Internet at <http://www.epa.gov/ttn/chief/net/2002inventory.html#biogenic> last accessed April 19, 2005.

U.S. Environmental Protection Agency (2005b) Draft 2002 National Emission Inventory (NEI). Available on the Internet at <http://www.epa.gov/ttn/chief/net/2002inventory.html> last accessed April 19, 2005.

Western Regional Air Partnership (2003a) Western Regional Air Partnership (WRAP) 2002 area source inventory version 1. Prepared for Central Regional Air Planning Association, Oklahoma City, OK, by E.H. Pechan & Associates, Inc., Durham, NC. Available on the Internet at <ftp://ftp.cenrap.org/ei/UNC%20Task%204B/arinv.WRAP2002_v3_ida.txt.onlyWRAP.cep.gz> last accessed December 27, 2004.

Western Regional Air Partnership (2003b) Western Regional Air Partnership (WRAP) 2002 point source inventory version 1. Prepared for Central Regional Air Planning Association, Oklahoma City, OK, by E.H. Pechan & Associates, Inc., Durham, NC. Available on the Internet at <ftp://ftp.cenrap.org/ei/UNC%20Task%204B/ptinv.WRAP2002_v1_WRAPonly_ida.txt.gz> last accessed December 27, 2004.

Western Regional Air Partnership (2003c) Western Regional Air Partnership (WRAP) states 2003 nonroad emissions version 2 (no shipping) autumn season. Prepared for Central Regional Air Planning Association, Oklahoma City, OK, by ENVIRON International Corporation, Novato, CA. Available on the Internet at <ftp://ftp.cenrap.org/ei/UNC%20Task%204B/nrinv.Environ_WRAP_aut03_v2_ida.txt.gz> last accessed December 27, 2004.

Western Regional Air Partnership (2003d) Western Regional Air Partnership (WRAP) states 2003 nonroad emissions version 2 (no shipping) spring season. Prepared for Central Regional Air Planning Association, Oklahoma City, OK, by ENVIRON International Corporation, Novato, CA. Available on the Internet at <ftp://ftp.cenrap.org/ei/UNC%20Task%204B/nrinv.Environ_WRAP_spr03_v2_ida.txt.gz> last accessed December 27, 2004.

Western Regional Air Partnership (2003e) Western Regional Air Partnership (WRAP) states 2003 nonroad emissions version 2 (no shipping) summer season. Prepared for Central Regional Air Planning Association, Oklahoma City, OK, by ENVIRON International Corporation, Novato, CA. Available on the Internet at <ftp://ftp.cenrap.org/ei/UNC%20Task%204B/nrinv.Environ_WRAP_sum03_v2_ida.txt.gz> last accessed December 27, 2004.

Western Regional Air Partnership (2003f) Western Regional Air Partnership (WRAP) states 2003 nonroad emissions version 2 (no shipping) winter season. Prepared for Central Regional Air Planning Association, Oklahoma City, OK, by ENVIRON International Corporation, Novato, CA. Available on the Internet at <ftp://ftp.cenrap.org/ei/UNC%20Task%204B/nrinv.Environ_WRAP_win03_v2_ida.txt.gz> last accessed December 27, 2004.

Western Regional Air Partnership (2003g) California, Oregon, Washington shipping emissions version 1. Prepared for Central Regional Air Planning Association, Oklahoma City, OK, by Zachariah Adelman (zac@unc.edu). Available on the Internet at <ftp://ftp.cenrap.org/ei/UNC%20Task%204B/nrinv.WRAP_shipping03_v1_ida.txt.gz> last accessed December 27, 2004.

Wilson D.L., Fanjoy J.N., and Billings R.S. (2004) Gulfwide emission inventory study for the regional haze and ozone modeling effort. Final report prepared for U.S. Department of the Interior, Minerals Management Service, Gulf of Mexico OCS Region, New Orleans, LA by Eastern Research Group, Inc., Morrisville, N.C.

APPENDIX D

DOCUMENTATION OF METHODS AND GRAPHICAL AND TABULAR SUMMARIES OF DATA FOR TASK 7

SOURCE APPORTIONMENT ANALYSES

Documentation for Task 7 is provided in the form of the attached two draft journal articles, “Source Apportionment of $PM_{2.5}$ at a Rural Site in Louisiana Using Positive Matrix Factorization” and “Source Apportionment of $PM_{2.5}$ at Hercules-Glades, Missouri, Using Positive Matrix Factorization”.

Source Apportionment of $PM_{2.5}$ at a Rural Site in Louisiana Using Positive Matrix Factorization

Steven G. Brown, Anna Frankel, Sean M. Raffuse, Hilary R. Hafner and Paul T. Roberts

Sonoma Technology, Inc., Petaluma, CA

Brett A. Anderson

United States Environmental Protection Agency Region 7
Air Planning and Development Branch
901 N. 5th Street
Kansas City, KS 66101

ABSTRACT

Speciated $PM_{2.5}$ data collected as part of the Interagency Monitoring of Protected Visual Environments (IMPROVE) program at Sikes, Louisiana, from March 2001 through February 2004 were analyzed using the multivariate receptor model Positive Matrix Factorization (PMF). Two hundred ninety-six samples and 27 species were utilized, including the organic carbon (OC) and elemental carbon (EC) analytical temperature fractions from the thermal optical reflectance (TOR) method. Eight factors were identified, with good comparison between predicted and measured $PM_{2.5}$ mass (slope = 0.99, r^2 = 0.97) and good orthogonality between factors. Bootstrapping over 300 runs was used to determine the concentrations and uncertainties of each species in the factor profiles. A coal combustion factor was the largest contributor to mass (27% of the median mass on all days and 38% on the worst visibility days) and to ammonium sulfate, which is consistent with coal-fired power plant emissions as the main source of SO_2 in the Ohio and Mississippi River Valleys. Southeastern aged aerosol was responsible for 21% of the mass, and an urban carbonaceous aerosol factor accounted for another 23%. Oil combustion and industrial metals factors were minor contributors to the mass (8% and 7%, respectively). Nitrate contributed 5% of the median mass over all days, and less than 1% of the mass on the worst visibility days, which mostly occurred in the spring through fall. Soil and local burning emissions were generally event-driven, and while they were 5% and 4% of the overall mass, they were only 2% and 1% of the mass on the worst visibility days. Conditional Probability Function (CPF) analysis applied to air mass trajectories and trajectories paired with the emission inventory

to find emission impact potential (EIP) both helped better identify the factors and their source regions.

IMPLICATIONS

A relatively new subset of $PM_{2.5}$ data, the analytical carbonaceous fractions, was used to enhance the identification of factors in this source apportionment work. These carbonaceous fractions helped differentiate and quantify carbonaceous aerosol factors that otherwise would not have been separated and apportioned as well. A more realistic treatment of XRF data close to the detection limit was used to better characterize the known analytical uncertainties of, and provide a better fit for, certain species. Bootstrapping was used to better quantify the composition and uncertainties in the factor profiles by compiling results from 300 individual runs. Lastly, emission inventory data were paired with air mass trajectories to better understand the source regions affecting factors with sulfate. All of these techniques were used to improve the confidence in, and to aid policy makers in understanding, the results.

INTRODUCTION

Particles with diameters of less than 2.5 microns ($PM_{2.5}$) impact human health[1-4] and visibility.[5-7] The EPA has identified a number of $PM_{2.5}$ constituents, such as manganese, arsenic, lead, and diesel particulate matter (DPM), which pose a public health risk in urban areas.[8] Visibility regulations are also promulgated by the EPA directing states to reduce the worst-20% visibility days in their Class 1 areas. To better address these issues, it is vital to understand the composition and characteristics of the sources contributing to $PM_{2.5}$. The Sikes site is in a Class 1 area located in rural Louisiana near the Kisatchie National Forest, approximately 100 miles from nearby urban areas such as Shreveport, Louisiana and Jackson, Mississippi. Sikes is generally impacted by transported aerosol from these urban areas and others such as New Orleans, Houston, and St. Louis. This site is also impacted by regional dust events from the Great Plains and local burning in the area.

In previous analyses of $PM_{2.5}$ data using receptor models with only the total organic carbon (OC) and elemental carbon (EC) fractions, it has been difficult to separate different sources of carbonaceous aerosols, such as gasoline-, diesel-fueled vehicles, aged aerosol transport, and fire emissions. Much of the $PM_{2.5}$ emitted from these sources is carbonaceous,[9-13] and a simple ratio of OC to EC is typically insufficient to quantitatively separate various source types. In urban areas, attempts using receptor modeling and data analysis[14-16] to better determine the gasoline-diesel split, for example, have begun to rely on carbon fractions resulting from the Thermal Optical Reflectance (TOR) protocol[17,18] technique. In rural areas, where the aerosol impacting a site is more aged, motor vehicle and diesel emissions will impact the site together, and will be indistinguishable.[19-21] However, the use of the fractions may better apportion the carbonaceous aerosol between the local and aged transported air masses, and possibly better apportion the contribution from burning or other combustion sources.

METHODS

Data

$PM_{2.5}$ data from March 2001 through February 2004 were collected as part of the Interagency Monitoring of Protected Visual Environments (IMPROVE) program[22] at the Sikes site, shown in Figure 1. These 24-hr samples were collected on Nylon, Teflon, and quartz fiber filters. Teflon filters were analyzed by gravimetric analysis for mass and by x-ray fluorescence (XRF) for elements. The Nylon filter was analyzed by ion chromatography (IC) for sulfate, nitrate, nitrite, and chloride. Ammonium (NH_4^+) was not analyzed, but its mass can be inferred from ionic balance with sulfate and nitrate.[23]

Quartz fiber filters were analyzed by the TOR method[17] to obtain eight thermally resolved fractions of carbonaceous aerosol. OC is volatilized in four steps, all in a helium atmosphere: (1) OC1 consists of the volatilized OC up to 120°C, (2) OC2 from 120° to 250°, (3) OC3 from 250° to 450°, and (4) OC4 from 450° to 550°. After the OC4 section is complete, a 2% O_2/98% He atmosphere is introduced to obtain EC1, and the temperature is then increased to 700°C for EC2 and to 850°C for EC3. A correction for the pyrolysis of OC is made. Pyrolyzed organic carbon (OP) is emitted when the O_2/He atmosphere is first introduced. This amount of OP is defined as the amount detected after the introduction of the O_2/He atmosphere at 550°C until the monitored filter reflectance returns to its original value. As reported, EC1 includes the OP fraction; thus, OP was subtracted from EC1 to achieve the correct EC1 concentration.

Data from the IMPROVE program are routinely validated before being made publicly available; therefore, the overall data quality was very good. Only valid samples from the IMPROVE data were used. Additional quality control (QC) checks performed in this study include comparison of reconstructed fine mass to measured mass and comparison of XRF sulfur to IC sulfate. Only species with good variability (i.e., signal/noise greater than 0.2 when not accounting for seasonal variability) and at least 25% of the data above detection were used. In particular, no sodium or chloride data were used in this analysis; therefore, no sea salt factor could be identified, though the impact of sea salt at this site was expected to be minimal. The final data set contained 296 samples with 27 species (see Table 1).

Source Apportionment With PMF

PMF is a multivariate factor analysis tool applied to a wide range of data, including 24-hr speciated $PM_{2.5}$ data, size-resolved aerosol data, deposition data, air toxics data, and VOC data.[14-16,20,21,24-34] Simply, PMF decomposes a matrix of ambient data into two matrices, which then need to be interpreted by the analyst to discern the source types they represent. The method is considered briefly here and described in greater detail elsewhere.[35,36]

An ambient data set can be viewed as a data matrix X of *i* by *j* dimensions, in which *i* number of samples and *j* chemical species were measured. The goal of multivariate receptor modeling is to identify a number of sources *p* that best characterize the $PM_{2.5}$ at a site, the species profile *f* of each source, and the amount of mass *g* contributed by each source to each individual sample:

$$X_{ij} = \sum_{k=1}^{p} g_{ik} f_{kj} + e_{ij} \qquad (1)$$

One strength of PMF is that results are constrained by a penalty function so that no sample can have a negative source contribution and no species can have a negative concentration in any source profile. Another strength of PMF, compared to other source apportionment tools such as principle component analysis (PCA), is that each data point can be weighed individually. This feature allows the analyst to adjust the influence of each data point, depending on the confidence in the measurement, and retain data that might otherwise be screened out. Data below detection can be retained for use in the model, with the associated uncertainty adjusted so these data points are given less weight in the model solution (i.e., these data have less influence on the solution than measurements above the detection limit). By individually weighing data, samples with some species missing or below detection do not need to be excluded as a whole, rather the analyst can adjust the uncertainty so these data have little or no impact on the final solution. The PMF solution minimizes the object function Q(E), based upon these uncertainties (*u*):

$$Q = \sum_{i=1}^{n} \sum_{j=1}^{m} \left[\frac{x_{ij} - \sum_{k=1}^{p} g_{ik} f_{kj}}{u_{ij}} \right]^2 \qquad (2)$$

Methods used in analysis for replacing and developing uncertainty values for missing and below-detection-limit data were drawn from previous work with PMF.[20,21,25,26,28,37] Since the solution found by PMF relies on both concentration data and on error estimates, these error estimates must be chosen judiciously so that they reflect the quality and reliability of each data point. The missing and below-detection-limit data are assigned less weight compared to actual measured values, so these data are less important to the solution.[20,21,25,26,28,37] Data below the minimum detection limit (MDL) were substituted with MDL/2; missing data were substituted with the median concentration. Similar to previous studies, the uncertainty for data above detection was calculated as the sum of the analytical uncertainty (UNC) plus one-third the MDL, uncertainty for data below detection was 5/6*MDL, and uncertainty for missing data was four times the median. Additionally, it has shown that XRF data reported above MDL but below approximately 10*MDL are more uncertain[38]; therefore, these data were assigned an uncertainty twice as high as concentrations above this threshold, i.e., 2*(UNC+MDL/3).

The robust mode was used in this analysis to reduce the influence of outliers; between 5 and 13 factors were explored. The uncertainty of the amount of each species in a given factor was determined by bootstrapping 300 runs and calculating the interquartile range of the factor loading over these runs. This was done using multiple starting points and rotations, so that the range of solutions PMF gives can be used as a measure of the confidence in a given factor. Scaled residuals were between -3 and 3 for all species demonstrating a good fit of the modeled results. The factors also showed oblique edges, which has been proposed as an additional check of the quality of the rotation.[39] A multi-linear regression (MLR) was applied to scale the factors back into the original μg/m^3 units by regressing the total measured $PM_{2.5}$ mass against the unscaled factor strength contributions:

$$X_{ij} = \sum_{k=1}^{p} \left(s_k g_{ik} \right) \left(\frac{f_{kj}}{s_k} \right) \tag{3}$$

The resulting coefficients were then applied to each factor to regain the μg/m^3 units.

Conditional Probability Integrative Analysis

A conditional probability function (CPF) was applied to help interpret the results.[14,16,24,40] The transport patterns of the highest 10% concentration days of a given factor were compared to the climatological transport patterns. This comparison highlights the differences in transport and areas of influence between the general transport pattern (i.e., the climatology) and high concentration days of a given factor. Using the NOAA HYSPLIT model,[41] 96-hr backward trajectories were run for all sample dates, which were then mapped as a spatial probability density (D_0):

$$D_0 = \frac{D_c}{\hat{D}} \tag{4}$$

D_c = Density at grid cell c

$\hat{D}$ = Maximum density over all grid cells (typically the density at the receptor site)

$$D_c = \sum_{i=1}^{n} \kappa_R(r_n) \tag{5}$$

r_n = distance between grid cell center and hourly trajectory point n

$$K_R(r) = \text{kernel density function} = \begin{cases} \dfrac{3}{\pi R^2}\left[1-\left(\dfrac{r}{R}\right)^2\right]^2 & \text{for } r < R \\ 0 & \text{for } r \geq R \end{cases} \tag{6}$$

R = search radius

The search radius was determined dynamically by dividing the geographic extent of all endpoints by 30.[42,43] The density D_k was then computed using only backward trajectories for the highest 10% concentration days of a given factor k. Areas that have a higher than typical influence on the high concentration days are then highlighted by calculating the conditional probability P_k:

$$P_k = D_k - D_0 \tag{7}$$

This Conditional Probability Integrative Analysis (CoPIA) is very similar to the CPF analyses employed in other studies;[14,16,24,40] however, CoPIA is adapted to take advantage of tools available in a geographic information system (GIS) framework. Ensemble backward trajectories were run every 6 hours to account for variability over a 24-hr sampling period. Emissions data, such as point source and fire locations, were overlaid on the CoPIA analysis to identify specific emissions sources in likely source areas.

Emission Impact Potential (EIP) Calculations

While trajectory analyses such as CoPIA can help identify transport patterns and likely areas of influence, only a broad conclusion can be reached, such as "the factor showed influence from the Ohio River Valley". However, this analysis only accounts for transport, and not the spatial distribution or magnitude of emissions. For example, a large, distant source and a small nearby source could influence a site in a similar way. To gain a better understanding of the source regions for a given factor, a GIS-tool was used to weight county-level emission inventory data by the trajectory kernel density of the highest 10% concentration days for a given factor. For a given factor, SO_2 emissions were weighted by the frequency and residence time of modeled backward trajectories passing over each county to estimate the potential for emissions from each county to impact the site. This is called the emission impact potential (EIP). This simple analysis technique is useful for characterizing general patterns and developing a preliminary conceptual model of factors affecting visibility conditions, but without the need for, and as an initial step toward, full-scale photochemical modeling efforts.

The EIP of a given county is calculated as:

$$EIP = \frac{E_p * D_0}{f\,(\text{distance})} \tag{8}$$

where

$$\begin{aligned} E_p &= \text{county total emissions of pollutant } p \\ D_0 &= \text{spatial probability density at the county centroid} \\ f &= \text{function of distance between county and receptor} \end{aligned}$$

The EIP may be divided by a distance function to roughly account for dilution and increased uncertainty in model outputs far from the receptor site. However, for this study, $f = 1$, assuming vertical dilution is similarly small compared to the horizontal transport distance for all areas and kernel density sufficiently accounts for horizontal dilution and uncertainty. This tool is used for simple analysis only and does not account for atmospheric chemistry, deposition, or other effects, but is expected to qualitatively provide insight into the potential sources affecting mass.

RESULTS AND DISCUSSION

Preliminary Data Analysis

Preliminary data analysis was conducted to gain insight into the trends and relationships among species that would impact later source apportionment with PMF. Inspection of the overall composition, changes in composition by season or on days of poor visibility, species relationships, and day-of-week trends assisted in identifying possible source types.

Annual Median Composition. Figure 2 shows the median $PM_{2.5}$ composition. Ammonium sulfate and nitrate concentrations are calculated from sulfate and nitrate concentrations, assuming full neutralization by ammonium. OC is represented by OC mass (OMC), equal to 1.4 times OC,[44,45] which takes into account the mass of oxygen and hydrogen associated with the carbon, though this factor may actually be higher than 1.4.[44,46] As shown in Figure 2, ammonium sulfate is the dominant component (accounting for 48% of the average mass), followed by OMC (34%). Ammonium nitrate, EC, and soil account for the remaining mass. Dominance of ammonium sulfate is typical of the eastern half of the United States, and the significant portion of mass from OMC demonstrates the importance of determining its source regions.

Seasonal Composition. Changes in $PM_{2.5}$ mass and composition between seasons (Figures 3a and 3b) may reflect differences in transport regimes or source strengths. Mass is highest in spring through fall, with a summer peak, and then drops off significantly in the winter. Ammonium sulfate contributions to mass range between a peak in the spring (54% of the mass) and a low (44%) in the winter. OMC accounts for between 30% of the mass in spring and 38% of the mass in the fall. In spring and summer, soil contributions are between 7% and 9%, while in fall and winter soil contributions are less than 5%. Nitrate accounts for 10% of the mass in winter, but is less than 4% of the mass during the warmer months of spring and summer. While changes in soil concentrations are due to wind-blown dust impacts likely from the arid western plains, the changes in ammonium sulfate and OMC suggest different source influences during these two seasons, even though total mass is similar. These seasonal differences are expected to be observed in PMF analysis and may be because of changes in sources or transport, which will be analyzed further using results from PMF analysis.

Composition on Poor Visibility Days. To investigate which components (i.e., OMC, sulfate, soil, etc.) have the greatest impact on days with severely impaired visibility, the $PM_{2.5}$ composition on the worst-20% visibility days (referred to as the worst visibility days in the remainder of this article) was examined (Figure 4a). Using the IMPROVE equation,[22,23] which likely does not fully account for extinction by OC,[47] the total light extinction (b_{ext}) contribution of each chemical component was calculated. On poor visibility days, which occurred in all months but predominantly in spring and summer, the average $PM_{2.5}$ mass was 16.1 $\mu g/m^3$ with 54% of the mass attributable to ammonium sulfate, 33% to OMC, and the remaining 13% to other components. This composition is actually similar to the median composition during all days, suggesting that the meteorological conditions and total mass are important in determining the visibility degradation on a given day. The analysis of the estimated contributions to light extinction in Figure 4b further shows the importance of ammonium sulfate becuase it dominates the light extinction (71% on average), followed by OMC (17%), ammonium nitrate (6%), and EC (5%). Since ammonium sulfate and OMC account for 88% of the light extinction on the worst visibility days, these components are likely the best candidates for emission reductions to help improve visibility.

Species Relationships. Species relationships were investigated because the degree of covariation among species impacts how species and sources are allocated in source apportionment. It is important to understand these relationships before conducting source apportionment to ensure that PMF results fit within in the context of the data. One example, Figure 5a, shows the fair relationship between ammonium sulfate and selenium ($r^2 = 0.36$), which is typical of coal combustion, although the amount of scatter also suggests other existing sources of these species. Potassium, often used as a tracer for wood smoke,[48,49] had some correlation in a number of samples with EC (Figure 5b) and OC (not shown), which are also emitted by wood combustion.[48,50] The relationship between potassium and OC and EC indicates that a smoke factor may be found by PMF, but that the majority of the carbonaceous aerosol is likely not associated with burning. In addition to the expected good relationships within the OC and EC fractions, the pyrolyzed organic fraction, OP, and the first EC fraction, EC1, showed a fairly good relationship (Figure 5c), especially in the summer and fall. These results may in part be due to analytical bias since these fractions are analyzed sequentially, but they may also suggest that there is a source of OP/EC1 in addition to a source of the other OC fractions.

PMF Results

Eight factors were resolved for the ambient $PM_{2.5}$ at Sikes and identified as (1) coal combustion, (2) southeastern aged aerosol, (3) urban carbonaceous, (4) oil combustion, (5) industrial metals, (6) nitrate, (7) soil, and (8) burning. Factor profiles with the standard deviation over 300 runs graphed as the error bars are shown in Figure 6, and a time series of all samples (every third day) are shown in Figure 7. The PMF solution accounted for the measured mass well, with a slope of 0.99 and r^2 of 0.97 between reconstructed and measured mass (Figure 8). The average compositions over all seasons and on the worst visibility days during the time period are shown in Figure 9. Figure 10 shows CoPIA plots for coal combustion, southeastern aged aerosol, urban carbonaceous, and industrial metals. Figure 11 shows air mass trajectories on days of high soil contributions, demonstrating likely Saharan dust episodes. Figure 12 shows air mass trajectories on days of high burning influence with fire locations from MODIS. Lastly, Figure 13 shows SO_2 EIP analysis results by county and by state for coal combustion, aged aerosol, and oil combustion.

The coal combustion factor was the largest contributor to mass (27% of the median mass on all days and 38% on the worst visibility days), which is consistent with coal emissions as the main source of ammonium sulfate in the region. A southeastern aged aerosol factor was responsible for another 21% of the mass on all days, and 28% of the mass on the worst visibility days. Carbonaceous aerosol from urban areas, most likely mobile sources, accounted for 23% of the mass overall, and 19% on the worst visibility days. Oil combustion and smelter operation factors were minor contributors to the mass (8% and 7%, respectively), and contributed even less on the worst visibility days (6% and 5%, respectively). A nitrate factor was significant only during the winter; while it contributed 5% of the median mass over all days, it accounted for less than 1% of the mass on the worst visibility days, which mostly occurred in the spring through fall, when nitrate concentrations were low. Soil and local burning emissions were both event-driven factors; and while they were 5% and 4% of the overall mass, they were only 2% and 1% of the mass on the worst visibility days, indicating that soil- and burn-events are likely not the key contributors to visibility degradation at Sikes. Overall, and similar to the basic data analysis results, the factor contributions on the worst visibility days were not much different than on average.

A coal combustion factor was identified by typical tracers of coal combustion—sulfate, selenium, and hydrogen.[20,25,26,51] This factor was the largest component of the mass on all days (27%), as well as on the worst visibility days (38%). Since most of the factor's mass derives from ammonium sulfate, this factor is likely more important in terms of visibility extinction. Ammonium sulfate accounted for half the mass at Sikes, and most of the sulfate is found in this factor; the remaining sulfate is found in the oil combustion and secondary transport factors. This factor was highest on days with transport from the Ohio River and Mississippi Valleys, where many coal-fired power plants are located and which have been identified as a significant area for the origin of sulfate transport in other studies in the mid-Atlantic and Northeast.[20,25,26,51] Additionally, EIP analysis using the top 10% concentration days of this factor with the SO_2 emission inventory further shows the high amount of influence from the Indiana-Alabama corridor, as about two-thirds of the EIP comes from these regions. This analysis also shows that the EIP is actually dominated by only a few counties in a given state, where there are major coal combustion facilities. While CoPIA showed possible influence from the State of Mississippi as well, the small amount of EIP indicates that this area likely affects Sikes less than regions located further away.

A southeastern aged aerosol factor was identified by sulfate and carbonaceous aerosol, predominantly the OP and EC1 fractions, consistent with earlier data analysis and demonstrating the usefulness of the carbonaceous fractions. In addition to carbonaceous aerosol, sulfate accounted for about 50% of this factor's mass. This factor was generally highest during the summer, when photochemistry increases, and comprised 21% of the mass over all days, and was the second highest component of the mass on the worst visibility days (28%). The transport regime when this factor was high differed from the coal combustion factor, and was characterized by slow-moving air masses from Louisiana, Mississippi, and Alabama. A combination of various anthropogenic and biogenic sources in these areas is likely for the carbonaceous component. The sulfate component can be further interpreted using EIP analysis, which shows that, unlike the coal combustion factor, SO_2 emissions emanate from a number of counties throughout the southeastern United States and Texas. Fifty-one percent of the SO_2 EIP influence comes from Louisiana, Mississippi, and Alabama, demonstrating the degree of local influence on this factor.

Urban carbonaceous aerosol, most likely from mobile sources, was another identified factor, and contributed 23% of the mass, on average, and 19% of the mass on the worst visibility days. Except for one spike, this factor had very little seasonal variability, which would be consistent with a persistent source, such as mobile emissions. Similar to the secondary transport factor, this factor was characterized by slow-moving air masses, though this factor was predominantly because of influence from urban areas along the Mississippi River in Missouri, Arkansas, Tennessee, and Louisiana.

Oil combustion was identified by its typical markers, nickel and vanadium.[14,20,21,24-26,52,53] This factor originates from the numerous oil refineries and drilling stations in Louisiana, Texas, and in the Gulf of Mexico, as well as the use of oil burning for energy in these areas. A small amount of the ammonium sulfate was also associated with this factor, and the factor contributed 8% of the median mass. On the worst visibility days, the factor had a similar concentration, but since the overall $PM_{2.5}$ mass was higher, the factor contributed only 6% to the total. Sulfate was the main component of the mass of this factor, and nearly 50% of the SO_2 EIP came from Louisiana, as expected. Other contributions came from the southeastern United States, Texas, Florida, and the Gulf of Mexico.

Another industrial factor, associated with copper, lead, zinc, manganese, and arsenic, was also identified. This factor contributed 7% of the median mass, and again was similar in concentration on the worst visibility days, when it was 5% of the mass. This factor comes from a source region different than the oil combustion factor; air masses on the industrial metals factor's highest concentration days come from the north along the Mississippi River, where numerous industrial facilities are located. Figure 10d shows the CoPIA results, indicating potential influence of these facilities.

An ammonium nitrate factor was identified, since it has a very strong seasonal signal that is independent of other components. It is highest in the winter, and is extremely low in the other warmer months, when nitrate production would be limited simply because of the ambient temperature. This factor was 5% of the median mass, but was minimal (< 1%) on the worst visibility days, which mostly occurred in the warmer months. This factor was highest under conditions of slow-moving cool air masses from Arkansas, Missouri, and the Mississippi River area, likely from a combination of on-road mobile sources and stationary sources.

A soil factor was identified by silicon, iron, and titanium and was, in general, an event-driven factor. There were only a few large events when this factor showed high concentrations, including the two biggest events on July 1 and July 31, 2002. These two samples had the highest concentrations of the soil factor, nearing 10 $\mu g/m^3$, while typically the factor averaged only 0.6 $\mu g/m^3$ (5% of the mass). Trajectories on these days (Figure 11) suggest that the high soil factor days in July 2002 may have been Saharan dust episodes; 10-day backward trajectories show fast transport over the Atlantic Ocean. Other days with high concentrations of this factor appear to be caused by transport over the Great Plains. Despite the large spikes in the soil factor concentrations, none of the highest concentration days occurred on the worst visibility days, indicating that while soil contributions to ambient $PM_{2.5}$ are event-driven, this factor is not significant on the worst visibility days.

A wood and biomass burning factor was identified by the presence of potassium[48-50,54] and a small amount of carbonaceous aerosol. This factor also included calcium, which may be caused by entrainment of soil with the smoke.[55,56] The analytical carbonaceous fractions aided in identifying and quantifying this factor, since runs using only a total OC and EC did not effectively resolve this factor. Air mass trajectories were combined with fire location satellite data to better identify this factor, and the combination suggests this factor is significant only when local burning and conducive meteorology occur. On two of the highest concentration days of this factor, August 4, 2003, and April 19, 2001, air mass trajectories show transport from nearby fire locations (Figure 12). Overall, this factor accounted for only 4% of the median mass, and only 2% on the worst visibility days. None of the highest concentration days of this factor were among the worst visibility days, indicating that while burning is episodic, it does not appear to be an important contributor to poor visibility at Sikes.

CONCLUSIONS

PMF was applied to speciated $PM_{2.5}$ data collected as part of the IMPROVE program at Sikes, Louisiana, from March 2001–February 2004. Modeled results accounted for the mass and were consistent with known sources and their locations. The use of the analytical OC/EC fractions, better uncertainty estimates for data near the detection limit, and bootstrapping all helped better apportion and quantify the uncertainties in the identified factors. Eight factors were identified: (1) coal combustion, (2) southeastern aged aerosol, (3) urban carbonaceous, (4) oil combustion, (5) smelter, (6) nitrate, (7) soil, and (8) burning. CPF analysis and emission inventory data were used to confirm the identification of sources. Calculating EIP by combining trajectory density with county-level emission inventory data helped identify the source regions for particular factors. Results showed that a combination of local (such as burning, nitrate, and carbonaceous aerosol) and regional (coal combustion, oil combustion, and industrial metals) impact the site. However, on the worst visibility days, coal combustion, urban carbonaceous, and southeastern aged aerosol factors were the largest contributors to the mass. Event-driven factors such as biomass/wood burning and soil were clearly evident, though their impact was minimal on the worst visibility days.

ACKNOWLEDGMENTS

This work was supported by the Central States Regional Air Planning Association (CENRAP) by contract number 904780.

REFERENCES

1. Dockery, D.W.; Pope, C.A., III Acute respiratory effects of particulate air pollution; *Annu Rev Public Health* **1994**, *15*, 107-132.
2. Dockery, D.W.; Pope, C.A.; Xu, X.P.; Spengler, J.D.; Ware, J.H.; Fay, M.E.; Ferris, B.G.; Speizer, F.E. An association between air pollution and mortality in six U.S. cities; *New Engl. J. Med.* **1993**, *329*, 1753-1759.
3. Wu, J.; Lurmann, F.; Winer, A.; Lu, R.; Turco, R.; Funk, T. Development of an individual exposure model for application to the Southern California Children's Health Study; *Atmos. Environ.* **2005**, *39*, 259-273.
4. Gilliland, F.; Avol, E.; Kinney, P.; Jerret, M.; Dvonch, T.; Lurmann, F.; Buckley, T.; Breysse, P.; Keeler, J.; de Villiers, T. *et al.* Air pollution exposure assessment for epidemiologic studies of pregnant women and children: lessons learned from the Centers

for Children's Environmental Health and Disease Prevention Research; *Environ Health Perspect* **2005**, in press.

5. Malm, W.C.; Schichtel, B.A.; Pitchford, M.L.; Ashbaugh, L.L.; Eldred, R.A. Spatial and monthly trends in speciated fine particle concentration in the United States; *Journal of Geophysical Research-Atmospheres* **2004**, *109*(D3).
6. Watson, J.G. 2002 Critical review -- Visibility: science and regulation; *J. Air & Waste Manag. Assoc.* **2002**, *52*(6), 628-713.
7. Delucchi, M.A.; Murphy, J.J.; McCubbin, D.R. The health and visibility cost of air pollution: a comparison of estimation methods; *Journal of Environmental Management* **2002**, *64*(2), 139-152.
8. U.S. Environmental Protection Agency *Highway vehicle emission estimates-II*, 1995.
9. Watson, J.G.; Chow, J.C.; Lurmann, F.W.; Musarra, S.P. Ammonium nitrate, nitric acid, and ammonia equilibrium in wintertime Phoenix, Arizona; *J. Air & Waste Manag. Assoc.* **1994**, *44*, 405-412.
10. Lowenthal, D.H.; Zielinska, B.; Chow, J.C.; Watson, J.G.; Gautam, M.; Ferguson, D.H.; Neuroth, G.R.; Stevens, K.D. Characterization of heavy-duty diesel vehicle emissions; *Atmos. Environ.* **1994**, *28*, 731-744.
11. Schauer, J.J.; Cass, G.R. Source apportionment of wintertime gas-phase and particle-phase air pollutants using organic compounds as tracers; *Environ. Sci. Technol.* **2000**, *34*(9), 1821-1832.
12. Kleeman, M.J.; Schauer, J.J.; Cass, G.R. Size and composition distribution of fine particulate matter emitted from motor vehicles; *Environ. Sci. Technol.* **2000**, *34*, 1132-1142.
13. Schauer, J.J.; Kleeman, M.J.; Cass, G.R.; Simoneit, B.R.T. Measurement of emissions from air pollution sources. 2. C_1 through C_{30} organic compounds from medium duty diesel trucks; *Environ. Sci. Technol.* **1999**, *33*(10), 1578-1587.
14. Kim, E.; Hopke, P.K.; Edgerton, E.S. Source identification of Atlanta aerosol by positive matrix factorization; *J. Air & Waste Manage. Assoc.* **2003**, *53*, 731-739.
15. Maykut, N.; Knowle, K.; Larson, T.V. *Seattle $PM_{2.5}$ characterization studies*; Draft report prepared by Puget Sound Air Pollution Control Agency, Seattle, WA, 1998.
16. Kim, E.; Hopke, P.K.; Edgerton, E.S. Improving source identification of Atlanta aerosol using temperature resolved carbon fractions in positive matrix factorization; *Atmos. Environ.* **2004**, *38*, 3349-3362.
17. Chow, J.C.; Watson, J.G.; Pritchett, L.C.; Pierson, W.R.; Frazier, C.A.; Purcell, R.G. The DRI thermal/optical reflectance carbon analysis system: description, evaluation and applications in U.S. air quality studies; *Atmos. Environ.* **1993**, *27A*(8), 1185-1201.
18. Chow, J.C.; Watson, J.G.; Crow, D.; Lowenthal, D.H.; Merrifield, T. Comparison of IMPROVE and NIOSH carbon measurements; *Aerosol Sci. Technol.* **2001**, *34*, 23-34.
19. Zhao, W.; Hopke, P.K. Source apportionment for ambient particles in the San Gorgonio wilderness; *Atmos. Environ.* **2004**, *38*, 5901-5910.
20. Poirot, R.L.; Wishinski, P.R.; Hopke, P.K.; Polissar, A.V. Comparative application of multiple receptor methods to identify aerosol sources in northern Vermont; *Environ. Sci. Technol.* **2001**, *35*(23), 4622-4636.
21. Song, X.-H.; Polissar, A.V.; Hopke, P.K. Sources of fine particle composition in the northeastern U.S.; *Atmos. Environ.* **2001**, *35*, 5277-5286.

22. Malm, W.C.; Sisler, J.F.; Huffman, D.; Eldred, R.A.; Cahill, T.A. Spatial and seasonal trends in particulate concentration and optical extinction in the United States; *J. Geophys. Res.* **1994**, *99*(D1), 1347-1370.

23. Overview of IMPROVE and visibility. <http://vista.cira.colostate.edu/improve/Overview/Overview.htm> last accessed August 4, 2004. By IMPROVE.

24. Kim, E.; Hopke, P.K. Improving source identification of fine particles in a rural northeastern U.S. area utilizing temperature-resolved carbon fractions; *J. Geophys. Res.* **2004**, *109*(D9).

25. Lee, J.H.; Yoshida, Y.; Turpin, B.J.; Hopke, P.K.; Poirot, R.L.; Lioy, P.J.; Oxley, J.C. Identification of sources contributing to mid-Atlantic regional aerosol; *J. Air & Waste Manage. Assoc.* **2002**, *52*, 1186-1205.

26. Polissar, A.V.; Hopke, P.K.; Poirot, R.L. Atmospheric aerosol over Vermont: chemical composition and sources; *Environ. Sci. Technol.* **2001**, *35*(23), 4604-4621.

27. Yakovleva, E.; Hopke, P.K.; Wallace, L. Receptor modeling assessment of particle total exposure assessment methodology data; *Environ. Sci. Technol.* **1999**, *33*(20), 3645-3652.

28. Ramadan, Z.; Song, X.-H.; Hopke, P.K. Identification of sources of Phoenix aerosol by positive matrix factorization; *J. Air & Waste Manage. Assoc.* **2000**, *50*, 1308-1320.

29. Zhou, L.; Kim, E.; Hopke, P.K.; Stanier, C.O.; Pandis, S. Advanced factor analysis on Pittsburgh particle size-distribution data; *Aerosol Sci. Technol.* **2004**, *38*(S1), 118-132.

30. Anttila, P.; Paatero, P.; Tapper, U.; Jarvinen, O. Source identification of bulk wet deposition in Finland by positive matrix factorization; *Atmos. Environ.* **1995**, *29*(14), 1705-1718, published without a date.

31. Brown, S.G.; Hafner, H.R.; Shields, E. Source apportionment of Detroit air toxics data with positive matrix factorization. Paper no. 41 presented at the *Air & Waste Management Association Symposium on Air Quality Measurement Methods and Technology, Research Triangle Park, NC, April 19-22* STI-2450, 2004.

32. Brown, S.G.; Hafner, H.R. Source apportionment of VOCs in the Houston, Texas, area. Presented at the *NARSTO Workshop on Innovative Methods for Emission-Inventory Development and Evaluation, Austin, TX, October 14-16* STI-2356, 2003.

33. Buzcu, B.; Fraser, M. Positive matrix factorization analysis of volatile organic compound concentrations in Houston, TX. Paper presented at *NARSTO Workshop on Innovative Methods for Emission-Inventory Development and Evaluation, Austin, TX, October 14-17,* Rice University, Houston, TX, 2003.

34. Zhao, W.; Hopke, P.K.; Karl, T. Source identification of volatile organic compounds in Houston, TX; *Environmental Science and Technology* **2004**, *38*, 1338-1347.

35. Paatero, P. Least squares formulation of robust non-negative factor analysis; *Chemometrics and Intelligent Laboratory Systems* **1997**, *37*, 23-35.

36. Paatero, P.; Tapper, U. Positive matrix factorization: a non-negative factor model with optimal utilization of error estimates of data values; *Environmetrics* **1994**, *5*, 111-126.

37. Hopke, P.K. *A guide to Positive Matrix Factorization*; by the Department of Chemistry, Clarkson University, Potsdam, NY, 2003.

38. White, W.H.; Eldred, R.A.; Feeney, P.J.; McDade, C.E.; Perley, B.P.; Shadoan, D.J.; Wakabayashi, P.H. Behavior of fine-particle elemental data near the detection limit. Paper No. 24 for presentation at the *Air and Waste Management Association's Regional*

and Global Perspectives on Haze: Causes, Consequences and Controversies – Visibility Specialty Conference, Asheville, NC, October 25-29, 2004.

39. Paatero, P.; Hopke, P.K.; Begum, B.A.; Biswas, S.W. A graphical diagnostic method for assessing the rotation in factor analytical models of atmospheric pollution; *Atmos. Environ.* **2004**, in press.
40. Ashbaugh, L.L.; Malm, W.C.; Sader, W.Z. A residence time probability analysis of sulfur concentrations at Grand Canyon National Park; *Atmos. Environ.* **1985**, *19*(8), 1263-1270.
41. Draxler, R.R.; Hess, G.D. *Description of the Hysplit 4 modeling system*; ERL ARL-224; by NOAA, 1997.
42. McCoy, J.; Johnston, K. *Using ArcGIS Spatial Analyst*; ESRI., 2001.
43. Cressie, N.A.C. *Statistics for spatial data*; John Wiley & Sons, Inc., 1993.
44. Turpin, B.; Saxena, P. Species contributions to $PM_{2.5}$ mass concentrations: revisiting common assumptions for estimating organic mass. Presented at the *Air & Waste Management Association International Specialty Conference, $PM_{2.5}$: A Fine Particle Standard, Long Beach, CA, January 28-30*, 1998.
45. Turpin, B.J.; Huntzicker, J.J.; Larson, S.M.; Cass, G.R. Los Angeles summer midday particulate carbon-primary and secondary aerosol; *Environ. Sci. Technol.* **1991**, *25*, 1788-1793.
46. Turpin, B.J.; Lim, H.-J. Species contribution to $PM_{2.5}$ mass concentrations: revisiting common assumptions for estimating organic mass; *Aerosol Sci. Technol.* **2001**, *35*(10), 602-610.
47. Lowenthal, D.; Kumar, N. $PM_{2.5}$ mass and light extinction reconstruction in IMPROVE; *J. Air & Waste Manage. Assoc.* **2003**, *53*(9), 1109-1120.
48. Fine, P.M.; Cass, G.R.; Simoneit, B.R.T. Chemical characterization of fine particle emissions from the fireplace combustion of wood types grown in the Midwestern and Western United States; *Environmental Engineering Science* **2004**, *21*(3), 387-409.
49. Poirot, R. *Tracers of opportunity: Potassium*, 1998.
50. Schauer, J.J.; Kleeman, M.J.; Cass, G.R.; Simoneit, B.R.T. Measurement of emissions from air pollution sources. 3. C_1 through C_{29} organic compounds from fireplace combustion of wood; *Environ. Sci. Technol.* **2001**, *35*(9), 1716-1728.
51. Song, X.H.; Polissar, A.V.; Hopke, P.K. Sources of fine particle composition in the northeastern U.S.; *Atmos. Environ.* **2001**, *35*(31), 5277-5286.
52. Kim, E.; Hopke, P.K. Source apportionment of fine particles at Washington, DC, utilizing temperature-resolved carbon fractions; *J. Air & Waste Manage. Assoc.* **2004**, *54*(7), 773-785.
53. Zheng, M.; Cass, G.R.; Schauer, J.J.; Edgerton, E.S. Source apportionment of $PM_{2.5}$ in the southeastern United States using solvent-extractable organic compounds as tracers; *Environ. Sci. Technol.* **2002**, *36*, 2361-2371.
54. Fine, P.M.; Cass, G.R.; Simoneit, B.R.T. Organic compounds in biomass smoke from residential wood combustion: emissions characterization at a continental scale; *Journal of Geophysical Research-Atmospheres* **2002**, *107*(D21).
55. Anderson, B.A.; Davis, M.F. Integrating source and receptor analytical methods for a fine particulate and ozone: a case study. Presented at the *Air and Waste Management Association's Regional and Global Perspectives on Haze: Causes, Consequences and Controversies – Visibility Specialty Conference, Asheville, NC, October 25-29*, 2004.

56. Guyon, P.; Graham, B.; Roberts, G.C.; Mayol-Bracero, O.L.; Maenhaut, W.; Artaxo, P.; Andreae, M.O. Sources of optically active aerosol particles over the Amazon forest; *Atmos. Environ.* **2004**, *38*, 1039-1051.

About the Authors

Steven G. Brown is an Air Quality Analyst and Project Manager, Anna Frankel is an Air Quality Data Analyst, Sean M. Raffuse is an Air Quality Analyst, Hilary R. Hafner is Senior Manager of the Air Quality Data Analysis Division, and Paul T. Roberts is Executive Vice President at Sonoma Technology, Inc. Brett A. Anderson is with the Air Planning and Development Branch of the United States Environmental Protection Agency Region 7. Address correspondence to: Steven G. Brown, Sonoma Technology, Inc., 1360 Redwood Way, Suite C, Petaluma, CA 94954; phone: (707) 665-9900; e-mail: sbrown@sonomatech.com.

Keywords

Source apportionment
PMF
$PM_{2.5}$
Louisiana
Receptor modeling
IMPROVE

Table 1. Summary statistics of species used in PMF analysis (in μg/m^3) for Sikes March 2001–February 2004 (N=296).

Species	Median	Mean	Standard Dev	N Missing	N below 10*MDL and above MDL	N below MDL	% below MDL
AS	0.0004	0.0004	0.0003	28	243	55	18
BR	0.0020	0.0025	0.0016	28	2	0	0
CA	0.0230	0.0354	0.0402	28	1	15	5
CU	0.0004	0.0005	0.0003	28	237	5	2
EC1	0.4548	0.5652	0.3664	50	28	1	0
EC2	0.0704	0.0792	0.0500	50	266	27	9
EC3	0	0.0066	0.0101	50	105	194	65
FE	0.0224	0.0474	0.0795	28	0	0	0
H	0.4256	0.4997	0.2903	28	0	0	0
K	0.0570	0.0731	0.0549	28	1	0	0
MN	0.0007	0.0012	0.0016	28	61	51	17
NI	0.0002	0.0002	0.0003	28	168	112	37
NO3	0.2642	0.4042	0.4566	27	119	2	1
OC1	0.0645	0.1245	0.1944	0	177	94	31
OC2	0.3425	0.4037	0.3150	0	128	6	2
OC3	0.7250	0.8459	0.6227	0	134	1	0
OC4	0.5573	0.6454	0.4269	0	19	1	0
OP	0.2191	0.2679	0.2521	50	155	35	12
PB	0.0011	0.0013	0.0008	28	67	3	1
RB	0.0005	0.0006	0.0003	28	208	85	28
SE	0.1203	0.2004	0.2792	28	122	1	0
SI	2.9655	3.2557	2.1163	28	16	0	0
SO4	0.0003	0.0005	0.0006	27	1	0	0
SR	0.0022	0.0058	0.0099	28	218	46	15
TI	0.0006	0.0011	0.0013	28	33	17	6
V	0.0039	0.0044	0.0023	28	93	73	24
ZN	0.0004	0.0004	0.0003	28	0	0	0

Figure 1. Location of the Sikes, Louisiana, IMPROVE air quality monitoring site (SIKE1).

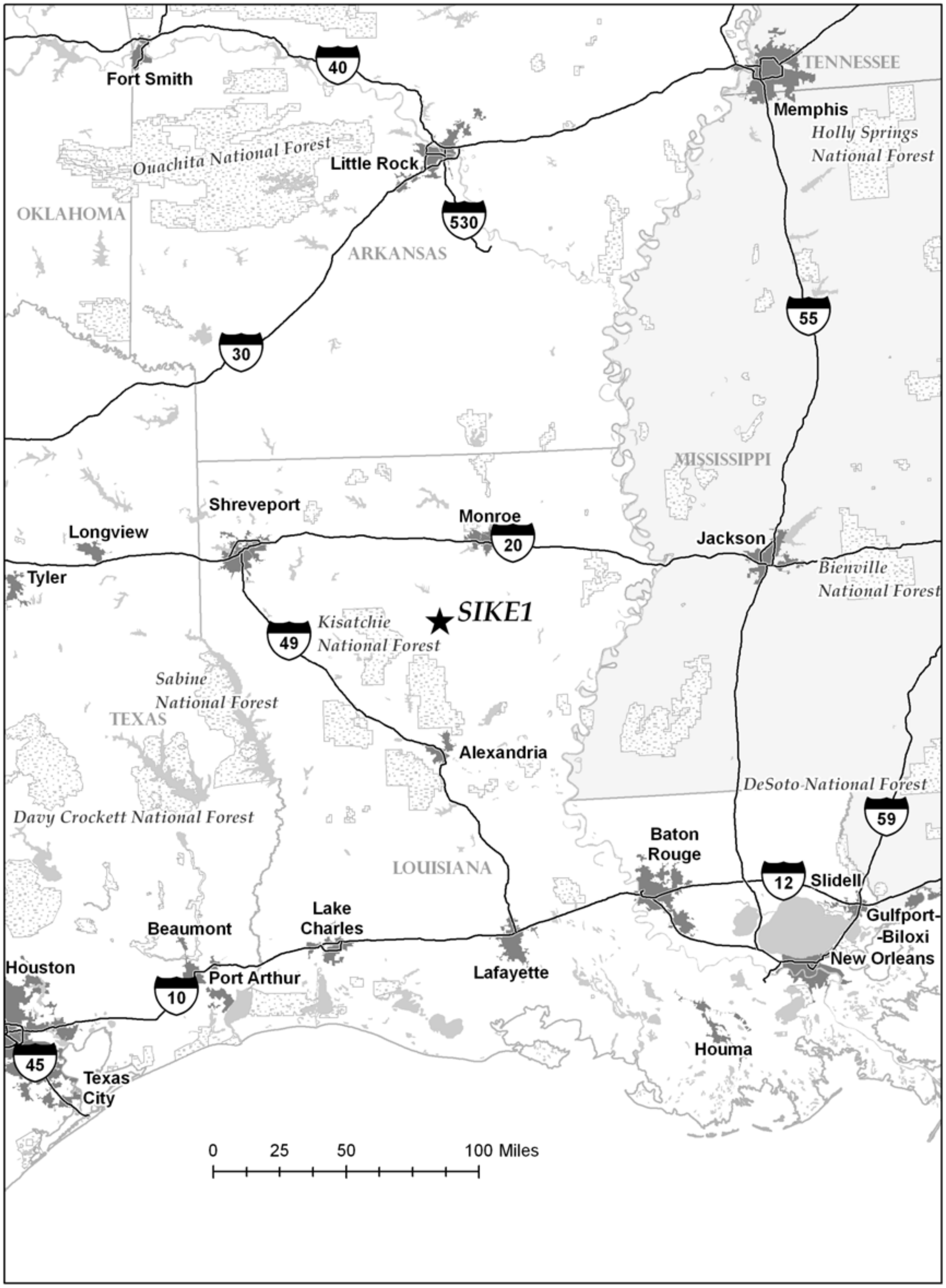

Figure 2. Average $PM_{2.5}$ composition by major component (OMC = 1.4*OC) for all valid data, March 2001–February 2004.

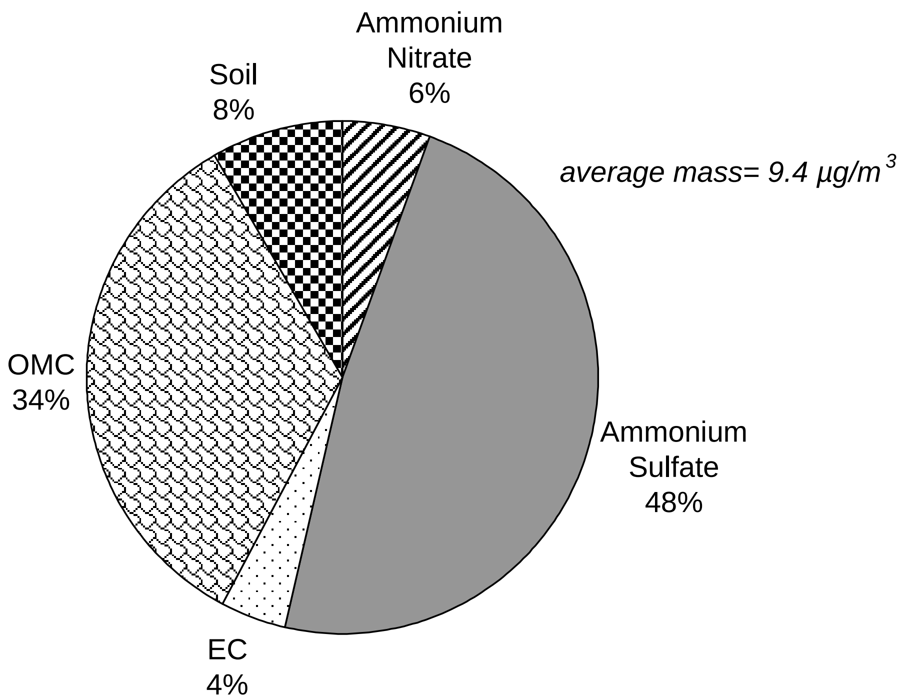

Figure 3a. Average composition (μg/m^3) by season (spring = March through May, summer = June through August, etc.) at Sikes, March 2001–February 2004.

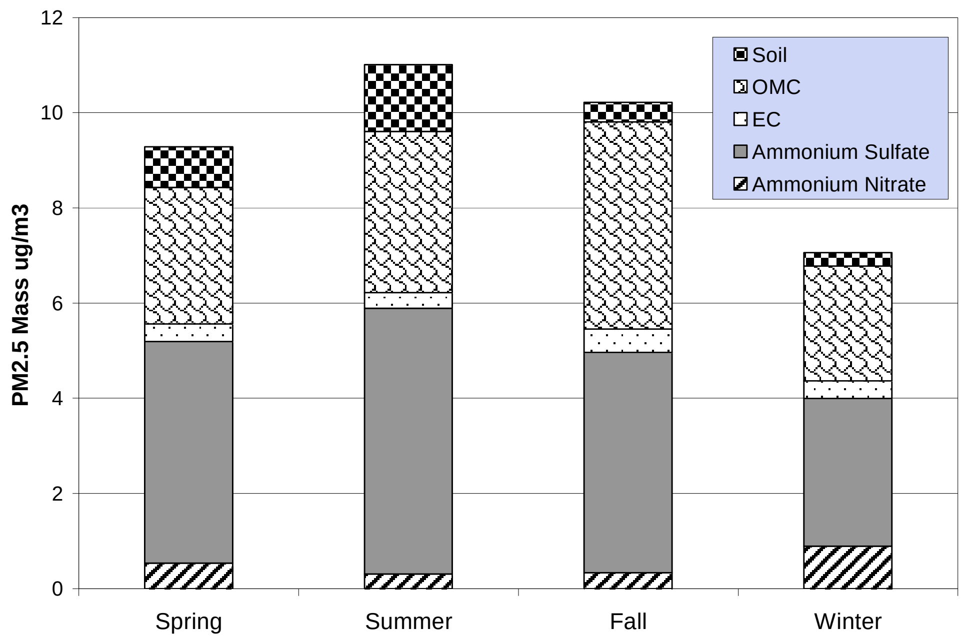

Figure 3b. Average composition (percentage) by season (spring = March through May, summer = June through August, etc.) at Sikes, March 2001–February 2004.

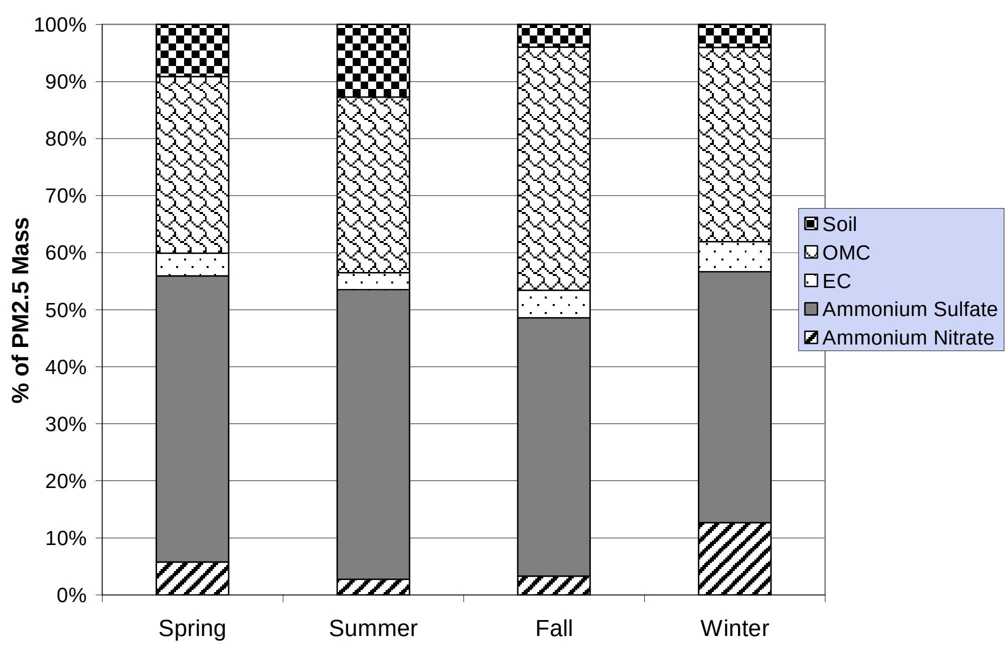

Figure 4a. Average composition on the worst-20% visibility days at Sikes, March 2001-February 2004.

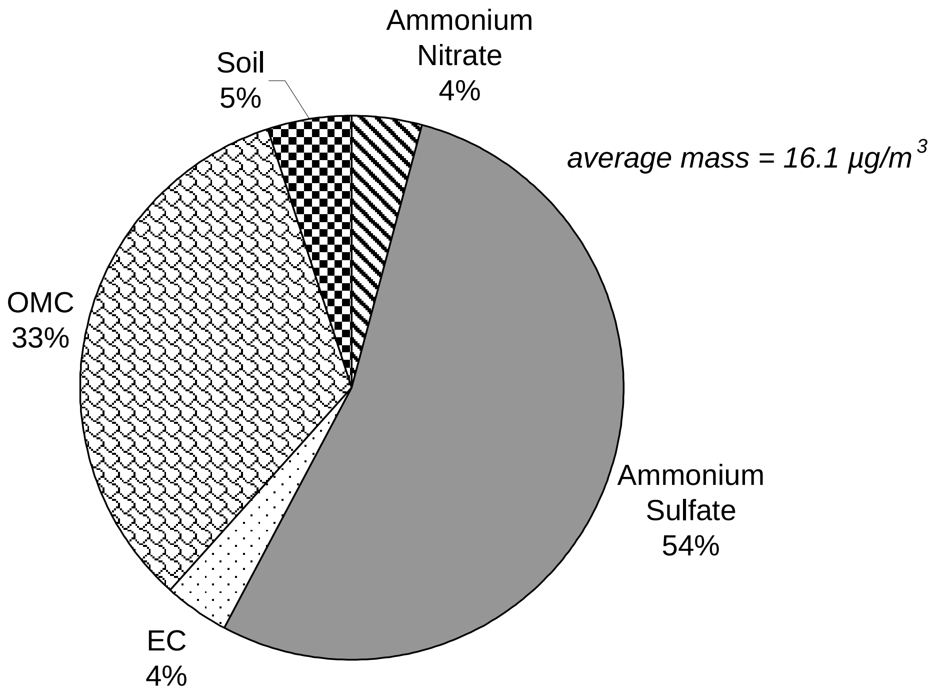

Figure 4b. Average composition of b_{ext} (light extinction by aerosol) based on the IMPROVE visibility equation on the worst-20% visibility days at Sikes, March 2001–February 2004.

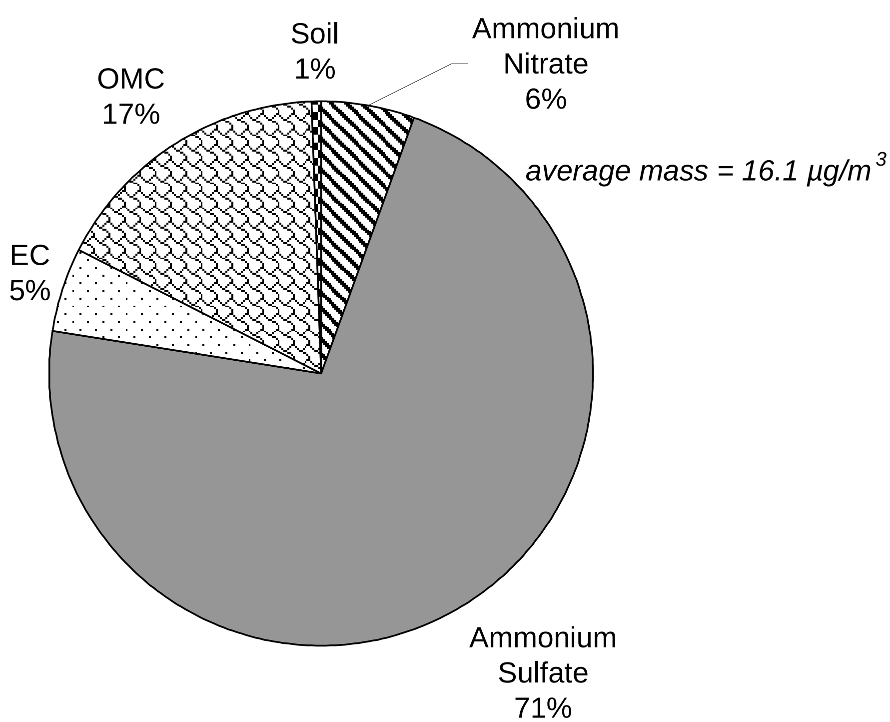

Figure 5a. Scatter plot of ammonium sulfate versus selenium by season (µg/m^3) where 1 = spring, 2 = summer, etc.

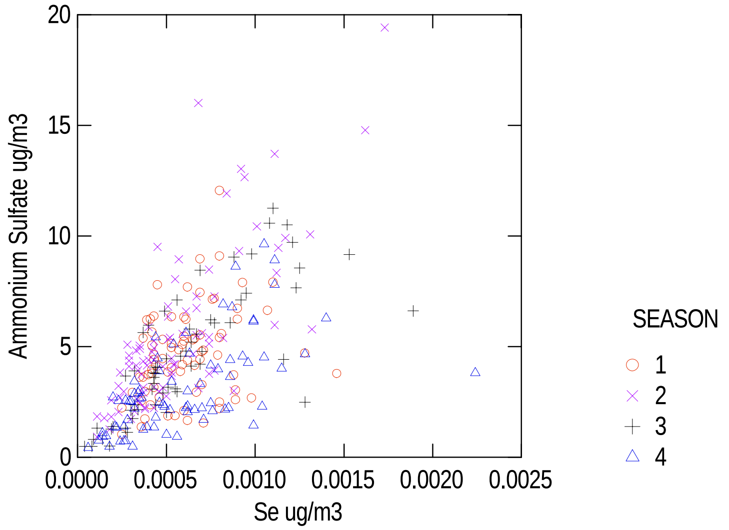

Figure 5b. Scatter plot of potassium (K) versus total EC by season (µg/m^3) where 1 = spring, 2 = summer, etc.

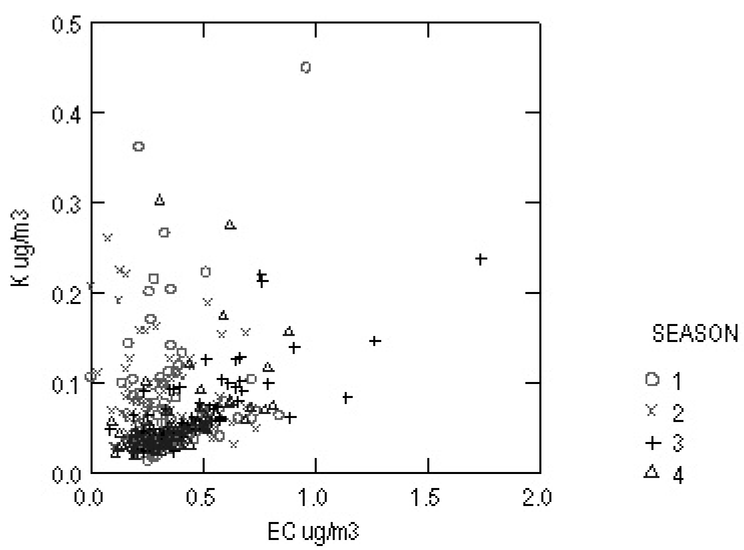

Figure 5c. Scatter plot of EC1 versus OP by season (µg/m^3) where 1 = spring, 2 = summer, etc.

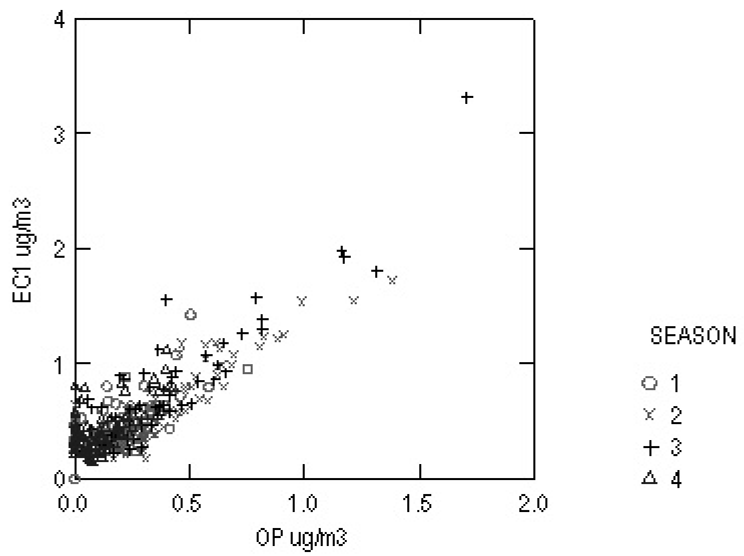

Figure 6. Factor profiles (percent of species in each factor). Error bars indicate the standard deviation from bootstrapping 300 runs.

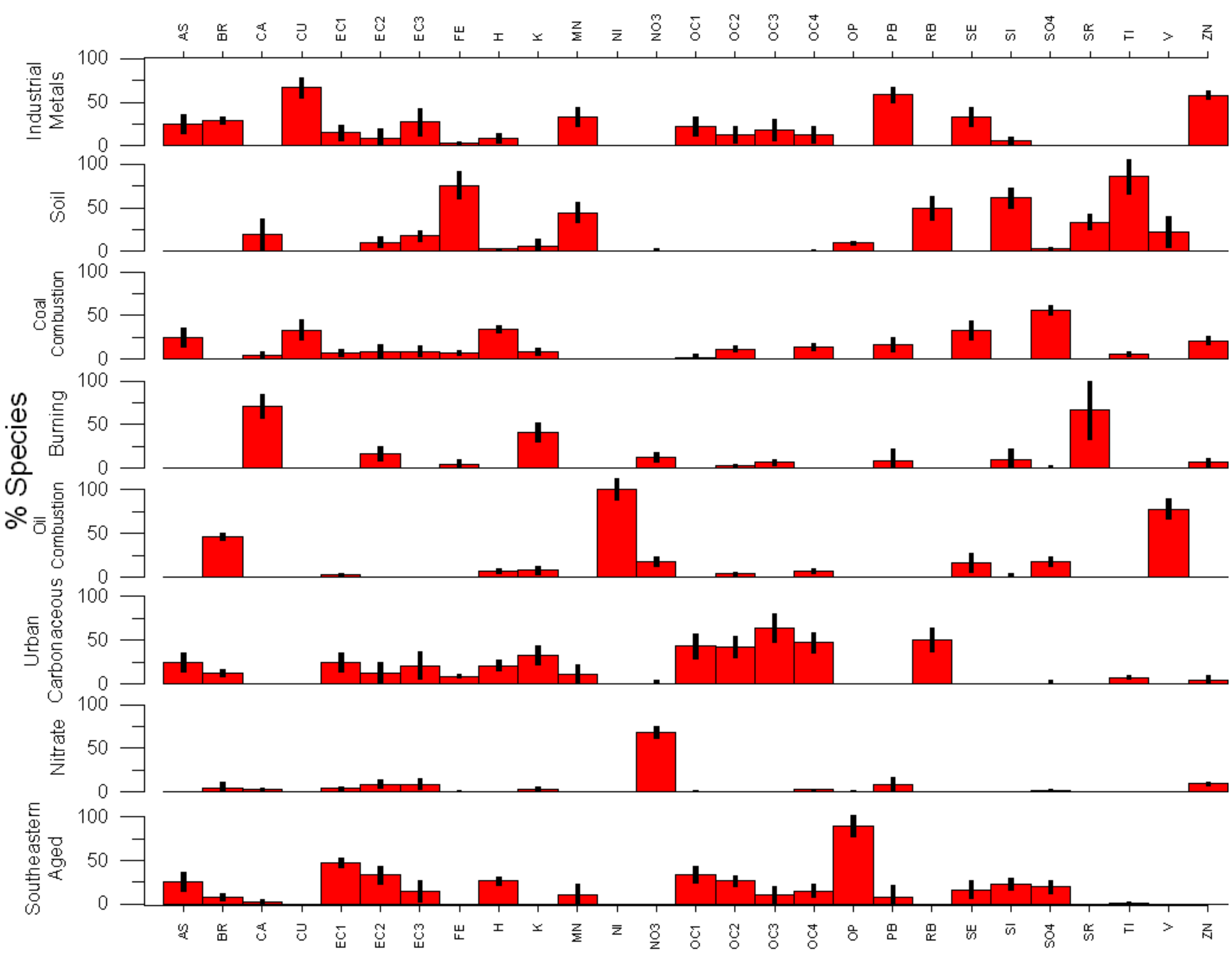

Figure 7. Time series of factor strengths by date ($\mu g/m^3$).

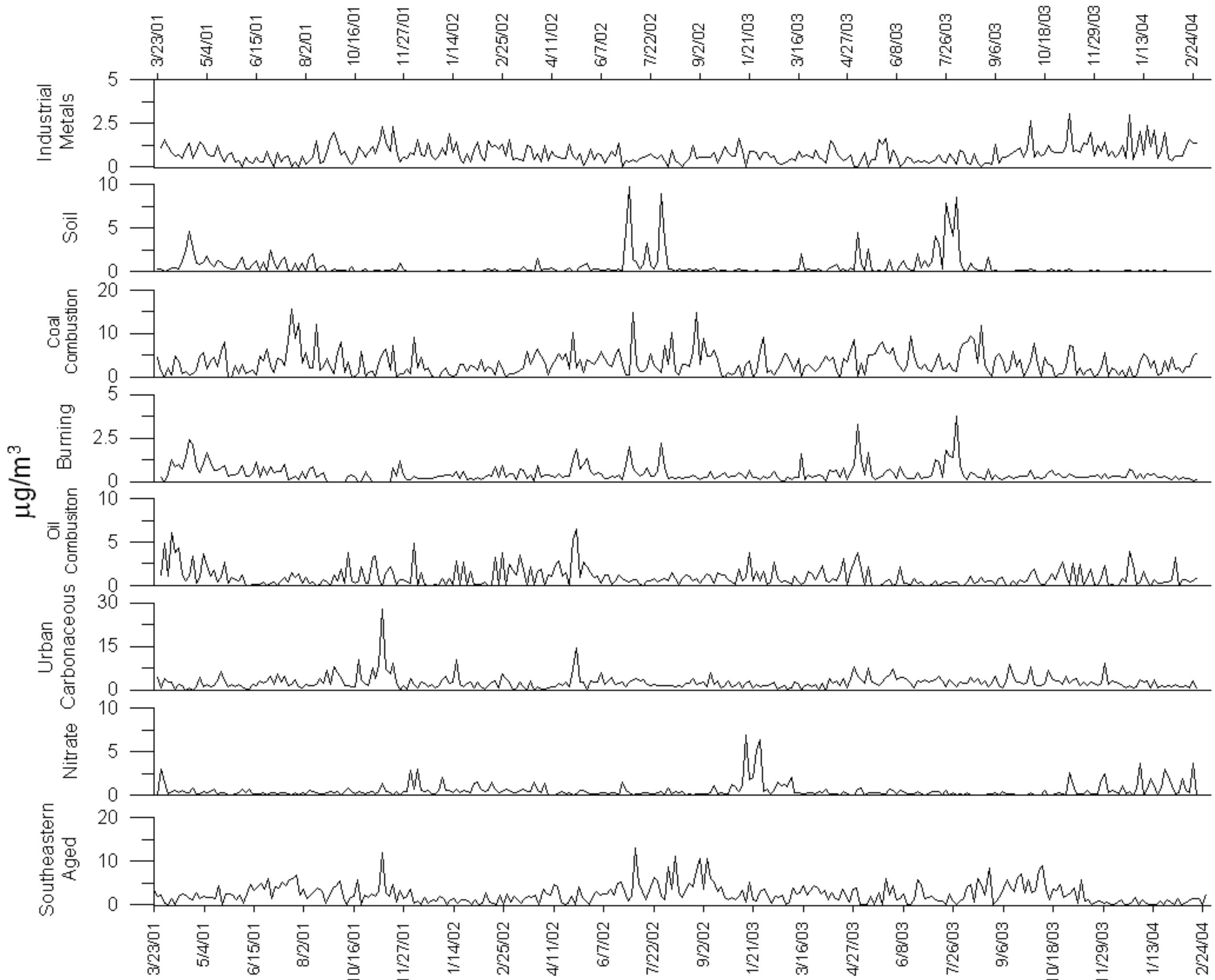

Figure 8. Reconstructed mass versus measured $PM_{2.5}$ mass.

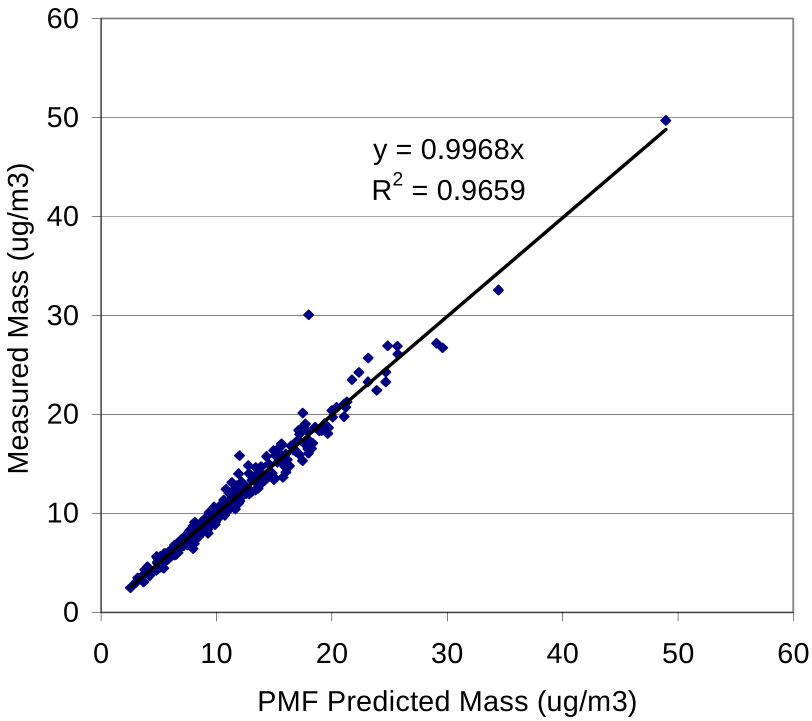

Figure 9. Average factor contribution estimates for (a) all samples and (b) the worst-20% visibility days.

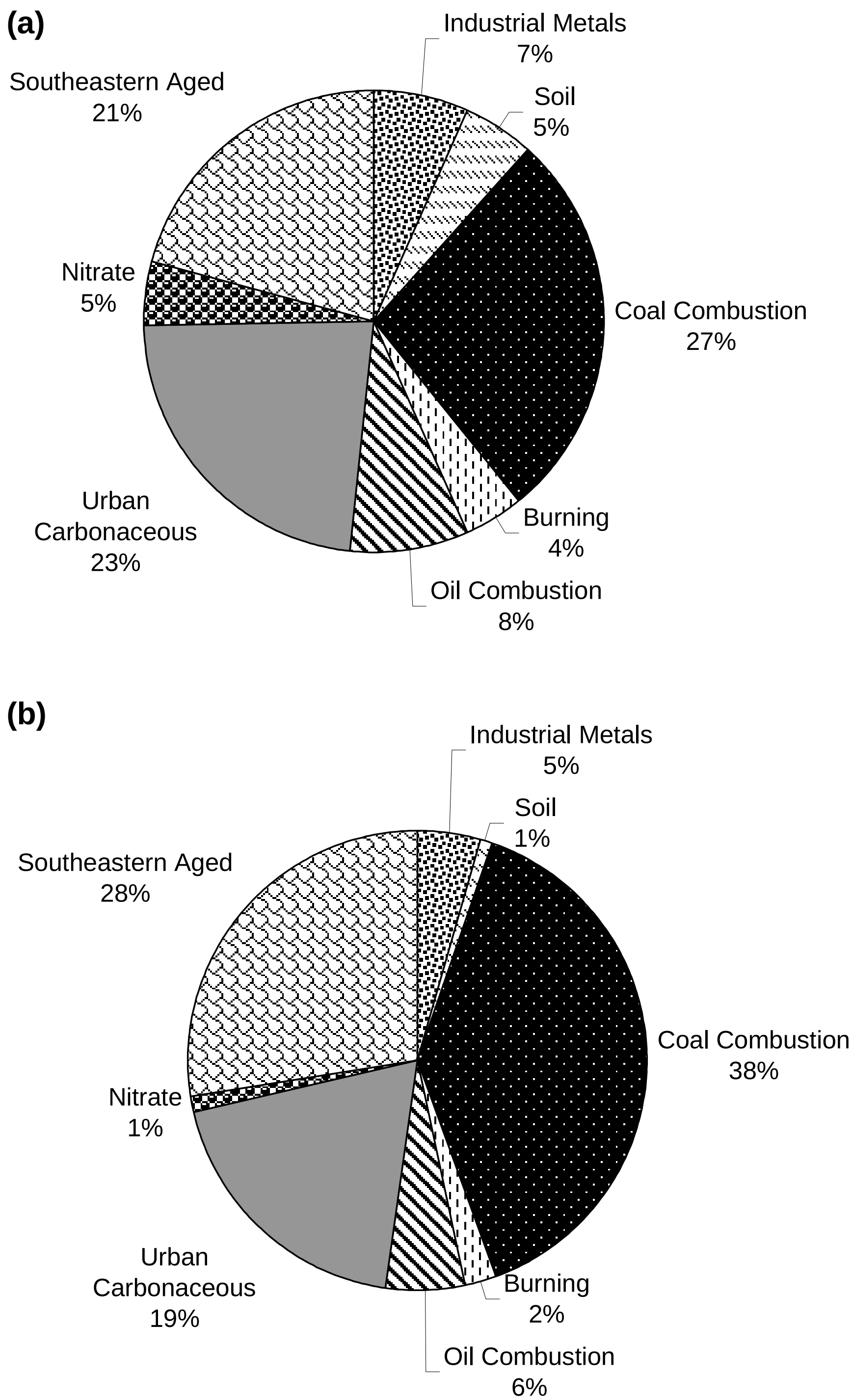

Figure 10. CoPIA plots for (a) coal combustion, (b) urban carbonaceous, (c) southeastern aged aerosol, and (d) industrial metals factors.

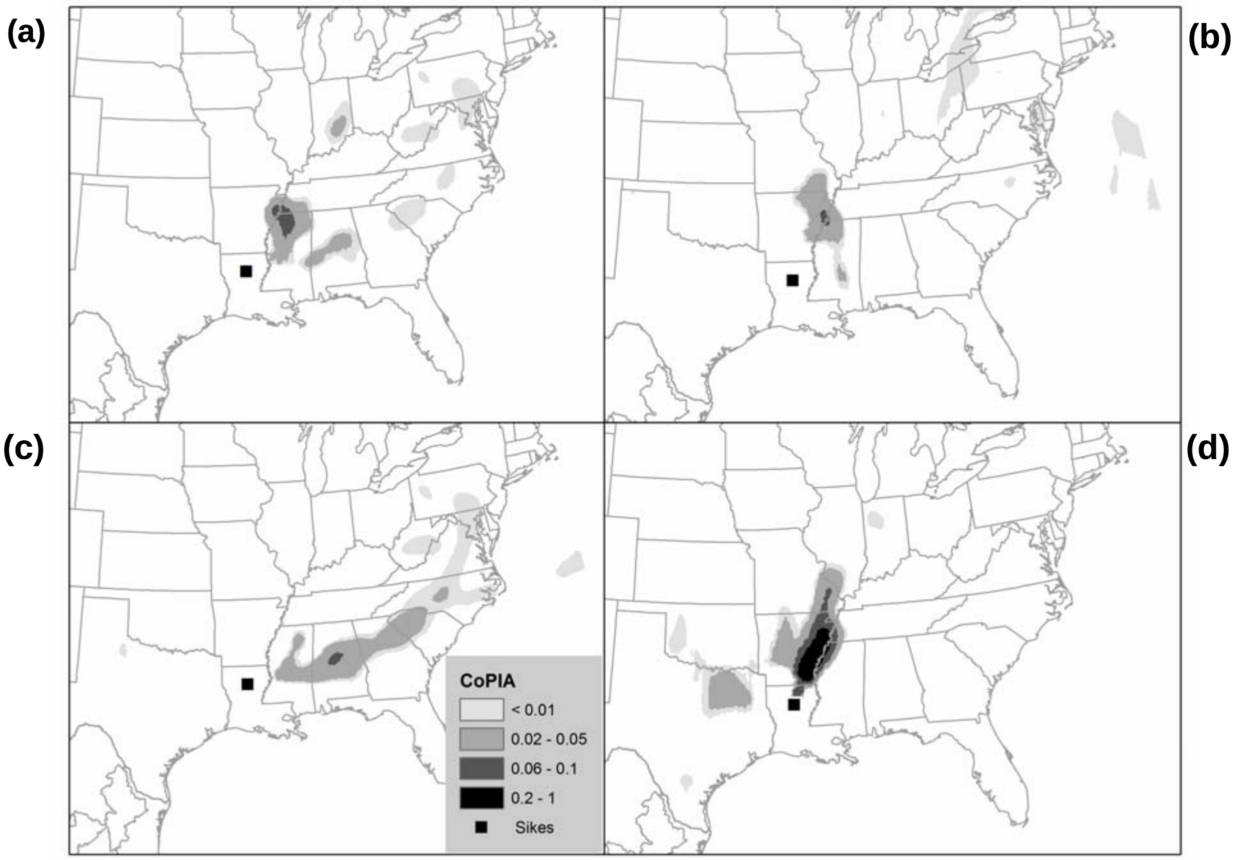

Figure 11. 10-day air mass back trajectories using the NOAA HYSPLIT model with 500 m and 1000 m ending heights on (a) July 1, 2002, and (b) July 31, 2002.

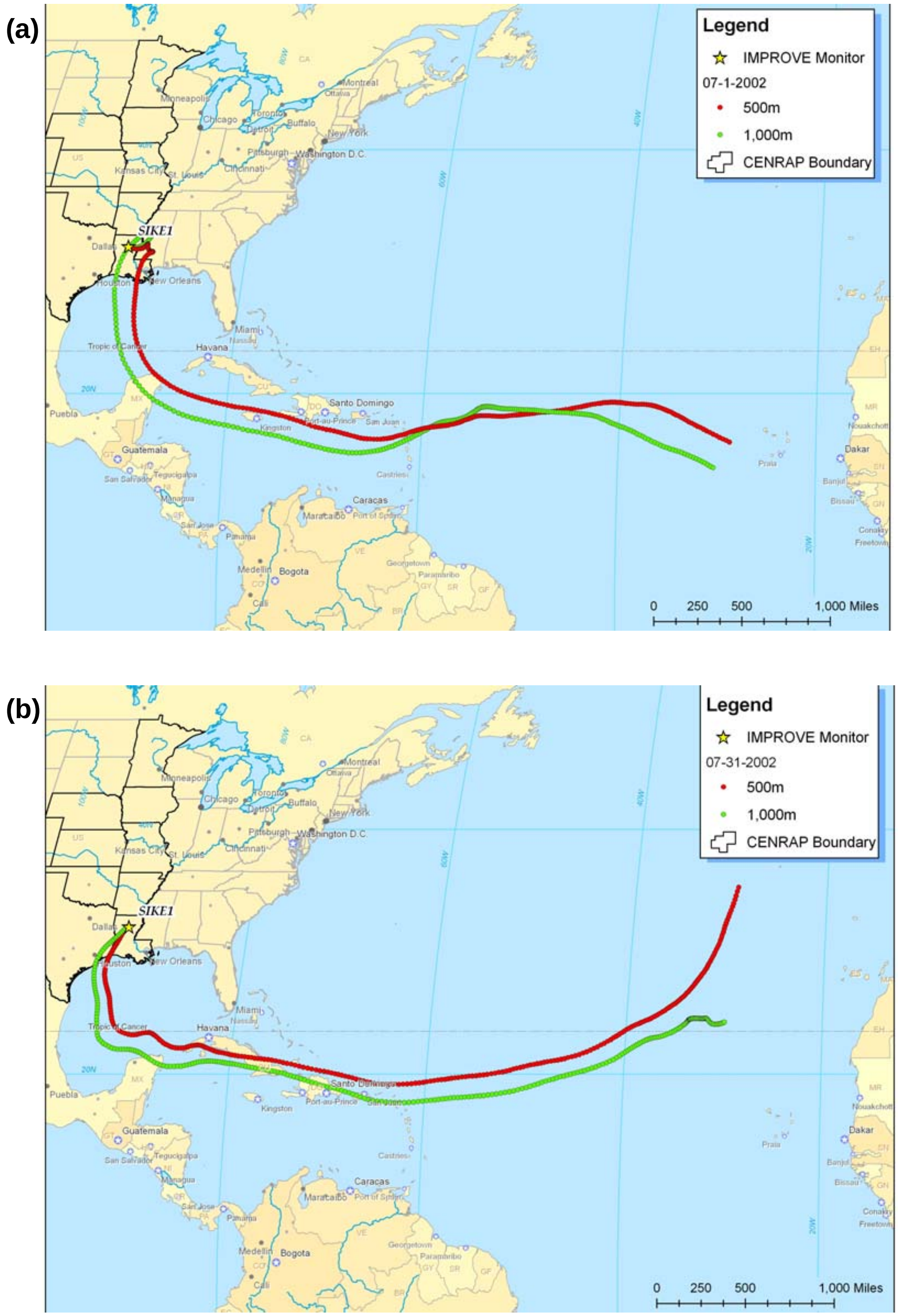

Figure 12. Three-day air mass backward trajectories using the NOAA HYSPLIT model with 250 m, 500 m, and 1000 m ending heights and fire locations on (a) August 4, 2003, and (b) April 19, 2001.

(a)

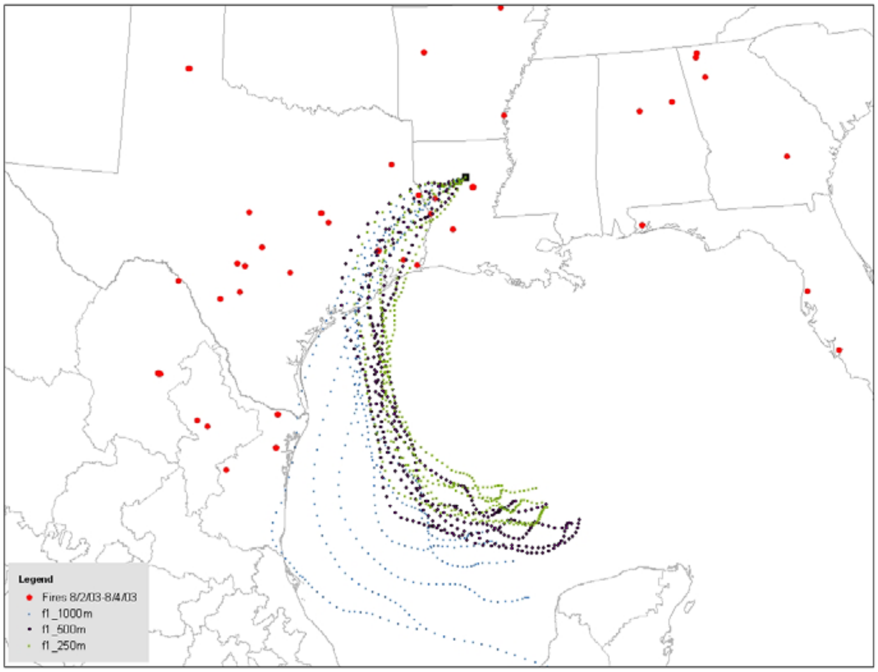

(b)

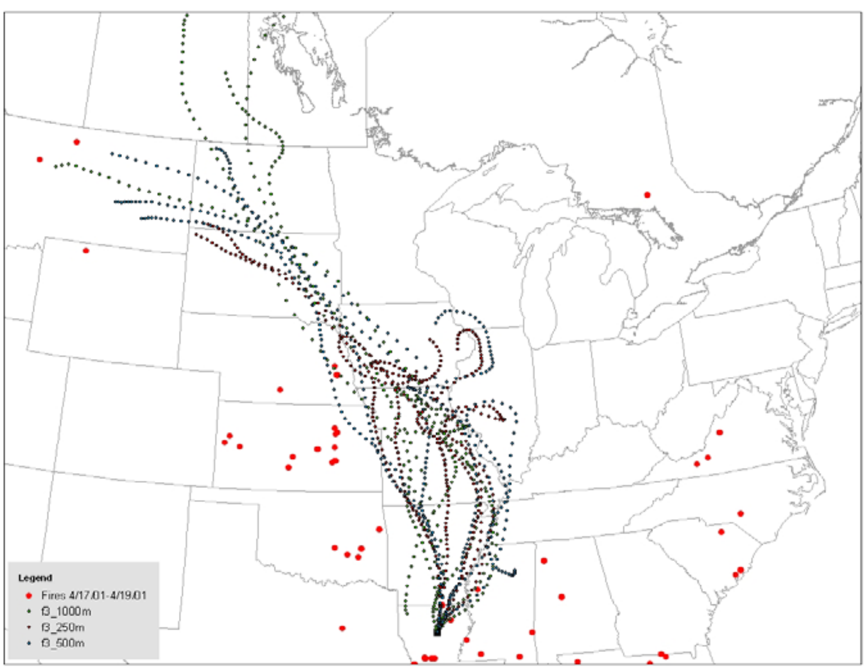

Figure 13. SO_2 EIP analysis for coal combustion, southeastern aged aerosol, and oil combustion factors by (a) county and (b) state.

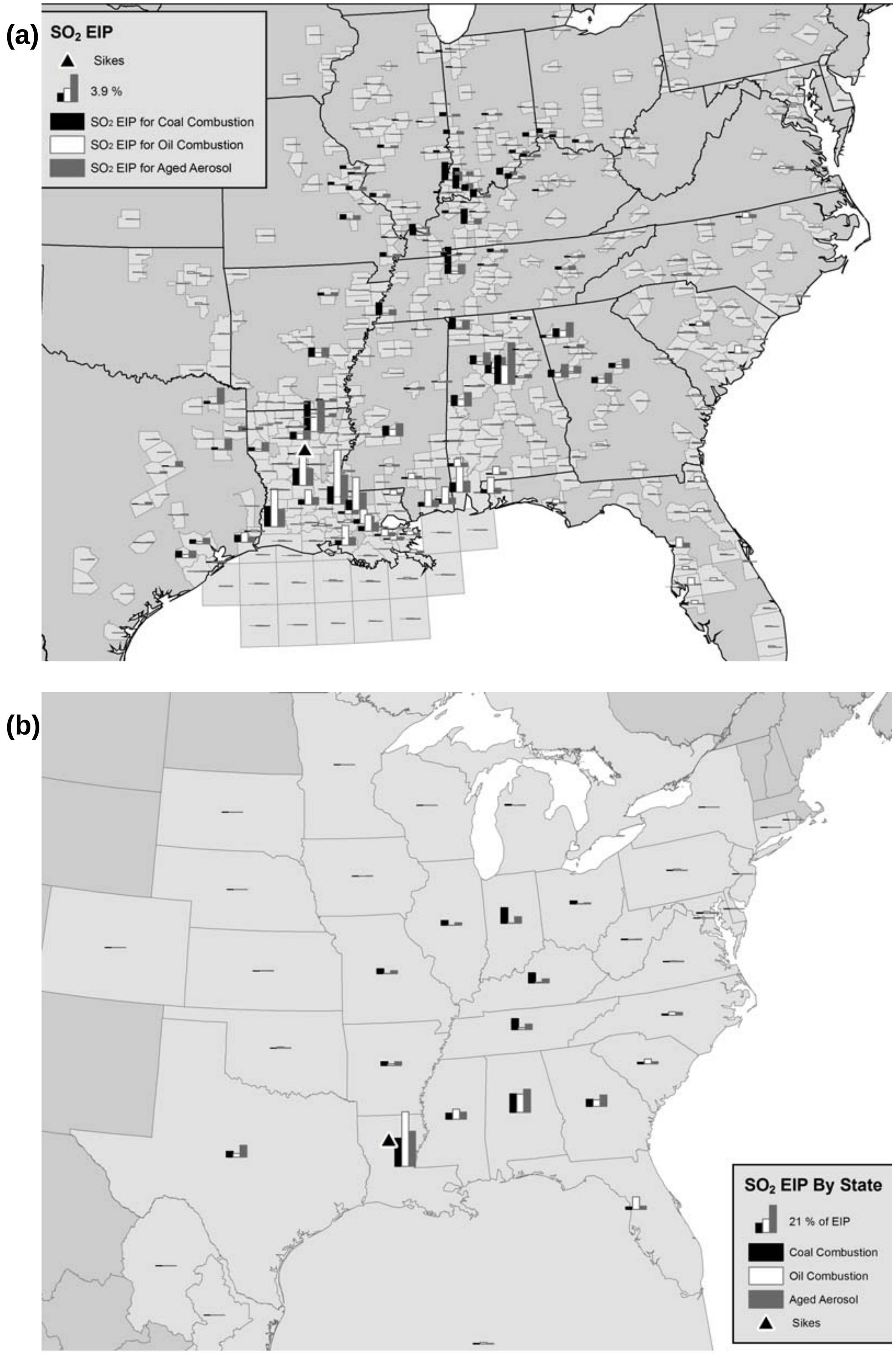

Source Apportionment of $PM_{2.5}$ at Hercules-Glades, Missouri, Using Positive Matrix Factorization

Steven G. Brown, Anna Frankel, Sean M. Raffuse, Hilary R. Hafner and Paul T. Roberts

Sonoma Technology, Inc., Petaluma, CA

Brett A. Anderson

United States Environmental Protection Agency Region 7
Air Planning and Development Branch
901 N. 5th Street
Kansas City, KS 66101

ABSTRACT

Speciated $PM_{2.5}$ data collected as part of the Interagency Monitoring of Protected Visual Environments (IMPROVE) program at Hercules-Glades, Missouri, from March 2001 through February 2004 were analyzed using the multivariate receptor model, Positive Matrix Factorization (PMF). Over 300 samples with 23 species were utilized, including the organic carbon (OC) and elemental carbon (EC) analytical temperature fractions from the thermal optical reflectance (TOR) method. Eight factors were identified, with a good comparison between predicted and measured mass (slope = 0.98, r^2 = 0.99). Bootstrapping over 300 runs was used to determine the concentrations and uncertainties of each species in the factor profiles. A coal combustion factor was the largest contributor to mass (34% of the average mass on all days and 49% on the worst visibility days) and to ammonium sulfate, and was predominantly from coal-fired power plant emissions of SO_2 in the Ohio and Mississippi River Valleys. Urban southeastern carbonaceous aerosol was responsible for another 20% of the average mass, and 18%, on average, during the worst visibility days. A background aged aerosol factor was also identified, accounting for 10% of the average mass, and 9% on the worst visibility days. Oil combustion and Mississippi River industrial metals operations factors were minor contributors to the mass (8% and 5%, respectively). Nitrate contributed 11% of the average mass over all days and on the worst visibility days, due to nitrate episodes in the winter. Soil and burning were generally event-driven, and were 5% and 7% of the overall mass, and 4% and 6% of the mass on the worst visibility days, though a few high mass days were dominated by these source types. Conditional Probability Function (CPF) analysis applied to air mass trajectories and trajectories

paired with emission inventory to find emission impact potential (EIP) both helped better identify the factors and their source regions.

IMPLICATIONS

A subset of $PM_{2.5}$ data, the analytical carbonaceous fractions, was used to enhance the identification of factors in this source apportionment work. These carbonaceous fractions helped better differentiate and quantify carbonaceous aerosol factors that otherwise may not have been separated and apportioned as well. A more realistic treatment of x-ray fluorescence (XRF) data close to the detection limit was used to better characterize the known analytical uncertainties of, and provide a better fit for, certain species. Bootstrapping was used to better quantify the composition and uncertainties in the factor profiles by compiling results from 300 individual runs. Lastly, emission inventory data were paired with air mass trajectories to better understand the source regions affecting factors with sulfate. All of these techniques were used to improve the confidence in, and to aid policy makers in understanding, the results.

INTRODUCTION

Particles with diameters of less than 2.5 microns ($PM_{2.5}$) impact human health[1-4] and visibility.[5-7] The EPA has identified a number of $PM_{2.5}$ constituents, such as manganese, arsenic, lead, and diesel particulate matter (DPM), which pose a public health risk in urban areas.[8] There are also visibility regulations promulgated by the EPA directing states to reduce the worst-20% visibility days in their Class 1 areas. To better address these issues, it is vital to understand the composition and characteristics of the sources contributing to $PM_{2.5}$. Hercules-Glades is a Class 1 area located in southern rural Missouri near the border with Arkansas, approximately 50 miles from the closest urban area, Springfield, and less than 150 miles from larger urban centers such as Little Rock, Arkansas and Memphis, Tennessee. Sikes is generally impacted by transported aerosol from these urban areas and others such as St. Louis, Kansas City, and Indianapolis. This site is also impacted by regional dust events from the Great Plains and emissions from agricultural burns and forest fires in the area.

In previous analyses of $PM_{2.5}$ data using receptor models with only the organic carbon (OC) and elemental carbon (EC) values, it has been difficult to separate different sources of carbonaceous aerosols, such as gasoline-, diesel-fueled vehicles, aged aerosol transport, background aerosol, and fire emissions. Much of the $PM_{2.5}$ in these sources is carbonaceous,[9-13] and a simple ratio of OC to EC is typically insufficient to quantitatively separate various source types. In urban areas, attempts using receptor modeling and data analysis[14-16] to better determine the gasoline-diesel split, for example, have begun to rely on the carbon fractions resulting from the Thermal Optical Reflectance (TOR) protocol[17,18] technique. In rural areas, where the aerosol impacting a site is more aged, the motor vehicle and diesel emissions will generally impact the site together, and will be indistinguishable.[19-21] However, the use of the fractions may better apportion the carbonaceous aerosol between the local and aged transported air masses, and possibly better apportion the contribution from burning or other combustion sources.

METHODS

Data

$PM_{2.5}$ data from March 2001 through February 2004 were collected as part of the IMPROVE program[22] at the Hercules-Glades site, shown in Figure 1. These 24-hr samples were collected on Nylon, Teflon, and quartz fiber filters. Teflon filters were analyzed by gravimetric analysis for mass and by x-ray fluorescence (XRF) for elements. The Nylon filter was analyzed by ion chromatography (IC) for sulfate, nitrate, nitrite, and chloride. Ammonium (NH_4^+) was not analyzed, but its mass can be inferred from ionic balance with sulfate and nitrate.[23]

Quartz fiber filters were analyzed by the TOR method[17] to obtain eight thermally resolved fractions of carbonaceous aerosol. OC is volatilized in four steps, all in a helium atmosphere: (1) OC1 consists of the volatilized OC up to 120°C, (2) OC2 from 120° to 250°, (3) OC3 from 250° to 450°, and (4) OC4 from 450° to 550°. After the OC4 section is complete, a 2% O_2/98% He atmosphere is introduced to obtain EC1, and the temperature is then increased to 700°C for EC2 and to 850°C for EC3. A correction for the pyrolysis of OC is made. Pyrolyzed organic carbon (OP) is emitted when the O_2/He atmosphere is first introduced. This amount of OP is defined as the amount detected after the introduction of the O_2/He atmosphere at 550°C until the monitored filter reflectance returns to its original value. As reported, EC1 includes the OP fraction; thus, OP was subtracted from EC1 to get the correct EC1 concentration.

Data from the IMPROVE program are routinely validated before being made publicly available; therefore, the overall data quality was very good. Only valid samples from the IMPROVE data were used. Additional quality control (QC) checks performed in this study include comparison of reconstructed fine mass to measured mass and comparison of XRF sulfur to IC sulfate. Only species with good variability, such as those with a signal/noise ratio greater than 0.2 (not accounting for seasonal variability) and at least 25% of the data above detection, were used. In particular, no sodium or chloride data were used in this analysis; therefore, no sea salt factor could be identified, though the impact of sea salt at this site was expected to be minimal. Also, nickel was not used because more than 50% of the data were below detection, so vanadium will be used as the only marker for oil combustion in the PMF analysis. The final data set contained 328 samples with 23 species (see Table 1).

Source Apportionment With PMF

PMF is a multivariate factor analysis tool that has been applied to a wide range of data, including 24-hr speciated $PM_{2.5}$ data, size-resolved aerosol data, deposition data, air toxics data, and VOC data.[14-16,20,21,24-34] Simply, PMF decomposes a matrix of ambient data into two matrices, which then need to be interpreted by the analyst to discern the source types they represent. The method is considered briefly here and described in greater detail elsewhere.[35,36]

An ambient data set can be viewed as a data matrix X of *i* by *j* dimensions, in which *i* number of samples and *j* chemical species were measured. The goal of multivariate receptor modeling is to identify a number of sources *p* that best characterize the $PM_{2.5}$ at a site, the species profile *f* of each source, and the amount of mass *g* contributed by each source to each individual sample:

$$X_{ij} = \sum_{k=1}^{p} g_{ik} f_{kj} + e_{ij} \tag{1}$$

One strength of PMF is that results are constrained by a penalty function so that no sample can have a negative source contribution and no species can have a negative concentration in any source profile. Another strength of PMF, compared to other source apportionment tools such as principle component analysis (PCA), is that each data point can be weighed individually. This feature allows the analyst to adjust the influence of each data point, depending on the confidence in the measurement. Data below detection can be retained for use in the model, with the associated uncertainty adjusted so these data points are given less weight in the model solution (i.e., these data have less influence on the solution than measurements above the detection limit). By individually weighing data, samples with some species missing or below detection do not need to be excluded as a whole, rather the analyst can adjust the uncertainty so these data also have little or no impact on the final solution. The PMF solution minimizes the object function Q(E), based upon these uncertainties (u):

$$Q = \sum_{i=1}^{n} \sum_{j=1}^{m} \left[\frac{x_{ij} - \sum_{k=1}^{p} g_{ik} f_{kj}}{u_{ij}} \right]^2 \qquad (2)$$

Methods used in this analysis for replacing and developing uncertainty values for missing and below-detection-limit data were drawn from previous work with PMF.[20,21,25,26,28,37] Since the solution found by PMF relies on both concentration data and on error estimates, these error estimates must be chosen judiciously so that they reflect the quality and reliability of each data point. The missing and below-detection-limit data are assigned less weight compared to actual measured values, so these data are less important to the solution.[20,21,25,26,28,37] Data below the minimum detection limit (MDL) were substituted with MDL/2; missing data were substituted with the median concentration. Similar to previous studies, the uncertainty for data above detection was calculated as the sum of the analytical uncertainty (UNC) plus one-third the MDL, uncertainty for data below detection was 5/6*MDL, and uncertainty for missing data it was four times the median. Additionally, it has shown that XRF data reported above MDL but below approximately 10*MDL are more uncertain;[38] therefore, these data were assigned an uncertainty twice as high as concentrations above this threshold, i.e., 2*(UNC+MDL/3).

The robust mode was used in this analysis to reduce the influence of outliers; between 5 and 13 factors were explored. The uncertainty of the amount of each species in a given factor was determined by bootstrapping 300 runs and calculating the interquartile range of the factor loading over these runs. This was done using multiple starting points and rotations, so that the range of solutions PMF gives can be used as a measure of the confidence in a given factor. Scaled residuals were inspected and were between -3 and 3 for all species demonstrating a good fit of the modeled results. The factors also showed oblique edges, which has been proposed as an additional check of the quality of the rotation.[39] A multi-linear regression (MLR) was applied to scale the factors back into the original μg/m^3 units by regressing the total measured $PM_{2.5}$ mass against the unscaled factor strength contributions:

$$X_{ij} = \sum_{k=1}^{p} \left(s_k g_{ik}\right)\left(\frac{f_{kj}}{s_k}\right) \tag{3}$$

The resulting coefficients were then applied to each factor to regain the μg/m^3 units.

Conditional Probability Integrative Analysis

A conditional probability function (CPF) was applied to help interpret the results.[14,16,24,40] The transport patterns of the highest 10% concentration days of a given factor were compared to the climatological transport patterns. This comparison highlights the differences in transport and areas of influence between the general transport pattern (i.e., the climatology) and high concentration days of a given factor. Using the NOAA HYSPLIT model,[41] 96-hr backward trajectories were run for all sample dates, which were then mapped as a spatial probability density (D_0):

$$D_0 = \frac{D_c}{\hat{D}} \tag{4}$$

D_c = Density at grid cell c

$\hat{D}$ = Maximum density over all grid cells (typically the density at the receptor site)

$$D_c = \sum_{i=1}^{n} \kappa_R(r_n) \tag{5}$$

r_n = distance between grid cell center and hourly trajectory point n

$$K_R(r) = \text{kernel density function} = \begin{cases} \dfrac{3}{\pi R^2}\left[1-\left(\dfrac{r}{R}\right)^2\right]^2 & \text{for } r < R \\ 0 & \text{for } r \geq R \end{cases} \tag{6}$$

R = search radius

The search radius was determined dynamically by dividing the geographic extent of all endpoints by 30.[42,43] The density D_k was then computed using only backward trajectories for the highest 10% concentration days of a given factor k. Areas that have a higher than typical influence on the high concentration days are then highlighted by calculating the conditional probability P_k:

$$P_k = D_k - D_0 \tag{7}$$

This Conditional Probability Integrative Analysis (CoPIA) is very similar to the CPF analyses employed in other studies;[14,16,24,40] however, CoPIA is adapted to take advantage of tools available in a geographic information system (GIS) framework. Ensemble backward trajectories were run every 6 hours to account for variability over a 24-hr sampling period. Emissions data, such as point source and fire locations, were overlaid on the CoPIA analysis to identify specific emissions sources in likely source areas.

Emission Impact Potential (EIP) Calculations

While trajectory analyses such as CoPIA can help identify transport patterns and likely areas of influence, only a broad conclusion can be reached, such as "the factor showed influence from the Ohio River Valley". However, this analysis only accounts for transport, and not the spatial distribution or magnitude of emissions. For example, a large, distant source and a small nearby source could influence a site in a similar way. To gain a better understanding of the source regions for a given factor, a GIS-tool was used to weight county-level emission inventory data by the trajectory kernel density of the highest 10% concentration days for a given factor. For a given factor, SO_2 emissions were weighted by the frequency and residence time of modeled backward trajectories passing over each county to estimate the potential for emissions from each county to impact the site. This is called the emission impact potential (EIP). This simple analysis technique is useful for characterizing general patterns and developing a preliminary conceptual model of factors affecting visibility conditions, but without the need for, and as an initial step toward, full-scale photochemical modeling efforts.

The EIP of a given county is calculated as:

$$EIP = \frac{E_p * D_0}{f(\text{distance})} \tag{8}$$

where

E_p = county total emissions of pollutant p

D_0 = spatial probability density at the county centroid

f = function of distance between county and receptor

The EIP may be divided by a distance function to roughly account for dilution and increased uncertainty in model outputs far from the receptor site. However, for this study, $f = 1$, assuming vertical dilution is similarly small compared to the horizontal transport distance for all areas and the kernel density sufficiently accounts for horizontal dilution and uncertainty. This tool is used for simple analysis only, and does not account for atmospheric chemistry, deposition, or other effects, but is expected to qualitatively provide insight into the potential sources affecting mass.

RESULTS AND DISCUSSION

Preliminary Data Analysis

Preliminary data analysis was conducted to gain insight into the trends and relationships among species that would impact later source apportionment with PMF. Inspection of the overall composition, changes in composition by season or on days of poor visibility, species relationships, and day-of-week trends assisted in identifying possible source types.

Annual Median Composition. Figure 2 shows the median $PM_{2.5}$ composition. Ammonium sulfate and nitrate concentrations are calculated from sulfate and nitrate concentrations, assuming full neutralization by ammonium. OC is represented by OC mass (OMC), equal to 1.4 times OC,[44,45] which takes into account the mass of oxygen and hydrogen associated with the carbon, though this factor may actually be higher than 1.4.[44,46] As shown in Figure 2, ammonium sulfate is the dominant component (accounting for 48% of the average mass), followed by OMC (27%). Ammonium nitrate is 13%, soil is 8%, and EC is 4%. Dominance of ammonium sulfate is typical of the eastern half of the United States, and the significant portion of mass from OMC demonstrates the importance of determining its source regions. Ammonium nitrate concentrations are significant mainly in the winter, and are important to wintertime $PM_{2.5}$ and visibility episodes.

Seasonal Composition. Changes in $PM_{2.5}$ mass and composition between seasons (Figures 3a and 3b) may reflect differences in transport regimes, atmospheric chemistry, or source strengths. Mass is highest in spring through fall, with a summer peak, and then drops off significantly in the winter. Ammonium sulfate contributions to mass range between a peak in the summer (60% of the mass) and a low (30%) in the winter. This large swing in sulfate concentrations is likely caused by meteorology affecting both transport and chemistry. OMC concentrations are similar throughout the year, accounting for between 25% and 30% of the mass. In spring and summer, soil contributions are between 9% and 12%, caused by wind-blown dust impacts likely from the arid western plains, while in fall and winter soil contributions are 5% or less. Nitrate accounts for 35% of the mass in winter, and is at a minimum in summer (4%). These seasonal differences are expected to be observed in PMF analysis and may be because of changes in sources or transport, which will be analyzed further using results from PMF analysis.

Composition on Poor Visibility Days. To investigate which components (i.e., OMC, sulfate, soil, etc.) have the greatest impact on days with severely impaired visibility, the $PM_{2.5}$ composition on the worst-20% visibility days (referred to as the worst visibility days in the remainder of this article) was examined (Figure 4a). Using the IMPROVE equation,[22,23] which likely does not fully account for extinction by OC,[47] the total light extinction (b_{ext}) contribution of each chemical component was calculated. On poor visibility days, which occurred in all months but predominantly in summer, the average $PM_{2.5}$ mass was 17.3 $\mu g/m^3$ with 55% of the mass attributable to ammonium sulfate, 24% to OMC, 12% to ammonium nitrate, and the remaining mass to soil and EC. Sulfate is an even larger part of the mass on these worst visibility days than on average. The analysis of the estimated contributions to light extinction in Figure 4b further shows the importance of ammonium sulfate because it dominates the light extinction (68% on average), followed by ammonium nitrate (14%) and OMC (13%), though the contribution from OMC is likely underestimated. This shows that while sulfate is by far the most important component of visibility extinction, wintertime episodes caused by nitrate and OMC are also important, and both regimes need to be considered when developing control measures.

Species Relationships. Species relationships were investigated because the degree of covariation among species impacts how species and sources are allocated in source apportionment. It is important to understand these relationships before conducting source apportionment to ensure that PMF results fit within in the context of the data. One example, Figure 5a, shows the fair relationship between ammonium sulfate and selenium (r^2 = 0.63), which is typical of coal combustion, although the amount of scatter also suggests other existing sources of these species. Potassium, often used as a tracer for wood smoke,[48,49] had some correlation in a number of samples with EC (Figure 5b) and OC (not shown), which are also emitted by wood combustion.[48,50] The relationship between potassium and OC and EC indicates that a smoke factor may be found by PMF, but that the majority of the carbonaceous aerosol is likely not associated with burning. Metals typically emitted from industrial processes, such as smelting, including arsenic, lead, and zinc, showed fairly good correlations, an example of which is shown between zinc and lead in Figure 5c. These relationships will be useful in determining non-coal combustion sources of industrial emissions.

PMF Results

Eight factors were resolved for the ambient $PM_{2.5}$ at Hercules-Glades and identified as (1) coal combustion, (2) urban carbonaceous, (3) background aged aerosol, (4) oil combustion, (5) industrial metals, (6) nitrate, (7) soil, and (8) burning. Factor profiles with the standard deviation over 300 runs graphed as the error bars are shown in Figure 6, and a time series of all samples (every third day) are shown in Figure 7. The PMF solution accounted for the measured mass well, with a slope of 0.98 and r^2 of 0.98 between reconstructed and measured mass (Figure 8). The average compositions over all seasons and on the worst visibility days during the time period are shown in Figure 9. Figure 10 shows CoPIA plots for coal combustion, urban carbonaceous, nitrate, and industrial metals. Figure 11 shows air mass trajectories on a day of high soil, July 1, 2002, demonstrating a likely Saharan dust episode. Figure 12 shows air mass trajectories on days of high burning influence with fire locations from MODIS. Lastly, Figure 13 shows SO_2 EIP analysis results by county and by state for coal combustion, aged aerosol, and oil combustion.

The coal combustion factor was the largest contributor to mass (34% of the median mass on all days and 49% on the worst visibility days), and accounted for most of the ammonium sulfate. Carbonaceous aerosol from urban areas, most likely from mobile sources, accounted for 20% of the mass overall, and 18% on the worst visibility days. A background aged aerosol factor was responsible for another 10% of the mass on all days, and 9% of the mass on the worst visibility days. Oil combustion and industrial metals factors were more minor contributors to the mass (8% and 5%, respectively), and contributed much less on the worst visibility days (2% and 1%, respectively). A nitrate factor was significant only during the winter, and was 11% of the mass, on average, and on the worst visibility days, due to wintertime nitrate episodes. Soil and local burning emissions were both event-driven factors, and while they were 5% and 7% of the overall mass and only 4% and 6% of the mass on the worst visibility days, soil- and burn-events occurred where these factors were likely the largest impact on visibility. Overall, regional coal combustion and urban aerosol accounted for most of the mass on the worst visibility days, with regional coal combustion likely responsible for most of the visibility degradation caused by the high amount of ammonium sulfate.

A coal combustion factor was identified by typical tracers of coal combustion—sulfate, selenium, and hydrogen.[20,25,26,51] This factor was the largest component of the mass on all days (34%), and accounted for half of the mass on the worst visibility days (49%). Since most of the factor's mass is from ammonium sulfate, this factor is likely even more important in terms of visibility extinction. Ammonium sulfate accounted for 65% the mass at Hercules-Glades, and most of the sulfate is found in this factor; the remaining sulfate is found in the urban industrial, oil combustion, and background aged aerosol factors. This factor was highest on days with transport from the Ohio River area, where many coal-fired power plants are located and which has been identified as a significant area for the origin of sulfate transport in other studies in the mid-Atlantic and Northeast.[20,25,26,51] EIP analysis corroborates this, showing more than half of the SO_2 EIP comes from this area. In the county-level map, it is clear that a handful of sources in a few counties are responsible for most of the SO_2 emissions impacting Hercules-Glades.

An urban carbonaceous aerosol factor, mostly likely from mobile sources, accounted for 20% of the mass, and 18% on the worst visibility days. It consisted of all of the analytical carbonaceous fractions except OP, zinc, bromine, and hydrogen. This factor was highest with slow-moving air masses from the south, with influences from the urban areas in Arkansas, Tennessee, Mississippi, and Louisiana. This factor did not show a weekday-weekend difference; because mobile emissions are low close to the site, no weekday-weekend effect is expected. Except for one event, this factor did not show a large seasonal difference, which would be expected from a mobile source/urban signature. On the worst visibility days, the factor's mass was similar to its average contribution, but since the overall mass was higher, this factor contributed less to the worst visibility days on average.

A background aged aerosol factor was composed mostly of carbonaceous aerosol, predominantly the OP and EC1 fractions, consistent with earlier data analysis. The separation of this factor was made possible by the use of the carbonaceous fractions. This factor was higher during the summer, when there would be increased photochemistry, and comprised 10% of the mass over all days, and 9% on the worst visibility days. CPF analysis showed that transport patterns on the highest concentration days of this factor are no different than the average climatology, indicating that this factor is simply a background aged aerosol factor. There is likely a biogenic component to this factor, as it was significantly lower in the winter than in other months, consistent with biogenic emissions. This factor is possibly a combination of various background anthropogenic and biogenic emissions in the region, and is not attributable to any single primary source type.

Oil combustion was identified by its typical marker, vanadium.[14,20,21,24-26,52,53] As expected, this factor is highest on days with transport from the numerous oil refineries and drilling stations in Louisiana, Texas, Florida, and in the Gulf of Mexico. This factor contributed 8% of the mass, and on the worst visibility days, the factor contributed only 2% to the total. Most of the mass of this factor is from sulfate, and SO_2 EIP analysis shows that about half of the influence is from Texas and Louisiana alone, with other areas such as Florida also contributing.

Another industrial factor, consisting of copper, lead, zinc, and arsenic, was also identified. This factor was a minor part of the median mass (5%), but it contained most of the mass of the toxic pollutants lead and arsenic. This factor comes from a source region different than the oil combustion, coal combustion, and urban industrial factors. Similar to coal combustion, EIP analysis showed this factor was influenced by Indiana, Kentucky, Illinois, and Tennessee, but also showed significant influence from Louisiana and Texas. Part of this factor may be coal combustion, but it is likely representative of the variety of smelting and other industrial operations in these areas. Figure 10d shows the CoPIA results combined with point source locations of smelter and ore processing facilities, indicating potential influence of these facilities.

An ammonium nitrate factor was identified because it has a very strong seasonal signal independent of other components. It is highest in the winter, and is extremely low in warmer months, when nitrate production would be limited because of the ambient temperature. This factor was 11% of the mass on average and on the worst visibility days. In the winter, this factor accounted for on average 34% of the mass and was responsible for some visibility extinction episodes. This factor was highest under conditions of slow moving cool air masses from the rural areas of northwest Missouri, Iowa, Nebraska, and Kansas.

A soil factor was identified by silicon, iron, and titanium and was fairly low except during dust events. There were only a few large events when this factor had high concentrations, including the biggest event on July 1 2002, which was also seen at Sikes, Louisiana. This sample had the highest concentration of the soil factor by far, at 19.6 $\mu g/m^3$, while typically the factor averaged only 0.6 $\mu g/m^3$ (5% of the mass). Trajectories (Figure 11) suggest that this high soil factor day may have been Saharan dust episodes; 10-day backward trajectories show fast transport over the Atlantic Ocean. Other days with high concentrations of this factor appear to be caused by transport over the Great Plains. Despite the large spikes in the soil factor concentrations, none of the highest concentration days occurred on the worst visibility days, indicating that while there can be events in which the soil contribution to ambient $PM_{2.5}$ is important, this factor is not as important as others during the worst visibility days.

A wood and biomass burning factor was identified by the presence of potassium[48-50,54] and a small amount of carbonaceous aerosol. The analytical carbonaceous fractions aided in identifying and quantifying this factor, since runs using only a total OC and EC did not effectively resolve this factor. Air mass trajectories were combined with fire location satellite data to better identify this factor, and the combination suggests this factor is significant only when local burning and conducive flow patterns from fire locations occur. On the two highest concentration days of this factor, April 12, 2003, and May 9, 2003, air mass trajectories show transport from nearby fire locations (Figure 12). Samples where this factor showed high concentrations were usually caused by nearby fires, rather than long-range multi-day transport. Overall, this factor accounted for 7% of the median mass, and 6% on the worst visibility days. Some of the days with high burning factor concentrations were episodes of poor visibility, but on average this factor was less important than coal combustion and other factors. However, this is likely a lower limit of burning influence; PMF would not be able to fully quantify a burning factor because the factor profile likely varies with every episode because of source distance, fuel type, and atmospheric chemistry during transport. With sampling every day during the spring and summer, or use of organic molecular markers such as levoglucosan,[48,50,53-58] this factor will likely be better estimated.

CONCLUSIONS

PMF was applied to speciated $PM_{2.5}$ data collected as part of the IMPROVE program at Hercules-Glades, Missouri, from March 2001-February 2004. Modeled results accounted for the mass and were consistent with known sources and their locations. The use of the analytical OC/EC fractions, better uncertainty estimates for data near the detection limit, and bootstrapping all helped better apportion and quantify the uncertainties in the identified factors. Nine factors were identified as: (1) coal combustion, (2) urban carbonaceous, (3) background aged aerosol, (4) oil combustion, (5) industrial metals, (6) nitrate, (7) soil, and (8) burning. CPF analysis and emission inventory data were used to confirm the identification of sources. Calculating EIP by combining trajectory density with county-level emission inventory data helped identify the source regions for particular factors. Results showed that a combination of local (such as burning, nitrate, urban carbonaceous, and industrial metals) and regional (coal combustion, background aerosol, and oil combustion) factors impact the site. However, on the worst visibility days, coal combustion accounted for about half of the mass, with urban carbonaceous aerosol and nitrate during the winter also important. Event-driven factors such as biomass/wood burning and soil were clearly evident, though their impact was important only during their severe events.

ACKNOWLEDGMENTS

This work was supported by the Central States Regional Air Planning Association (CENRAP) by contract number 904780.

REFERENCES

1. Dockery, D.W.; Pope, C.A., III Acute respiratory effects of particulate air pollution; *Annu Rev Public Health* **1994**, *15*, 107-132.

2. Dockery, D.W.; Pope, C.A.; Xu, X.P.; Spengler, J.D.; Ware, J.H.; Fay, M.E.; Ferris, B.G.; Speizer, F.E. An association between air pollution and mortality in six U.S. cities; *New Engl. J. Med.* **1993**, *329*, 1753-1759.
3. Wu, J.; Lurmann, F.; Winer, A.; Lu, R.; Turco, R.; Funk, T. Development of an individual exposure model for application to the Southern California Children's Health Study; *Atmos. Environ.* **2005**, *39*, 259-273.
4. Gilliland, F.; Avol, E.; Kinney, P.; Jerret, M.; Dvonch, T.; Lurmann, F.; Buckley, T.; Breysse, P.; Keeler, J.; de Villiers, T. *et al.* Air pollution exposure assessment for epidemiologic studies of pregnant women and children: lessons learned from the Centers for Children's Environmental Health and Disease Prevention Research; *Environ Health Perspect* **2005**, in press.
5. Malm, W.C.; Schichtel, B.A.; Pitchford, M.L.; Ashbaugh, L.L.; Eldred, R.A. Spatial and monthly trends in speciated fine particle concentration in the United States; *Journal of Geophysical Research-Atmospheres* **2004**, *109*(D3).
6. Watson, J.G. 2002 Critical review -- Visibility: science and regulation; *J. Air & Waste Manag. Assoc.* **2002**, *52*(6), 628-713.
7. Delucchi, M.A.; Murphy, J.J.; McCubbin, D.R. The health and visibility cost of air pollution: a comparison of estimation methods; *Journal of Environmental Management* **2002**, *64*(2), 139-152.
8. U.S. Environmental Protection Agency *Highway vehicle emission estimates-II*, 1995.
9. Watson, J.G.; Chow, J.C.; Lurmann, F.W.; Musarra, S.P. Ammonium nitrate, nitric acid, and ammonia equilibrium in wintertime Phoenix, Arizona; *J. Air & Waste Manag. Assoc.* **1994**, *44*, 405-412.
10. Lowenthal, D.H.; Zielinska, B.; Chow, J.C.; Watson, J.G.; Gautam, M.; Ferguson, D.H.; Neuroth, G.R.; Stevens, K.D. Characterization of heavy-duty diesel vehicle emissions; *Atmos. Environ.* **1994**, *28*, 731-744.
11. Schauer, J.J.; Cass, G.R. Source apportionment of wintertime gas-phase and particle-phase air pollutants using organic compounds as tracers; *Environ. Sci. Technol.* **2000**, *34*(9), 1821-1832.
12. Kleeman, M.J.; Schauer, J.J.; Cass, G.R. Size and composition distribution of fine particulate matter emitted from motor vehicles; *Environ. Sci. Technol.* **2000**, *34*, 1132-1142.
13. Schauer, J.J.; Kleeman, M.J.; Cass, G.R.; Simoneit, B.R.T. Measurement of emissions from air pollution sources. 2. C_1 through C_{30} organic compounds from medium duty diesel trucks; *Environ. Sci. Technol.* **1999**, *33*(10), 1578-1587.
14. Kim, E.; Hopke, P.K.; Edgerton, E.S. Source identification of Atlanta aerosol by positive matrix factorization; *J. Air & Waste Manage. Assoc.* **2003**, *53*, 731-739.
15. Maykut, N.; Knowle, K.; Larson, T.V. *Seattle $PM_{2.5}$ characterization studies*; Draft report prepared by Puget Sound Air Pollution Control Agency, Seattle, WA, 1998.
16. Kim, E.; Hopke, P.K.; Edgerton, E.S. Improving source identification of Atlanta aerosol using temperature resolved carbon fractions in positive matrix factorization; *Atmos. Environ.* **2004**, *38*, 3349-3362.
17. Chow, J.C.; Watson, J.G.; Pritchett, L.C.; Pierson, W.R.; Frazier, C.A.; Purcell, R.G. The DRI thermal/optical reflectance carbon analysis system: description, evaluation and applications in U.S. air quality studies; *Atmos. Environ.* **1993**, *27A*(8), 1185-1201.

18. Chow, J.C.; Watson, J.G.; Crow, D.; Lowenthal, D.H.; Merrifield, T. Comparison of IMPROVE and NIOSH carbon measurements; *Aerosol Sci. Technol.* **2001**, *34*, 23-34.
19. Zhao, W.; Hopke, P.K. Source apportionment for ambient particles in the San Gorgonio wilderness; *Atmos. Environ.* **2004**, *38*, 5901-5910.
20. Poirot, R.L.; Wishinski, P.R.; Hopke, P.K.; Polissar, A.V. Comparative application of multiple receptor methods to identify aerosol sources in northern Vermont; *Environ. Sci. Technol.* **2001**, *35*(23), 4622-4636.
21. Song, X.-H.; Polissar, A.V.; Hopke, P.K. Sources of fine particle composition in the northeastern U.S.; *Atmos. Environ.* **2001**, *35*, 5277-5286.
22. Malm, W.C.; Sisler, J.F.; Huffman, D.; Eldred, R.A.; Cahill, T.A. Spatial and seasonal trends in particulate concentration and optical extinction in the United States; *J. Geophys. Res.* **1994**, *99*(D1), 1347-1370.
23. Overview of IMPROVE and visibility. <http://vista.cira.colostate.edu/improve/Overview/Overview.htm> last accessed August 4, 2004. By IMPROVE.
24. Kim, E.; Hopke, P.K. Improving source identification of fine particles in a rural northeastern U.S. area utilizing temperature-resolved carbon fractions; *J. Geophys. Res.* **2004**, *109*(D9).
25. Lee, J.H.; Yoshida, Y.; Turpin, B.J.; Hopke, P.K.; Poirot, R.L.; Lioy, P.J.; Oxley, J.C. Identification of sources contributing to mid-Atlantic regional aerosol; *J. Air & Waste Manage. Assoc.* **2002**, *52*, 1186-1205.
26. Polissar, A.V.; Hopke, P.K.; Poirot, R.L. Atmospheric aerosol over Vermont: chemical composition and sources; *Environ. Sci. Technol.* **2001**, *35*(23), 4604-4621.
27. Yakovleva, E.; Hopke, P.K.; Wallace, L. Receptor modeling assessment of particle total exposure assessment methodology data; *Environ. Sci. Technol.* **1999**, *33*(20), 3645-3652.
28. Ramadan, Z.; Song, X.-H.; Hopke, P.K. Identification of sources of Phoenix aerosol by positive matrix factorization; *J. Air & Waste Manage. Assoc.* **2000**, *50*, 1308-1320.
29. Zhou, L.; Kim, E.; Hopke, P.K.; Stanier, C.O.; Pandis, S. Advanced factor analysis on Pittsburgh particle size-distribution data; *Aerosol Sci. Technol.* **2004**, *38*(S1), 118-132.
30. Anttila, P.; Paatero, P.; Tapper, U.; Jarvinen, O. Source identification of bulk wet deposition in Finland by positive matrix factorization; *Atmos. Environ.* **1995**, *29*(14), 1705-1718, published without a date.
31. Brown, S.G.; Hafner, H.R.; Shields, E. Source apportionment of Detroit air toxics data with positive matrix factorization. Paper no. 41 presented at the *Air & Waste Management Association Symposium on Air Quality Measurement Methods and Technology, Research Triangle Park, NC, April 19-22* STI-2450, 2004.
32. Brown, S.G.; Hafner, H.R. Source apportionment of VOCs in the Houston, Texas, area. Presented at the *NARSTO Workshop on Innovative Methods for Emission-Inventory Development and Evaluation, Austin, TX, October 14-16* STI-2356, 2003.
33. Buzcu, B.; Fraser, M. Positive matrix factorization analysis of volatile organic compound concentrations in Houston, TX. Paper presented at *NARSTO Workshop on Innovative Methods for Emission-Inventory Development and Evaluation, Austin, TX, October 14-17,* Rice University, Houston, TX, 2003.
34. Zhao, W.; Hopke, P.K.; Karl, T. Source identification of volatile organic compounds in Houston, TX; *Environmental Science and Technology* **2004**, *38*, 1338-1347.

35. Paatero, P. Least squares formulation of robust non-negative factor analysis; *Chemometrics and Intelligent Laboratory Systems* **1997**, *37*, 23-35.

36. Paatero, P.; Tapper, U. Positive matrix factorization: a non-negative factor model with optimal utilization of error estimates of data values; *Environmetrics* **1994**, *5*, 111-126.

37. Hopke, P.K. *A guide to Positive Matrix Factorization*; by the Department of Chemistry, Clarkson University, Potsdam, NY, 2003.

38. White, W.H.; Eldred, R.A.; Feeney, P.J.; McDade, C.E.; Perley, B.P.; Shadoan, D.J.; Wakabayashi, P.H. Behavior of fine-particle elemental data near the detection limit. Paper No. 24 for presentation at the *Air and Waste Management Association's Regional and Global Perspectives on Haze: Causes, Consequences and Controversies – Visibility Specialty Conference, Asheville, NC, October 25-29*, 2004.

39. Paatero, P.; Hopke, P.K.; Begum, B.A.; Biswas, S.W. A graphical diagnostic method for assessing the rotation in factor analytical models of atmospheric pollution; *Atmos. Environ.* **2004**, in press.

40. Ashbaugh, L.L.; Malm, W.C.; Sader, W.Z. A residence time probability analysis of sulfur concentrations at Grand Canyon National Park; *Atmos. Environ.* **1985**, *19*(8), 1263-1270.

41. Draxler, R.R.; Hess, G.D. *Description of the Hysplit 4 modeling system*; ERL ARL-224; by NOAA, 1997.

42. McCoy, J.; Johnston, K. *Using ArcGIS Spatial Analyst*; ESRI., 2001.

43. Cressie, N.A.C. *Statistics for spatial data*; John Wiley & Sons, Inc., 1993.

44. Turpin, B.; Saxena, P. Species contributions to $PM_{2.5}$ mass concentrations: revisiting common assumptions for estimating organic mass. Presented at the *Air & Waste Management Association International Specialty Conference, $PM_{2.5}$: A Fine Particle Standard, Long Beach, CA, January 28-30*, 1998.

45. Turpin, B.J.; Huntzicker, J.J.; Larson, S.M.; Cass, G.R. Los Angeles summer midday particulate carbon-primary and secondary aerosol; *Environ. Sci. Technol.* **1991**, *25*, 1788-1793.

46. Turpin, B.J.; Lim, H.-J. Species contribution to $PM_{2.5}$ mass concentrations: revisiting common assumptions for estimating organic mass; *Aerosol Sci. Technol.* **2001**, *35*(10), 602-610.

47. Lowenthal, D.; Kumar, N. $PM_{2.5}$ mass and light extinction reconstruction in IMPROVE; *J. Air & Waste Manage. Assoc.* **2003**, *53*(9), 1109-1120.

48. Fine, P.M.; Cass, G.R.; Simoneit, B.R.T. Chemical characterization of fine particle emissions from the fireplace combustion of wood types grown in the Midwestern and Western United States; *Environmental Engineering Science* **2004**, *21*(3), 387-409.

49. Poirot, R. *Tracers of opportunity: Potassium*, 1998.

50. Schauer, J.J.; Kleeman, M.J.; Cass, G.R.; Simoneit, B.R.T. Measurement of emissions from air pollution sources. 3. C_1 through C_{29} organic compounds from fireplace combustion of wood; *Environ. Sci. Technol.* **2001**, *35*(9), 1716-1728.

51. Song, X.H.; Polissar, A.V.; Hopke, P.K. Sources of fine particle composition in the northeastern U.S.; *Atmos. Environ.* **2001**, *35*(31), 5277-5286.

52. Kim, E.; Hopke, P.K. Source apportionment of fine particles at Washington, DC, utilizing temperature-resolved carbon fractions; *J. Air & Waste Manage. Assoc.* **2004**, *54*(7), 773-785.

53. Zheng, M.; Cass, G.R.; Schauer, J.J.; Edgerton, E.S. Source apportionment of $PM_{2.5}$ in the southeastern United States using solvent-extractable organic compounds as tracers; *Environ. Sci. Technol.* **2002**, *36*, 2361-2371.
54. Fine, P.M.; Cass, G.R.; Simoneit, B.R.T. Organic compounds in biomass smoke from residential wood combustion: emissions characterization at a continental scale; *Journal of Geophysical Research-Atmospheres* **2002**, *107*(D21).
55. Sheesley, R.J.; Schauer, J.J.; Chowdhury, Z.; Cass, G.R.; Simoneit, B.R.T. Characterization of organic aerosols emitted from the combustion of biomass indigenous to South Asia; *Journal of Geophysical Research-Atmospheres* **2003**, *108*(D9).
56. Schauer, J.J.; Fraser, M.P.; Cass, G.R.; Simoneit, B.R.T. Source reconciliation of atmospheric gas-phase and particle-phase pollutants using organic compounds as tracers; **2001**, submitted for publication.
57. Brown, S.G.; Herckes, P.; Ashbaugh, L.; Hannigan, M.P.; Kreidenweis, S.M.; Collett, J.L., Jr. Characterization of organic aerosol in Big Bend National Park, Texas; *Atmos. Environ.* **2002**, *36*(38), 5807-5818.
58. Nolte, C.G.; Schauer, J.J.; Cass, G.R.; Simoneit, B.R.T. Highly polar organic compounds present in wood smoke and in the ambient atmosphere; *Environ. Sci. Technol.* **2001**, *35*(10), 1912-1919.

About the Authors

Steven G. Brown is an Air Quality Analyst and Project Manager, Anna Frankel is an Air Quality Data Analyst, Sean M. Raffuse is an Air Quality Analyst, Hilary R. Hafner is Senior Manager of the Air Quality Data Analysis Division, and Paul T. Roberts is Executive Vice President at Sonoma Technology, Inc. Brett A. Anderson is with the Air Planning and Development Branch of the United States Environmental Protection Agency Region 7. Address correspondence to: Steven G. Brown, Sonoma Technology, Inc., 1360 Redwood Way, Suite C, Petaluma, CA 94954; phone: (707) 665-9900; e-mail: sbrown@sonomatech.com.

Keywords

Source apportionment
PMF
$PM_{2.5}$
Missouri
Receptor modeling
IMPROVE

Table 1. Summary statistics of species used in PMF analysis (in μg/m^3) for Hercules-Glades March 2001–February 2004 (N=328).

Species	Median	Mean	Standard Dev	N Missing	N below 10*MDL and above MDL	N below MDL	% below MDL
AS	0.0003	0.0003	0.0002	1	253	81	24
BR	0.0018	0.0022	0.0014	1	4	0	0
CU	0.0005	0.0005	0.0003	1	213	17	5
EC1	0.43	0.48	0.24	1	47	0	0
EC2	0.084	0.092	0.054	1	294	25	7
EC3	0.0031	0.0076	0.0097	1	145	189	57
FE	0.026	0.045	0.086	1	0	0	0
H	0.42	0.50	0.29	1	0	0	0
K	0.048	0.060	0.049	1	3	0	0
MN	0.0008	0.0012	0.0016	1	81	49	15
NO3	0.41	1.1	1.36	2	91	3	1
OC1	0.063	0.11	0.12	0	200	106	32
OC2	0.28	0.35	0.24	0	175	8	2
OC3	0.54	0.69	0.58	0	201	3	1
OC4	0.44	0.53	0.42	0	64	0	0
OP	0.20	0.22	0.17	1	188	32	10
PB	0.0016	0.0018	0.0011	1	44	0	0
SE	0.0005	0.0006	0.0004	1	130	4	1
SI	0.12	0.20	0.29	1	14	0	0
SO4	2.60	3.29	2.61	2	1	0	0
TI	0.0025	0.0060	0.011	1	26	16	5
V	0.0002	0.0005	0.0008	1	145	124	37
ZN	0.0046	0.0051	0.0027	1	3	0	0

Figure 1. Location of the Hercules-Glade, Missouri, IMPROVE air quality monitoring site.

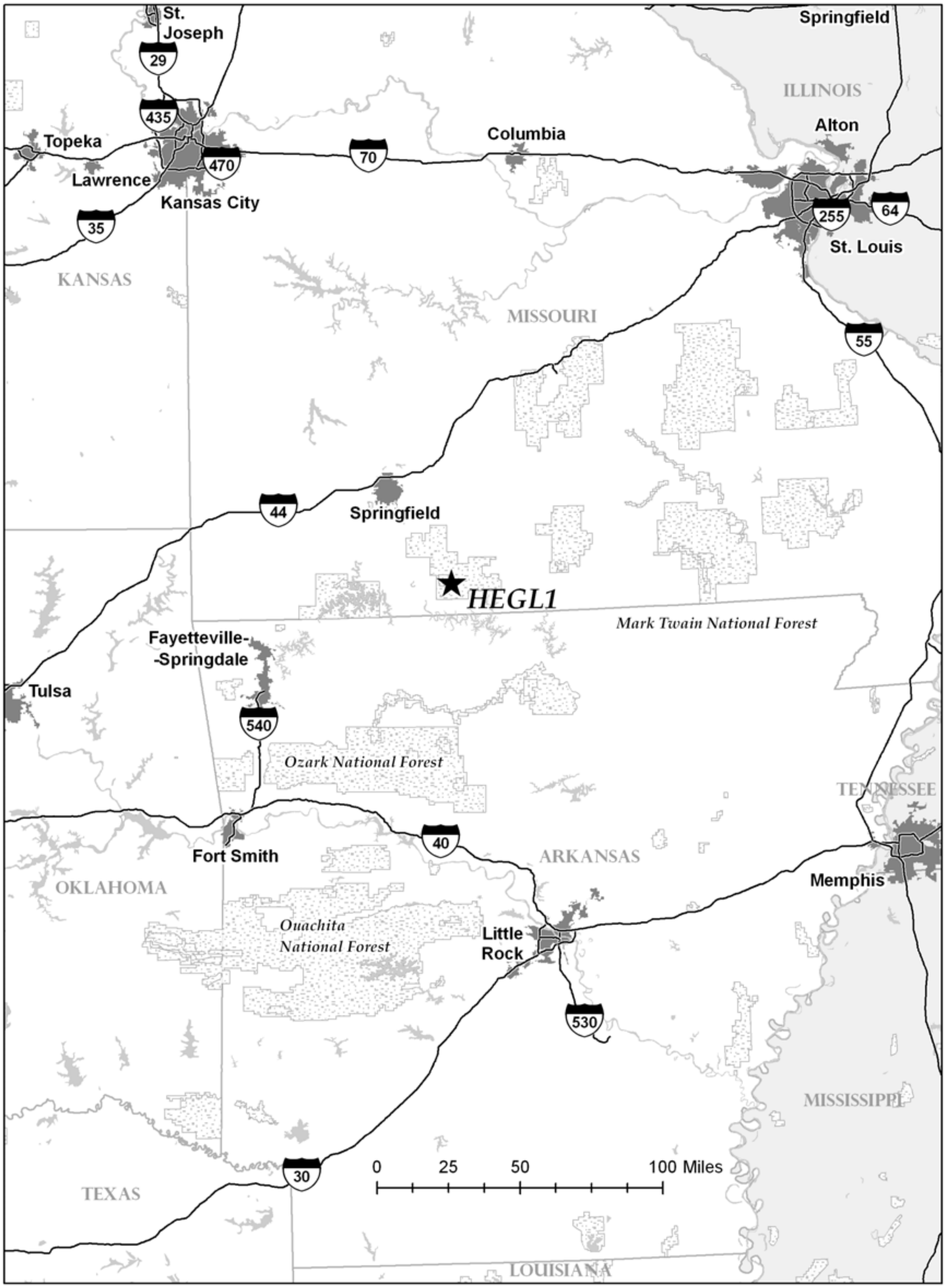

Figure 2. Average $PM_{2.5}$ composition by major component (OMC = 1.4*OC) for all valid data March 2001–February 2004.

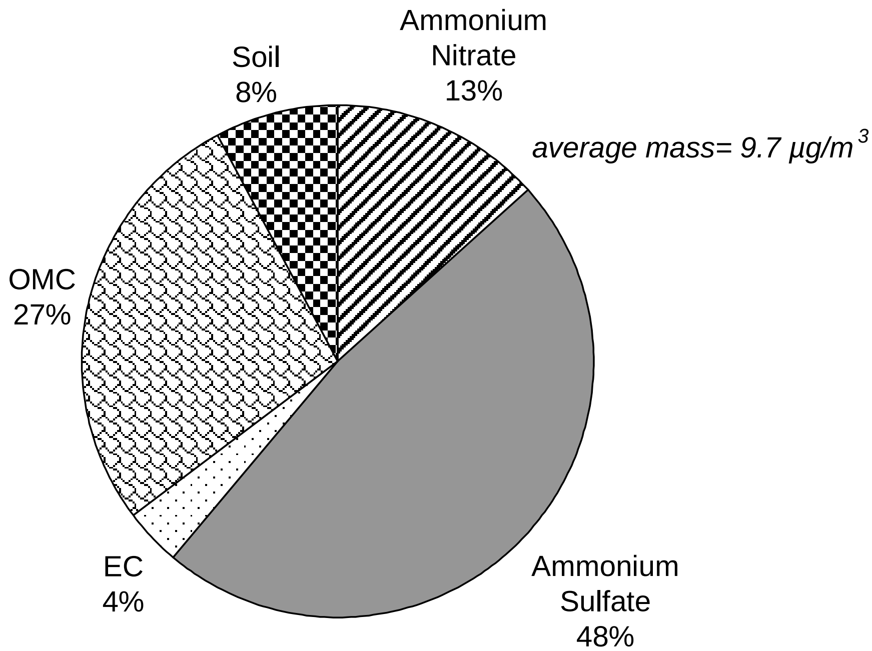

Figure 3a. Average composition (µg/m^3) by season (spring = March through May, summer = June through August, etc.) at Hercules-Glade, March 2001–February 2004.

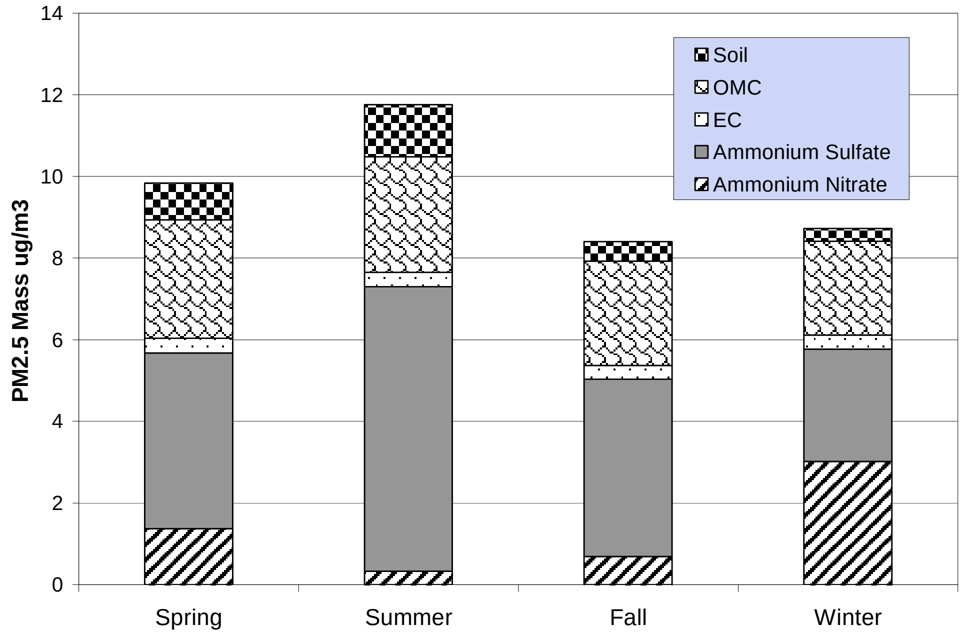

Figure 3b. Average composition (percentage) by season (spring = March through May, summer = June through August, etc.) at Hercules-Glade, March 2001–February 2004.

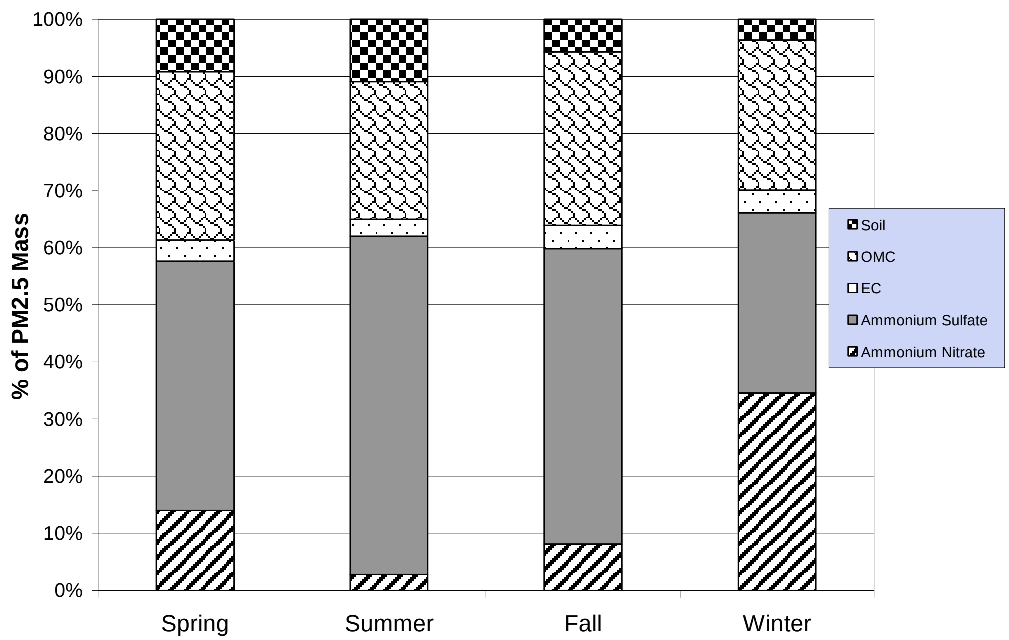

Figure 4a. Median composition on the worst-20% visibility days at Hercules-Glade, March 2001–February 2004.

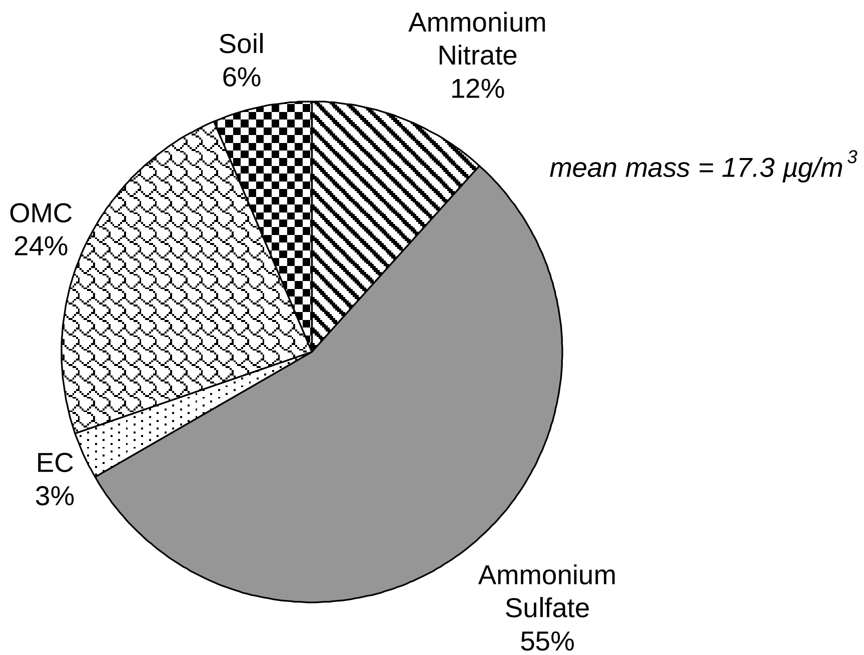

Figure 4b. Median composition of b_{ext} (aerosol extinction) based on the IMPROVE visibility equation on the worst-20% visibility days at Hercules-Glade, March 2001–February 2004.

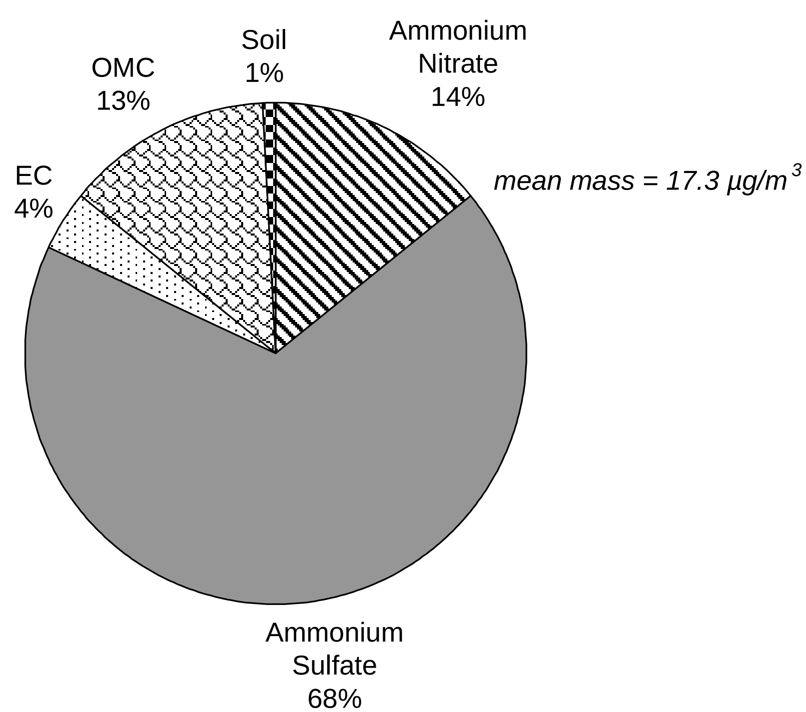

Figure 5a. Scatter plot of ammonium sulfate versus selenium by season ($\mu g/m^3$) where 1 = spring, 2 = summer, etc.

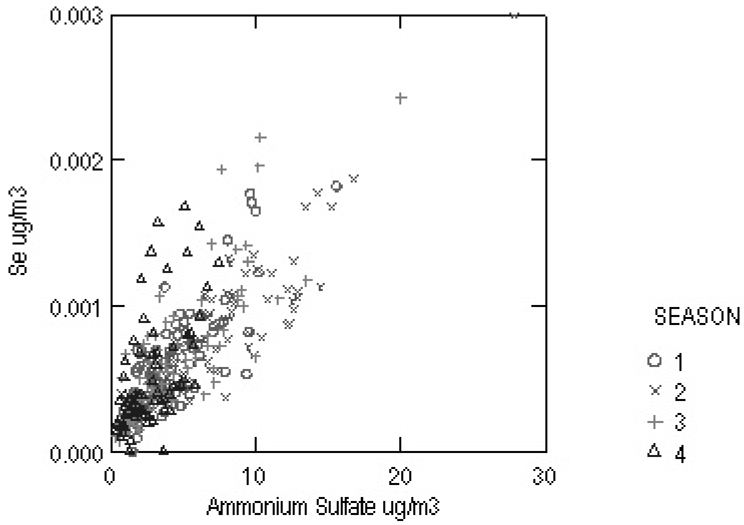

Figure 5b. Scatter plot of potassium versus EC by season ($\mu g/m^3$) where 1 = spring, 2 = summer, etc.

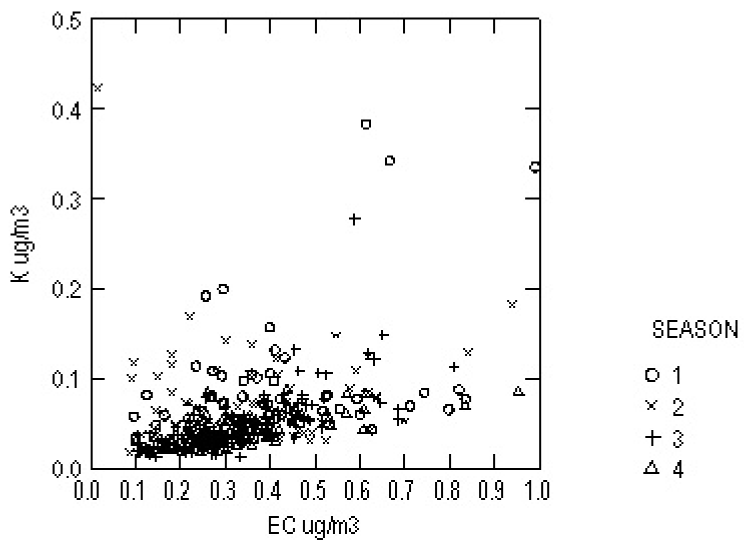

Figure 5c. Scatter plot of lead (PB) versus zinc (ZN) by season ($\mu g/m^3$) where 1 = spring, 2 = summer, etc.

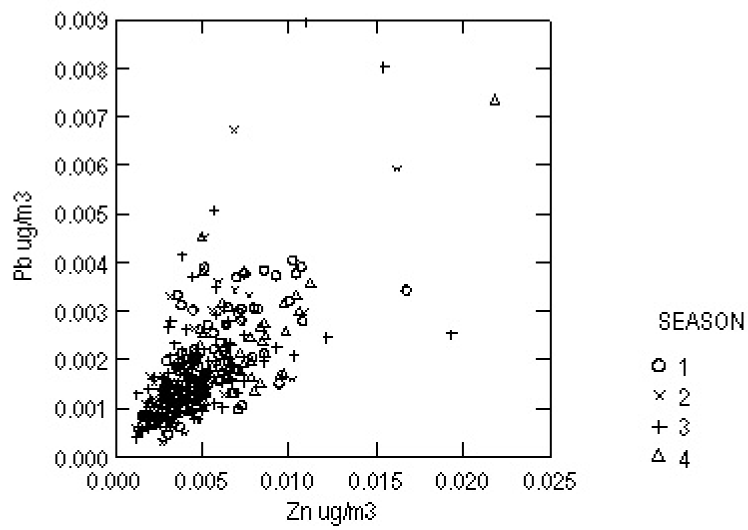

Figure 6. Factor profiles (percent of species in factor). Error bars represent the standard deviation of the factor loading over 300 runs.

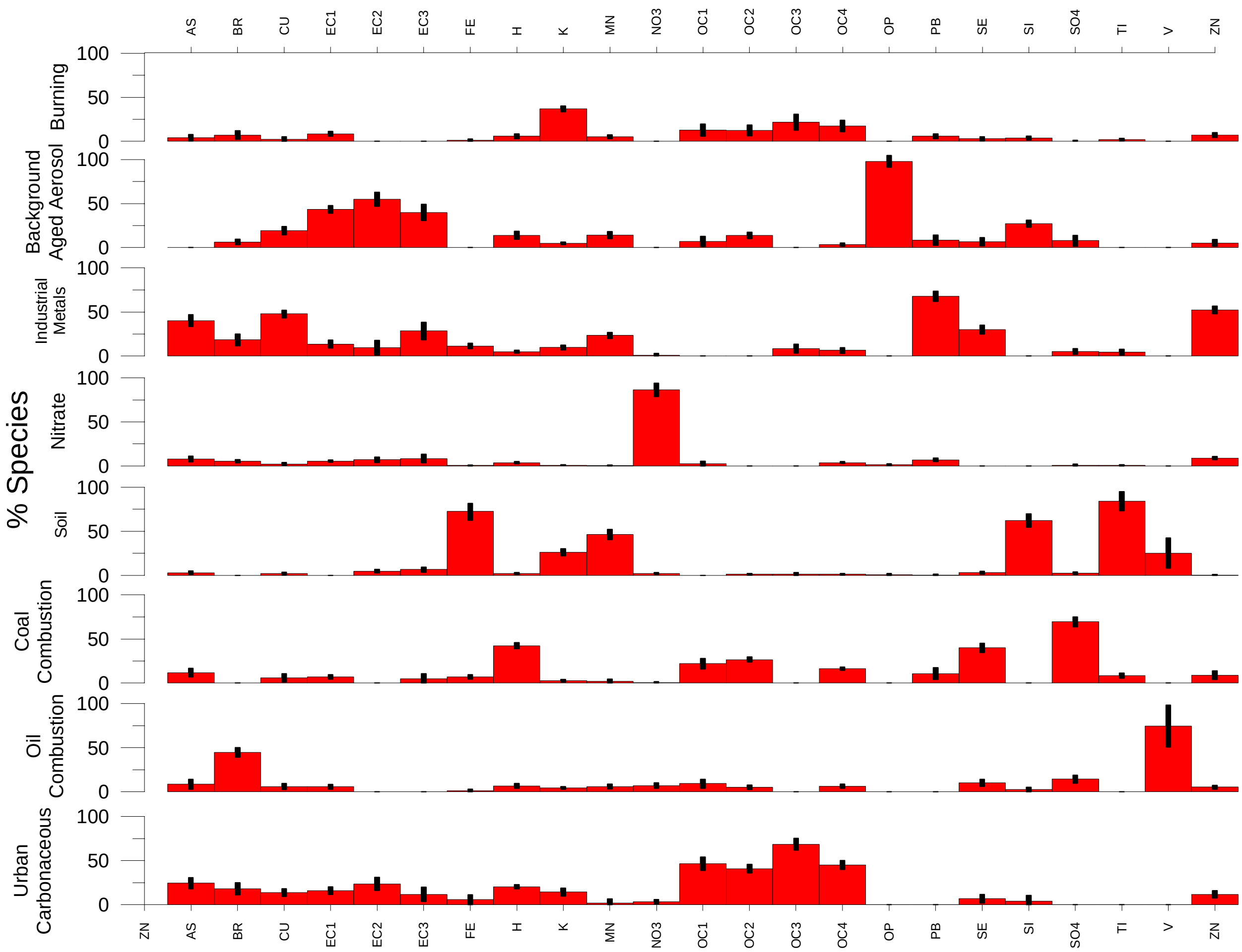

Figure 7. Time series of factor strengths by date ($\mu g/m^3$).

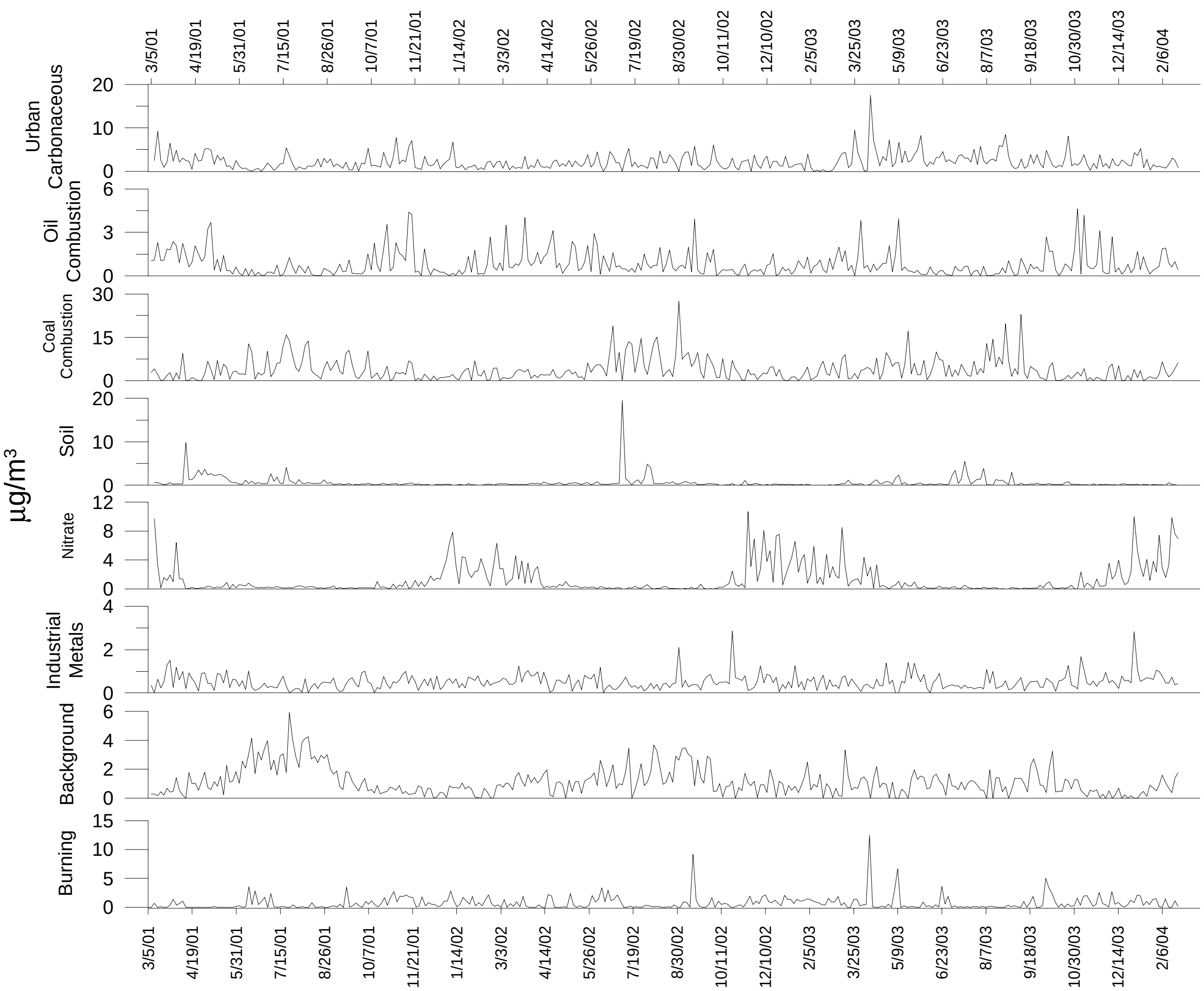

Figure 8. Reconstructed mass versus measured $PM_{2.5}$ mass.

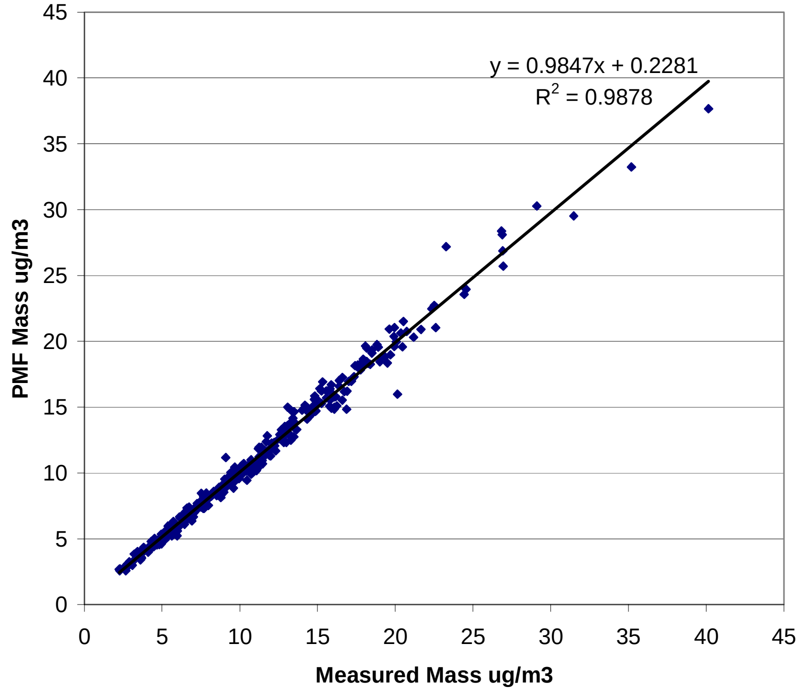

Figure 9. Average factor contribution estimates for (a) all samples and (b) the worst-20% visibility days.

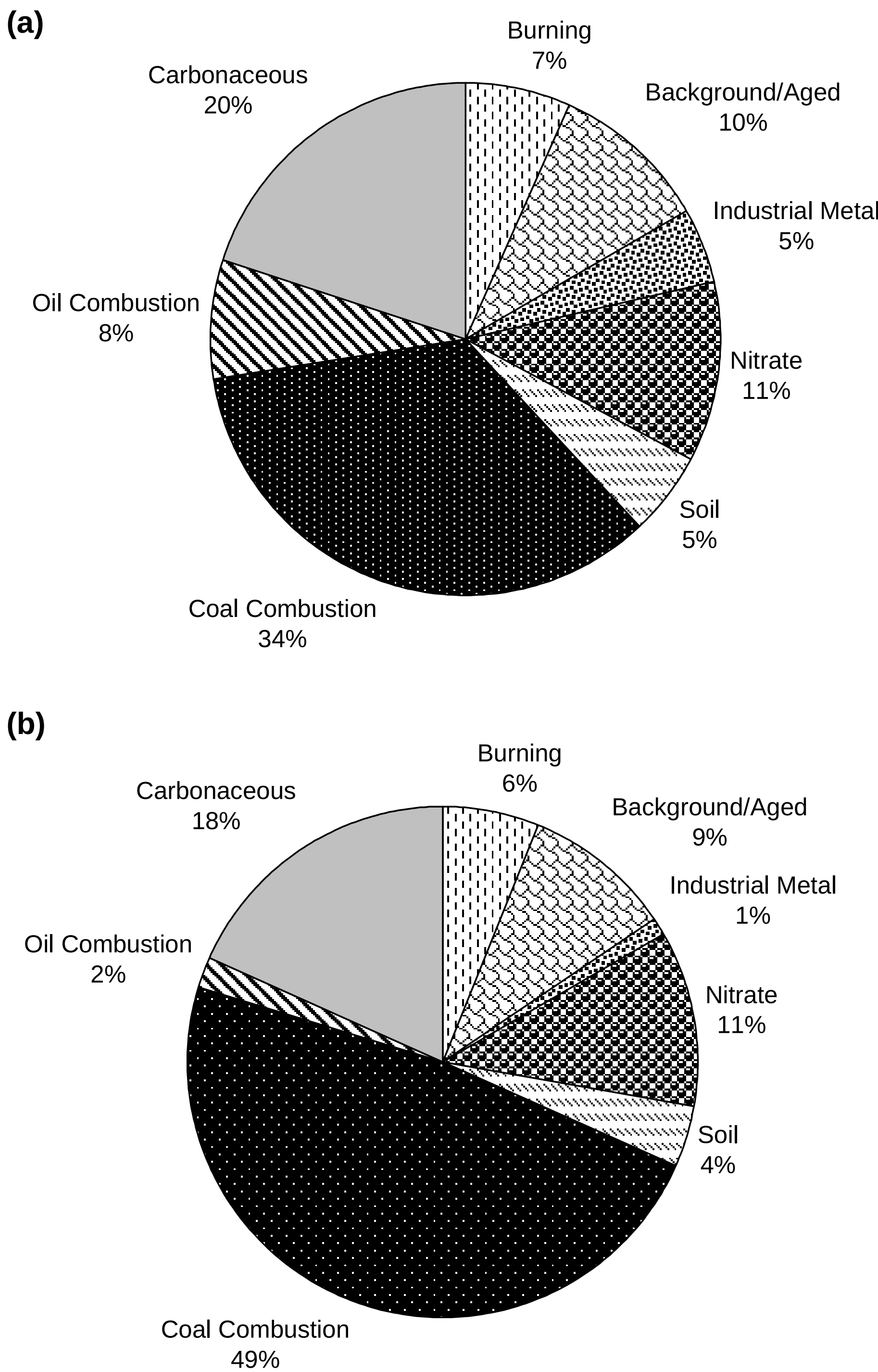

Figure 10. CPF plots for (a) coal combustion, (b) urban carbonaceous, (c) nitrate, and (d) industrial metals.

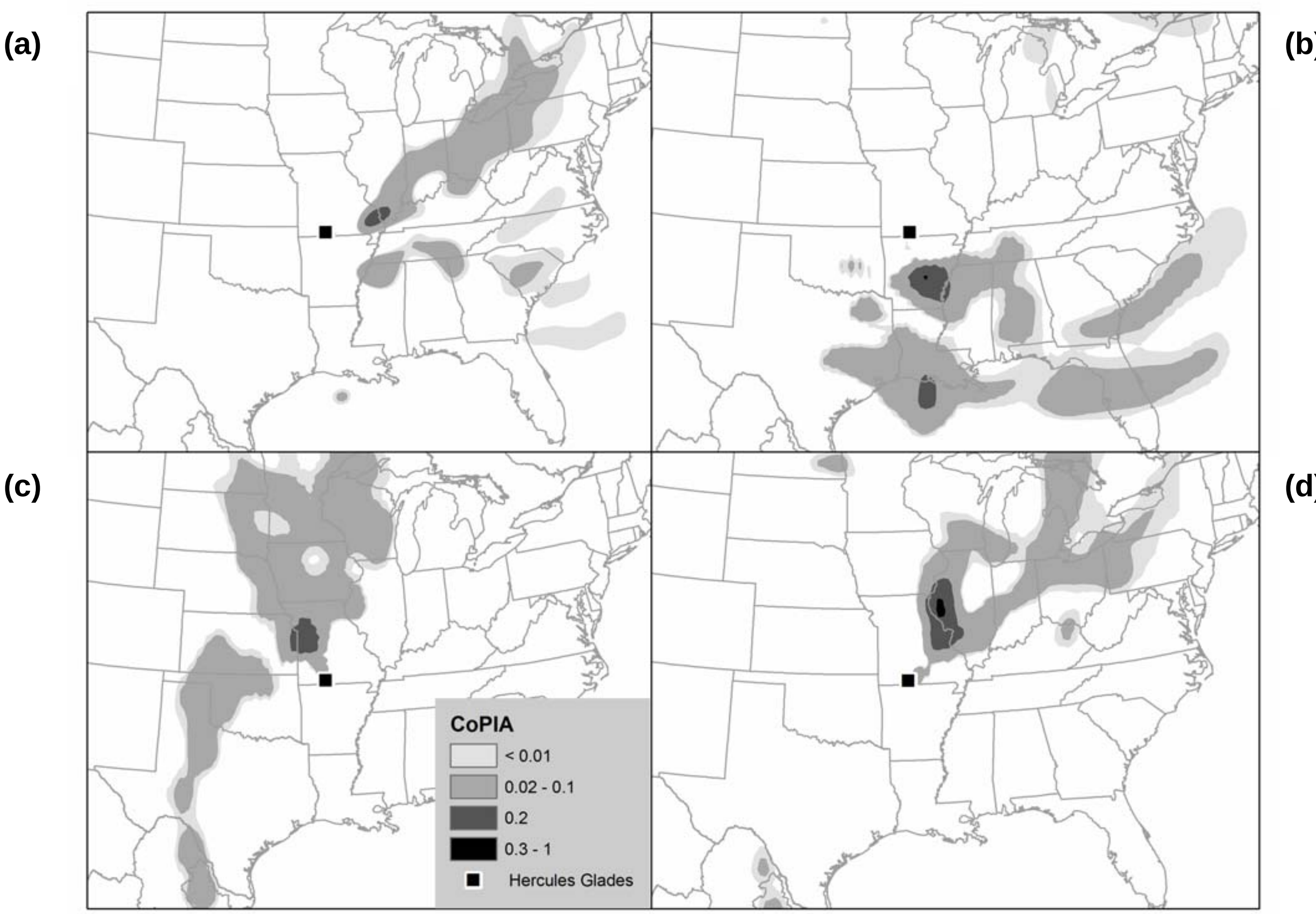

Figure 11. Air mass trajectories on the dust event day of July 1, 2002.

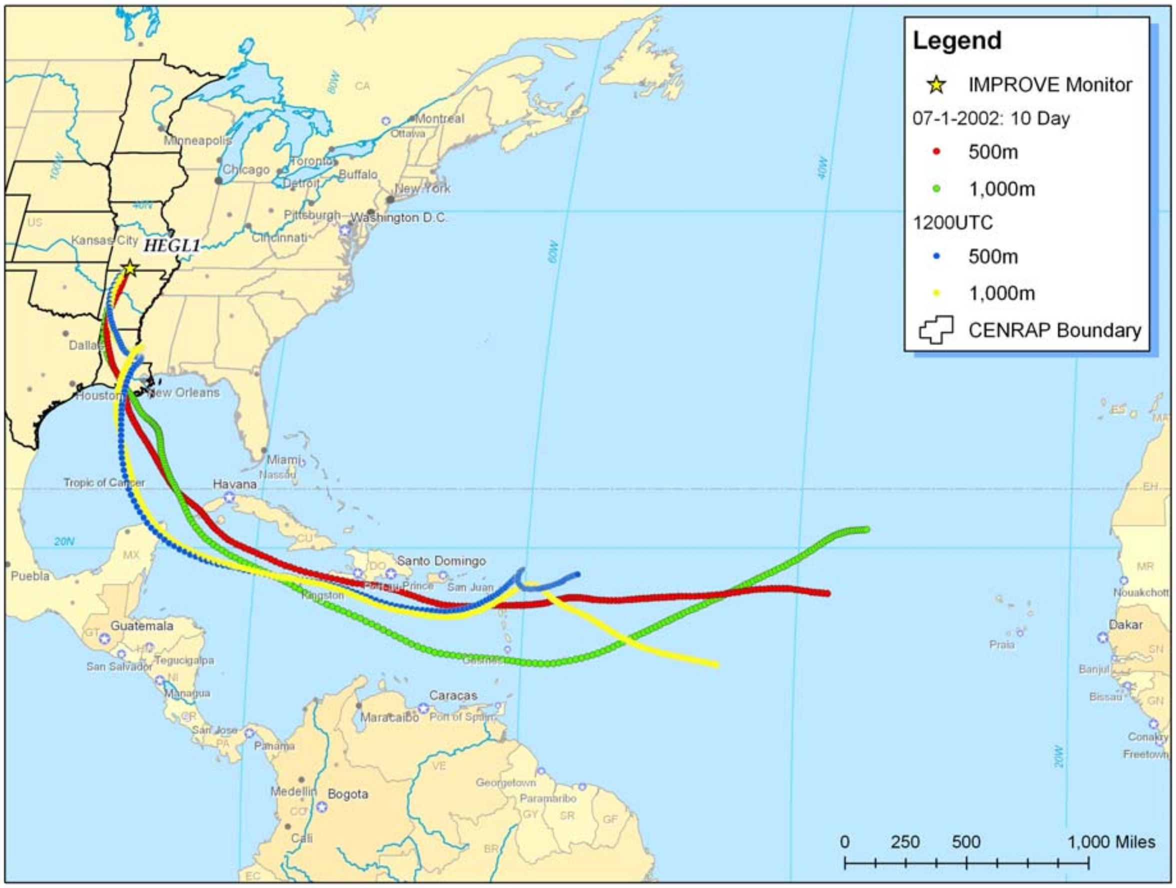

Figure 12. Air mass trajectories with ending heights of 250 m, 500 m, and 1000 m and fire locations on the burning event days of (a) April 12, 2003, and (b) May 9, 2003.

(a)

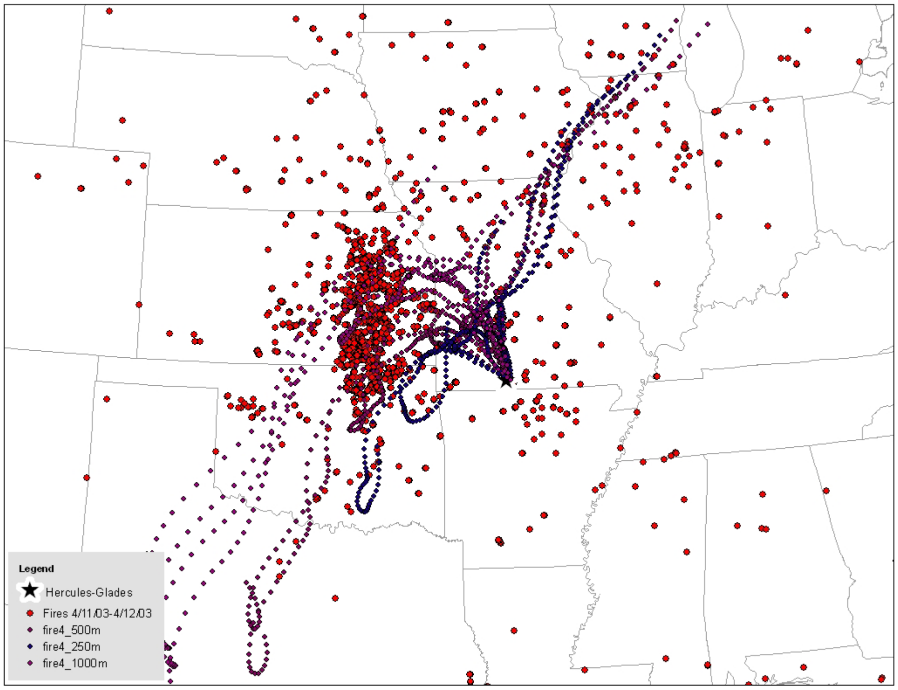

(b)